TIGHT-BINDING ENERGY BANDS OF

PEROVSKITE TYPE TRANSITION METAL OXIDES

by

Harutun George Karian

A Dissertation Submitted to the

Graduate Faculty in Partial Fulfillment of

The Requirements for the Degree of

DOCTOR OF PHILOSOPHY

Major Subject: Physical Chemistry

Approved:

In Charge of Major Work

Head of Major Department

Dean of Graduate College

Iowa State University
Ames, Iowa

1969

PLEASE NOTE:

Not original copy.
Several pages have
broken print. Filmed
as received.

TABLE OF CONTENTS

TABLE OF CONTENTS (Continued)

TABLE OF CONTENTS (Continued)

PART I. THEORY

INTRODUCTION

Transition metal oxides have been receiving increasing attention from experimentalists and theorists alike, as model systems in which to study the solid state. Tungsten bronzes, for example, properly doped, form a basis for the study of a major portion of the field of solid state physics, in that depending upon the temperature and concentration of alkali metal, they can be insulators, semiconductors, metals, or super-conductors. ReO_3 has been found to be a "good metal", reduced potassium tantalate $KTaO_{2+x}$ has been found to be a semi metal, and some compounds such as $SrTiO_3$ are found to be semiconductors. The cubic tungsten bronzes, (stoichiometry A_xWO_3, where A is an alkali metal), ReO_3, $KTaO_3$, and $SrTiO_3$ all have a common structural feature; the transition metal is octahedrally co-ordinated with oxygens, and, except for the case of ReO_3 (which has the perovskite structure without the central hole filled by a non-transition metal atom) are all perovskite structures.

A major question to be answered for these systems is "how does one think chemically about their stability, and physically about their transport properties?" For the chemist, the easiest approach is the localized molecular orbital picture with each metal ion in a site of O_h symmetry. Levels are guessed at, electrons are counted, and depending upon the last levels to be filled, inferences are made

regarding the possibilities for conduction bands, generally labeled according to the transformation properties of the orbitals in question under O_h point symmetry. The solid state theorist, on the other hand, is very aware that an exact many body calculation to infer stabilities is not possible. He, therefore, uses an independent particle model with the meaningful results (to him) being energy as a function of wave vector, and Fermi surface contours. He realizes that point symmetry designations completely break down as soon as translational symmetry is forced upon the wave functions, and has a tendency to listen with a respectful, but somewhat distant ear to point symmetry, bond order, electronegativity etc., type arguments from his chemical cohorts in the solid state chemistry field. For the average chemist, on the other hand, vision, intuition, and comprehension become somewhat blurred as soon as an $E(\underline{k})$ vs. $\underline{k}$ plot is waved enthusiastically before his eyes as his theorist friend explains what the Fermi Surface must look like from the most recent band calculation.

Objectives of the Thesis Work

The present work is one attempt to provide the beginnings of a translation between these two groups via tight binding calculations of the band structures of some representative, important and interesting cubic transition metal oxides.

The work is aimed at chemists via a delineation of orbitals
participating in valence and conduction bands, and a com-
parison of how the molecular orbital model flows over into
the band picture as translational symmetry is added. For
the physicists, we do indeed exhibit energy vs. wave vector
plots and discuss their validity in terms of transport and
optical properties.

Recently, overlap calculations (1) were used to provide
a "zeroth order" method of thinking about the possibilities
for orbitals forming conduction bands in the cubic tungsten
bronzes. We will now outline the theory of the first
order method for thinking about transport properties of
perovskite type metal oxides; in particular, we use ReO_3
as a model to discuss the method.

The tight-binding energy bands of a series of perovskite
type transition metal oxides: ReO_3, $Na_xWO_3(x=1.0)$, $KTaO_3$
are calculated and the results are discussed in Parts II
and III of the thesis. The crystal orbital properties which
will be discussed in subsequent Parts II and III are:

1) Density of States

2) Joint Density of States

3) Fermi Surface

4) Results of the Mulliken Population Analysis

Before we discuss the tight-binding approximation (TBA) used in obtaining energy bands of crystals, we shall make a brief excursion into the Hartree-Fock (H-F) approximation. The purpose of this preliminary discussion is to show the "rigorous" equations from which we will systematically descend in rigor by a series of hopefully justified approximations.

HARTREE - FOCK APPROXIMATION

Let us assume that the electronic state of a unit cell (molecular unit) in a crystal is characterized by a particular wave vector, $\underline{k}$, in reciprocal space. If we further assume that the electronic configuration is a closed-shell, i.e., $M_{\underline{k}}$ doubly-occupied energy bands, the total wave function $\Phi(\underline{k})$ is approximated as an antisymmetrized product (ASP) of crystal spin-orbitals $u_q(\underline{k},\underline{x}_q)$

$$\Phi(\underline{k}) = \mathcal{A}\left\{ u_1(\underline{k},\underline{x}_1) \cdots u_{2M_{\underline{k}}}(\underline{k},\underline{x}_{2M_{\underline{k}}}) \right\}$$

where $\mathcal{A}$ is the antisymetrizer operator defined by

$$\mathcal{A} = (2M_{\underline{k}})^{-\frac{1}{2}} \sum_P (-1)^P P. \tag{1}$$

In the above, p is the parity of the P th permutation. In other words, we can express $\Phi(\underline{k})$ as a single-Slater determinant

$$\Phi(\underline{k}) = (2M_{\underline{k}})^{-\frac{1}{2}} \begin{vmatrix} u_1(\underline{k},\underline{x}_1) & u_1(\underline{k},\underline{x}_2) \cdots & u_1(\underline{k},\underline{x}_{2M_{\underline{k}}}) \\ u_2(\underline{k},\underline{x}_2) & u_2(\underline{k},\underline{x}_2) \cdots & u_2(\underline{k},\underline{x}_{2M_{\underline{k}}}) \\ \cdots & \cdots & \cdots \\ u_{2M_{\underline{k}}}(\underline{k},\underline{x}_1) \cdots & & u_{2M_{\underline{k}}}(\underline{k},\underline{x}_{2M_{\underline{k}}}) \end{vmatrix}$$

$$\tag{2}$$

From the properties of a determinant, we satisfy, as usual, the Pauli exclusion principle while allowing for double occupancy of the M_k energy bands. It is important to stress that M_k for all possible $\underline{k}$ vectors need not be the same.

The spin-orbital $u_q(\underline{k},\underline{x}_q)$ has a space ($\underline{r}$) - spin (ξ) coordinate $\underline{x}_q=(\underline{r}_q, \xi_q)$. We shall adapt the usual convention for an odd μ electron where

$$u_\mu(\underline{k},\underline{x}_\mu) = \Psi_j(\underline{k},\underline{r}_\mu)\,\alpha(\mu)$$

and $$u_{\mu+1}(\underline{k},\underline{x}_{\mu+1}) = \Psi_j(\underline{k},\underline{r}_{\mu+1})\,\beta(\mu+1)$$

where the functions α and β are the usual eigenfunctions of the single electron spin operators $\hat{S}^2$ and $\hat{S}_z$. The crystal orbital is labeled by j. So that there will be no confusion between the sum indices α and β used further on, the spin functions as the above is the only place we mention the spin functions explicitly.

The crystal Hamiltonian $\mathcal{H}$, defined for a fixed nuclear framework and $\underline{k}$ in the Born-Oppenheimer approximation, is

$$\mathcal{H} = \sum_\mu^{2M_k} h(\underline{r}_\mu) + \sum_{\mu<\nu}^{2M_k} g(\underline{r}_\mu,\underline{r}_\nu) \tag{3}$$

where $h(\underline{r}_\mu)=-\nabla_\mu^2 - 2\sum_\delta Z/r_{\delta\mu}$ and $g(\underline{r}_\mu,\underline{r}_\nu)=2/r_{\mu\nu}$.

The one-electron and two-electron operators are expressed in Rydberg energy units (13.6 e.v.). μ and V label interacting electrons. γ labels the atomic site having a bare nuclear charge Z_γ. In the valence shell approximation Z_γ becomes the effective nuclear charge (bare nuclear charge minus the sum of the non-valence electrons).

The quantum mechanical treatment of $\langle \mathcal{H} \rangle_{\underline{k}}$ equal to $\langle A \Phi(\underline{k}) | \mathcal{H} | A \Phi(\underline{k}) \rangle$ proceeds in three steps:

1) The expectation value of the operator is expressed in terms of the permutation operators and the identity $A = A^2$ yields the form amenable to further expansion (2)

$$\langle \mathcal{H} \rangle_{\underline{k}} = \sum_P (-1)^P \langle \Phi(\underline{k}) | \mathcal{H} | P\Phi \rangle .$$

2) Assuming the closed shell electronic configuration, integration of the spin part of the above expression gives the resulting total energy $E(\underline{k})$ in terms of space type integrals

$$E(\underline{k}) = \langle \mathcal{H} \rangle_{\underline{k}} = 2 \sum_{g=1}^{M_k} h_g(\underline{k}) + \sum_{g,s}^{M_k} (2J_{gs}(\underline{k}) - K_{gs}(\underline{k}))$$

3) We now wish to find the best possible orbitals u_μ to form $\Phi(\underline{k})$ (restricted to a single-determinantal form) by minimizing $E(\underline{k})$ under the constraint

$$\langle \Psi_g(\underline{k},\underline{r}_\mu) | \Psi_s(\underline{k},\underline{r}_\nu) \rangle - \delta_{gs} = 0 .$$

To do so, we define the functional F($\underline{k}$) as follows:

$$F(\underline{k}) = E(\underline{k}) - \sum_{g,s}^{M_k} L_{gs}(\underline{k}) \left(\langle \Psi_g(\underline{k},\underline{r}_\mu) | \Psi_s(\underline{k},\underline{r}_v) \rangle - \delta_{gs} \right).$$

We then use variational techniques to find the conditions by which an arbitrarily small variation in the crystal orbital yields a vanishing of the resulting small variation of the functional F($\underline{k}$) or δF=0. We thereby obtain the following set of Hartree-Fock equations which satisfy the above

$$\left[h(\underline{r}_\mu) + \sum_s (2C_s(\underline{k},\underline{r}_\mu) - \mathcal{X}_s(\underline{k},\underline{r}_\mu) \right] \Psi_g(\underline{k},\underline{r}_\mu)$$
$$= \sum_s \Psi_s(\underline{k},\underline{r}_v) \cdot L_{gs}(\underline{k}) \quad . \tag{4}$$

In the three steps above we use the following notation:

$$h_g(\underline{k}) = \langle \Psi_g(\underline{k},\underline{r}_\mu) | -\nabla_\mu^2 - \sum_\gamma 2Z_\gamma / r_{\gamma\mu} | \Psi_g(\underline{k},\underline{r}_\mu) \rangle$$

$$J_{gs}(\underline{k}) = \langle \Psi_g(\underline{k},\underline{r}_\mu) | C_s(\underline{k},\underline{r}_\mu) | \Psi_g(\underline{k},\underline{r}_\mu) \rangle$$

$$K_{gs}(\underline{k}) = \langle \Psi_g(\underline{k},\underline{r}_\mu) | \mathcal{X}_s(\underline{k},\underline{r}_\mu) | \Psi_g(\underline{k},\underline{r}_\mu) \rangle$$

$L_{gs}(\underline{k})$ = the matrix elements of the lagrangian multipliers.

$C_s(\underline{k},\underline{r}_\mu)$ and $\mathcal{X}_s(\underline{k},\underline{r}_\mu)$ are Coulombic and exchange operators respectively. $J_{gs}(\underline{k})$ and $K_{gs}(\underline{k})$ are the corresponding Coulomb and exchange integrals. $C_s(\underline{k},\underline{r}_\mu)$ is defined by its operational meaning on $\Psi_g(\underline{k},\underline{r}_\mu)$:

$$C_s(\underline{k},\underline{r}_\mu)\Psi_g(\underline{k},\underline{r}_\mu) = 2\int d\underline{r}_v \frac{\Psi_s(\underline{k},\underline{r}_v)^* \Psi_s(\underline{k},\underline{r}_v)}{|\underline{r}_\mu - \underline{r}_v|} \Psi_g(\underline{k},\underline{r}_\mu).$$

Likewise $\mathcal{L}_s(\underline{k},\underline{r}_\mu)$ is defined by

$$\mathcal{L}_s(\underline{k},\underline{r}_\mu)\,\Psi_g(\underline{k},\underline{r}_\mu)=2\int d\underline{r}_v\,\Psi_s(\underline{k},\underline{r}_\mu)^*\,\frac{\Psi_s(\underline{k},\underline{r}_\mu)\,\Psi_g(\underline{k},\underline{r}_v)}{|\underline{r}_\mu-\underline{r}_v|}\ .$$

Summing over s, we obtain the total Coulomb and exchange operators $C(\underline{k},\underline{r}_\mu)$ and $\mathcal{X}(\underline{k},\underline{r}_\mu)$:

$$C(\underline{k},\underline{r}_\mu)=\sum_s C_s(\underline{k},\underline{r}_\mu)\ \text{such that}$$

$$C(\underline{k},\underline{r}_\mu)\,\Psi_g(\underline{k},\underline{r}_\mu)=2\int d\underline{r}_v\,\frac{\rho_{\underline{k}}(\underline{r}_v|\underline{r}_v)}{|\underline{r}_\mu-\underline{r}_v|}\,\Psi_g(\underline{k},\underline{r}_\mu)\ .$$

$$\mathcal{X}(\underline{k},\underline{r}_\mu)=\sum_s \mathcal{X}_s(\underline{k},\underline{r}_\mu)\ \text{such that}$$

$$\mathcal{X}(\underline{k},\underline{r}_\mu)\,\Psi_g(\underline{k},\underline{r}_\mu)=2\int d\underline{r}_v\,\frac{\rho_{\underline{k}}(\underline{r}_v|\underline{r}_\mu)}{|\underline{r}_\mu-\underline{r}_v|}\,\Psi_g(\underline{k},\underline{r}_v)\ .$$

$$\rho_{\underline{k}}(\underline{r}_v|\underline{r}_\mu)=\text{Fock-Dirac density matrix}\tag{5}$$
$$=2\sum_{s=1}^{M_{\underline{k}}}\Psi_s(\underline{k},\underline{r}_v)^*\,\Psi_s(\underline{k},\underline{r}_\mu)$$

The one-electron operator on μ or the Fock operator $\mathcal{F}(\underline{k},\underline{r}_\mu)$ is defined in terms of the above operators as

$$\mathcal{F}(\underline{k},\underline{r}_\mu)=h(\underline{r}_\mu)+C(\underline{k},\underline{r}_\mu)-\tfrac{1}{2}\mathcal{X}(\underline{k},\underline{r}_\mu)\ .\tag{6}$$

We now have the mathematical formalism to approach the TBA method in a manner similar to Roothaan's procedure for molecular orbitals in the closed shell electronic config-

uration (3). The latter approach is technically called the ASP-SCF-MO-LCAO method, but SCF-MO-LCAO is the description most often found in literature.

Let us consider the rhenium oxide (cubic) crystal as a model for perovskite transition metal oxides in showing why the Roothaan approach is inadequate for the whole crystal to obtain energy levels. ReO_3 is the molecular unit which is repeated periodically through the crystal because of translational symmetry. The electronic system of ReO_3 without inclusion of translational symmetry is no different than that of an isolated molecule. In order to make ReO_3 part of the crystal and hence to consider the entire crystal as an immense molecule, we must investigate the effects of translational symmetry on the molecular orbital functions. From the discussion in Appendix J, we find that the molecular orbitals upon forming a periodic crystal become crystal orbitals which are explicitly functions of the wave vector in reciprocal space. We will show in the next section how the TBA method encompasses both the Roothaan procedure and translational symmetry.

TBA METHOD

The crystal orbital $\Psi_j(\underline{k}, \underline{r}_\mu)$ is analytically expressed as a linear combination of Bloch sums, $b_{q\alpha}(\underline{k}, \underline{r})$ giving

$$\Psi_j(\underline{k}, \underline{r}_\mu) = \sum_{q\alpha} C_{qj}^{\alpha}(\underline{k}) b_{q\alpha}(\underline{k}, \underline{r}_\mu) \tag{7}$$

where the expansion coefficients are $C_{qj}^{\alpha}(\underline{k})$. The double sum over atomic orbital quantum numbers q and atomic sites α is expressed in condensed form as $q\alpha$.

The Bloch sums $q\alpha$ are expressed in terms of an atom orbital $q\alpha$ by the sum over the p lattice translation vectors. We refer to the discussion of translational symmetry aspects of the TBA problem in Appendix J which gives

$$b_{q\alpha}(\underline{k}, \underline{r}_\mu) = \sum_{p=0}^{G} \exp(i\underline{k} \cdot \underline{R}_p) \cdot \phi_{q\alpha}(\underline{r}_\mu - \underline{\rho}_\alpha - \underline{R}_p). \tag{8}$$

G is the number of unit cells in a microcrystal. The corresponding "ground domain (G)" on the lattice translation vector set is expressed differently (Appendix J) with the choice here being the inequality for j components of $\underline{R}_p$

$$-\frac{(G-1)}{2} \leq (\underline{R}_p)_j \leq \frac{(G-1)}{2} \qquad (j=1,2,3).$$

We shall define $\underline{R}_o$ as the null vector, i.e.

$$(\underline{R}_o)_j = 0 \qquad (j=1,2,3).$$

which locates the q atomic orbital at $\mathcal{P}_\alpha$ in the unit cell.
Figures 1 and 2 show the vector notation on the μ electron
position vectors $\underline{r}_\mu - \mathcal{P}_\alpha$ and $\underline{r} - \mathcal{P}_\alpha$ $-\underline{R}_p$.

By Equation 7, the crystal orbitals, $\Psi_j(\underline{k},\underline{r}_\mu)$ are
expanded in a linear combination of atomic orbitals (LCAO)
to form TBA energy bands (see Table 1 for a comparison of
MO and crystal orbitals). The j th energy band, $E_j(\underline{k})$
is obtained from the Schrodinger equation defined by the
effective one-electron operator $\mathcal{F}(\underline{k},\underline{r}_\mu)$ (Equation 6) on
electron μ in crystal orbital $\Psi_j(\underline{k},\underline{r}_\mu)$ (for the canonical
case discussed below).

$$\mathcal{F}(\underline{k},\underline{r}_\mu)\,\Psi_j(\underline{k},\underline{r}_\mu) = E_j(\underline{k})\;\Psi_j(\underline{k},\underline{r}_\mu). \qquad (9)$$

SCF Iterative Process

We substitute Equation 7 into Equation 4 to obtain a
form amenable to a MO-LCAO-SCF type treatment of tight-
binding energy bands. We begin with the Hartree-Fock
equations:

$$\mathcal{F}(\underline{k},\underline{r}_\mu)\,\Psi_n(\underline{k},\underline{r}_\mu) = \sum_m \Psi_m(\underline{k},\underline{r}_\mu)\,L_{mn}(\underline{k})$$

and finally obtain

$$\mathcal{F}(\underline{k},\underline{r}_\mu)\left\{\sum_{s\beta} b_{s\rho}(\underline{k},\underline{r}_\mu)c_{sn}^\beta(\underline{k})\right\} = \sum_{s\beta}\left\{\sum_m c_{sm}^\beta(\underline{k})L_{mn}(\underline{k})b_{s\beta}(\underline{k},\underline{r}_\mu)\right\}.$$

$$(10)$$

If we multiply Equation 10 by $\Psi_p(\underline{k},\underline{r}_\mu)^*$ and integrate,
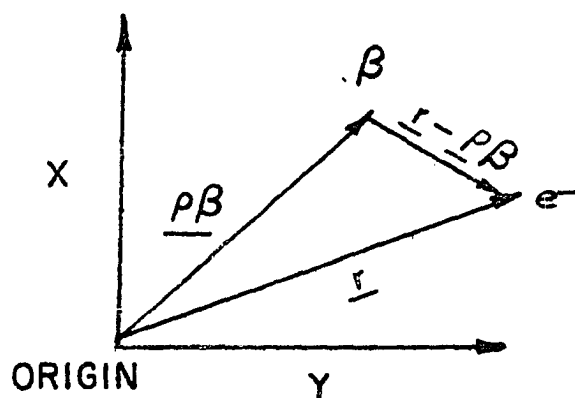
Figure 1. Definition of position vector $\underline{r} - \underline{\rho}_\beta$ of an electron (e^-) with respect to atomic site β.
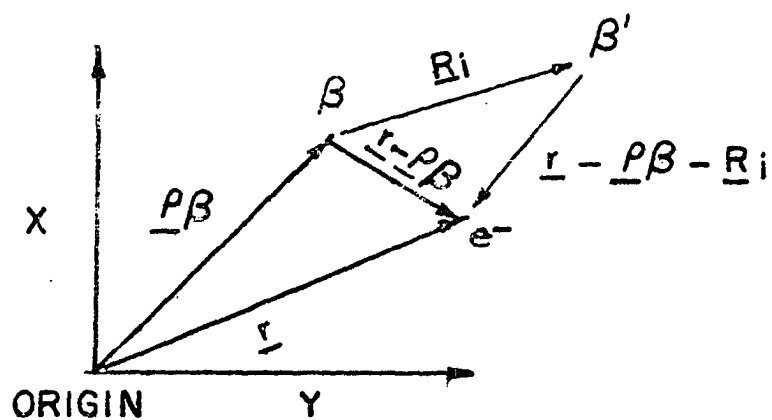
Figure 2. Definition of position vector $\underline{r} - \underline{\rho}_\beta - \underline{R}_i$ after translation $\underline{R}_i$.

Table 1 Comparison of molecular and crystal orbitals

Orbital i	One-electron wave function	Normalization condition	The q th basis set[a]	Linear combination of basis set
MOLECULAR	$\Psi_i(\underline{r})$	$\langle \Psi_i(\underline{r})_\mu \vert \Psi_i(\underline{r})_\mu \rangle = 1$	atomic orbital function $\phi_{q\alpha}$	$\Psi_i(\underline{r}) = \sum_{q\alpha} c_{iq}^{\alpha}(\underline{r})_\mu \phi_{q\alpha}$
CRYSTAL	$\Psi_i(\underline{k},\underline{r})$	$\langle \Psi_i(\underline{k},\underline{r})_\mu \vert \Psi_i(\underline{k},\underline{r})_\mu \rangle = 1$	Bloch sum function $b_{q\alpha}$	$\Psi_i(\underline{k},\underline{r})_\mu =$ $\sum_{q\alpha} c_{iq}^{\alpha}(\underline{k}) b_{q\alpha}(\underline{k},\underline{r})_\mu$

[a]The basis set functions are normalized.

we obtain

$$\sum_{q\alpha} c_{qp}^{\alpha *}(\underline{k})\left\{\sum_{s\beta} \langle b_{q\alpha}(\underline{k},\underline{r}_\mu)| \mathcal{F}(\underline{k},\underline{r}_\mu)| b_{s\beta}(\underline{k},\underline{r}_\mu)\rangle c_{sn}^{\beta}(\underline{k})\right\} =$$

$$\sum_{q\alpha} c_{qp}^{\alpha *}(\underline{k})\sum_{s\beta m}(\sum c_{sm}^{\beta}(\underline{k}) \ L_{mn}(\underline{k}) \ \langle b_{q\alpha}(\underline{k},\underline{r}_\mu)| b_{s\beta}(\underline{k},\underline{r}_\mu)\rangle \quad . \tag{11}$$

.We define the Hamiltonian matrix $H(\underline{k})$ with elements between Bloch sums as

$$H_{q\alpha s\beta}(\underline{k}) = \langle b_{q\alpha}(\underline{k},\underline{r}_\mu)| \mathcal{F}(\underline{k},\underline{r}_\mu)| b_{s\beta}(\underline{k},\underline{r}_\mu)\rangle \tag{12}$$

and an overlap matrix $\underset{\sim}{\Delta}(\underline{k})$ with elements between Bloch sums that are

$$\Delta_{q\alpha s\beta}(\underline{k}) = \langle b_{q\alpha}(\underline{k},\underline{r}_\mu)| b_{s\beta}(\underline{k},\underline{r}_\mu)\rangle \ .$$

Thus, we have the following matrix form:

$$\underset{\sim}{H}(\underline{k}) = \underset{\sim}{b}^\dagger \mathcal{F}(\underline{k}) \ \underset{\sim}{b}$$

$$\text{and } \underset{\sim}{\Delta}(\underline{k}) = \underset{\sim}{b}^\dagger \underset{\sim}{b} \tag{13}$$

with $\underset{\sim}{b} = (b_{1\alpha}....b_{A\alpha}b_{1\beta} ....b_{B\beta} ...b_{1\gamma} ....b_{C\gamma})$ is the Bloch sums matrix ($\underline{k}$ dependence implied) for A,B and C Bloch sums specified for α,β,γ atomic sites.

Furthermore, the coefficient matrix is defined as

$$\underset{\sim}{C}(\underline{k}) = (\underset{\sim}{C}_1(\underline{k}) \ \underset{\sim}{C}_2(\underline{k}) \ ...\underset{\sim}{C}_n(\underline{k}) \ ... \ \underset{\sim}{C}_{M_{\underline{k}}})$$

where the submatrix $\underset{\sim}{C}_n(\underline{k})$ is a column matrix of the expansion coeffients of the nth crystal orbital function into a Bloch sums basis set.

Then, Equation 11 for a particular $q\alpha$ term becomes

$$H_{q\alpha s\beta}(\underline{k}) \; C_{sn}^{\beta}(\underline{k}) = \sum_m L_{mn}(\underline{k}) \sum_{s\beta} \Delta_{q\alpha s\beta}(\underline{k}) \; C_{sm}^{\beta}(\underline{k}) \; .$$

In matrix notation, we obtain

$$\underset{\sim}{H}(\underline{k}) \; \underset{\sim}{C}_n(\underline{k}) \sum_m (\underset{\sim}{\Delta}\underset{\sim}{C}_m(\underline{k}) \;) \; L_{mn}(\underline{k}) \; .$$

If we diagonalize $\underset{\sim}{L}$ by some unitary matrix, the resulting similarity transformation is

$$\underset{\sim}{U}^{\dagger} \underset{\sim}{L} \; \underset{\sim}{U} = \underset{\sim}{E}(\underline{k}) \quad \text{where} \quad (\underset{\sim}{E}(\underline{k}))_{mn} = E_n(\underline{k}) \, \delta_{mn} \; .$$

Thus, we obtain the canonical form of the H-F equations which are now written as

$$\underset{\sim}{H}(\underline{k}) \; \underset{\sim}{C}_n(\underline{k}) = E_n(\underline{k}) \; \underset{\sim}{C}_n(\underline{k}) \underset{\sim}{\Delta}(\underline{k}) \; .$$

From matrix algebra, we know that a non-trivial solution of the coefficient matrix , $\underset{\sim}{C}$, exists if and only if the following determinant vanishes, i.e. we seek a solution of the secular determinant written as

$$\left| \underset{\sim}{H}(\underline{k}) - E(\underline{k}) \underset{\sim}{\Delta}(\underline{k}) \right| = 0 \; . \tag{14}$$

The Fock-Dirac density matrix defined in Equation 5 can be expanded in terms of Bloch sums using Equation 8 to give

$$\underline{P}_{\underline{k}}(\underline{r}_v | \underline{r}_\mu) = 2 \sum_n \Psi_n(\underline{k}, \underline{r}_v)^* \Psi_n(\underline{k}, \underline{r}_\mu)$$

$$= \sum_{q\alpha, s\beta} b_{q\alpha}^*(\underline{k}, \underline{r}_v) b_{s\beta}(\underline{k}, \underline{r}_\mu) \; p_{\underline{k}}(q\alpha, s\beta) \; . \tag{15}$$

The bond order matrix $p_{\underline{k}}(q\alpha, s\beta)$ is defined as

$$p_{\underline{k}}(q\alpha,s\beta) = 2 \sum_{m=1}^{M_{\underline{k}}} C_{qm}^{\alpha*}(\underline{k}) \ C_{sm}^{\beta}(\underline{k}) \ . \tag{16}$$

The bond order matrix can be varied in a SCF process to obtain the best crystal orbitals which lead to a minimum in the total electronic energy $E(\underline{k})$ under the constraint of orthonormality on the crystal orbitals.

Using Equations 6, 12, and 16, the Hamiltonian matrix elements $H_{q\alpha s\beta}(\underline{k})$ can be expressed as

$$H_{q\alpha s\beta} = \langle b_{q\alpha}(\underline{k},\underline{r}_\mu) | h(\underline{r}_\mu) | b_{s\beta}(\underline{k},\underline{r}_\mu) \rangle$$
$$+ \sum_{t\gamma, v\delta} p_{\underline{k}}(t\gamma, v\delta) \cdot$$
$$\left\{ 2\langle b_{t\gamma}(\underline{k},\underline{r}_v) b_{v\delta}(\underline{k},\underline{r}_v) | b_{q\alpha}(\underline{k},\underline{r}_\mu) b_{s\beta}(\underline{k},\underline{r}_\mu) \rangle \right.$$
$$\left. - \langle b_{t\gamma}(\underline{k},\underline{r}_v) b_{q\alpha}(\underline{k},\underline{r}_\mu) | b_{v\delta}(\underline{k},\underline{r}_v) b_{s\beta}(\underline{k},\underline{r}_\mu) \rangle \right\}.$$

The one-electron operator on μ in state $\underline{k}$ becomes

$$\mathcal{F}(\underline{k},\underline{r}_\mu) = -\nabla_\mu^2 - \sum_\tau 2Z_\tau/r + \sum_{t\gamma, v\delta} \hat{p}_{\underline{k}}(t\gamma, v\delta) \cdot$$
$$\left\{ 2\langle b_{t\gamma}(\underline{k},\underline{r}_v) b_{v\delta}(\underline{k},\underline{r}_v) | - \langle b_{t\gamma}(\underline{k},\underline{r}_v) | b_{v\delta}(\underline{k},\underline{r}) \right\} .$$
$$\tag{17}$$

The SCF process which is outlined below is for the canonical case and gives us a means of controlling TBA calculations:

1) Guess $p_{\underline{k}}(t\gamma,v\delta)$ for each $t\gamma,v\delta$ pair.

2) Calculate the Hamiltonian and overlap matrix elements (the latter type are omitted if we start with an orthogonal basis set ; if the basis set is non-ortho-

gonal we have the option of varying parameters in
the analytical form of the atomic wave functions at this
point in the SCF process).

3) Solve the secular determinant in Equation 14 to
yield energies and coefficients for crystal orbitals.

4) Use some type of population analysis to calculate
the new bond order matrix and repeat steps 2-4 until a
self-consistency condition is reached.

In the next section, we shall transform the Fock
operator defined in Equation 17 for a particular $\underline{k}$ vector into
an average Fock operator over all momentum or wave vector
space. The transformation is called the " unitary trans-
formation of the Fock operator".

Unitary Transformation of the Fock Operator

The bond order matrix can only be obtained in step 4 of
the SCF iterative process $\underline{if}$ the Fermi level ($E_{M_{\underline{k}}}(\underline{k}) = E_f$)
is known. But the Fermi level can only be found
as some average quantity over the entire $\underline{k}$ space (further
discussion of the procedure for finding E_f is in Part II).
Thus, the present form of the Fock operator is useless for
our present purposes in the TBA method

However, we can reasonably define an effective Fock
operator which is applicable to all $\underline{k}$ states. The average

of the $\mathcal{F}(\underline{k},\underline{r}_\mu)$ operators on electron μ over the G unit
cells (or $\underline{k}$ vectors) in the microcrystal is

$$\mathcal{F}^{Ave}(\underline{r}_\mu) = \frac{1}{G} \sum_{\underline{k}} \mathcal{F}(\underline{k},\underline{r}_\mu) \qquad (18)$$

Furthermore, Equation 18 can be rewritten

$$\mathcal{F}^{Ave}(\underline{r}_\mu) = \frac{1}{G} \sum_{\underline{k}} \exp(i\underline{k}\cdot\underline{R}_j)\exp(-i\underline{k}\ \underline{R}_j)\mathcal{F}(\underline{k},\underline{r}_\mu) \qquad (19)$$

where $\exp(-i\underline{k}\cdot\underline{R}_j)$ is a phase factor for an arbitrary
translation vector $\underline{R}_j$.

By using Equation 19, we are able to show that the
average of $\mathcal{F}(\underline{k},\underline{r}_\mu)$ over G $\underline{k}$ wave vectors is nothing more
than unitary transformation. Ziman (4) shows how such an
unitary transformation can be used to generate a Wannier
function (function of position only in reciprocal space)
from the corresponding Bloch sum. Since Bloch sums occur
explicitly in the form of $\mathcal{F}(\underline{k},\underline{r}_\mu)$ it, therefore, seems
reasonable to transform the Bloch sums into localized atomic
orbitals if we define Bloch sums by Equation 8.

The unitary transformation of the Fock operator $\mathcal{F}(\underline{k},\underline{r}_\mu)$
is shown in Appendix K. The results are summarized here
for the resulting LCAO form of the Fock operator. Using
arbitrary labels α, β, and γ for atomic sites, we have:

$$\mathcal{F}^{Ave.}(\underline{r}_\mu) = -\nabla_\mu^2 - \sum_\tau 2Z_\tau/r_{\tau\mu} + \sum_{q\alpha, t\beta} \sum p^{Ave.}(q\alpha, t\beta) \cdot$$

$$\sum_{j=0}^{G} \left\{ 2\langle \phi_{q\alpha}(\underline{r}-\underline{P}_\alpha-\underline{R}_j) \; \phi_{t\beta}(\underline{r}-\underline{P}_\beta) \rangle | \right.$$

$$\left. -\langle \phi_{q\alpha}(\underline{r}-\underline{P}_\alpha-\underline{R}_j) | \phi_{t\beta}(\underline{r}-\underline{P}_\beta) \rangle \right\}$$

and $p^{Ave.}(q\alpha, t\beta) = \dfrac{2}{G} \sum_{\underline{k}} \sum_m^M c_{qm}^{\alpha*}(\underline{k}) c_{tm}^{\beta}(\underline{k})$. (20)

What we now have is a Fock operator which is identical in form to that used in molecular orbital calculations, i.e. the LCAO form. The effect of translational symmetry is now contained only in the bond order matrix $p^{Ave}(q\alpha, t\beta)$ just the expansion coefficients of the crystal orbitals.

In summary to this point, we have justifiably transformed the H-F equations for a crystal into the LCAO form in which Roothaan's procedure may be applied to the energy and overlap matrices and the effects of translational symmetry remain only in coefficients which are solutions of the resulting secular determinant. An important point is that the periodicity of the crystal lattice is still preserved since the electron position vectors used in conjuction with the atomic orbitals explicitly show the dependence on the translation vectors.

We now discuss the approximations which will be used in TBA calculations.

Approximations Used in the TBA Method

Population analysis of crystal orbitals

The charge density of the m th crystal orbital is

$$\Psi_m^*(\underline{k},\underline{r}_\mu)\Psi_m(\underline{k},\underline{r}_\mu) = \sum_{p\alpha}\sum_{t\beta} c_{pm}^{\alpha*}(\underline{k})c_{tm}^{\beta}(\underline{k})\, b_{p\alpha}^*(\underline{k},\underline{r}_\mu)b_{t\beta}(\underline{k},\underline{r}_\mu)\, .$$

(21)

The sum over t is over the entire Bloch sum basis set and therefore contains the term $p\alpha$. Integration of Equation 21 gives

$$\langle\Psi_m(\underline{k},\underline{r}_\mu)|\Psi_m(\underline{k},\underline{r}_\mu)\rangle = \sum_{p\alpha}\sum_{t\beta} c_{pm}^{\alpha*}(\underline{k})c_{tm}^{\beta}(\underline{k})\cdot\langle b_{p\alpha}(\underline{k},\underline{r})|b_{t\beta}(\underline{k},\underline{r})\rangle.$$

If the Bloch sums are normalized, i.e. $\langle b_{p\alpha}(\underline{k},\underline{r})| b_{p\alpha}(\underline{k},\underline{r})\rangle$ equals one, the above equation becomes

$$\langle\Psi_m(\underline{k},\underline{r})|\Psi_m(\underline{k},\underline{r}_\mu)\rangle = \sum_{p\alpha}|c_{pm}^{\alpha}(\underline{k})|^2 + \sum_{t\beta\neq p\alpha} c_{pm}^{\alpha*}(\underline{k})c_{tm}^{\beta}(\underline{k})\cdot$$

$$\langle b_{p\alpha}(\underline{k},\underline{r}_\mu)|b_{t\beta}(\underline{k},\underline{r}_\mu)\rangle$$

$$= \sum_{p\alpha} n_{pm}^{\alpha}(\underline{k})$$

(22)

where $n_{pm}^{\alpha}(\underline{k})$ is the occupation number defined by Flodmark to be expressed as

$$n_{pm}^{\alpha}(\underline{k}) = \left(|c_{pm}^{(k)}|^2 + \sum_{t\neq p} c_{pm}^{\alpha*}(\underline{k})c_{tm}^{\beta}(\underline{k})\langle b_{p\alpha}(\underline{k},\underline{r}_\mu)|b_{t\beta}(\underline{k},\underline{r}_\mu)\rangle\right)$$

(23)

If the crystal orbital m is normalized to one, the sum over the occupation numbers is also one; therefore this quantity defined by Flodmark(5) is the fraction of double occupancy

which is attributed to Bloch sum $p\alpha$.

The analogy with Mulliken's population analysis (6) is implied by Flodmark's definition where Bloch sums are used instead of atomic orbitals. However, justification for using such a quantity for population analysis is lacking since the overlap of Bloch sums $p\alpha$ and $t\beta$ is not clear from a geometrical point of view. That is, the Mulliken procedure to divide overlap charge between centers α and β depends on the maximum of the charge distribution being located midway between overlapping centers situated in real space. Since the Bloch sum is a function in complex space, we have no valid way of showing where it overlaps with a Bloch sum on another site in real space unless the exponential terms drop out in the overlap expression.

In real space, we also have problems with the Mulliken population analysis. For instance, diffuse atomic orbitals, eg., $4s$ on K, have a maximum in charge distribution in regions of other atoms such as oxygen in $KTaO_3$. However, workers in molecular orbital calculations of transition metal complexes continue to divide the overlap charge density equally between neighboring atoms. Fenske (7) has analyzed differences in calculated results and concludes that either dividing charge or placing overlap charge on one center gives essentially the same result. If we proceed in the same spirit to Bloch sum charge distributions, the

only problem is to relate the quantity $n_{qm}^{\alpha}(\underline{k})$ to atomic orbitals, i.e., somehow we need to get rid of the phase factor $\exp(i\underline{k}\ \underline{R}_p)$. We attain this end by defining the population of orbitals $q\alpha$, $n_{q\alpha}$, as

$$n_{q\alpha} = \frac{2}{G} \sum_{\underline{k}} \sum_{m}^{M_k} n_{qm}^{\alpha}(\underline{k}).$$ (24)

where $n_{q\alpha}$ equals the number of electrons in orbital q_α and M_k, as defined in Equation 1 is the number of doubly occupied bands. Proceeding in the same manner as we did to perform a unitary transformation of the Fock operator, we identify Equation 24 with an unitary transformation of the occupation number. The essential steps for this transformation are shown in Appendix K giving

$$n_{q_\alpha} = p^{Ave}(q\alpha,q\alpha) + \sum_{t\beta \neq q\alpha} p^{Ave}(q\alpha,t\beta) \sum_{p=1}^{G} \cdot$$

$$\left\langle \phi_q(\underline{r} - \underline{\rho}_\alpha - \underline{R}_p) \middle| \phi_{t\beta}(\underline{r} - \underline{\rho}_\beta) \right\rangle$$ (25)

in terms of bond order matrices, $p^{Ave}(q\alpha,t\beta)$.

Because of the LCAO nature of our TBA approach, particularly in $n_{q\alpha}$ and $A_q^{Ave}(\underline{r}_\mu)$, we shall refer to the population analysis used as the Mulliken type. Even though the occupation numbers reflect the properties of crystal orbitals in complex space if analyzed individually, we may utilize the the density of states vs. Mulliken population analysis to obtain an average distribution of occupation numbers in a particular energy range. Then, the occupation numbers can in a sense be related to real space since the integration over

the distribution of occupation numbers vs. energy up to the Fermi energy gives the population n_q identically as Equation 25.

Richardson's approximation

We will now simplify the TBA Fock operator in a manner identical to that used by Richardson (8) and discussed thoroughly by Fenske (7) and Basch-Gray (9). The essential part of the Richardson approximation is the application of Mulliken's approximation (10) to Coulomb and exchange parts of the Fock operator (molecular). We shall leave the details of the simplification to these three references (7, 8, 9) and only show the results of Appendix A.

$$\overset{Ave}{\mathcal{F}}\cdot(\underline{r}_\mu) = -\frac{2}{\nabla_\mu} + \sum_\gamma \sum_p V_\gamma (\underline{r}_\mu - \mathcal{P}_\gamma - \underline{R}_p) \qquad (26)$$

where V_γ is the potential for atomic site γ located at $\mathcal{P}_\gamma + \underline{R}_p$. Explicitly each potential term is expressed in Fenske's Coulomb, exchange, and nuclear attraction operator notation:

$$V_\gamma(\underline{r}_\mu - \mathcal{P}_\gamma - \underline{R}_p) = \sum_{q\gamma} n_{q\gamma} \left| 2 \langle \phi_{q\gamma}(\underline{r}_\nu - \mathcal{P}_\gamma - \underline{R}_p) \phi_{q\gamma}(\underline{r}_\nu - \mathcal{P}_\gamma - \underline{R}_p) | \right.$$

$$- \langle \phi_{q\gamma}(\underline{r}_\nu - \mathcal{P}_\gamma - \underline{R}_p) | \phi_{q\gamma}(\underline{r}_\nu - \mathcal{P}_\gamma - \underline{R}_p) \rangle \Big\}$$

$$- z_\gamma \langle 1/r_{\gamma\mu} | \qquad . \qquad (27)$$

Crystal potential

Since charge distributions described by crystal orbitals can be directly related to occupation numbers $n_{qm}^\alpha(\underline{k})$ (m th crystal orbital for $q\alpha$ th Bloch sum), the unitary trans-

formation of $n_{qm}^{\alpha}(\underline{k})$ and $\mathcal{F}'(\underline{k},\underline{r}_\mu)$ to eliminate $\underline{k}$ dependence in $n_{q\alpha}$ and $\mathcal{F}^{ve}(\underline{r}_\mu)$ yields the LCAO form. Thus, the resulting linear combination of atomic potentials in Equation 27 can be properly referred to as the "crystal potential," U, i.e.,

$$U \text{ (crystal)} = \sum_\gamma \sum_p V_\gamma (\underline{r}_\mu \mathcal{P}_\gamma - \underline{R}_p) \qquad (28)$$

Variation of the atomic orbital population or Bloch sum occupation number of electrons in energy bands gives the TBA method a handle by which self-consistency of both atomic charge and population can be obtained. The advantage of this potential over a potential in the single-particle model (e.g. a point charge model) is that shielding effects of diffuse charge distributions are included automatically. The exchange interactions which increase with decrease in bond distance are an important factor in these shielding effects.

The self-consistency of the $q\alpha$th atomic orbital population, say for the second iteration, is obtained by the formula

$$n_{q\alpha}^2 \text{ (assumed)} = \frac{\lambda \cdot n_{q\alpha}^0 \text{ (assumed)} + n_{q\alpha}^1 \text{ (calculated)}}{\lambda + 1} \qquad (29)$$

$n_{q\alpha}$(calculated) is obtained using the Mulliken population analysis after eigenvectors of $E(\underline{k})$ vs. $\underline{k}$ and the Fermi energy are determined. The superscripts denote the iteration.

The assumed population values are weighted by a damping constant λ (taken to be +8 in our calculations) to prevent the oscillations of the difference between the calculated and assumed values of $n_{q\alpha}$ from diverging in early

stages of iteration. The condition for self-consistency is obtained when the difference between assumed and calculated occupied Bloch sum charge distributions is less than 1%.

The dependence of the populations on the $\underline{k}$ vector and the location of the Fermi energy poses the ultimate problem in using our method. Since the value of the Fermi energy can only be obtained after a complete $E(\underline{k})$ vs. $\underline{k}$ calculation, we use the same potential for all $\underline{k}$ vectors to obtain self-consistency for the first Brillouin zone.

Mattheiss (11) has recently calculated the band structure of ReO_3 at the symmetry points, Γ, X, M and R, using the augmented-plane-wave (APW) method (12) and has invoked the Slater-Koster (13) interpolation scheme to obtain $E(\underline{k})$ over the remainder of the zone. We find it hard to make an assessment of the relative merits of our method compared to his excellent and experienced approach in which a "muffin tin" potential is adjusted to fit optical spectra (14) and De Haas-Van Alphen results (15). We do feel that our approach might give a better description of the lower valence bands, e.g., the bands involving 2s and 2p states, and will be adequate, for our purposes, in describing states in the neighborhood of the Fermi energy. We mention, in particular, three characteristics of the present approach that we feel are desirable, and are lacking in the APW method:

1)   Self-consistency of charge distribution can be obtained at all points in the Brillouin zone.

2)   The potential in the present method is calculated using no adjustable parameters; Coulomb and exchange effects are included in explicit evaluation of all two-center Coulomb and exchange integrals.

3)   The present method explicitly utilizes a population analysis to relate contributions of individual orbitals to energy bands.

Atomic orbital energy

Let us assume the effective atomic Hamiltonian operator, H_{eff}^{β}, for atom β located at $\underline{P}_{\beta} + \underline{R}_j$

$$H_{eff}^{\beta}(\underline{r}_{\mu} \underline{P}_{\beta} - \underline{R}_j) = - \nabla_{\mu}^2 + V_{\beta}(\underline{r}_{\mu} \underline{P}_{\beta} - \underline{R}_j) \tag{30}$$

has an eigenfunction $\phi(\underline{r}_{\mu} \underline{P}_{\beta} - \underline{R}_j)$ or

$$H_{eff}^{\beta}(\underline{r}_{\mu} \underline{P}_{\beta} - \underline{R}_j)\phi_{q\beta}(\underline{r}_{\mu} \underline{P}_{\beta} - \underline{R}_j) = \epsilon_{q\beta} \phi_{q\beta}(\underline{r}_{\mu} \underline{P}_{\beta} - \underline{R}_j).$$

$\epsilon_{q\beta}$, then, is the orbital energy of an electron, located at $\underline{r}_{\mu} \underline{P}_{\beta} - \underline{R}_j$, which has a set of quantum numbers n_q, ℓ_q and m_q indicated by q. $V_{\beta}(\underline{r}_{\mu} \underline{P}_{\beta} - \underline{R}_j)$ is expressed explicitly in Equation 27 in terms of Coulomb, exchange and nuclear attraction operators.

The evaluation of $\epsilon_{q\beta}$ can be made by either of the following approaches:

1) Use atomic spectra data to obtain what is commonly called the valence state ionization energy (VSIE).

2) Using an analytical expression for the atomic orbital function $\phi_{q\beta}$, one may calculate the orbital energy exactly.

Let us briefly discuss the first approach to explain why we prefer the second.

Atomic spectra data provided by Moore (16) has been the prime source of valence state ionization energies (assumed to equal the negative of the orbital energy) which are used in semi-empirical methods. The difficulties with the semi-empirical method are twofold:

1) One needs to average the energy of multiplets. This can be a difficult process when a large number of states exist for an atom or ion.

2) Atomic spectra may not be available for a particular atom of interest. Cotton and Harris (17) found this to be a problem for rhenium, even though sufficient data is available for platinum.

Therefore, in the present method, we calculate the atomic orbital energy in terms of average values of two-electron interaction integrals $g(q,t)$. Slater (18) uses the "average energy of configuration" method to express $g(q,t)$ as linear combinations of Slater-Condon parameters $F^k(n\ell,n'\ell')$ and $G^k(n\ell,n'\ell')$ (see Table 2).

Using an analytical expression for $\phi_{q\beta}(\underline{r} - \underline{f}_\beta - \underline{R}_j)$, we compute $\epsilon_{q\beta}$ by

$$\epsilon_{q\beta} = \langle \phi_{q\beta}(\underline{r}_\mu - \underline{f}_\beta - \underline{R}_j) \mid -\nabla_\mu^2 - 2Z_\beta/r_{\beta\mu} \mid \phi_{q\beta}(\underline{r}_\mu - \underline{f}_\beta - \underline{R}_j) \rangle$$

$$+ \left[\sum_{t \neq q} n_t g(q,t) \right] + (n_q - 1) g(q,q) \tag{31}$$

where n_q and n_t are the population of atomic orbitals qβ and tβ respectively. $g(q,t)$ is the average electronic interaction of electron μ in orbital qβ with electron γ in orbital tβ. Even though the analytical form of the atomic orbital will be frozen (orbital function parameters kept constant) during the SCF iteration process, our choice of atomic orbital functions will be taken using neutral atoms for the following reasons. Semi-empirical MO calculations for transition metal complexes in recent years (19) have led to near-neutral atoms in the calculated molecule. Recent work by Fenske (7) using a more semi-quantitative method has also led to this result. Furthermore, the philosophy which has prevailed during the history of MO calculations of transition metal complexes is Pauling's (20) "electroneutrality principle." Simply, Pauling suggests that the initial electronic charge distributions on isolated metal and ligand (eg. oxygen) atoms become evenly smeared about the molecule when bonding occurs between metal and ligand orbitals. The result is a neutral atom

constitution in molecules, if we consider the atoms in molecule picture or LCAO. In conclusion, we can effectively use Equation 31 to obtain atomic orbital energies; in other words, we say that the $\phi_{q\beta}$ are eigenfunctions of the above effective Hamiltonian within the given approximations.

The Slater approach is preferred since this method effectively takes an average of energies of the various multiplet states which exist for any atom or ion. This method is presently being utilized by Fenske (7).

The Slater-Condon parameters (21, 22), kinetic energy (22) and nuclear-attraction integrals can be calculated from the analytical radial functions for atomic orbitals. Also, Mann (23) has tabulated most of the necessary integrals and parameters which are computed in the SCF process. However, we will evaluate all one-center integrals from atomic functions (see Appendix F).

Table 2. Two-electron interaction integrals (18) used for perovskite oxide calculations

q	t	$g(q,t)$
ns^a	ns	$F^0(ns,ns)$
ns	np	$F^0(ns,np)-G^1(ns,np)/6$
np	np	$F^0(np,np)-2F^2(np,np)/25$

[a]n stands for the principal quantum number.

Table 2(Cont.)

q	t	g(q,t)
ns	nd	$F^0(ns,nd)-G^2(ns,nd)/10$
np	nd	$F^0(np,nd)-G^1(np,nd)/15-3G^3(np,nd)/70$
nd	nd	$F^0(nd,nd)-2F^2(nd,nd)/63-2F^4(nd,nd)/63$

Approximations used in evaluating energy matrix elements between atomic orbitals

The following notation will be used in this thesis to label vectors which belong to interaction sets. $\underline{\rho}_j^{\beta\alpha}$ is the vector to the j th neighbor of the type α from the atom at $\underline{\rho}^\beta$ (the vector defined from the origin to the lattice point β).

As an illustration of this notation, the vector set for the Re-O_1 interactions would be $\underline{\rho}_1$Re-O_1 and $\underline{\rho}_2$Re-O_1 with coordinates $(a/2,0,0)$ and $(-a/2,0,0)$, respectively. An additional example would be the O_1-O_2 interaction set with four vectors: $\underline{\rho}_j O_1$-O_2 with j=1 to 4 and with coordinates $(-a/2,a/2,0)$, $(a/2,a/2,0)$, $(a/2,-a/2,0)$ and $(-a/2,-a/2,0)$. The choice in labeling the j th vector is purely arbitrary for any interaction set.

The use of frozen analytical expressions for atomic orbital functions (see section on atomic orbital energy) for neutral atoms is assumed throughout the following

approximations to Hamiltonian matrix elements which arise between atomic orbitals. The Pauling electroneutrality principle is used again to justify use of the Hamiltonian operator for electron μ on atom γ (located at $\underline{\rho}_\gamma$).

$$H_{eff}^{\gamma}(\underline{r}_\mu - \underline{\rho}_\gamma) = -\nabla_\mu^2 + V_\gamma(\underline{r}_\mu - \underline{\rho}_\gamma)$$

Therefore, $H_{eff}^{\gamma}(\underline{r}_\mu - \underline{\rho}_\gamma)\phi_q(\underline{r}_\mu - \underline{\rho}_\gamma) = \epsilon_{q\gamma}\phi_{q\gamma}(\underline{r}_\mu - \underline{\rho}_\gamma)$. $\qquad$ (32)

There are two classes of matrix elements for which we desire to approximate by known techniques familiar to molecular orbital calculations of transition metal complexes. Namely,

$$1) \quad \langle \phi_{q\alpha}(\underline{r}_\mu - \underline{\rho}_\alpha - \underline{R}_j) | -\nabla_\mu^2 + V_\beta(\underline{r}_\mu - \underline{\rho}_\beta - \underline{R}_p) | \phi_{s\beta}(\underline{r}_\mu - \underline{\rho}_\beta - \underline{R}_p) \rangle$$

and $\qquad$ (33)

2) the potential integrals which need to be evaluated can be represented generally by integral I

$$I = \langle \phi_{q\alpha}(\underline{r}_\mu - \underline{\rho}_\alpha - \underline{R}_j) | V_\gamma(\underline{r}_\mu - \underline{\rho}_\gamma - \underline{R}_n) | \phi_{s\beta}(\underline{r}_\mu - \underline{\rho}_\beta - \underline{R}_p) \rangle. \qquad (34)$$

The electron position vector notation for the two classes of integrals shall be expressed in terms of the interaction vectors $\underline{\rho}_j^{\beta\alpha}$ defined above. Let us first consider class one and make the necessary vector notational changes. To do so we let $\underline{r}_\mu$ equal $\underline{r}'_\mu - \underline{\rho}_\beta + \underline{R}_p$. Then we express Equation 33 as

$$\langle \phi_{q\alpha}(\underline{r}_\mu - \underline{\rho}_\alpha - \underline{R}_j) | -\nabla_\mu^2 + V_\beta(\underline{r}_\mu - \underline{\rho}_\beta - \underline{R}_p) | \phi_{s\beta}(\underline{r}_\mu - \underline{\rho}_\beta - \underline{R}_p) \rangle =$$

$$\langle \phi_{q\alpha}(\underline{r}'_\mu - \underline{\rho}_\alpha + \underline{\rho}_\beta + \underline{R}_p - \underline{R}_j) | -\nabla_\mu^2 + V_\beta(\underline{r}'_\mu) | \phi_{s\beta}(\underline{r}'_\mu) \rangle .$$

$$(35)$$

We may remove the primes from $\underline{r}'_\mu$ above since it is a dummy index of integration. Then $\underline{P}^{\beta\alpha}_j$ is expressed as

$$\underline{P}^{\beta\alpha}_j = \underline{P}_\alpha - \underline{P}_\beta + \underline{R}_p - \underline{R}_j$$

so that the integral becomes

$$\left\langle \phi_{q\alpha}(\underline{r} - \underline{P}^{\beta\alpha}_j) \left| -\nabla^2_\mu + V_\beta(\underline{r}_\mu) \right| \phi_{s\beta}(\underline{r}_\mu) \right\rangle .$$

The Hamiltonian (effective) operates on function $\phi_{s\beta}(\underline{r}_\mu)$ as in Equation 32, the function is an eigenfunction. Therefore, the eigenvalue $\in_{s\beta}$, a constant, comes out of the integral and leaves the overlap integral to give the following approximation for class one integrals

$$\left\langle \phi_{q\alpha}(\underline{r}_\mu - \underline{P}^{\beta\alpha}_j) \left| -\nabla^2_\mu + V_\beta(\underline{r})_\mu \right| \phi_{s\beta}(\underline{r}_\mu) \right\rangle$$

$$= \in_{s\beta} \left\langle \phi_{q\alpha}(\underline{r} - \underline{P}^{\beta\alpha}_j) \left| \phi_{s\beta}(\underline{r}) \right\rangle . \tag{36}$$

Let us now discuss the three types of I integrals which exist in class two. The substitution of $\underline{r}_\mu = \underline{r}'_\mu + \underline{P}_\beta + \underline{R}_p$ into Equation 34, proceeding as above,we obtain the following form of I which facilitates discussion of the three possiblities, i.e.

$$I = \left\langle \phi_{q\alpha}(\underline{r} - \underline{P}^{\beta\alpha}_j) \left| V_\gamma(\underline{r} - \underline{P}^{\beta\gamma}_p) \right| \phi_{s\beta}(\underline{r}_\mu) \right\rangle . \tag{37}$$

The subscript p in the position vector in the potential term denotes the possibility of different interaction vectors other than the j th type. We may have

1) When $\underline{\rho}_j^{\beta\alpha} = \underline{\rho}_p^{\beta\gamma}$, we have the two-center integral

$$I_1 = \langle \phi_{s\beta\uparrow}(\underline{r}) | V(\underline{r} - \underline{\rho}_j^{\beta\alpha}) | \phi_{q\alpha\uparrow}(\underline{r} - \underline{\rho}_j^{\beta\alpha}) \rangle . \tag{38}$$

Basch and Gray (9) and later Fenske (7) have suggested a convenient way for evaluating this integral:

$$I_1 = \langle \phi_{s\beta\uparrow}(\underline{r}) | -\nabla_\mu^2 + V(\underline{r} - \underline{\rho}_j^{\beta\alpha}) | \phi_{q\alpha\uparrow}(\underline{r} - \underline{\rho}_j^{\beta\alpha}) \rangle$$

$$- \langle \phi_{s\beta}(\underline{r}) | -\nabla_\mu^2 | \phi_{q\alpha\uparrow}(\underline{r} - \underline{\rho}_j^{\beta\alpha}) \rangle . \tag{39}$$

Equation 36 is used again to re-express the first term in I_1 which gives

$$I_1 = \epsilon_{q\alpha} \langle \phi_{s\beta\uparrow}(\underline{r}) | \phi_{q\alpha\uparrow}(\underline{r} - \underline{\rho}_j^{\beta\alpha}) \rangle +$$

$$\langle \phi_{s\beta\uparrow}(\underline{r}) | \nabla_\mu^2 | \phi_{q\alpha\uparrow}(\underline{r} - \underline{\rho}_j^{\beta\alpha}) \rangle . \tag{40}$$

The kinetic integral can be expressed in terms of overlap integrals and evaluated using a method described in Appendix D.

2) When $\underline{\rho}_j^{\beta\alpha} = 0$, one obtains another type of two-center integral, I_2, which involves an analytical expression for the potential $V(\underline{r} - \underline{\rho}_p^{\beta\gamma})$ where

$$I_2 = \langle \phi_{q\alpha\mu}(\underline{r}) | V(\underline{r} - \underline{\rho}_p^{\beta\gamma}) | \phi_{s\beta\gamma}(\underline{r}) \rangle . \tag{41}$$

The evaluation of this type of integral is discussed in Appendix E, eg, nuclear attraction, Coulomb (24), etc., type.

3) Finally, when $\underline{\rho}_j^{\beta\alpha} \neq \underline{\rho}_p^{\beta\gamma}$ one has to deal with three-center potential integrals, I_3, where

$$I_3 = \langle \phi_q(r_{\alpha^-\rho}\ \underline{\rho}_j^{\beta\alpha})\ |V_\gamma(r_{-\mu}\underline{\rho}_p^{\beta\gamma}|\ \phi_{s\beta}(r_{-\mu})\rangle. \tag{42}$$

The Mulliken approximation (10) was used to reduce the three-center integrals to linear combinations of two-center integrals of the type I_2 multiplied by an overlap integral, i.e.,

$$I_3 = \frac{\langle \phi_{q\alpha}(r_{-\rho}\ \underline{\rho}_j^{\beta\alpha})\ |\ \phi_{s\beta}(r_{-\mu})\rangle}{2}$$

$$\cdot \left[\langle \phi_{q\alpha}(r_{-\mu})|\ V_\gamma(r_{-\mu}(\underline{\rho}_p^{\beta\gamma} - \underline{\rho}_j^{\beta\alpha}))|\ \phi_{q\alpha}(r)\rangle \right.$$

$$\left. + \langle \phi_{s\beta}(r_{-\mu})|\ V_\gamma(r_{-\mu}\ \underline{\rho}_p^{\beta\gamma})|\ \phi_{s\beta}(r_{-\mu})\rangle \right]. \tag{43}$$

Encouragement for using the Mulliken approximation (despite its shortcomings for evaluating three-center nuclear attraction integrals) comes from the fact that Flodmark (5) has utilized the Mulliken approximation in his TBA method which is basically very similar to ours. Furthermore, as will be seen in the following chapter, the atomic potential is taken to be a simplified SCF potential via Mulliken's approximation. Thus, it is consistent to use it here. In any case, some estimate should be made for the I_3 integrals which are probably important parameters contributing to band energies.

Formulation of the Secular Determinant Between Bloch Sums

Using Equation 7 to express crystal orbitals as a linear combination of Bloch sums, we obtain the following matrix formulation

$$\Psi_p(\underline{k},\underline{r}_\mu) = \sum_{q\alpha} b_{q\alpha}(\underline{k},\underline{r}_\mu)\, c_{qp}^\alpha(\underline{k}) \tag{44}$$

$$= \underline{b}\, \underline{C}_p$$

where $\underline{C}_p$ is the submatrix of $\underline{C}$ which is represented as a column vector

$$\underline{C}_p = \begin{pmatrix} c_{1p}^\alpha(\underline{k}) \\ \vdots \\ c_{pp}^\alpha(\underline{k}) \end{pmatrix}$$

and $\underline{b}$ is defined in Equation 13 for the Bloch sums on atomic site α. Using the formulism outlined in the section "SCF iterative process" we obtain the secular determinant shown in Equation 13 for matrix elements between Bloch sums. However, there is one important exception : we now use the TBA Fock operator (Equation 20) to obtain energy matrix elements of $\underline{H}(\underline{k})$ instead of the $\underline{k}$ dependent operator $\mathcal{F}(\underline{k},\underline{r}_\mu)$.

The solutions of the secular determinant and the corresponding coefficient matrix is described in Appendix A. The flow chart for the computer calculation is given in Appendix B. Let us now proceed to express the Hamiltonian and overlap matrix elements in terms of matrix elements between atomic orbital functions.

Overlap and Hamiltonian Matrix Elements Between Atomic Orbital Functions

Let $F(\underline{r}_\mu)$ be a general operator on electron μ. When $F(\underline{r}_\mu)=1$ or $F(\underline{r}_\mu)= \overset{Ave}{\mathcal{F}} \cdot (\underline{r}_\mu)$ one has an overlap or Hamiltonian matrix element $\langle b_{q\alpha}(\underline{k},\underline{r}_\mu)| F(\underline{r}_\mu)|b_{s\beta}(\underline{k},\underline{r}_\mu)\rangle$ for Bloch sums $b_{q\alpha}(\underline{k},\underline{r}_\mu)$ and $b_{s\beta}(\underline{k},\underline{r}_\mu)$. Expansion of the matrix element into the corresponding atomic orbitals proceeds by the definition of Bloch sums in Equation 8 which gives the following expression

$$F_{q\alpha s\beta}(\underline{k}) = \langle b_{q\alpha}(\underline{k},\underline{r}_\mu)| F(\underline{r}_\mu)| b_{s\beta}(\underline{k},\underline{r}_\mu)\rangle$$

$$= \sum_{\underline{R}_t} \sum_{\underline{R}_j} \exp(-i\underline{k}\cdot(\underline{R}_t -\underline{R}_j) \cdot N_q^{-\frac{1}{2}} N_s^{-\frac{1}{2}} \cdot$$

$$\cdot \langle \phi_{q\alpha}(\underline{r}-\underline{\rho}_\alpha-\underline{R}_t)| F(\underline{r}_\mu)| \phi_{s\beta}(\underline{r}-\underline{\rho}_\beta-\underline{R}_j)\rangle \tag{45}$$

where the subscripts q and s for the functions ϕ represent different sets of n, ℓ, and m quantum numbers.

Equation 45 can be reduced to a single sum over $\underline{R}_p$ (as shown in Appendix C) giving

$$F_{q\alpha s\beta}(\underline{k}) = G N_q^{-\frac{1}{2}} N_s^{-\frac{1}{2}} \sum_p \exp(-i\underline{k}\cdot\underline{R}_p) \cdot$$

$$\cdot \langle \phi_{q\alpha}(\underline{r}-\underline{\rho}_\alpha\underline{R}_p)| F(\underline{r}_\mu)| \phi_{s\beta}(\underline{r}-\underline{\rho}_\beta)\rangle \tag{46}$$

where $\underline{R}_p$ equals $\underline{R}_t -\underline{R}_j$ and G is the number of unit cells taken in a microcrystal.

If we substitute $\underline{r}_\mu = \underline{r}'_\mu + \underline{f}_\beta$ into Equation 46, $F_{q\alpha s\beta}(\underline{k})$ becomes

$$F_{q\alpha s\beta}(\underline{k}) = GN_q^{-\frac{1}{2}}N_s^{-\frac{1}{2}} \cdot$$

$$\cdot \sum_{p=1}^{G} \exp(-i\underline{k}\cdot\underline{R}_p)\langle\phi_q \; (\underline{r}'_\mu \; \underline{f}_\alpha-\underline{R}_p + \underline{f}_\beta)$$

$$|F(\underline{r}'_\mu + \underline{f}_\beta)|\phi_{s\beta}(\underline{r}_\mu)\rangle. \tag{47}$$

Since $F(\underline{r}_\mu)$ is a general operator which possesses the translational symmetry of the crystal, $F(\underline{r}_\mu)$ equals $F(\underline{r}'+\underline{f}_\beta)$. After dropping the primes (dummy indices of integration) and defining $\underline{R}_p$ as

$$\underline{R}_p = \underline{f}_j^{\beta\alpha} - \underline{f}_1^{\beta\alpha} \;\; (j=1,2,\ldots,\ldots V) \;\; (\text{for } \alpha \neq \beta \text{ and}$$

V vectors in the j th interaction set)

we obtain the form of the matrix element in terms of the j th interaction vector, $\underline{f}_j^{\beta\alpha}$, and $\underline{f}_1^{\beta\alpha}$ (the convention of taking the interaction vector corresponding to j=1 and setting it equal to $\underline{f}_\alpha-\underline{f}_\beta$; this is for $\alpha \neq \beta$). Thus,

$$F_{q\alpha s\beta}(\underline{k}) = G\,N_q^{-\frac{1}{2}}\,N_s^{-\frac{1}{2}} \sum_{j=1}^{V} \exp(-i\underline{k}\cdot(\underline{f}_j^{\beta\alpha} - \underline{f}_1^{\beta\alpha})) \cdot$$

$$\cdot\langle\phi_q \; (\underline{r}_\mu - \underline{f}_j^{\beta\alpha})|F(\underline{r}_\mu)|\phi_{s\beta}(\underline{r}_\mu)\rangle. \tag{48}$$

Equation 48 is simplified by the approximations stated in the previous section for the energy matrix elements and the steps are shown in Appendix L for the cases $q \neq s$, $\alpha \neq \beta$; $q \neq s, \alpha = \beta$; and $q=s, \alpha=\beta$ which occur in the $\underset{\sim}{H}(\underline{k})$. The corresponding overlap matrix elements are discussed first

in Appendix L to establish various additional conventions necessary to simplify some matrix elements (cases $q \neq s, \alpha = \beta$ and $q=s, \alpha = \beta$) computationally into cosine and sin terms resulting from application of Euler's relation ($\exp(i\theta) = \cos(\theta) + i\sin(\theta)$) to the exponential terms in Equation . In addition, the explicit form of the Bloch sum normalization constant $N_{q\alpha}$ is shown in Appendix L to be derived from a formulation of the diagonal overlap integral $\Delta_{q\alpha q\alpha}(\underline{k})$. We, therefore, refer to Appendix L for the essential details and summarize the results here for overlap and Hamiltonian matrix elements between Bloch sums as well as the normalization constant:

1) Matrix elements for $q \neq s$ and $\alpha \neq \beta$

$$\Delta_{q\alpha s\beta}(\underline{k}) = G\ N_{q\alpha}^{-\frac{1}{2}} N_{s\beta}^{-\frac{1}{2}} \sum_{j=1}^{V} \exp(-i\underline{k}\cdot(\underline{\rho}_{j}^{\beta\alpha} - \underline{\rho}_{1}^{\beta\gamma})) \cdot$$

$$\langle \phi_{q\alpha}(\underline{r}_{\mu} - \underline{\rho}_{j}^{\beta\alpha}) | \phi_{s\beta}(\underline{r}_{\mu}) \rangle.$$

$$H_{q\alpha s\beta}(\underline{k}) = G\ N_{q\alpha}^{-\frac{1}{2}} N_{s\beta}^{-\frac{1}{2}} \sum_{j=1}^{V} \exp(-i\underline{k}\cdot(\underline{\rho}_{j}^{\beta\alpha} - \underline{\rho}_{1}^{\beta\alpha})) \cdot$$

$$\Big[\langle \phi_{q\alpha}(\underline{r}_{\mu} - \underline{\rho}_{j}^{\beta\alpha}) | \phi_{s\beta}(\underline{r}_{\mu}) \rangle \epsilon_{q\alpha}$$

$$-\langle \phi_{q\alpha}(\underline{r}_{\mu} - \underline{\rho}_{j}^{\beta\alpha}) | -\nabla_{\mu}^{2} | \phi_{s\beta}(\underline{r}_{\mu}) \rangle$$

$$+\langle \phi_{q\alpha}(\underline{r}_{\mu} - \underline{\rho}_{j}^{\beta\alpha}) | \phi_{s\beta}(\underline{r}_{\mu}) \rangle \cdot$$

$$\sum_{p}' \sum_{\gamma}' \Big\{ \langle \phi_{q\alpha}(\underline{r}_{\mu}) | V_{\gamma}(\underline{r}_{\mu} - (\underline{\rho}_{p}^{\beta\gamma} - \underline{\rho}_{j}^{\beta\alpha})) | \phi_{q\beta}(\underline{r}_{\mu}) \rangle$$

$$+\langle \phi_{s\beta}(\underline{r}_{\mu}) | V_{\gamma}(\underline{r} - \underline{\rho}_{p}^{\alpha\gamma}) | \phi_{s\beta}(\underline{r}_{\mu}) \rangle \Big\} \Big].$$

(49)

2) Matrix elements for $q \neq s$ and $\alpha = \beta$

$$\Delta_{q\alpha s}(\underline{k}) = G\ N_{q\alpha}^{-\frac{1}{2}}N_{s\alpha}^{-\frac{1}{2}} \cdot \left[\underline{SOO} \right.$$

$$+ \left\{ \sum_{j=1,2}^{V} \exp(-\underline{k}\cdot\underline{\rho}_j^{\alpha\alpha}) + (-1)^{\ell_q+\ell_s}\exp(-\underline{k}\cdot\underline{\rho}_{j+1}^{\alpha\alpha}) \right.$$

$$\left. \left. \cdot\ S(\underline{\rho}_j^{\alpha\alpha})\right\}\right]$$

$$H_{q\alpha s\alpha}(\underline{k}) = G\ N_{q\alpha}^{-\frac{1}{2}}N_{s\alpha}^{-\frac{1}{2}} \left[\left\{\underline{SOO}\cdot\in_{s\alpha} + \underline{VOO}\right\}\right.$$

$$+ \left\{\sum_{j=1,2}^{V} \exp(-\underline{k}\cdot\underline{\rho}_j^{\alpha\alpha}) + (-1)^{\ell_q+\ell_s}\exp(-\underline{k}\cdot\underline{\rho}_{j+1}^{\alpha\alpha})\right\} \cdot$$

$$\cdot\ S(\underline{\rho}_j^{\alpha\alpha})\left\{\in_{s\alpha} + \langle\phi_{q\alpha}(\underline{r}_\mu)|\ V_\gamma(\underline{r}_\mu - (\underline{\rho}_p^{\alpha\gamma} - \underline{\rho}_j^{\alpha\alpha})|\phi_{q\alpha}(\underline{r}_\mu)\rangle\right.$$

$$\left.\left. + \langle\phi_{s\alpha}(\underline{r}_\mu)|\ V_\gamma(\underline{r}_\mu - \underline{\rho}_p^{\alpha\gamma})|\phi_{s\alpha}(\underline{r}_\mu)\rangle\right\}\right] \tag{50}$$

where groups of integrals indicated by $S(\underline{\rho}_j^{\alpha\alpha})$, $\underline{SOO}$ and

$\underline{VOO}$ which are expanded as

$$\underline{VOO} = \sum_p'' \sum_\gamma'' \langle\phi_{q\alpha}(\underline{r}_\mu)|\ V_\gamma(\underline{r}_\mu - \underline{\rho}_p^{\alpha\alpha})|\phi_{s\alpha}(\underline{r}_\mu)\rangle$$

$$\underline{SOO} = \langle\phi_{q\alpha}(\underline{r}_\mu)|\phi_{s\alpha}(\underline{r}_\mu)\rangle$$

$$S(\underline{\rho}_j^{\alpha\alpha}) = \langle\phi_{q\alpha}(\underline{r}_\mu - \underline{\rho}_j^{\alpha\alpha})|\phi_{s\alpha}(\underline{r}_\mu)\rangle.$$

The convention taken in the Equations above is the translation vectors are grouped for

$$\underline{\rho}_{j+1}^{\alpha\alpha} = -\underline{\rho}_j^{\alpha\alpha}$$

in order to express the exponential terms into cosine and

sin terms by

$$\left[\exp(-i\underline{k}\cdot\underline{\rho}_j^{\alpha\alpha}) + (-1)^{\ell_q+\ell_s}\exp(-i\underline{k}\cdot\underline{\rho}_{j+1}^{\alpha\alpha})\right] = 2\cos(\underline{k}\cdot\underline{\rho}_j^{\alpha\alpha})$$

for an even sum $\ell_q + \ell_s$ and is $+1 \cdot 2 \cdot \sin(\underline{k} \cdot \underline{\rho}_j^{\alpha\alpha'})$ for an odd sum $\ell_q + \ell_s$.

3) Matrix elements for q=s and $\alpha = \beta$

The diagonal elements of $\overset{\Delta}{}$ and H are conveniently obtained from the form stated for (q≠s and $\alpha = \beta$) ; therefore, the cosine expression of exponential terms results since $\ell_q + \ell_s$ would always be even for q=s. The requirement that the Bloch sums be normalized to unity yields the expression of the normalization constant which for the qα case would be

$$N_{q\alpha} = G \left[1 + 2 \sum_{j=1,2}^{V} \cos(\underline{k} \cdot \underline{\rho}_j^{\alpha\alpha}) \, S(\underline{\ell}_j^{\alpha\alpha}) \right].$$ (51)

The evaluation of the above matrix elements is therefore reduced by a series of approximations using exact diatomic integrals: overlap and related integrals (kinetic energy), Coulomb, exchange and nuclear attraction type. In addition, the exact evaluation of one-center integrals have been discussed in the section "Atomic Orbital Energy" under the approximations of the TBA method. Further discussion of these diatomic integrals are in Appendices D (overlap and related integrals) and E (potential integrals).

The word "exact" deserves some discussion at this point in the thesis. The analytical expression for the atomic wave functions (the subject of the next section) is approximate; but methods are available to solve diatomic

integrals rapidly and efficiently using available numerical techniques programed into Fortran IV language and the IBM 360-65 model computer. Then , we properly refer to the latter as exact within the usual round-off errors encounted in machine computations. In order to minimize such errors, we use double precision numbers in overlap, Coulomb, exchange and nuclear attraction programs to give an accuracy of something like 10^{-6} Hartree energy units (27.2 e.v.).

The choice of atomic orbital functions in the TBA method is the crux of how exactly our calculated energy bands and crystal orbital properties correspond to reality. In our realm of theoretical investigations, the H-F crystal equations provide the indicator of how well we are approaching exactness. Hopefully, such an indicetor approximates as well the experimental phenomenon . In other words, we must approach the H-F limit in order to make the TBA amenable to the present state of the art of the quantum chemisty of diatomic molecules; thereby the correlation problem of crystals can become tractible. The approximations that we have strived to make in a justifiable manner would be useless if we unwisely used atomic orbital functions.

In the discussion of the atomic orbital energy, we have suggested that the choice of neutral atomic wave functions may be justified using the Pauling electro-

neutrality principle. Let us approach the atomic wave function problem from this a priori notion, i.e. neutral atoms in a crystal, and consider how the available tables of the numerical SCF functions for neutral atoms may be used to obtain analytical functions which have the proper radial and nodal behavior .

ATOMIC WAVE FUNCTIONS

The atomic wave function, ϕ_q, is taken as a product of the radial function $R_{n\ell}(\underline{r})$ and spherical harmonics function $Y_{\ell m}(\theta, \phi)$ or

$$\phi_q = R_{n\ell}(\underline{r})Y_{\ell m}(\theta, \phi). \tag{52}$$

The type of radial function used in the TBA calculations was of the Slater orbital type (STO), i.e.,

$$R_{n\ell}(\underline{r}) = Nr^{n-1}\exp(-\zeta r) \tag{53}$$

where ζ is the orbital exponent and N is the normalization constant.

The radial function may be of the single orbital exponent type shown above or a linear combination of STO's, i.e.,

$$R_{n\ell}(\underline{r}) = \sum_i C_i N_i r_i^{n-1}\exp(-\zeta_i \cdot r)$$

$$\text{where } N_i = \frac{(2\zeta_i)^{n+\frac{1}{2}}}{(2n_i!)^{\frac{1}{2}}} \tag{54}$$

There are many ways of choosing a basis set. If a single orbital exponent STO is desired, the ζ parameter may be adjusted so that the radial function matches the numerical values of SCF functions in the tail-off region, as Gerstein et al. (1) have done. Brown and Fitzpatrick (25), who have

investigated radial functions of all transition metal series, would call this type of fit to the outer region of the SCF radial function a Burns' type orbital (26). They refer to the Clementi type orbital (27) as one that better describes the inner region of SCF radial functions (particularly in the region of the maximum peak). Since both types of orbitals are STO's differing only in a choice of ζ , neither one will show radial nodes. Nevertheless, Brown and Fitzpatrick (25) find that both types of orbitals can be used in overlap integral calculations and give sufficiently accurate values for cases involving first-row transition metals. The Richardson (28) linear combination of STO's fits Watson's SCF functions (29) for the titanium 3d, 4s and 4p orbitals at varying charge better than single exponent STO's. In the case of 4s and 4p titanium orbitals, only Richardson orbitals will properly describe the respective Bloch sums, since SCF radial function values remain negative in the region of interest in TBA calculations and no single STO function can describe this behavior.

Brown and Fitzpatrick have further concluded that Basch and Gray 5d, 6s and 6p functions (30) (which are linear combinations of STO's) are necessary for tantalum, tungsten and rhenium cases where overlap integrals using them are calculated. They compared Burn's orbitals with the Basch-Gray functions and found that the use of functions fitted to the outer regions of tungsten 5d orbitals produce overlap

integral values which are too large. The arguments in favor of using 6s and 6p functions to accurately describe behavior in the overlap region are the same for titanium 4s and 4p orbitals.

Ruedenberg (private communication, Ames, Iowa, 1969) has suggested that higher quantum number radial functions can be fitted with lower n STO's to represent the radial behavior correctly in evaluating two-center Coulomb and exchange integrals for which the available programs go to n=3. The extrema of the SCF function to be fitted are produced by the coefficients of the linear combination of STO's (always nodeless functions by themselves). The coefficients and orbital exponents can be found by a least squares fit procedure (31).

The atomic radial functions which form an orthogonal basis set are generally obtained in the present work by the following recipe:

1) For s and p orbitals we start with single STO's with the same l quantum numbers and Schmidt orthogonalize to form the valence shell functions which are orthogonalized linear combinations of STO's (as in Equation 54). For 5d orbitals, we use the orthonormal Basch-Gray functions which are linear combinations of 3d, 4d and 5d STO's.

2) If the n quantum number of the valence shell is greater than 3, the least squares fit of n=3 STO's is made to the Schmidt orthogonalized radial function.

The main problem in the above procedure is obtaining the single STO's necessary for the s and p functions in the first step. Besides providing numerical values for SCF functions, Mann (23) tabulates the location of the maximum in the radial function, r_{max}. If one differentiates the radial function with respect to r, the radial distance, and equates the expression to zero, the tabulated maximum distance can be related to the orbital exponent of a single STO:

$$\frac{\partial P_{n\ell}}{\partial r}\Bigg)_\zeta = \frac{\partial}{\partial r}\Bigg)_\zeta \left[R_{n\ell} \cdot r\right] = \frac{\partial}{\partial r}\Bigg)_\zeta (N \exp(-\zeta r)r^n) = 0$$

$$= N\, n \exp(-\zeta r)r_{max}^{n-1} - N\zeta \exp(-\zeta r)r_{max}^n = 0$$

where $r = r_{max}$

Thus, $\zeta = \dfrac{n}{r_{max}}$.

(55)

Therefore, the necessary orbital exponents can be obtained.

The np orbitals for Na(n=3), K(n=4) and Sr(n=5) are not given in the ground state configuration by Mann; thus, one needs to approximate the ζ_{np} for the single STO representation. If one takes the ratio of ζ_{6p}/ζ_{6s} (2.372/2.398) from Basch-Gray single STO representation for Re (charge = +1) and multiplies it by the neutral atom ns(n= 3,4,5,6) orbital exponent, one can obtain the single STO representation for neutral atoms.

The Schmidt orthogonalization procedure for the 1s, 2s and 3s single STO basis set provides an example of obtaining a 3s atomic orbital function, say for Na . Let the non-orthogonal STO's be represented by a row vector $\underset{\sim}{v}$:

$$\underset{\sim}{v} = (v_1\ v_2\ v_3) = (1s\ 2s\ 3s) \tag{56}$$

The v_i functions exist in Hilbert space and have a set of inner products $\langle v_i | v_k \rangle$ which are represented by an overlap matrix $\underset{\sim}{S}$. Therefore, we seek the similarity transformation $\underset{\sim}{T}^\dagger \underset{\sim}{S} \underset{\sim}{T} = \underset{\sim}{I}$ which maps $\underset{\sim}{v}$ into $\underset{\sim}{u}$ (a column vector of orthogonal functions). The transpose of $\underset{\sim}{u}$ is related to $\underset{\sim}{v}$ by the upper triangular matrix $\underset{\sim}{T}$: $\underset{\sim}{u}^t = \underset{\sim}{v}\ \underset{\sim}{T}$ or

$$\begin{pmatrix} u_1 \\ u_2 \\ u_3 \end{pmatrix}^t = \begin{pmatrix} 1s' \\ 2s' \\ 3s' \end{pmatrix}^t = (1s\ 2s\ 3s) \begin{pmatrix} T_{11} & T_{12} & T_{13} \\ & T_{22} & T_{23} \\ 0 & & T_{33} \end{pmatrix} \tag{57}$$

where the primes denote orthogonal functions, i.e. $\langle u_j | u_k \rangle = \delta_{jk}$ (normalization is generally imposed as well). The matrix $\underset{\sim}{T}$ can be separated into a set of three column vectors which are identified with the expansion coefficients of the v_i bases into orthogonal functions, i.e.

$$u_j = \sum_i T_{ij}\ v_i \quad j=1,2,3 \text{ equations are obtained from}$$

the coefficients

$$\left.\begin{matrix} T_{11} & T_{12} & T_{13} \\ & T_{22} & T_{23} \\ & & T_{33} \end{matrix}\right\} \quad \text{giving}$$

$$u_1 \equiv 1s' = T_{11}(1s)$$

$$u_2 \equiv 2s' = T_{12}(1s) + T_{22}(2s)$$

$$u_3 \equiv 3s' = T_{13}(1s) + T_{23}(2s) + T_{33}(3s) \qquad (58)$$

As mentioned above, the d STO basis set for 5d functions $(v_1 = 3d, v_2 = 4d, v_3 = 5d)$ is chosen from Basch-Gray (30). The double zeta representation used by Basch-Gray for $v_3 = 5d$ is necessary to properly describe the outer 5d radial behavior. Even though we cannot apply the simple formula in Equation 55 for this case, we could in principle do so and continue through step two above for $u_1 = 3d$ and $u_2 = 4d$ using Mann's data for r_{max}. However, the respective ζ_{3d} and ζ_{4d} values are close for neutral (Mann) and +1 cases (Basch-Gray) and, therefore, to remain consistent, we use the entire Basch-Gray $v_i(i=1,3)$ basis set for third-row transition metals.

We justify the use of the Basch-Gray 5d functions for the neutral atom using Gianturco's (32) investigation of the size of the d orbital of vanadium as a function of oxidation state. The primary result of this study was that the 3d wave function varies slowly with charge in removing 4s electrons from the $3d^3 4s^2$ configuration, and finally the removal of d electrons from the $3d^3$ configuration shows a small change, even though it is greater than in the former case. It is reasonable to assume that the behavior of the third-row transition metals is similar to the first-row transition metals; therefore, it

would be useful to show that the Basch-Gray 5d functions for configuration $5d^4 6s^1 6p^1 (Re^{+1})$ differ little from the neutral atom $(5d^5 6s^2)$ numerical radial functions provided by Mann.

A plot of Basch-Gray vs. Mann functions is shown in Figure 3. The Basch-Gray values vary from the Mann values at the extrema, but generally fit the SCF function over a wide range of radial distance: 3.5 to 8.0 a.u.

Once we have a set of u_j functions, we may apply any least squares fit program to obtain a new set of functions F_j which have a new basis f_k, or

$$F_j = \sum_k c_{jk} f_k (\zeta_k) \qquad (59)$$

F_j is related to u_j (quantum numbers n', ℓ', m') by the minimization of the deviation, D (31):

$$D = \sum_p (u_j(r_p) - F_j(r_p))^2 r_p \qquad (60)$$

over a mesh of radial values r_p. The necessary constraints for this minimization are

$$\frac{\partial D}{\partial c_{jk}} = 0 \qquad \frac{\partial D}{\partial \zeta_k} = 0. \qquad (61)$$

Each f_k function with orbital exponent ζ_k has quantum numbers $n=3$, ℓ', m'.

For example, a 6s function, u_6, is fitted by a function F_6 which is a linear combination of six 3s STO's:
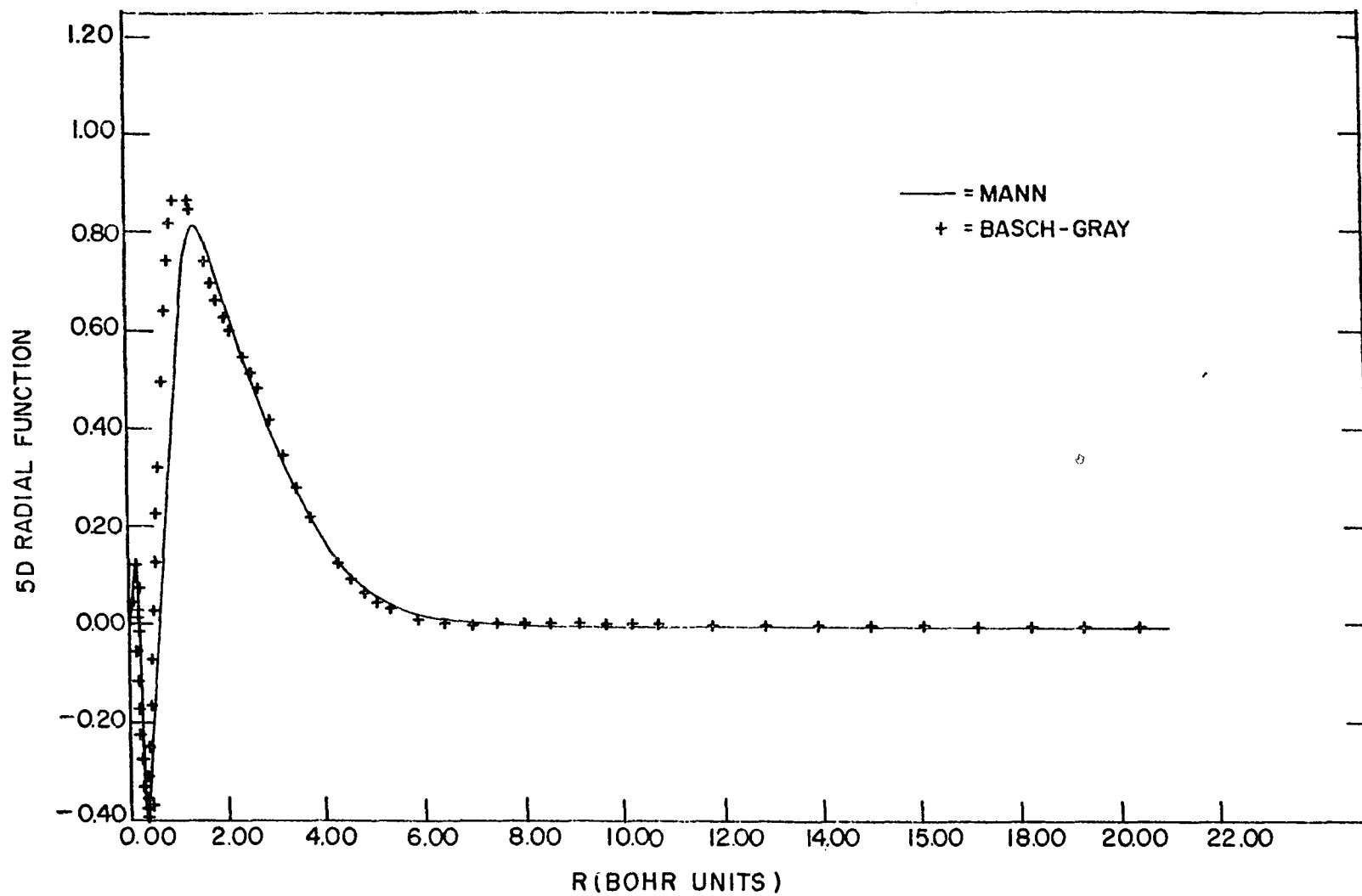
Figure 3. P(5d) vs. R.

$$F_6 = c_{61} \; 3s(\zeta_1) + c_{62} \; 3s(\zeta_2) + c_{63} \; 3s(\zeta_3)$$

$$+ \; c_{64} \; 3s(\zeta_4) + c_{65} \; 3s(\zeta_5) + c_{66} \; 3s(\zeta_6) \qquad (62)$$

Thus, as a matter of convenience, each F_j is expanded into the same number of bases as the corresponding u_j functions, eg. the upper k limits on F_j = 5d, 6s and 6p least squares fit functions is 4, 6, and 5 respectively.

OVERLAP EFFECTS, MADELUNG EFFECTS AND THE OVERLAP CRITERION

In 1952, Wolfsberg and Helmholz (33) suggested a semi-empirical method based on two approximations:

1) Diagonal energy matrix elements are approximated as the negative of the valence state ionization energy (VSIE) of a particular orbital q, i.e.

$$H_{qq} = - \text{VSIE}$$

2) Off-diagonal energy matrix elements are calculated by the expression

$$H_{pq} = \frac{\Delta}{2} pq \left\{ H_{pp} + H_{qq} \right\} .$$

Richardson (8) points out that such approximations, as crude as they are, incorporate many aspects of chemical intuition, eg., overlap of bonding orbitals and electro-negativity. Furthermore, Jørgenson (34) analyzes the semi-empirical approach in terms of the physical nature of the chemical bond. He concludes that diagonal energy matrix elements are dominated by the Madelung potential, i.e., Madelung effects, and off-diagonal energy matrix elements vary as two-center kinetic energy effects. Ruedenberg (35) relates the lowering of two-center kinetic energy, due to interference effects (changes in atomic orbitals upon bonding), to be the crucial phenomenon which gives stability to molecules after potential energy is cancelled by nuclear-nuclear repulsions.

In this theoretical investigation, we are interested in applying chemical concepts to an amalgamation of quantum chemistry and solid state physics, i.e., the TBA. However, we are still unable to determine stabilities of crystals or cohesive energy for many reasons. For example, two reasons which we feel are important are:

1) The magnitude of the correlation energy is unknown.

2) The Madelung potential cannot be evaluated exactly in terms of Coulomb, exchange and nuclear attraction integrals (computationally very laborous, even for a computer).

In other words, the crystal is a giant molecule; even with the inclusion of translational symmetry, the multi-center integral bottleneck exists for a large number of sometimes difficult integrals (eg. three-center Coulomb integrals). Even though three and even four-center integrals are tractable now on the computer, the task to do a rigorous calculation would be both costly and unreasonable.

We propose a semi-rigorous method which will be based on three objectives:

1) To study a series of related crystals to observe possible trends and, thereby, propose some theoretical model. No computations will be attempted on an absolute energy scale.

2) To apply a SCF-MO-LCAO treatment to crystals in order to use a theoretical handle instead of an empirical one to control calculation of energy bands.

3) To use the LCAO procedure when conditions are satisfied by some well defined and pertinent criterion. We suggest that the "overlap criterion" (1) is a reasonable way for choosing a TBA interaction model.

Besides chemical intuition, the overlap criterion is based directly on many important mathematical relations which are explicitly expressed in terms of overlap integrals. Here are three quantities which depend directly on overlap and occur throughout the TBA formulism:

1) The expression for $H_{q\alpha}$ s_{β} $(\underline{k})$ in Equation 49 is essentially a function of overlap and two-center kinetic energy integrals (can be expressed as a linear combination of overlap integrals).

2) The normalization constant for the Bloch sums is a function of overlap integrals (Equation 51). Evaluation of this quantity is possible so long as the overlap is adequately small. Otherwise, the cosine terms by becoming negative when $(\frac{\pi}{2} \leqslant \underline{k} \cdot \underline{f}_j^{\alpha\alpha} \leqslant \pi)$ causes the value of $N_{q\alpha}$ to become negative. Since an imaginary value for $N_{q\alpha}^{\frac{1}{2}}$ could result, the TBA is limited by overlap.

3) Because of quantity number 2, the TBA Fock operator is only possible if the identity approximately exists: $N_{q\alpha}^{-\frac{1}{2}} N_{q\alpha}^{-\frac{1}{2}} \cdot G = 1$ (see Appendix K).

If the off-diagonal energy matrix elements are related to bonding of atomic orbitals, we may suggest that differences between energy levels for molecular orbitals (isolated molecule) or crystal orbitals (solid state) are determined to a large extent by overlap effects.

Let us now consider the Madelung potential and its effect on the TBA. Ros and Schuit (36) and Basch and Gray (9) have placed much importance on shielding effects on the point charge model for doing molecular orbital calculations of transition metal complexes.

The lack of explicit evaluation of Coulomb and exchange integrals, the latter particularly, leads to deficiencies in the point charge model, eg. suggested by Fenske (7). The ordering of molecular orbitals is critically affected by the shielding effects. Since exchange integrals converge exponentially to zero, we suggest that the similar behavior of overlap integrals points to the possibility that the "important" effects of the Madelung potential are only within bonding distances, i.e., where overlap is maximum.

In principle, we continue to include more neighboring atoms in the Madelung potential, oscillating as it may with each additional neighboring atom, until convergence occurs. Finally, we obtain an external potential (excluding nearest neighbor effects) which acts equally upon the metal

atom or the ligand (assuming the Pauling electroneutrality principle is valid). Thus, the whole molecular orbital correlation diagram is shifted on some arbitrary energy scale. The analogous energy band behavior has the same result, if we trust that the TBA model resembles the molecular orbital situation within the overlap criterion.

In points 2) and 3) we show additional evidence that the overlap criterion has quantitative consequences in the TBA. Particularly, the third point exemplifies the connection of the overlap criterion to a choice of the TBA interaction model. That is, the one-electron operator $\mathcal{F}^{Ave}(r_\mu)$ converges to the molecular case in the limit

$$\frac{G}{N_{q_\alpha}^{\frac{1}{2}} N_{s_\beta}^{\frac{1}{2}}} = 1$$

In the present TBA method we calculate the overlap integrals for various overlap pairs which are involved with possible bonding orbitals . Then the overlap criterion is applied to notice from tabulated overlap integrals if any values are exceptionally large. If such values occur, we go to the quantitative aspect of the overlap criterion and see how the normalization constant of Bloch sums are affected. At this junction we decide whether a TBA type calculation is reasonable and proceed accordingly to find a series of substances which apply.

Use of the Overlap Criterion to Choose a TBA Model

In order to make TBA calculations practical, the Bloch sums must be limited to a small set of interacting neighbors. The overlap criterion mentioned above is used to choose a TBA model which can be applied to transition-metal oxides. In Table 3, various overlap pairs in the ReO_3 structure are listed to indicate that overlap is adequately small in the nearest-neighbor metal-oxygen interactions and next-nearest-neighbor metal-metal interactions to limit the size of the interaction set to these atoms.

Table 3. Overlap Integrals

a	b	S_{AB}	R(a.u.)	θ_B	ϕ_B
$5d_z{}^2$	$5d_z{}^2$	.008460	7.0818	90	0
		.027642	7.0818	0	0
$5d_{xz}$	$5d_{xz}$	-.014323	7.0818	90	0
		.002067	7.0818	90	90
$5d_{x^2-y^2}$	$5d_{x^2-y^2}$	.021248	7.0818	90	0
		.002067	7.0818	0	0
$6s$	$6s$	.000000	7.0818	90	0
$6p_z$	$6p_z$	.077021	7.0818	90	0
$5d_z{}^2$	$2s$	-.102873	3.5409	90	0
		.205746	3.5409	0	0
$5d_z{}^2$	$2p_z$	.143401	3.5409	180	0
$5d_{xz}$	$2p_x$	.096507	3.5409	0	0
$5d_{x^2-y^2}$	$2s$	.178181	3.5409	90	0

Table 3(Cont.)

a	b	S_{AB}	R(a.u.)	θ_B	ϕ_B
$5d_{x^2-y^2}$	$2p_x$	.124189	3.5409	90	180
6s	2s	.275805	3.5409	90	0
$6p_z$	2s	.427884	3.5409	0	0
$6p_z$	$2p_z$	.115660	3.5409	90	0
2s	2s	.006946	5.0076	90	45
$2p_x$	2s	.005662	5.0076	90	45
$2p_z$	$2p_z$	.001119	5.0076	90	45

In Table 1, S_{AB} is the overlap integral between orbitals a and b. θ_B and ϕ_B are the polar angles of the location of center B with respect to center A as the origin. The radial distances R are obtained by geometrical considerations using the lattice constant (37) of 7.0810 a.u.. These integral values represent the true atomic overlap orbital after proper rotation of spherical harmonics from the elliptical coordinate system through the given polar angles. The overlap integral values listed are part of the TBA output.

The TBA interaction model for rhenium trioxide is shown in Figure 4. Re, O_1, O_2, and O_3 are the four atoms which make up the unit cell and a is the lattice constant. The primed oxygen atoms belong to other unit cells but make up a part of the nearest-neighbor rhenium-oxygen interaction set.
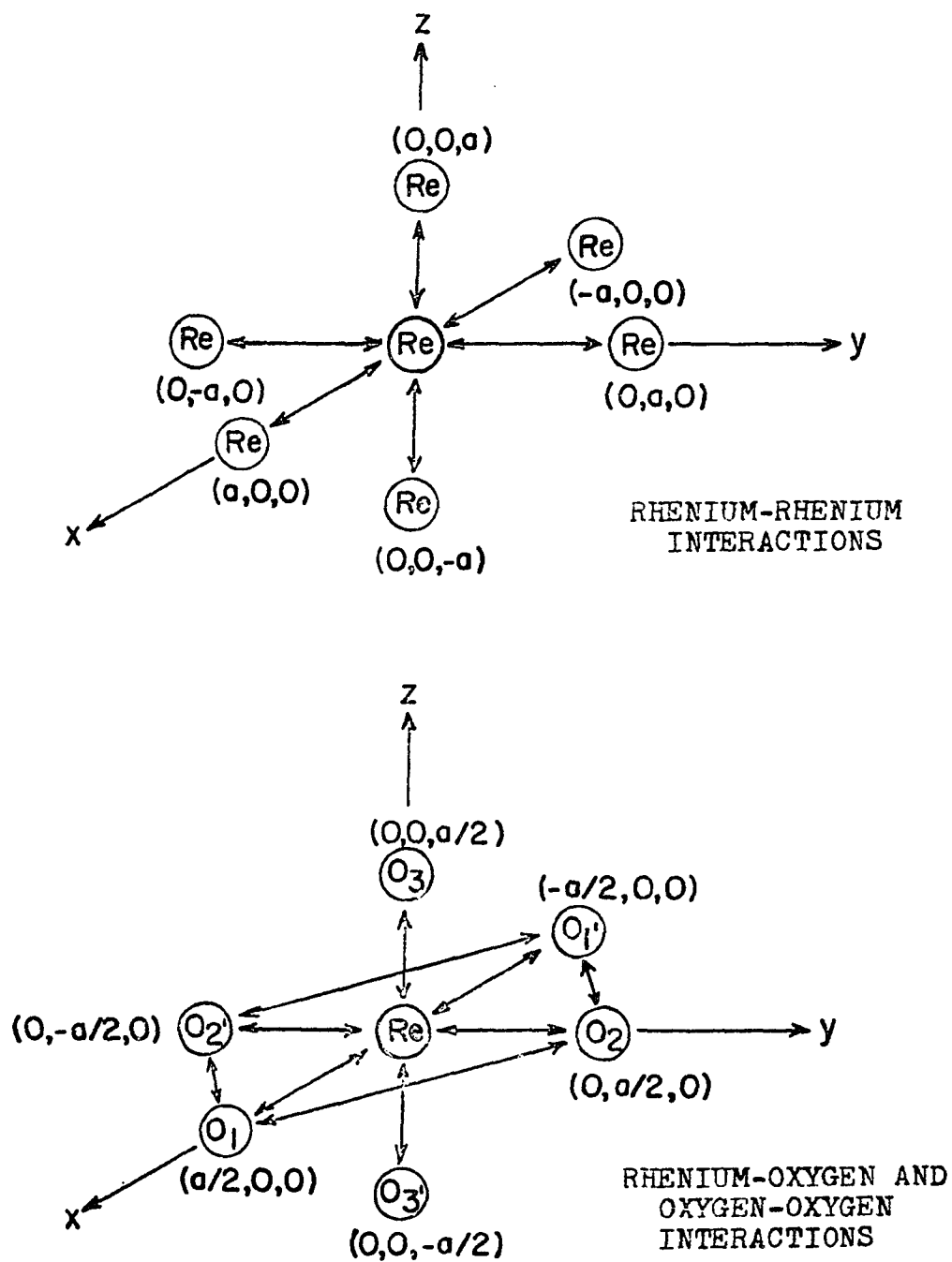
Figure 4. TBA interaction model.

The next-nearest-neighbor rhenium atoms are located at positions $(\pm a,0,0)$, $(0,\pm a,0)$ and $(0,0,\pm a)$.

In general, the crystal lattice of perovskite transition metal oxides contain the structure ABO_3 shown in Figure 5. A is a transition metal and B is either vacant as far as ReO_3 or filled by a non-transition metal such as alkali metals Na and K. B is commonly referred to as the perovskite hole in the transition metal oxide crystal lattice. In the recent paper on the overlap criterion (1), Na-Na overlap in tungsten bronzes was conveniently shown by considering sodium as filling the perovskite hole. However, for our purposes, the octahedral arrangement of oxygen atoms about a particular transition metal (as it was for ReO_3 in Figure 3) and the B atom located at the corner of the unit cell is taken as the model for TBA interactions.

From our discussions of overlap and Madelung effects, we can propose a model for the interaction set of perovskite oxides in general. Even though sodium-sodium interactions have been postulated to be important in describing the conduction band picture of sodium tungsten bronzes (38), overriding evidence exists, both theoretically (39, 40, 41) and experimentally (14, 42) that transition-metal and oxygen valence orbitals are the important contributors to the lowest conduction band. Since Na-Na 3s and 3p overlap has been found to be strong (1), one must seek a possible

explanation other than overlap effects to explain this dilemma. We propose that Madelung effects push sodium energy bands out of the conduction picture into high energy regions. The nearest-neighbor Madelung effects between sodium atoms are then considered to be unimportant compared to nearest-neighbor interactions between sodium and other types of atoms in the lattice. Thus, the important effect of orbital overlap and potential interactions between alkali metals (eg. Na and K) and transition-metal or oxygen atoms in the same unit cell makes the TBA model complete for nearest-neighbor interactions.

The inclusion of metal-metal (A-A) interactions tests the model (39) which proposes that t_{2g} d states mainly make up the lowest conduction band. The model (39, 40), which proposes that π bonded oxygen and transition metal d states are more important, is of course tested by the nearest-neighbor aspect of the TBA method.

We will now apply the above TBA method to the series of perovskite transition metal oxides: ReO_3, Na_xWO_3 (for our present calculations we will take x to be 1.0) and $KTaO_3$. Rhenium trioxide will be discussed first (Part II) since it is the simplest of the three to treat in the TBA. In order to obtain meaningful results (Part III) for sodium tungsten bronze and potassium tantalate ($KTaO_3$), we will scale their crystal potentials and charge distributions to

● — RHENIUM

◯ — OXYGEN
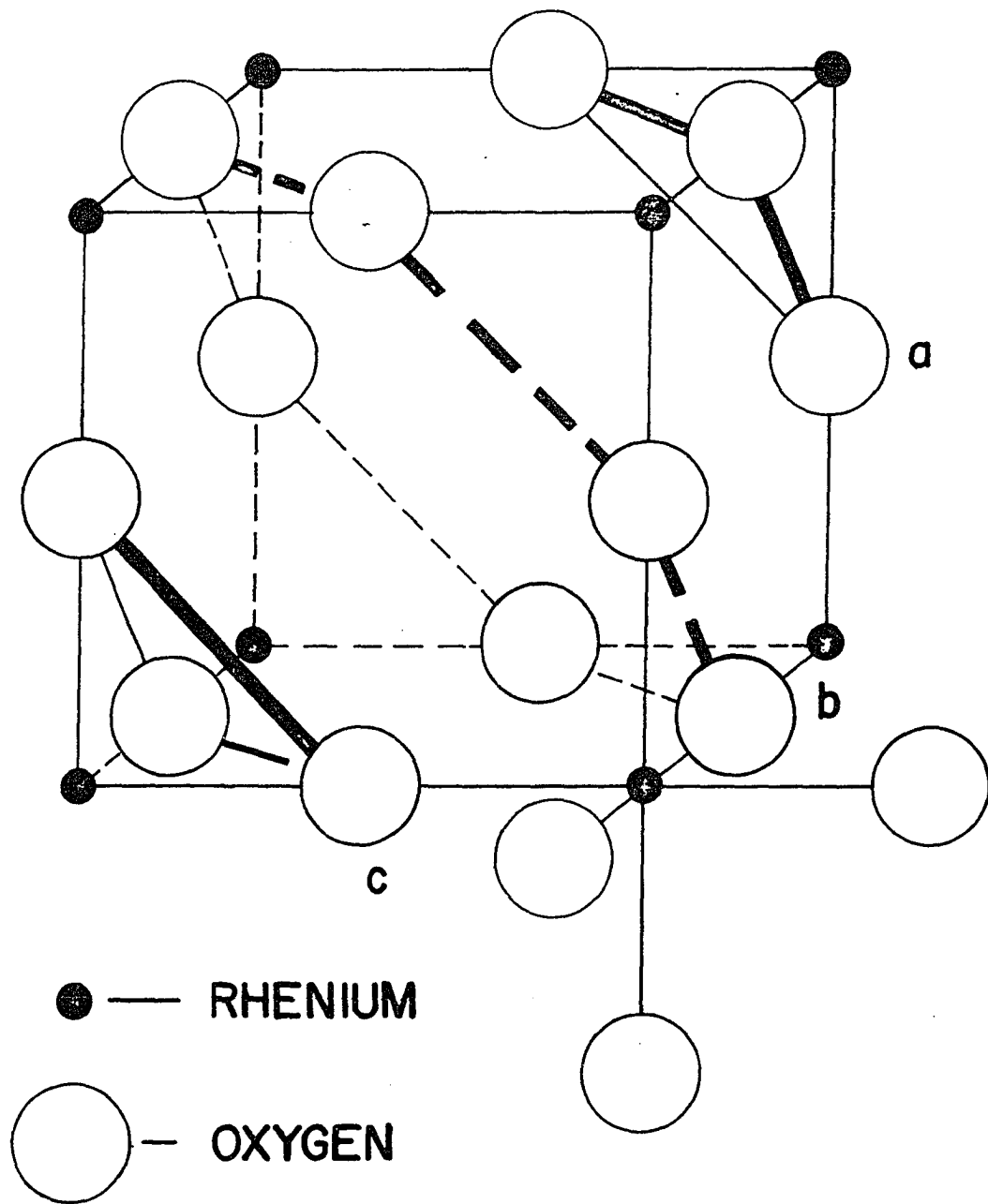
ReO$_3$ STRUCTURE

Figure 5. Perovskite crystal lattice.

the ReO_3 model. Hopefully, we then can obtain a theoretical model of perovskite transition metal oxides which gives a realistic picture of crystal orbitals in the LCAO limit; thereby we hope to delineate the nature of the admixture of atomic orbitals which form conduction and valence bands as a function of the wave vector.

SUMMARY

The LCAO procedure is to be used to obtain the crystal potential and energy bands for transition metal oxides. The option to obtain self-consistency of charge distribution throughout all $E(\underline{k})$ vs. $\underline{k}$ allows one to approach the accurate APW potential proposed by Mattheiss. The use of the Bloch sum basis set allows one to exactly determine the participation of atomic orbitals in various symmetry crystal orbitals or bands. The effects of translational symmetry on the traditional LCAO-MO picture can, therefore, be determined despite knowledge of the inherent weaknesses which exist for the tight-binding method. By using the overlap criterion, one can decide which oxides can be considered to be adequately described.

Thus, one imposes all the rigor which is practically possible for the LCAO-MO procedure in evaluating two-center overlap and potential integrals and approximating other multi-center integral values. Also, one uses good atomic orbital functions (descriptive of both inner and outer properties).

As in the molecular case, we seek interpretation of molecular properties (including translational symmetry) in terms of atomic properties, e.g., potential, orbital energy, and orbital functions.

PART II. TIGHT-BINDING ENERGY BANDS

OF RHENIUM TRIOXIDE

INTRODUCTION

Recently, L. F. Mattheiss (11) has reported an APW calculation of the energy bands and Fermi surface of ReO_3. His is the first effort to theoretically describe quantitatively the electronic structure of ReO_3 and provide a model for the perovskite transition metal oxides. He parameterizes the crystal potential via the Slater-Koster (13) tight-binding interpolation scheme between symmetry points. This provides a handle for empirically controlling his calculations. The results of his semi-empirical approach are not in disagreement with present experimental data (14, 15). The tight-binding method proposed in Part I has been applied to ReO_3 to obtain an entirely different theoretical model of ReO_3, but agreement with the same experimental data appears to be comparable for the two approaches.

Rhenium trioxide and the perovskite transition metal oxides provide a group of substances which form a borderline between a strictly APW (free electron) and a strictly tight-binding (localized electron) application. From Table 3, we see, using an overlap criterion, that the TBA might provide a reasonable picture of the band structure of ReO_3. As a matter of fact, Mattheiss has had to modify the APW potential or Muffin Tin potential to make the APW method applicable. The question of which method is better cannot really be answered since entirely different crystal potentials are used.

Even though the APW method can accurately be corrected
for ReO_3, the problem of obtaining self-consistency and
quantitative information concerning the distribution of
atomic orbital contributions to crystal orbitals which form
valence and conduction bands remains. The TBA method
described in this thesis solves this problem by utilizing
the Mulliken population analysis (6) of the Bloch sums
basis set.

Since Bloch sums are directly related to atomic orbitals
by Equation 8, we have for the first time obtained a
theoretical handle, instead of an empirical handle, to
control band calculations. Even though we require an em-
pirical quantity, the lattice constant, to do calculations
at present (a minimization of energy with respect to bond
length is not practical), we are completely independent of
empirical parameters in the crystal potential. Our potential
is based upon the Fock operator used in making LCAO-SCF-MO
calculations for closed-shell systems. Thus, charge dis-
tributions which are assumed before the first cycle of the
TBA calculation are calculated at the end of that cycle by
the Mulliken population analysis. The calculated charge dis-
tribution is essentially put into cycle two (properly weighted
by a damping constant) and so forth. Thus, when the oscilla-
tions of assumed and calculated charge distributions for each
atomic orbital become sufficiently small, we are confident

that the TBA energy bands have converged enough to give us useful quantitative information.

Because of its nature, the TBA method invoked in this thesis may be called a semi-rigorous[a] molecular orbital calculation which includes the effects of translational symmetry on the electronic structure.

Obviously, we cannot obtain the exact solution of the Schrödinger equation of electrons in a solid, but because of the Born-von Kármán periodic boundary (43), the Born-Oppenheimer approximation (44) and the unique nature of the loosely-packed structure of ReO_3, we may use a Bloch sum basis set and solve the eigenvalue problem of the electronic structure in a solid variationally using a linear combination of atomic potentials as the crystal potential. But even at this point, we cannot proceed in an ab initio manner. Instead, we proceed to make systematic approximations as Ruedenberg (39) has stressed we must do, and continue to do so until the calculation is both theoretically founded and practical. The multi-center integral problem has plagued progress of the TBA approach to solids previously. Even though we still are unable to evaluate three-center integrals practically, we resort to the Mulliken approximation (10). The evaluation of all necessary two-center Coulomb, exchange, nuclear attraction,

---

[a]A work suggested by Kaufmann (45) and considered by the author elsewhere (46).

overlap and kinetic energy integrals makes our method at least a good first order attempt to describe the electronic structure of a group of substances, namely the perovskite transition metal oxides. It is important to stress that we evaluate off-diagonal elements in the Hamiltonian matrix as explicitly as possible and do not resort to any semi-empirical approximations such as the Wolfsberg-Helmholz (33) or extended Hückel approximations (47). For the above reasons, we use the description semi-rigorous when referring to the present TBA method.

We will now discuss the calculation of TBA energy bands of ReO_3 in two steps:

1) The input data which consists of the crystal potential, orbital energies and orbital functions.

2) The output data which consists of $E(\underline{k})$ vs. $\underline{k}$, the density of states, particularly at the Fermi energy, the results of the Mulliken population analysis, the correlation of the joint density of states with the imaginary part of the dielectric constant, and the Fermi surface.

THE CRYSTAL POTENTIAL

We have calculated all Coulomb, C, exchange, X, and nuclear attraction integrals necessary for the crystal potential (see "Atomic Potential", Chapter I) in the TBA interaction model for ReO_3, eg., Re-Re, Re-O_1, O_1-O_2, etc., interactions. The "crystal potential", which is a linear combination of atomic potentials, (Equation 28) is thereby calculated by evaluating matrix elements of the classes shown in Equations 33 and 34. Only the type in Equation 41 needs to be expanded into C, X, and nuclear attraction integrals

The charge distributions of crystal orbitals $|\Psi_i(\underline{k},\underline{r})|^2$ (i = occupied orbitals) are divided by the Mulliken population analysis (6) to give Bloch sum (in reciprocal space) or atomic orbital (in real space) populations n_q for the q bases. The self-consistency procedure outlined in Part I is applied to ReO_3.

Since we wish to use the ReO_3 structure to parameterize a series of oxides, the obvious place to start is the crystal potential.

An additional calculation of C, X, and nuclear attraction integrals to be used in the crystal potential for $NaWO_3$ and $KTaO_3$ was performed using the ReO_3 structure (Re, O_1, O_2, O_3 orbitals for the same lattice constant) with Na and K atomic orbitals situated at the (111) corner positions, i.e. in the

perovskite positions of a hypothetical perovskite oxide
$AReO_3$ (A=Na or K). We scale these results for the $NaWO_3$ and
$KTaO_3$ cases using the following procedure:

1) Using a set of C, X, and nuclear attraction integrals,
$\langle a\,a|b\,b'\rangle$, $\langle a\,b|a\,b'\rangle$ and $\langle 1/r_A|b\,b'\rangle$ respectively (defined
in Equation 60 with b not necessarily = to b') we calculate
a scaling factor, S, as follows:

$$S_{\substack{ReO_3\\model}} = \left\{ \langle a\,a|b\,b'\rangle_{AReO_3} -\tfrac{1}{2}\langle a\,b|a\,b'\rangle_{AReO_3} \right\} / \langle 1/r_A|b\,b'\rangle_{AReO_3} . \qquad (60)$$

2) Using the respective lattice constants of $KTaO_3$ and
$Na_xWO_3(x=1.0)$ to obtain the appropriate interatomic distances,
we calculate all nuclear attraction integrals

$$\langle 1/r_A|b\,b'\rangle_{KTaO_3 \text{ or } NaWO_3} .$$

3) We calculate $[C-\tfrac{1}{2}X]_{KTaO_3 \text{ or } NaWO_3}$ used in the crystal
potential (Equation 28) by

$$[C-\tfrac{1}{2}X]_{\substack{KTaO_3\\or\\NaWO_3}} = S_{\substack{ReO_3\\model}} \cdot \langle 1/r_A|b\,b'\rangle_{\substack{KTaO_3\\or\\NaWO_3}} \qquad (61)$$

for each a, b and b' set.

4) Using $[C-\tfrac{1}{2}X]_{KTaO_3 \text{ or } NaWO_3}$ values, we calculate all
matrix elements of the type $\langle b|V_A|b'\rangle$.

Justification for this scaling procedure stems from
Fenske's "point charge approximation" (7.) which for $\langle b|V_A|b'\rangle$

is $\langle b|V_A|b'\rangle \approx \sum_a 2n_a \langle 1/r_A|b\ b'\rangle -Z_A \langle 1/r_A|b\ b'\rangle$ or in other

words $\langle 1/r_A|b\ b'\rangle \approx C-\frac{1}{2}X$.

The scaling factor S calculated for set a, b, and b'
in step 1 above is introduced into Equation 61 by

$$\langle b|V_A|b'\rangle = \left(\sum_a 2n_a \cdot S -Z_A\right)\langle 1/r_A|b\ b'\rangle \qquad (62)$$

to give a general expression for point charge approximations
(Fenske's is for S = 1).

A $1/R_{AB}$ behavior is exhibited by Coulomb integrals at
sufficiently large interatomic distances R_{AB}, e.g. at R_{AB} from
center B, the charge distribution a$*$a on center A appears as
a point charge to center B. The exchange integral, however,
which behaves like an overlap integral $\langle a|b\rangle$, diminishes
exponentially with increase in R_{AB}. Hence, the point charge
approximation is good for first-row transition metal 3d
orbitals, i.e. a=3d gives S=0.99 (8_l).

If a=4s or 4p for first-row transition metals, we would
expect that the point charge approximation would not be
reasonable. The 4s and 4p orbitals have such a large $\langle r\rangle$
that for usual R_{AB} distances encountered in transition metal
oxides (3-4 a.u.), the diffuse a$*$a charge distribution still
has a finite value, eg. for Ti (23) $\langle r_{3d}\rangle= 1.487$ a.u. but
$\langle r_{4s}\rangle= 3.766$ a.u. The situation for rhenium is about the
same for titanium: $\langle r_{5d}\rangle= 1.800$ and $\langle r_{6s}\rangle= 3.694$ for
$R_{Re-O} = 3.5$ a.u.

Therefore, we introduce the parameter S into our calculations for two main reasons:

1) We facilitate the evaluation of $C-\frac{1}{2}X$ integral values by the fast and easy calculation of nuclear attraction integrals (Appendix E).

2) We quantitatively measure the shielding effects of diffuse charge distributions in showing why the simple point charge approximation is of no value to TBA calculations of perovskite transition metal oxides.

The result of the above analysis is shown in Table 4 using nuclear attraction integrals listed in Table 5.

We thereby avoid the extensive evaluation of Coulomb and exchange integrals each time, but also construct a crystal potential which is directly related to the ReO_3 model. As trends become obvious, we may calculate Coulomb and exchange integrals more accurately if desired as the TBA method is improved (evaluation of three-center integrals explicitly). Until then, our semi-rigorous method will be kept at the present level of approximation.

Table 4. Coulomb-exchange integrals and shielding parameters for perovskite transition metal oxides

Atomic orbitals[a]				C[b]	X[c]	$C-X/2$[d]	S[e]
i	j	k	l				
520	520	520	520	0.157796	0.000492	0.147225	0.980167
521	521	520	520	0.155405	0.000032	0.145206	0.966725
522	522	520	520	0.151178	0.000002	0.141270	0.940521
600	600	520	520	0.150008	0.001513	0.143033	0.952258
610	610	520	520	0.164212	0.003853	0.156877	1.044430
611	611	520	520	0.140568	0.000074	0.135848	0.904423
200	200	520	520	0.302454	0.030307	0.287300	1.009110
210	210	520	520	0.317908	0.024608	0.305604	1.073400
211	211	520	520	0.295973	0.004515	0.293715	1.031560
300	300	520	520	0.168116	0.003352	0.160795	0.718775
310	310	520	520	0.195724	0.008270	0.185090	0.827377
311	311	520	520	0.154021	0.000207	0.148696	0.664646
400	400	520	520	0.162177	0.002548	0.155445	0.694860
410	410	520	520	0.195055	0.006899	0.185106	0.827448
411	411	520	520	0.144611	0.000190	0.139614	0.624093

[a]The atomic orbitals i, j, k, and l which have quantum numbers n, ℓ, and m are indicated by the integer nℓm. The i and j orbitals are located on atom A and the k and l orbitals are located on atom B.

[b]The value of the Coulomb integral in atomic units of 27.2 e.v. are indicated by C. Electron 1 is in the orbitals i and j and electron 2 is in orbitals k and l.

[c]The value of the corresponding exchange integral is indicated by X and is in atomic units of 27.2 e.v.

[d]The value of the difference is corrected for the renormalization of 5d and 6s orbitals where necessary.

[e]The shielding parameter is indicated by S. It is evaluated by the following expression:

$$S = (C-X/2) / \left\langle \frac{1}{r_A} \Big| kl \right\rangle$$

Table 4(Cont.)

Atomic orbitals							
i	j	k	l	C	X	C-X/2	S
520	520	521	521	0.155405	0.000032	0.145206	0.979560
521	521	521	521	0.153452	0.000077	0.143359	0.967100
522	522	521	521	0.149478	0.000002	0.139681	0.942288
600	600	521	521	0.148305	0.000306	0.141980	0.957797
610	610	521	521	0.161381	0.000779	0.155627	1.049860
611	611	521	521	0.139752	0.000334	0.134934	0.910265
200	200	521	521	0.283718	0.002058	0.282689	1.083700
210	210	521	521	0.294120	0.001893	0.293173	1.123880
211	211	521	521	0.279989	0.005414	0.277282	1.062970
300	300	521	521	0.166610	0.001891	0.160144	0.715865
310	310	521	521	0.193123	0.004589	0.184469	0.836697
311	311	521	521	0.153731	0.001830	0.147724	0.670032
400	400	521	521	0.161516	0.002380	0.154986	0.702970
410	410	521	521	0.193911	0.006038	0.184531	0.836978
411	411	521	521	0.145001	0.001953	0.139225	0.631483
520	520	522	522	0.151178	0.000002	0.141270	0.977904
521	521	522	522	0.149478	0.000002	0.139681	0.966905
522	522	522	522	0.146040	0.000001	0.136468	0.944664
600	600	522	522	0.144715	0.000046	0.138655	0.959803
610	610	522	522	0.156117	0.000123	0.150855	1.044250
611	611	522	522	0.136795	0.000014	0.132230	0.915327
200	200	522	522	0.244397	0.000037	0.244378	1.024930
210	210	522	522	0.253269	0.000029	0.253254	1.062160
211	211	522	522	0.239959	0.000032	0.239943	1.006330
300	300	522	522	0.162769	0.000795	0.156961	0.729712
310	310	522	522	0.187294	0.002088	0.180044	0.837025
311	311	522	522	0.150326	0.000230	0.145206	0.675063
400	400	522	522	0.159128	0.001415	0.153238	0.712404
410	410	522	522	0.190297	0.003757	0.182140	0.846769
411	411	522	522	0.142617	0.000391	0.137675	0.640051

Table 4(Cont.)

Atomic orbitals							
$\underline{i}$	$\underline{j}$	$\underline{k}$	$\underline{l}$	C	X	C-X/2	S
520	520	520	600	0.006442	0.000083	0.006056	0.810935
521	521	520	600	0.005900	0.000002	0.005581	0.747330
522	522	520	600	0.005174	0.000000	0.004896	0.655604
600	600	520	600	0.005090	-0.001536	0.005685	0.761256
610	610	520	600	0.007292	-0.006265	0.010206	1.366580
611	611	520	600	0.003858	-0.000198	0.003874	0.518752
200	200	520	600	0.028791	-0.002830	0.030206	0.403997
210	210	520	600	0.030923	0.000000	0.030923	0.413587
211	211	520	600	0.028911	0.000000	0.028911	0.386670
300	300	520	600	0.004827	-0.000206	0.004103	0.409289
310	310	520	600	0.006681	-0.000129	0.005614	0.559965
311	311	520	600	0.003807	-0.000008	0.003171	0.316319
400	400	520	600	0.002754	-0.002333	0.003263	0.315859
410	410	520	600	0.003563	-0.003404	0.004382	0.424194
411	411	520	600	0.002163	-0.000170	0.001872	0.181092
520	520	600	600	0.150008	0.001513	0.143033	1.134460
521	521	600	600	0.148305	0.000306	0.141980	1.126110
522	522	600	600	0.144715	0.000046	0.138664	1.099810
600	600	600	600	0.142534	0.010168	0.135089	1.071450
610	610	600	600	0.153122	0.020046	0.141865	1.125200
611	611	600	600	0.134951	0.000921	0.132438	1.050430
200	200	600	600	0.257590	0.046575	0.234302	0.828300
210	210	600	600	0.260103	0.014386	0.252910	0.894082
211	211	600	600	0.257748	0.009476	0.253010	0.894436
300	300	600	600	0.156238	0.031179	0.139435	0.971801
310	310	600	600	0.173393	0.057084	0.143602	1.000840
311	311	600	600	0.147367	0.003679	0.144272	1.005510
400	400	600	600	0.149951	0.042908	0.127389	0.887846
410	410	600	600	0.169898	0.077311	0.130110	0.906810
411	411	600	600	0.138887	0.004384	0.135516	0.944487

Table 4(Cont.)

Atomic orbitals							
i	j	k	l	C	X	C-X/2	S
520	520	520	610	0.017103	0.000126	0.015655	3.824680
521	521	520	610	0.016178	0.000003	0.014861	3.630700
522	522	520	610	0.014837	0.000000	0.013632	3.330440
600	600	520	610	0.014625	-0.002370	0.015410	3.764830
610	610	520	610	0.018665	-0.006265	0.021431	5.235750
611	611	520	610	0.012294	-0.000310	0.012240	2.990310
200	200	520	610	0.057395	-0.004946	0.059868	0.786713
210	210	520	610	0.060451	0.000000	0.060451	0.794368
211	211	520	610	0.057836	0.000000	0.057836	0.760011
300	300	520	610	0.015239	-0.000361	0.015162	1.467910
310	310	520	610	0.006681	-0.000129	0.005614	1.829370
311	311	520	610	0.003806	-0.000008	0.003171	1.290160
400	400	520	610	0.011678	-0.003691	0.013298	1.326530
410	410	520	610	0.014045	-0.005606	0.016566	1.652520
411	411	520	610	0.010131	-0.000275	0.010097	1.007220
520	520	600	610	0.041916	0.000345	0.038839	1.703470
521	521	600	610	0.040436	0.000088	0.037582	1.648360
522	522	600	610	0.037771	0.000018	0.035135	1.541010
600	600	600	610	0.037026	-0.005150	0.039089	1.714450
610	610	600	610	0.044702	-0.014077	0.051517	2.259550
611	611	600	610	0.032449	-0.000959	0.032786	1.438000
200	200	600	610	0.110093	-0.006283	0.113235	0.889485
210	210	600	610	0.111291	0.000000	0.111291	0.874214
211	211	600	610	0.111854	0.000000	0.111854	0.878637
300	300	600	610	0.039407	-0.001287	0.039754	0.689140
310	310	600	610	0.046695	-0.000686	0.046689	0.808355
311	311	600	610	0.035417	-0.000052	0.035181	0.609100
400	400	600	610	0.031926	-0.015806	0.039534	0.684475
410	410	600	610	0.036706	-0.019612	0.046168	0.799325
411	411	600	610	0.028722	-0.001265	0.029137	0.500447

Table 4(Cont.)

Atomic orbitals				C	X	C-X/2	S
i	j	k	l				
520	520	610	610	0.164212	0.003853	0.156877	1.169900
521	521	610	610	0.161381	0.000779	0.155627	1.160580
522	522	610	610	0.156117	0.000123	0.150855	1.124990
600	600	610	610	0.153122	0.020046	0.141865	1.057950
610	610	610	610	0.168031	0.047714	0.144174	1.075170
611	611	610	610	0.129780	0.000014	0.129773	0.967776
200	200	610	610	0.313108	0.120665	0.252775	0.755407
210	210	610	610	0.317081	0.034146	0.300008	0.896561
211	211	610	610	0.315077	0.024790	0.302682	0.904552
300	300	610	610	0.165389	0.037250	0.146764	0.689023
310	310	610	610	0.185154	0.061839	0.154234	0.724093
311	311	610	610	0.155008	0.005051	0.152482	0.715821
400	400	610	610	0.154332	0.038066	0.135299	0.635198
410	410	610	610	0.174658	0.060805	0.144255	0.677244
411	411	610	610	0.142651	0.004550	0.140376	0.659033
520	520	521	611	0.011230	0.000008	0.010310	-10.731300
521	521	521	611	0.011030	0.000011	0.010128	-10.541900
522	522	521	611	0.010342	0.000000	0.009502	-9.890200
600	600	521	611	0.010369	-0.000062	0.010138	-10.551800
610	610	521	611	0.012331	-0.000190	0.012218	-12.717000
611	611	521	611	0.009475	-0.000239	0.009433	-9.818060
200	200	521	611	0.028137	-0.000015	0.028145	0.761270
210	210	521	611	0.028074	0.000000	0.028074	0.759336
211	211	521	611	0.029312	0.000000	0.029312	0.792835
300	300	521	611	0.011589	-0.000006	0.160144	5.911890
310	310	521	611	0.013859	-0.000004	0.013628	7.069160
311	311	521	611	0.010910	-0.000017	0.010736	5.568750
400	400	521	611	0.161518	0.002380	0.154986	5.125560
410	410	521	611	0.193911	0.006038	0.184531	6.021650
411	411	521	611	0.145001	0.001953	0.139225	4.893640

Table 4(Cont.)

Atomic orbitals							
i	j	k	l	C	X	C-X/2	S
520	520	611	611	0.140568	0.000074	0.131321	1.159280
521	521	611	611	0.139752	0.000334	0.134934	1.191180
522	522	611	611	0.136795	0.000014	0.132230	1.167310
600	600	611	611	0.134951	0.000921	0.133330	1.177020
610	610	611	611	0.143041	0.002057	0.142012	1.253660
611	611	611	611	0.129780	0.001885	0.128837	1.137350
200	200	611	611	0.227914	0.002059	0.226884	0.993315
210	210	611	611	0.229277	0.000827	0.228863	1.001980
211	211	611	611	0.229285	0.007324	0.225623	0.987794
300	300	611	611	0.148858	0.005383	0.146166	0.806322
310	310	611	611	0.163824	0.010215	0.158716	0.875554
311	311	611	611	0.143316	0.010757	0.137937	0.760926
400	400	611	611	0.144952	0.008990	0.140457	0.774828
410	410	611	611	0.163608	0.016365	0.155425	0.857399
411	411	611	611	0.137363	0.015336	0.129695	0.715460
520	520	200	200	0.302454	0.030307	0.287300	1.009110
521	521	200	200	0.283718	0.002058	0.282689	1.083700
522	522	200	200	0.244397	0.000037	0.244378	0.865343
600	600	200	200	0.257590	0.046575	0.234302	0.829664
610	610	200	200	0.313108	0.120665	0.252776	0.895080
611	611	200	200	0.227914	0.002059	0.226884	0.803397
200	200	200	200	0.199695	0.000028	0.199681	0.999925
210	210	200	200	0.203837	0.000040	0.203817	1.020640
211	211	200	200	0.197625	0.000001	0.197625	0.989629
300	300	200	200	0.190554	0.014012	0.183548	0.919137
310	310	200	200	0.228161	0.038600	0.208861	1.045890
311	311	200	200	0.171216	0.000330	0.171051	0.856556
400	400	200	200	0.179941	0.017658	0.171112	0.856862
410	410	200	200	0.221059	0.048655	0.196731	0.985152
411	411	200	200	0.157759	0.000400	0.157559	0.788994

Table 4(Cont.)

Atomic orbitals							
i	j	k	l	C	X	C-X/2	S
520	520	200	210	0.064313	0.005210	0.061708	1.250890
521	521	200	210	0.058865	-0.000423	0.059077	1.197560
522	522	200	210	0.040324	-0.000027	0.040337	0.817679
600	600	200	210	0.027597	-0.025030	0.040111	0.813104
610	610	200	210	0.038969	-0.082532	0.080236	1.626470
611	611	200	210	0.023021	-0.002228	0.024135	0.489245
200	200	200	210	0.024668	0.000000	0.024668	0.999927
210	210	200	210	0.026203	0.000000	0.026203	1.062250
211	211	200	210	0.023902	0.000000	0.023902	0.963877
300	300	200	210	0.018337	-0.000032	0.018353	0.743946
310	310	200	210	0.025005	-0.000033	0.025022	1.014260
311	311	200	210	0.014646	-0.000001	0.014646	0.597735
400	400	200	210	0.013147	-0.002449	0.014371	0.582534
410	410	200	210	0.016586	-0.004435	0.018804	0.762207
411	411	200	210	0.010941	-0.000036	0.010959	0.444207
520	520	210	210	0.317908	0.024608	0.305604	1.073400
521	521	210	210	0.294120	0.001893	0.293173	1.123880
522	522	210	210	0.253269	0.000029	0.253254	0.861054
600	600	210	210	0.260103	0.014386	0.252910	0.859884
610	610	210	210	0.317081	0.034146	0.300008	1.020020
611	611	210	210	0.229277	0.000827	0.228863	0.778125
200	200	210	210	0.203837	0.000040	0.203817	0.999892
210	210	210	210	0.208494	0.000061	0.208463	1.022680
211	211	210	210	0.201510	0.000001	0.201510	0.988574
300	300	210	210	0.192631	0.004927	0.190167	0.932927
310	310	210	210	0.231841	0.013406	0.225138	1.104490
311	311	210	210	0.172437	0.000142	0.172366	0.845599
400	400	210	210	0.180837	0.004503	0.178585	0.876108
410	410	210	210	0.222689	0.012495	0.226433	1.110842
411	411	210	210	0.158189	0.000132	0.158123	0.775725

Table 4(Cont.)

Atomic orbitals							
i	j	k	l	C	X	C-X/2	S
520	520	211	211	0.295973	0.004515	0.293715	1.031560
521	521	211	211	0.279989	0.005414	0.277282	1.062970
522	522	211	211	0.239959	0.000032	0.239943	0.867617
600	600	211	211	0.257748	0.009476	0.253010	0.914867
610	610	211	211	0.315077	0.024790	0.302682	1.094480
611	611	211	211	0.229285	0.007324	0.225623	0.815837
200	200	211	211	0.197625	0.000001	0.197625	1.000000
210	210	211	211	0.201510	0.000001	0.201510	1.019660
211	211	211	211	0.195747	0.000001	0.195747	0.990497
300	300	211	211	0.189881	0.002572	0.188595	0.954307
310	310	211	211	0.227376	0.007156	0.223798	1.132440
311	311	211	211	0.171234	0.001134	0.170667	0.863590
400	400	211	211	0.179956	0.003455	0.178228	0.901849
410	410	211	211	0.221590	0.009642	0.216769	1.096870
411	411	211	211	0.158248	0.001457	0.157519	0.797060
520	520	300	300	0.168116	0.003352	0.160795	1.005350
521	521	300	300	0.166610	0.001891	0.160144	1.001280
522	522	300	300	0.162769	0.000795	0.156961	0.981374
600	600	300	300	0.156238	0.031179	0.139435	0.871796
610	610	300	300	0.165389	0.037250	0.146764	0.917557
611	611	300	300	0.148858	0.005383	0.146166	0.913880
200	200	300	300	0.190554	0.014012	0.183548	0.954245
210	210	300	300	0.192631	0.004927	0.190167	0.988656
211	211	300	300	0.189881	0.002572	0.188595	0.980483
520	520	400	400	0.162177	0.002548	0.155445	0.936195
521	521	400	400	0.161518	0.002380	0.154986	0.983283
522	522	400	400	0.159128	0.001415	0.153238	0.972193
600	600	400	400	0.149951	0.042908	0.127389	0.808198
610	610	400	400	0.154332	0.038066	0.135299	0.858382
611	611	400	400	0.144952	0.008990	0.140457	0.891106

Table 4(Cont.)

Atomic orbitals							
$\underline{i}$	$\underline{j}$	$\underline{k}$	$\underline{l}$	C	X	C-X/2	S
200	200	400	400	0.179941	0.017658	0.171112	0.938618
210	210	400	400	0.180837	0.004503	0.178585	0.979611
211	211	400	400	0.179956	0.003455	0.178228	0.977652
520	520	300	310	0.059897	0.001203	0.057319	0.995078
521	521	300	310	0.058695	0.000736	0.056384	0.978838
522	522	300	310	0.055819	0.000350	0.053790	0.872514
600	600	300	310	0.048263	-0.049829	0.072547	1.259440
610	610	300	310	0.053318	-0.050633	0.078635	1.365130
611	611	300	310	0.044347	-0.011824	0.050259	0.933814
200	200	300	310	0.075673	-0.001605	0.076475	0.971049
210	210	300	310	0.077420	0.000000	0.077420	0.983049
211	211	300	310	0.075419	0.000000	0.075419	0.957641
520	520	400	410	0.065835	0.001214	0.063055	0.946059
521	521	400	410	0.065483	0.001016	0.062811	0.942398
522	522	400	410	0.063893	0.000636	0.061457	0.902923
600	600	400	410	0.074976	-0.074855	0.111434	1.671920
610	610	400	410	0.077166	-0.050681	0.102506	1.537970
611	611	400	410	0.050174	-0.020011	0.060180	0.922083
200	200	400	410	0.078509	-0.002148	0.079584	0.963838
210	210	400	410	0.079038	0.000000	0.079038	0.957225
211	211	400	410	0.079033	0.000000	0.079033	0.957165
520	520	310	310	0.195724	0.008270	0.185090	0.979354
521	521	310	310	0.193123	0.004589	0.184469	1.001280
522	522	310	310	0.187294	0.002088	0.180044	0.981374
600	600	310	310	0.173393	0.057084	0.143602	0.759831
610	610	310	310	0.185154	0.061839	0.154234	0.816087
611	611	310	310	0.163824	0.010215	0.158716	0.913880
200	200	310	310	0.228161	0.038600	0.208861	0.894648
210	210	310	310	0.231841	0.013406	0.225138	0.964370
211	211	310	310	0.227376	0.007156	0.223798	0.958630

Table 4(Cont.)

Atomic orbitals							
_i_	_j_	_k_	_l_	C	X	C-X/2	S
520	520	410	410	0.195055	0.006899	0.185106	0.959451
521	521	410	410	0.193911	0.006038	0.184531	0.956471
522	522	410	410	0.190297	0.003757	0.182140	0.944078
600	600	410	410	0.169898	0.077311	0.130110	0.674393
610	610	410	410	0.174658	0.060805	0.144255	0.747710
611	611	410	410	0.163608	0.016365	0.155425	0.805607
200	200	410	410	0.221059	0.048655	0.196731	0.938618
210	210	410	410	0.222689	0.012495	0.226433	0.979611
211	211	410	410	0.221590	0.009642	0.216769	0.977652
520	520	311	311	0.154021	0.000207	0.148696	1.010140
521	521	311	311	0.153731	0.001830	0.147724	1.003530
522	522	311	311	0.150326	0.000230	0.145206	0.986427
600	600	311	311	0.147367	0.003679	0.144272	0.980082
610	610	311	311	0.155088	0.005051	0.152482	1.035860
611	611	311	311	0.143316	0.010757	0.137937	0.937047
200	200	311	311	0.171216	0.000330	0.171051	0.889274
210	210	311	311	0.172437	0.000142	0.172366	0.738323
211	211	311	311	0.171234	0.001134	0.170667	0.996427
520	520	411	411	0.144611	0.000190	0.139614	1.004190
521	521	411	411	0.145001	0.001953	0.139225	0.882075
522	522	411	411	0.142617	0.000391	0.137675	0.990247
600	600	411	411	0.138887	0.004384	0.135516	0.974718
610	610	411	411	0.142651	0.004550	0.140376	1.009670
611	611	411	411	0.137363	0.015336	0.129695	0.932850
200	200	411	411	0.157759	0.000400	0.157559	0.998323
210	210	411	411	0.158189	0.000132	0.158123	1.001810
211	211	411	411	0.158248	0.001457	0.157519	0.997979

Table 5.   Nuclear attraction integrals[a] calculated for perovskite transition metal oxides in the rhenium trioxide model

Potential center A	Quantum numbers[b] of orbitals		Distance[c]	$\left\langle \frac{1}{r_A} \middle\| ij \right\rangle$
	i	j		
Re	520	520	7.08182	0.150204
O	520	520	3.54091	0.284707
AM[d]	520	520	6.13304	0.223707
Re	521	521	7.08182	0.148236
O	521	521	3.54091	0.260856
AM	521	521	6.13304	0.220473
Re	522	522	7.08182	0.144462
O	522	522	3.54091	0.238434
AM	522	522	6.13304	0.215100
Re	520	600	7.08182	0.007468
O	520	600	3.54091	0.074768
AM	520	600	6.13304	0.010329
Re	600	600	7.08182	0.126080
O	600	600	3.54091	0.282871
AM	600	600	6.13304	0.143481
Re	520	610	7.08182	0.004093
O	520	610	3.54091	0.076099
AM	520	610	6.13304	0.010025
Re	600	610	7.08182	0.022800
O	600	610	3.54091	0.127304
AM	600	610	6.13304	0.057758
Re	610	610	7.08182	0.134094
O	610	610	3.54091	0.334621
AM	610	610	6.13304	0.213003
Re	521	611	7.08182	-0.000961
O	521	611	3.54091	0.036971
AM	521	611	6.13304	0.001928
Re	611	611	7.08182	0.113278
O	611	611	3.54091	0.228411
AM	611	611	6.13304	0.181275

[a]The integral values are in atomic units of 27.2 e.v.

[b]The quantum numbers n, ℓ, and m are expressed as an integer nℓm. The indicated orbitals are on center B.

[c]The distance between potential center A and the indicated orbitals on center B is expressed in Bohr units.

[d]AM is any element which fills the perovskite hole.

Table 5(Cont.)

Potential center A	Quantum numbers of orbitals		Distance	$\left\langle \frac{1}{r_A} \middle| ij \right\rangle$
	i	j		
Re	200	200	3.54091	0.282406
O	200	200	5.00760	0.199696
AM	200	200	5.00760	0.199696
Re	200	210	3.54091	0.049331
O	200	210	5.00760	0.024670
AM	200	210	5.00760	0.024670
Re	210	210	3.54091	0.294121
O	210	210	5.00760	0.203839
AM	210	210	5.00760	0.203839
Re	211	211	3.54091	0.276554
O	211	211	5.00760	0.197625
AM	211	211	5.00760	0.197625
Re	300	300	6.13304	0.159940
O	300	300	5.00760	0.192349
AM	300	300	5.00760	0.192349
Re	300	310	6.13304	0.057602
O	300	310	5.00760	0.078755
AM	300	310	5.00760	0.078755
Re	310	310	6.13304	0.188992
O	310	310	5.00760	0.233456
AM	310	310	5.00760	0.233456
Re	311	311	6.13304	0.147204
O	311	311	5.00760	0.171279
AM	311	311	5.00760	0.171279
Re	400	400	6.13304	0.157621
O	400	400	5.00760	0.182302
AM	400	400	5.00760	0.182302
Re	400	410	6.13304	0.066650
O	400	410	5.00760	0.082570
AM	400	410	5.00760	0.082570
Re	410	410	6.13304	0.192929
O	410	410	5.00760	0.228046
AM	410	410	5.00760	0.228046
Re	411	411	6.13304	0.139031
O	411	411	5.00760	0.157838
AM	411	411	5.00760	0.157838

ATOMIC ORBITAL FUNCTIONS AND ENERGIES

Using the values of r_{max} from Mann's data (29), we used Equation 55 to obtain the orbital exponents of the rhenium 6s and 6p and other ns and np (n = 2,3,4) STO expansions resulting from Equation 54. The expansion coefficients were then found by the Schmidt orthogonalization procedure and listed in Table 6.

Using a least-squares-program proposed by Raffenetti (48), we have been able to express all principal quantum number STO's in terms of 3d, 3s and 3p STO's for the Basch-Gray 5d, 6s and 6p functions. The Basch-Gray functions are listed in Table 7. The Raffenetti least squares fits are shown below Table 7. The resulting functions are compared both graphically (Figures 6 to 8) and in Table 8. A comparison of radial expectation values for $\langle r^q \rangle$ in a.u. (q=2,-1,0,1,2) is given in Table 8. Outer region radial properties depend on reliable $\langle r \rangle$ and $\langle r^2 \rangle$ values while inner properties depend on $\langle r^{-1} \rangle$ and $\langle r^{-2} \rangle$ values. It can be seen that except for $\langle r^{-2} \rangle$ values, we obtained a least-squares fit function which appears to be adequate for making two-center integral calculations. The original SCF type functions will be used to evaluate all one-center integrals. Thus, the deficiencies in the nodal behavior at the nucleus, as exhibited by $\langle r^{-2} \rangle$, of the fitted functions need not be of concern in the TBA calculations. Cusachs (49) has made a careful study of radial properties vs. inner and outer behavior.
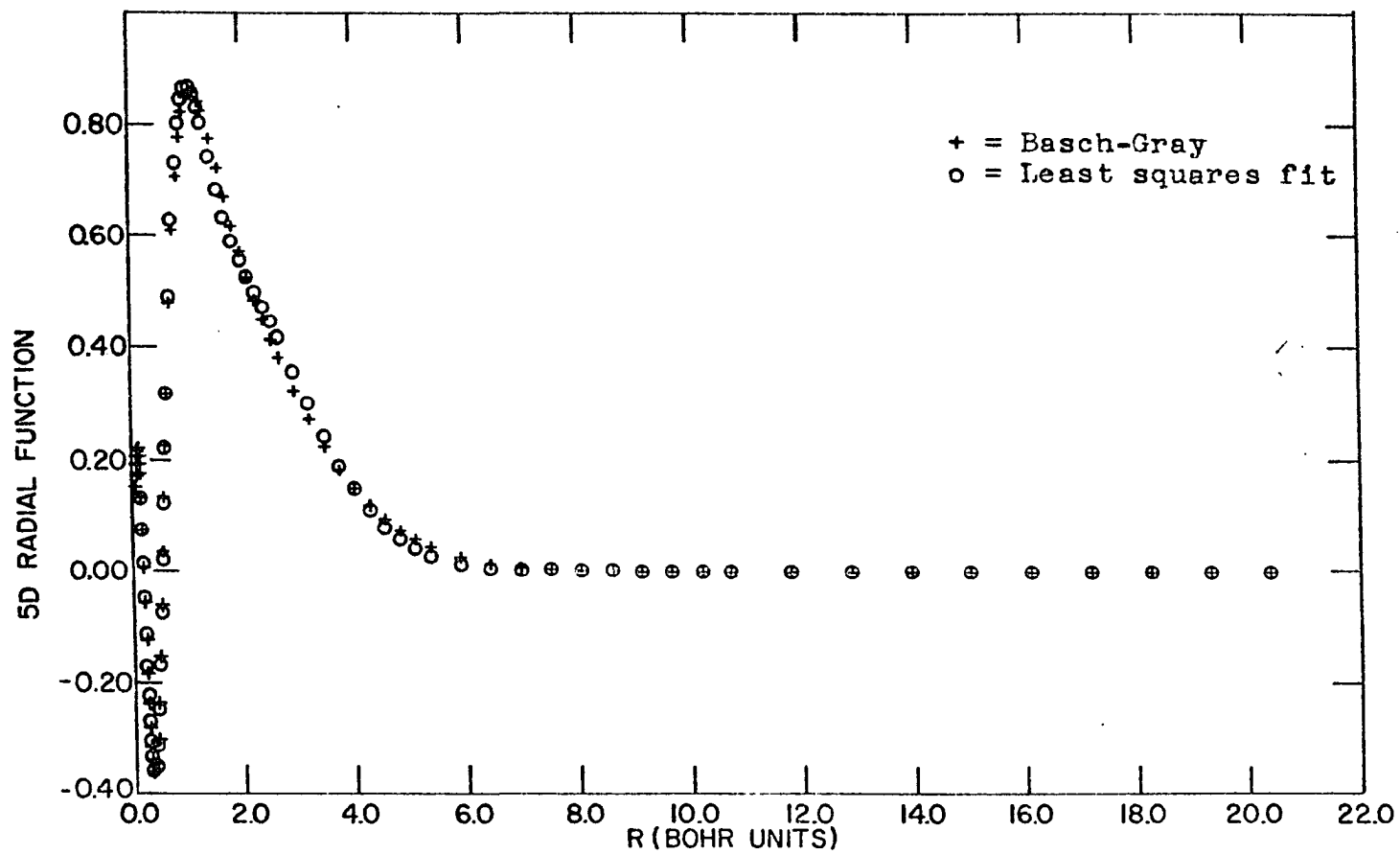
Figure 6. P(5d) vs. R.
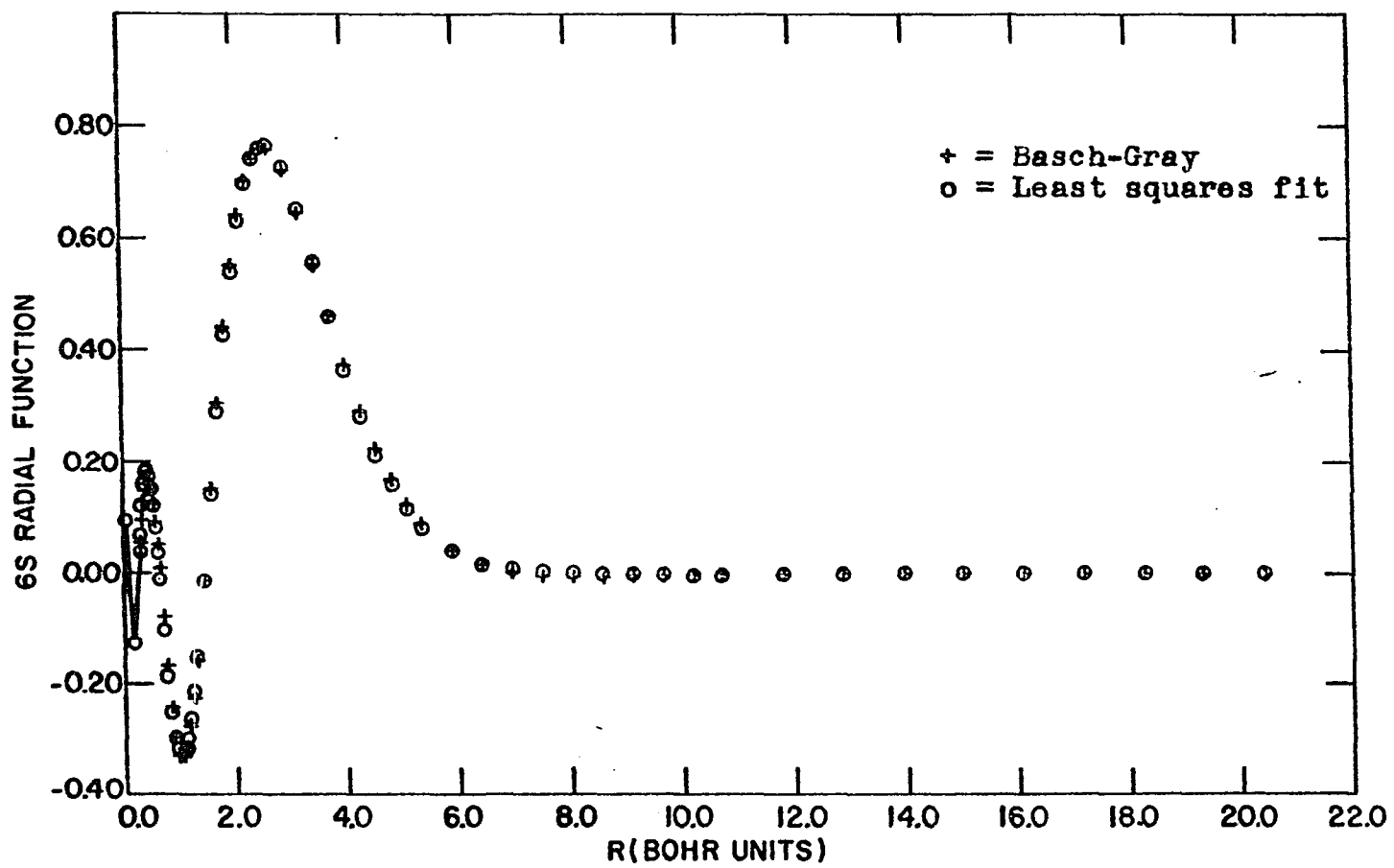
Figure 7. P(6s) vs. R.
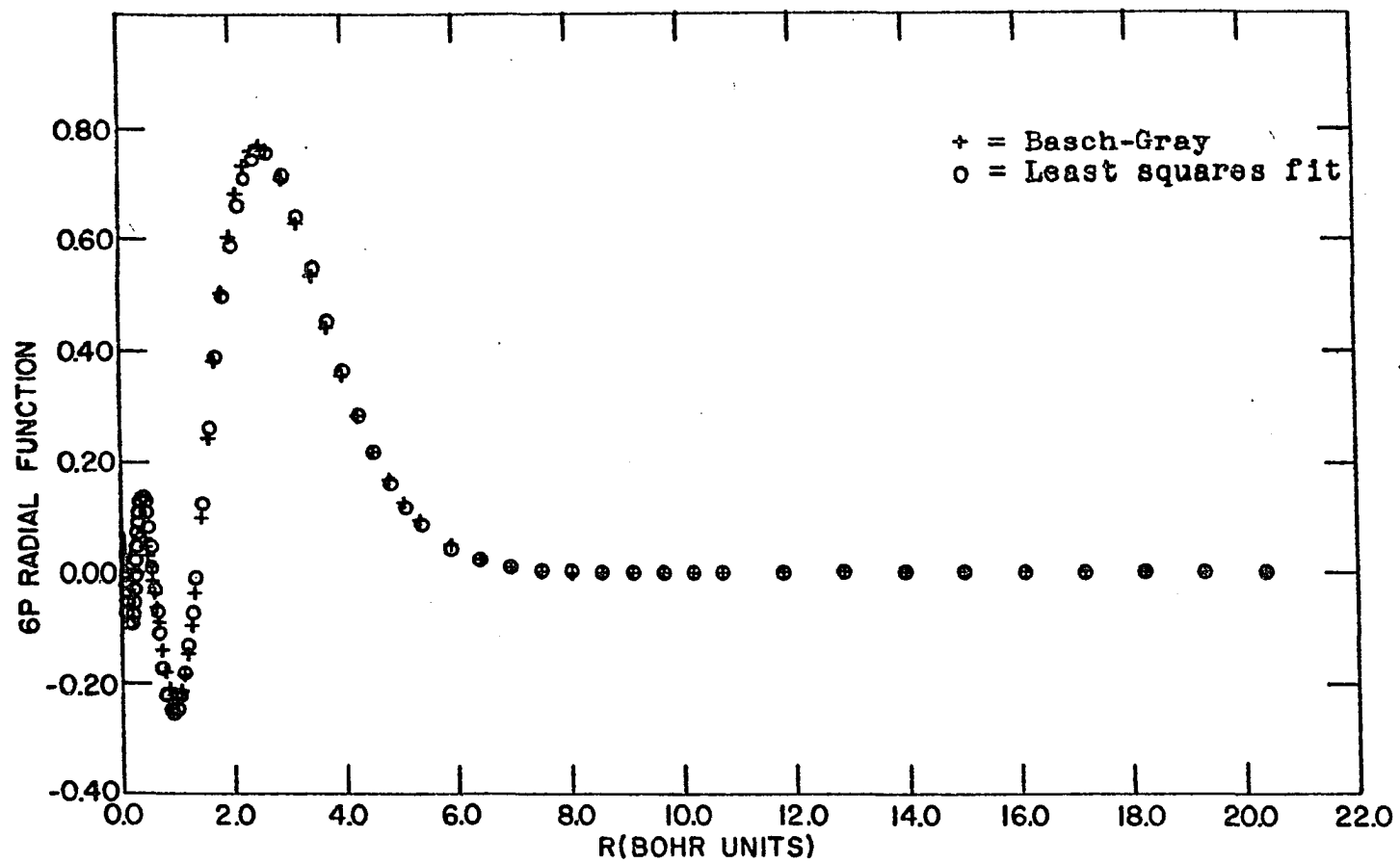
Figure 8. P(6p) vs. R.

Table 6. Coefficient matrix elements for Schmidt ortho-
gonalized atomic orbital radial function used
in tight-binding calculations of rhenium tri-
oxide energy bands

atom	u_j	$\underline{1}$	$\underline{j}$	T_{ij} [a]	n_i [b]	ζ_i [c]
OXYGEN	1s	1	1	1.000000	1	7.723800
	2s	1	2	-0.240748	1	7.723800
		2	2	1.028571	2	2.285810
OXYGEN	2p	1	1	1.000000	2	2.401410
RHENIUM	3d	1	1	1.000000	3	20.255000
	4d	1	2	-0.481633	3	20.255000
		2	2	1.109941	4	10.409000
	5d	1	3	0.123000	3	20.255000
		2	3	-0.334200	4	10.409000
		3	3	0.666200 [d]	5	5.343000
				0.591000	5	2.277000

[a] These are elements of matrix T which is upper tri-
angular, i.e.

$$T = \begin{pmatrix} T_{11} & T_{12} & T_{13} & \cdots \\ & T_{22} & T_{23} & \cdots \\ & & T_{33} & \cdots \\ 0 & & & T_{ij} \end{pmatrix}$$

The Schmidt orthogonalized functions, u_j , with
$n_j^{\prime} l_j^{\prime} m^{\prime}$ are taken as a linear combination of
v_i where

$$u_j = v_1 T_{1j} + v_2 T_{2j} + \cdots + v_j T_{jj} \quad \text{with } i=1, \ldots, n^{\prime}-l^{\prime} \text{ or } j.$$

Thus, the STO basis set v_i is mapped by T into a set of func-
tions u_j which are orthogonal or $\int u_j^* \cdot u_k \, dv = \delta_{jk}$.

[b] The principal quantum number n_i for STO v_i.

[c] The orbital exponent ζ_i for STO v_i.

[d] The rhenium 5d v_i is a double-zeta STO.

Table 6(Cont.)

atom	u_j	$\underline{i}$	$\underline{j}$	T_{ij}	n_i	ζ_i
RHENIUM	1s	1	1	1.000000	1	74.604500
	2s	1	2	-0.343106	1	74.604500
		2	2	1.057223	2	27.425000
	3s	1	3	0.182846	1	74.604500
		2	3	-0.671419	2	27.425000
		3	3	1.185138	3	15.012400
	4s	1	4	-0.100416	1	74.604500
		2	4	0.386493	2	27.425000
		3	4	-0.886654	3	15.012400
		4	4	1.253684	4	8.907850
	5s	1	5	0.043263	1	74.604500
		2	5	-0.168471	2	27.425000
		3	5	0.409206	3	15.012400
		4	5	-0.723755	4	8.907850
		5	5	1.157926	5	4.841620
	6s	1	6	-0.008305	1	74.604500
		2	6	0.032385	2	27.425000
		3	6	-0.079181	3	15.012400
		4	6	0.143364	4	8.907850
		5	6	-0.256261	5	4.841620
		6	6	1.024283	6	1.985020
RHENIUM	2p	1	1	1.000000	2	35.291400
	3p	1	2	-0.417916	2	35.291400
		2	2	1.083814	3	15.914866
	4p	1	3	0.212250	2	35.291400
		2	3	-0.670135	3	15.914866
		3	3	1.176621	4	8.885510
	5p	1	4	-0.079740	2	35.291400
		2	4	0.261209	3	15.914866
		3	4	-0.553094	4	8.885510
		4	4	1.106088	5	4.511780
	6p	1	5	0.017990	2	35.291400
		2	5	-0.059165	3	15.914866
		3	5	0.127640	4	8.885510
		4	5	-0.284291	5	4.511780
		5	5	1.032576	6	1.963498

Table 7.   Basch-Gray rhenium functions

Orbital	n^a	Expansion coefficient	Orbital exponent
5d[b]	3	0.1230	20.255
	4	-0.3342	10.409
	5	0.6662	5.343
	5	0.5910	2.277
6s[c]	1	-0.0140	74.535
	2	0.0505	28.821
	3	-0.1232	15.279
	4	0.2424	8.657
	5	-0.4845	4.682
	6	1.0860	2.398
6p[d]	2	0.0269	35.294
	3	-0.0751	18.084
	4	0.1546	10.041
	5	-0.3338	5.191
	6	1.0439	2.372

[a]The principal quantum number of the Slater type orbital basis.

[b]The least squares function is
$$5d=0.583504(1.54671)+0.668450(3.55414)$$
$$-0.505987(8.16695)+0.184065(18.76656)$$
where the number in parenthesis is the orbital exponent and the number preceding the parenthesis is the corresponding coefficient.

[c]The least squares function is
$$6s=-0.179520(0.99199)+2.034532(1.56188)$$
$$-1.246671(2.45917)-0.547268(3.87195)$$
$$+0.869837(6.09637)-0.307880(9.59870).$$

[d]The least squares function is
$$6p=-0.159442(0.99847)+1.256337(1.43424)$$
$$+0.789819(2.06021)-1.977675(2.95936)$$
$$+0.785272(4.25094).$$

Table 8. Analysis of least-squares-fit functions for rhenium atomic orbitals[a]

SCF type function[b]	Weighted self-overlap of SCF[c]	Weighted self-overlap of LSF type	Weighted mean-square deviation[d]	q	Radial expectation values[e]	
					$\langle r^q_{SCF} \rangle$	$\langle r^q_{LSF} \rangle$
Basch-Gray 5d	0.078989	0.078859	0.000128	-2	1.160198	1.171559
				-1	0.789875	0.788594
				0	0.999995	0.995184
				1	1.653259	1.631237
				2	3.349344	3.277541
				3	8.071030	7.942476
Basch-Gray 6s	0.042237	0.040340	0.001897	-2	1.997412	0.233403
				-1	0.422368	0.403403
				0	1.000026	0.998402
				1	2.803940	2.804037
				2	8.492696	8.512128
				3	27.353992	27.543308

[a]Least-squares-fit functions are referred to as LSF type. See Table 4.

[b]The function which is fitted is based upon self-consistent radial functions (SCF).

[c]The weighted self-overlap, S, is defined as $S = \sum_p \left[f(r_p) \right]^2 r_p$ where $f(r_p)$ is the value of the function at the radial distance r_p. (48, 30)

[d]The weighted mean-square deviation, D, is defined as: (48)

$$D = \sum_p \left[SCF(r_p) - LCF(r_p) \right]^2 r_p$$

[e]Atomic units.

Table 8(Cont.)

SCF type function	Weighted self-overlap of SCF	Weighted self-overlap of LSF type	Weighted mean-square deviation	Radial expectation values		
				q	$\langle r^q{}_{SCF} \rangle$	$\langle r^q{}_{LSF} \rangle$
Basch-Gray 6p	0.040575	0.038971	0.001604	-2	0.381871	0.184165
				-1	0.405748	0.389708
				0	0.999970	0.996415
				1	2.798682	2.795655
				2	8.436718	8.421913
				3	27.098299	27.076257

Table 9.   Comparison of Schmidt orthogonalized function radial expectation values with Mann's SCF results for neutral rhenium (a.u.)

Function	q	$\langle r^q_{SOF}{}^a \rangle$	$\langle r^q_{MANN} \rangle$
Basch-Gray 5d	-2	1.160198	1.160285
	-1	0.789875	0.722333
	1	1.653259	1.799927
	2	3.349344	3.845362
SCF[b] 6s	-2	0.769747	0.881567
	-1	0.338750	0.337196
	1	3.320042	3.694182
	2	11.857742	15.666920
LSF[c] 6s	-2	0.182571	0.881567
	-1	0.335347	0.337196
	1	3.330900	3.694182
	2	12.048085	15.666920

Radial expectation value

[a]The subscript SOF means Schmidt orthogonalized function.

[b]The single zeta Slater type orbital basis set based upon Mann's SCF r_{max} values are Schmidt orthogonalized to give analytical functions which are labeled SCF.

[c]The weighted mean square deviation of the least-squares-fit (LSF) function, D, is 0.003403.

The 5d and 6s radial functions for neutral rhenium in Table 6 were fitted by $n=3$ STO's and the calculated $\langle r^q \rangle$, radial expectation values, of our basis set for rhenium are compared with Mann's values in Table 9. The 6s and 6p least squares functions for the neutral rhenium atom are shown in Table 10.

Table 10.   Least squares functions for 6s and 6p orbitals

Orbital	Least squares function[a]

6s
1.46078(1.29317) - 0.93009(2.42117)
0.16555(4.53311) + 0.12909(8.48725)
-0.13028(15.8905) + 0.04871(29.7515)

6p
1.58713(1.30492) - 1.03977(2.25186)
0.02002(3.88597) + 0.24836(6.70589)
-0.10577(11.5721)

[a]The number in the parenthesis is the orbital exponent and the number preceding the parenthesis is the corresponding expansion coefficient.

Using programs based upon Appendix F, we have calculated the atomic orbital energy parameters (see Table 11) which will be put into the TBA calculation. The formulation for calculating Slater-Condon parameters is obtained from Ros and Schuit (36).

Table 11. ReO_3 orbital energy parameters[a]

Orbital	Two-electron interaction energy			One center kinetic energy	Core energy[b]	Orbital energy[c]
	$\underline{i}$	$\underline{j}$	$g(i,j)$			
OXYGEN 2s	1s	2s	2.206543	6.24103	-14.0796	-2.072135
	2p	2s	1.494784			
	2s	2s	1.615272			
OXYGEN 2p	1s	2p	2.350730	5.76677	-13.4445	-0.721791
	2s	2p	1.494784			
	2p	2p	1.677232			
RHENIUM 5d	1s	5d	1.579712	12.17131	-106.3099	-0.671732
	2s	5d	1.567410			
	2p	5d	1.572472			
	3s	5d	1.532340			
	3p	5d	1.536908			
	3d	5d	1.549390			

[a]Orbital energy parameters are in Rydberg units.

[b]The core energy of the j th orbital is expressed as the value of the integral $\langle \phi_j \mid -\nabla^2 - \dfrac{2Z_j}{r} \mid \phi_j \rangle$ where Z_j is the bare nuclear charge.

[c]This is the orbital energy for the neutral atom.

Table 11(Cont.)

Orbital	Two-electron inter-action energy			One center kinetic energy	Core energy	Orbital energy
	i	j	$g(i,j)$			
RHENIUM 5d	4s	5d	1.468756			
	4p	5d	1.470050			
	4d	5d	1.418938			
	4f[d]	5d	1.462356			
	5s	5d	1.211320			
	5p	5d	1.170556			
	5d	5d	1.076252			
	6s	5d	0.626782			
	6p	5d	0.619212			
RHENIUM 6s	1s	6s	0.674316	1.67557	-49.1369	-0.330855
	2s	6s	0.670548			
	2p	6s	0.671698			
	3s	6s	0.666742			
	3p	6s	0.667558			
	3d	6s	0.668898			
	4s	6s	0.661294			
	4p	6s	0.662210			
	4d	6s	0.663802			
	4f	6s	0.662356			

[d]Basch-Gray 4f functions have been used to evaluate $g(4f,j)$ terms.

Table 11(Cont.)

Orbital	Two-electron inter- action energy			One center kinetic energy	Core energy	Orbital energy
	i	j	g(i,j)			
RHENIUM 6s	5s	6s	0.639848			
	5p	6s	0.648272			
	5d	6s	0.626782			
	6s	6s	0.547078			
RHENIUM 6p	1s	6p	0.667286	1.679749	-48.39085	-0.134514
	2s	6p	0.664774			
	2p	6p	0.665388			
	3s	6p	0.661504			
	3p	6p	0.661774			
	3d	6p	0.663040			
	4s	6p	0.656248			
	4p	6p	0.656188			
	4d	6p	0.657898			
	4f	6p	0.656386			
	5s	6p	0.641836			
	5p	6p	0.640108			
	5d	6p	0.619212			
	6s	6p	0.474214			
	6p	6p	0.512740			

E($\underline{k}$) VS. $\underline{k}$ AND DENSITY OF STATES

The eigenvalues of crystal orbitals $\Psi_i(\underline{k},\underline{r})$ are $E_i(\underline{k})$ for the i th energy band. Since the energy is a periodic function of $\underline{k}$, the $\underline{k}$ vectors which are to be chosen for band calculations can be restricted to lie within a unit cell of wave vector or momentum space which is called the primitive Brillouin zone.

Rhenium trioxide and the perovskite transition metal oxides belong to the cubic space group O_h^1. In reciprocal or wave vector space, the first Brillouin zone is a cube with side $2\pi/\underline{a}$ where $\underline{a}$ is the lattice constant. For ReO_3, $\underline{a}$ is 3.7477 Å (37) All of the symmetry points and lines found in the simple cubic Brillouin zone can be placed on the surface of a polyhedron which is only 1/48 of the Brillouin zone volume (Figure 9). Thus, the choice of $\underline{k}$ vectors can be restricted further to lie within the 1/48 volume. Slater (50) lists the degeneracies of the $\underline{k}$ vectors which correspond to symmetry points and lines on the surface of the 1/48 Brillouin zone. A non-symmetry point within this surface represents a total of 48 points in the entire Brillouin zone because of the space group symmetry.

A convenient choice of 56 points shown in Table 12 was used to obtain the energy bands of ReO_3, $KTaO_3$ and $NaWO_3$. These points are evenly spaced in the 1/48 Brillouin zone with a cubic mesh of side $0.2\pi/\underline{a}$. This choice represents 1000 points in the entire Brillouin zone.
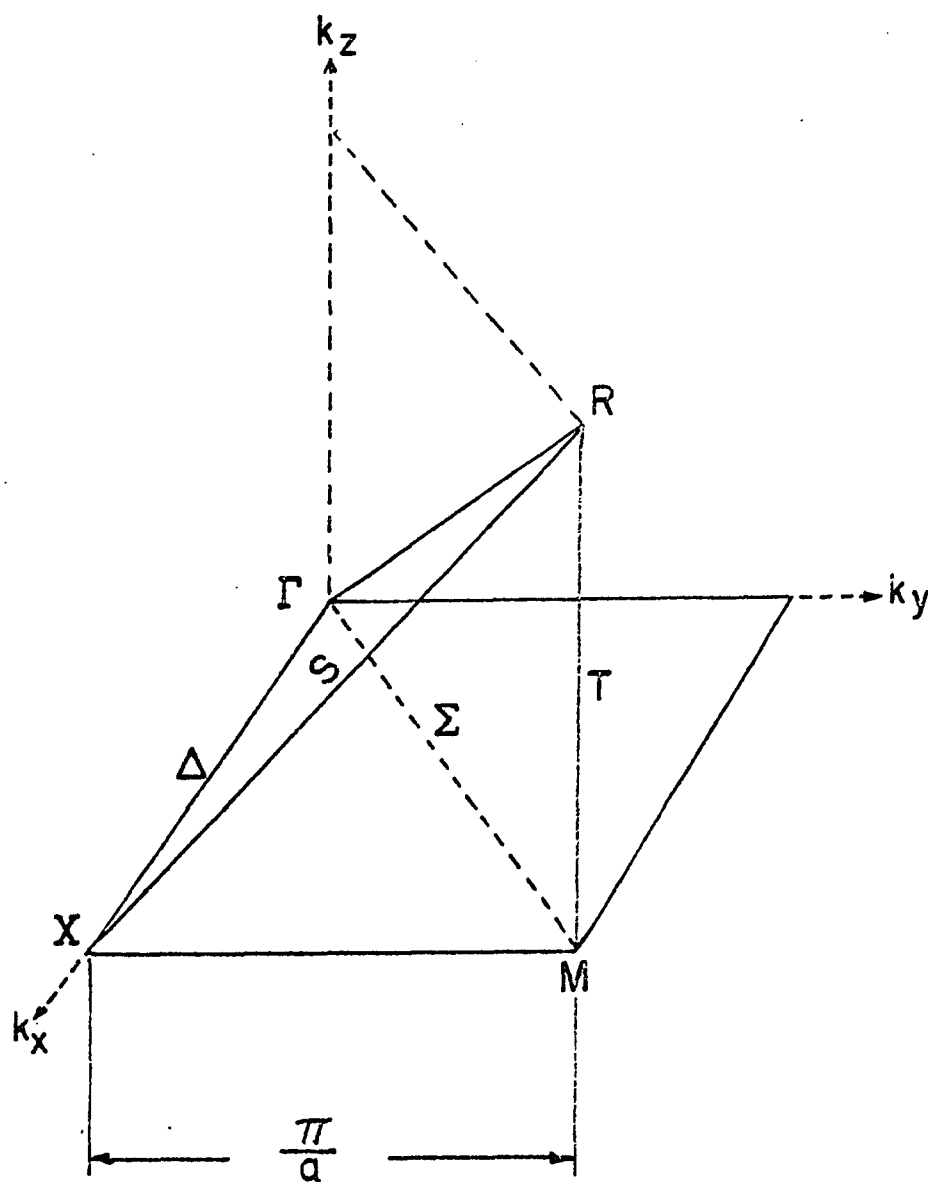
Figure 9. 1/48 Brillouin zone for O_h^1 structure.

Table 12. K vector basis used in energy band calculation of perovskite transition metal oxides in the 1/48 Brillouin zone

Number	$k_x{}^a$	k_y	k_z	g^b	Number	k_x	k_y	k_z	g
1	0	0	0	1	29	2	1	0	24
2	1	0	0	6	30	3	1	0	24
3	2	0	0	6	31	4	1	0	24
4	3	0	0	6	32	3	2	0	24
5	4	0	0	6	33	4	2	0	24
6	5	0	0	3	34	4	3	0	24
7	5	1	0	12	35	2	1	1	24
8	5	2	0	12	36	3	1	1	24
9	5	3	0	12	37	4	1	1	24
10	5	4	0	12	38	2	2	1	24
11	5	5	0	3	39	3	2	1	48
12	5	5	1	6	40	4	2	1	48
13	5	5	2	6	41	5	2	1	24
14	5	5	3	6	42	3	3	1	24
15	5	5	4	6	43	4	3	1	48
16	5	5	5	1	44	5	3	1	24
17	4	4	4	8	45	4	4	1	24
18	3	3	3	8	46	5	4	1	24
19	2	2	2	8	47	3	2	2	24
20	1	1	1	8	48	4	2	2	24
21	1	1	0	12	49	3	3	2	24
22	2	2	0	12	50	4	3	2	48
23	3	3	0	12	51	5	3	2	24
24	4	4	0	12	52	4	4	2	24
25	5	1	1	12	53	5	4	2	24
26	5	2	2	12	54	4	3	3	24
27	5	3	3	12	55	4	4	3	24
28	5	4	4	12	56	5	4	3	24

[a]The k_x, k_y and k_z components of $\underline{k}$ are in units of 0.2 $\pi/\underline{a}$ where $\underline{a}$ is the lattice constant.

[b]The number of points in the entire Brillouin zone are indicated.

In Figure G1 (Appendix G), we see the E($\underline{k}$) vs. $\underline{k}$ curve and the density of states histogram. The E($\underline{k}$) vs. $\underline{k}$ values for Γ, X, M, and R symmetry points are listed in Table G1 (Appendix G). Note that the E($\underline{k}$) vs. $\underline{k}$ curve is limited to the region 1.0 to -4.0 Rydberg units. This range was taken because we wish to show the important details of the energy bands in the region of the Fermi energy which has been found to be -1.4828 Rydbergs. Only the top and lowest bands which are excluded from Figure G1, are represented by the four examples in Tables G2 to G5 to roughly show their relative variation in $\underline{k}$ space.

The histogram for the density of states is determined as follows. We choose an increment of energy E and count the number of energy levels (E($\underline{k}$) calculated at 1000 $\underline{k}$ vectors) N(E) within a particular energy interval E to E+ΔE. Thus the density of states G(E) at an energy E in each unit cell volume is

$$G(E) = \frac{N(E)}{\Delta E} \cdot 2 \cdot p^{-1} \qquad (63)$$

where the factor of 2 is included to account for the spin degeneracy. p is the sum of $\underline{k}$ vectors taken, i.e. 1000 resulting from the present mesh taken for the 1/48 zone (Table 12). The energy axis is divided into increments E + n ΔE (n=0,1,2...) and the partitioned columns formed from G(E) produce the histogram.

There are 25 valence electrons considered in the ReO_3 calculation, seven from rhenium and six each from the three oxygen atoms. The computed energy bands must accommodate

these 25 electrons via the Pauli exclusion principle by
filling the energy bands below the Fermi level with two
electrons each.

In order to simplify the calculation of the Fermi energy,
we guess at which bands are definitely filled and consider
only those bands which are within the region of where we
expect the Fermi level to be. For ReO_3, we are left with nine
electrons which are to fill levels to the Fermi energy.

The determination of the Fermi energy is simple
arithmetic. The number of times an energy corresponding to
a given $\underline{k}$ is counted (on the basis of $\underline{k}$ vector degeneracies
listed in Table 12). Then, we number the lowest energy level
one and proceed numbering energies to the next lowest level
and so forth, until the list of energies is exhausted. For
example, if there are nine electrons or 4.5 electron pairs and
1000 $\underline{k}$ vectors in the Brillouin zone, 4500 energy states will
be occupied, and all higher energies will be unoccupied.
Thus, the approximate Fermi energy lies somewhere between
energy number 4500 and 4501. Generally, both energies have
the same value.

The density of states at the Fermi energy, $G(E_f)$, in the
independent particle model, is related to the electronic
specific heat, Ce, by $C_e = \gamma T$.

$$G(E_f) = 3\gamma / \pi^2 \underline{a}^3 k^2 No. \tag{64}$$

$\underline{a}$ is the lattice constant, k is Boltzmann's constant, and No
is Avagadro's number. If $G(E_f)$ is expressed as states

-e.v.$^{-1}$-cm^{-3}, γ is given by joules-mole^{-1}-deg^{-2}, and $\underline{a}$ is expressed in angstroms, evaluation of the physical constants gives (51):

$$G(E_f) = 4.242 \times 10^{26} \, \gamma \, /\underline{a}^3. \tag{65}$$

Taking the value of $G(E_f)$ at $\triangle E = .05$ Rydberg units, 21.1 electron states/Ryd.-unit cell or 2.94×10^{22} states -e.v.$^{-1}$-cm^{-3}, one obtains γ from Equation 65 and finds it to be 3.66×10^{-3} joules-mole^{-1}deg^{-2}.

Thus, by a measurement of the specific heat of ReO_3 at low temperatures such as Sandin and Keeson (52) have done for reduced TiO_2, the constant γ can be found and compared with our value. At this time, we know at least that our $N(E)$ vs. E at E_f correlates with the fact that ReO_3 is a conductor as it has been found experimentally (53).

The Fermi level actually lies close to a peak in the density of states which amounts to 64 electron states/Ryd.-unit cell. The value of 21.1 states/Ryd. was obtained by counting the number of states just above this peak. Since the gap between the Fermi level and the next higher peak is filled by a constant number of states (20-21) and the results (51) for sodium tungsten bronzes are of this magnitude, we feel that the value of 21.1 states/Ryd. is not unreasonable.

If rhenium trioxide is slightly reduced, eg. $ReO_{2.99}$, the specific heat at low temperatures should have an out-

standing increase above that of the pure substance to the extent that E_f lies above the $2p_N$ peak. Certainly, such measurements would help to test our density of states picture.

RESULTS OF THE MULLIKEN POPULATION ANALYSIS OF ReO_3

In Tables G2 to G5 (Appendix G), we show the results of the Mulliken population analyses. We use Equation 23 to obtain the % orbital contribution of atomic orbitals to crystal orbital $\underline{i}$ with eigenfunction $\Psi_i(\underline{k},\underline{r})$ (normalized to one) and eigenvalue $E_i(\underline{k})$ at the symmetry points Γ (gamma), X, M and R.

The main contribution to the crystal states immediately below the Fermi level comes from oxygen $2p_\pi$ orbitals. These orbitals form narrow bands which are rather insensitive to change in translational symmetry, as evidenced by the very flat group of bands at the Fermi level in Figure G1. The electrons in these bands are localized on the oxygens by the overlap criterion. The Re-O e_g type bands cross the Fermi level (see Figure 10 which is a magnification of the region about the Fermi level) and, therefore, contribute to the conduction band, but the direction of the "E_g" band-Fermi energy intersection contributes little to the 21.1 electron states/Ryd. discussed in the previous section. This is so because the derivative, $N(E)/\Delta E$, is small.

An interesting thing happens at the R symmetry point where stabilization of t_{2g} type bands ($R_{25'}$) brings d_π-$2p_\pi$ states very close to the Fermi level. A d_{xy} type band (M_3) also comes close to the Fermi level at the M symmetry point.

Figure 10. ReO_3 energy bands near Fermi energy (numbers label i th energy band).

The small curvature of the conduction bands at $R_{25'}$ and M_3 contribute mainly to the 21.1 electron states at the Fermi level. Then $d_\pi - 2p_\pi$ bands give rise to a large number of states from the Fermi level to -1.0 Rydbergs. Therefore, within the limits of our TBA, the Sienko-Goodenough $d_\pi - p_\pi$ model (39, 40) applies to ReO_3.

The localized O_h molecular orbital picture of ReO_3 qualitatively agrees with our bands at the Γ and R symmetry points, e.g. the t_{1u}(6p and 2p), $t_{2g}*-t_{2g}(5d_\pi -2p_\pi)$, e_g*-e_g $(5d_\sigma -2p_\sigma)$, and $a_{1g}*(6p)-a_{1g}(2s)$ orbitals are the main contributors to bands at Γ and R and are identified as such in Tables G2 to G5.

The self-consistent crystal potential (obtained by calculating 56 $\underline{k}$ vectors at .7 minutes/$\underline{k}$ vector) involved a lengthy and expensive computation without some prior educated guess about approximate charge distribution. We, therefore, sought a method to obtain the approximate charge distribution for a given $\underline{k}$ vector, in order to guess occupation numbers before executing an entire $E(\underline{k})$ vs. $\underline{k}$ calculation.

Three values of damping constant, λ , were tried. These values were 2, 4, and 8. The $\underline{k}$ vector was chosen to be (0.0,0.0,0.0) in an $E(\underline{k})$ calculation over 3 cycles. The Mulliken population analysis was accomplished by assuming that $E_{12}(\underline{k},\underline{r})=E_f$. In Figure 11 we see that λ =8 gives the best control over charge distribution oscillations (indicated by
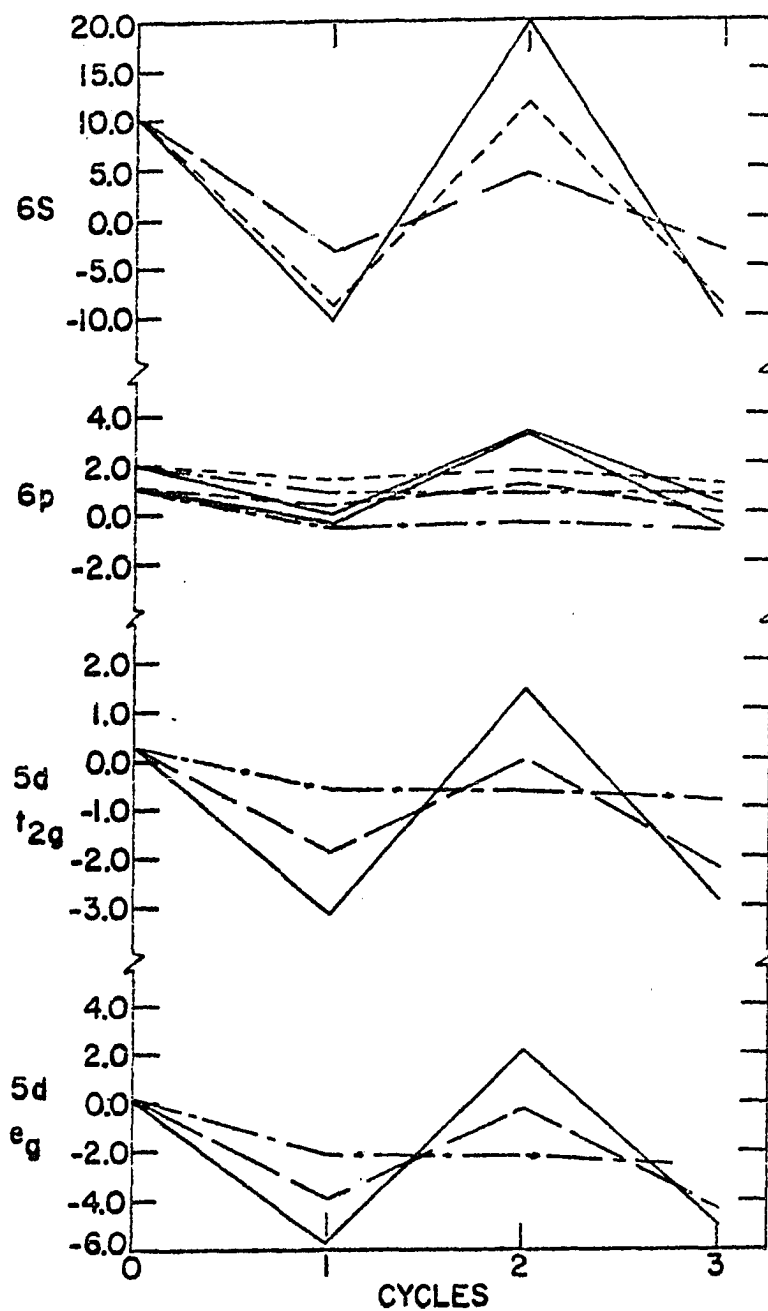
Figure 11. Variation of rhenium energy bands during three cycles (____ λ =2, --- λ =4, _ . ___ λ =8).

variation of metal band energies) which occur in the self-consistency cycling procedure. Furthermore, $\lambda = 8$ gave good convergence for the metal orbital charge distributions after 5 cycles at $\underline{k} = (0.0,0.0,0.0)$, (Figure 12).

Comparison of assumed-calculated charge distributions using $\lambda = 8$ for all $\underline{k}$ vectors with proper weighting of $\underline{k}$ vector degeneracies in the entire Brillouin zone can be made from Table 13.

The 6p type levels at Γ symmetry are spread widely apart, but converge to a narrow band near R symmetry. This phenomenon is an indication of the incomplete self-consistency of 6p charge distributions which have not yet converged to the same value for the $6p_z$, $6p_x$ and $6p_y$ Bloch sums.

Because of the convergence of other charge distributions (5d, 6s, 2s, 2p), we find that only 1 to 2 cycles using all 56 $\underline{k}$ vectors are necessary to approximate self-consistent tight-binding energy bands. The fact that the 6p states do not converge to SCF states is not a serious problem because of the small mixing of 6p states with other rhenium and oxygen states.
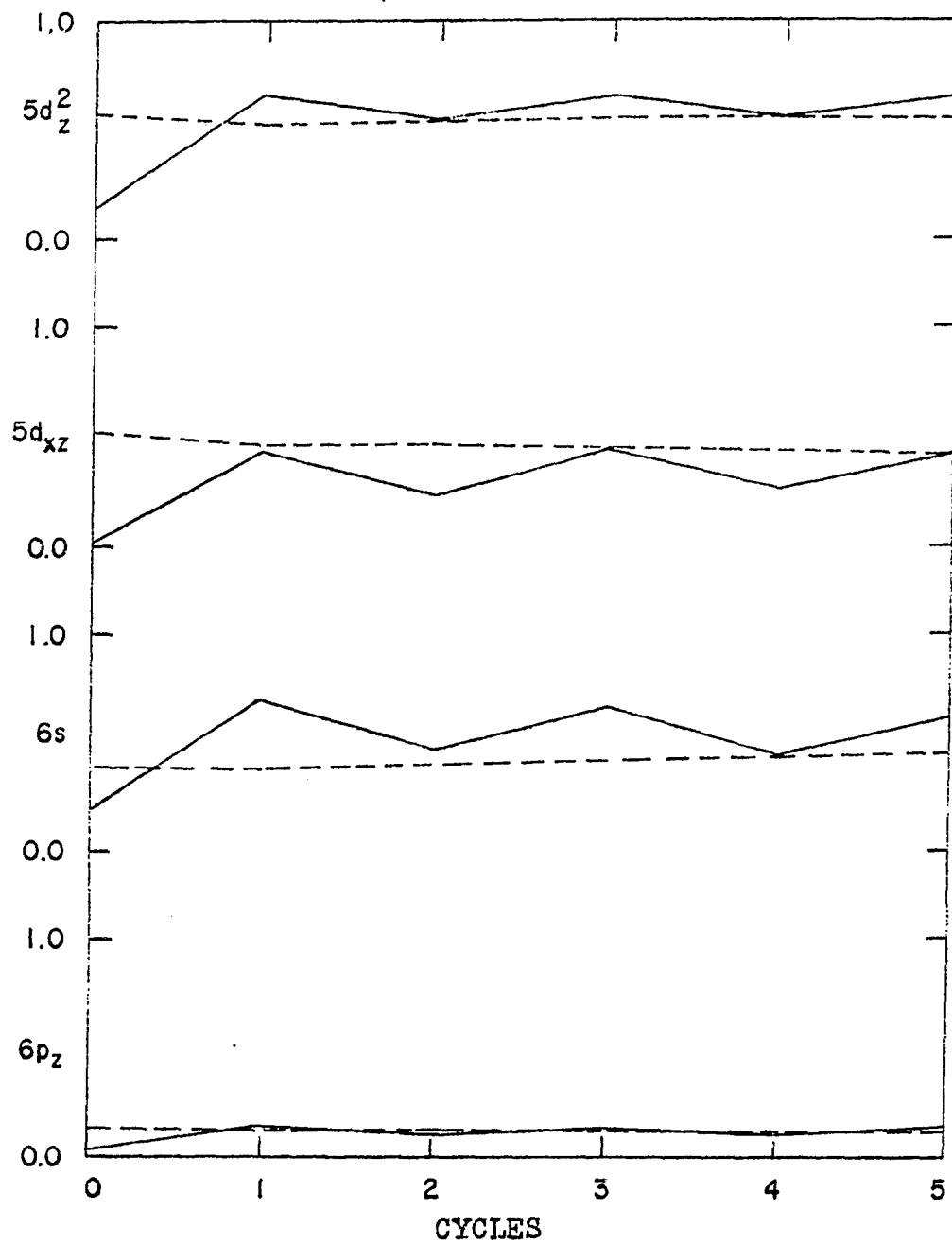
Figure 12. Variation of rhenium atomic orbital occupation numbers at $\lambda = 8$ (---- assumed and ____ calculated).

Table 13. ReO_3 charge distributions

Orbital	Initial charge distribution[a]	Cycle one for 56 k vectors		Cycle two for 56 k vectors	
		assumed	calc.	assumed	calc.
$5d_{z^2}$	0.570000	0.562463	0.508856	0.556507	0.594902
$5d_{xz}$	0.520000	0.419174	0.262088	0.401720	0.440543
$5d_{yz}$	0.520000	0.419321	0.255052	0.401069	0.412365
$5d_{x^2-y^2}$	0.570000	0.562664	0.440582	0.549099	0.601975
$5d_{xy}$	0.520000	0.419408	0.254642	0.401101	0.491285
$6s$	0.400000	0.466548	0.576255	0.478738	0.598266
$6p_z$	0.133333	0.121009	0.156211	0.124920	0.155003
$6p_x$	0.133333	0.122265	0.266513	0.138292	0.304171
$6p_y$	0.133333	0.121786	0.284138	0.139825	0.297851
$2s(1)$	1.000000	0.939621	0.820419	0.926371	0.825832
$2p_z(1)$	0.666667	0.750217	0.885612	0.765261	0.758865
$2p_x(1)$	0.666667	0.571473	0.755541	0.591925	0.745573
$2p_y(1)$	0.666667	0.750037	0.862680	0.762553	0.729168
$2s(2)$	1.000000	0.938646	0.883222	0.932488	0.890104
$2p_z(2)$	0.666667	0.750191	0.843977	0.760612	0.742527
$2p_x(2)$	0.666667	0.750509	0.788706	0.754753	0.594019
$2p_y(2)$	0.666667	0.567457	0.677464	0.579680	0.646704
$2s(3)$	1.000000	0.938929	0.906650	0.935343	0.906099
$2p_z(3)$	0.666667	0.573808	0.556071	0.571837	0.502240
$2p_x(3)$	0.666667	0.750621	0.740925	0.749544	0.593041
$2p_y(3)$	0.666667	0.750488	0.773804	0.753079	0.669813

[a]Values prior to iteration at $\underline{k}=(0.0,0.0,0.0)$.

THE CORRELATION OF THE JOINT DENSITY OF STATES WITH

THE IMAGINARY PART OF THE DIELECTRIC CONSTANT

In the reflectance method (54), one determines the reflectivity R which is given by

$$R = ((n-1)^2 + k^2)/((n+1)^2 + k^2) \tag{66}$$

where n is the real and k is the imaginary part of the refractive index. The complex dielectric constant, ϵ, is related to n and k by

$$\epsilon = \epsilon_1 - i\epsilon_2 = (n-ik)^2 \tag{67}$$

where the real part, ϵ_1, is n^2-k^2 and the imaginary part, ϵ_2, is 2nk. ϵ_2 is a function of a photon frequency, ω, (54) i.e.

$$\epsilon_2(\omega) = \frac{4\pi^2 e^2 \hbar}{2m^2\omega^2} \sum_{o,u} \int_{B.Z.} (2/(2\pi)^3) \cdot$$

$$\cdot \delta(\omega_{o,u}(\underline{k})-\omega) \cdot |M_{o,u}(\underline{k})|^2 \, d^3\underline{k} \tag{68}$$

where e, $\hbar$ and m are the electric charge, Planck's constant divided by 2π and the electron mass. The subscripts o and u refer to occupied and unoccupied bands, respectively. $\omega_{o,u}(\underline{k})$ corresponds to the electronic transition energy at a particular wave vector $\underline{k}$ or $\omega_{o,u}(\underline{k})=(E_u(\underline{k})-E_o(\underline{k}))/\hbar$. The momentum matrix element, $M_{o,u}(\underline{k})$, is expressed as $\langle \Psi_o(\underline{k},\underline{r})| - i\nabla|\Psi_u(\underline{k},\underline{r})\rangle$ between crystal orbitals o and u (Equation 7). $M_{o,u}(\underline{k})^* \cdot M_{o,u}(\underline{k})$ or $|M_{o,u}|^2$ is related to the transition probability of an electron in state o being promoted by some electromagnetic interaction, eg. light waves, into state u.

The delta function is defined by

$$\delta(\omega_{o,u}(\underline{k}) - \omega) = 1 \quad \text{if } | \omega_{o,u} - \omega| \leq (\Delta\omega/2)$$
$$= 0 \quad \text{otherwise} \tag{69}$$

The momentum matrix element can be considered to be constant throughout the Brillouin zone (B.Z.) and the factor $4\pi^2 e^2 \hbar/3m^2\omega^2$ may be taken as a constant as well. Thus, the behavior of ϵ_2 is determined essentially by the quantity

$$J_{o,u}(\omega) = \frac{1}{\Delta\omega}\int_{B.Z.} \frac{2}{(2\pi)^3} \delta(\omega_{o,u}(\underline{k}) - \omega)d^3k \tag{70}$$

which is the joint density of states for the two bands indexed by o and u. Feinleib (14) points out that this quantity could be an important parameter in energy band calculations. Accordingly, $J_{o,u}(\omega)\cdot\Delta\omega$ is the number of pairs of states in bands o and u with

$$\hbar(\omega - \Delta\omega/2) \leq (E_u(\underline{k})-E_o(\underline{k})) \leq \hbar(\omega + \Delta\omega/2) \tag{71}$$

Brust (55) suggests a sampling procedure which replaces the integral in Equation 70 by a finite sum. We have

$$J_{o,u}(\omega = \omega_i) = \frac{\Delta^3k}{\Delta\omega} \frac{2}{(2\pi)^3} \sum_{\underline{k}} \delta(\omega_{o,u}(\underline{k}) - \omega_i) \tag{72}$$

where $\underline{k}$ is a set of uniformly spaced sampling points lying within the first B.Z. The sum is defined for a set of values ω_i such that $\omega_{i+1} = \omega_i + \Delta\omega$. Δ^3k is the volume surrounding the sampling points. In our TBA calculations, we take a

cubic mesh of $\Delta^3 k = \left[.2 \frac{\pi}{a} \right]^3$ where $\underline{a}$ is the lattice constant. We chose a value of .04 Ryd. for Δ E to give the joint density of states vs. energy histogram. The degeneracy of $\underline{k}$ vectors is included in the sum which gives a total of 1000 sampling points in the Brillouin zone. The calculated joint density of states may be compared with ϵ_2 found by Feinleib (14). He determined optical properties of ReO_3 by the reflectance method over the photon energy range 0.1 to 22 e.v. In Table 14 we show a comparison of our peaks (Figure 13) in the joint density of states and the maxima in the ϵ_2 values found by Feinleib.

Table 14. Joint density of states peaks of ReO_3

Rydberg units	Electron-volts	Feinleib results
0.06	0.816	
0.16	2.18	2.30
0.26	3.54	4.20
0.46	6.26	
0.54	7.35	7.0
0.60	8.16	8.5
0.74	10.03	9.3
0.90	12.22	
1.14	15.52	14.0

We wish to obtain experimental verification from the ϵ_2 maxima Feinleib calculates from reflectivity data. The Feinleib peaks are placed along side the closest joint density
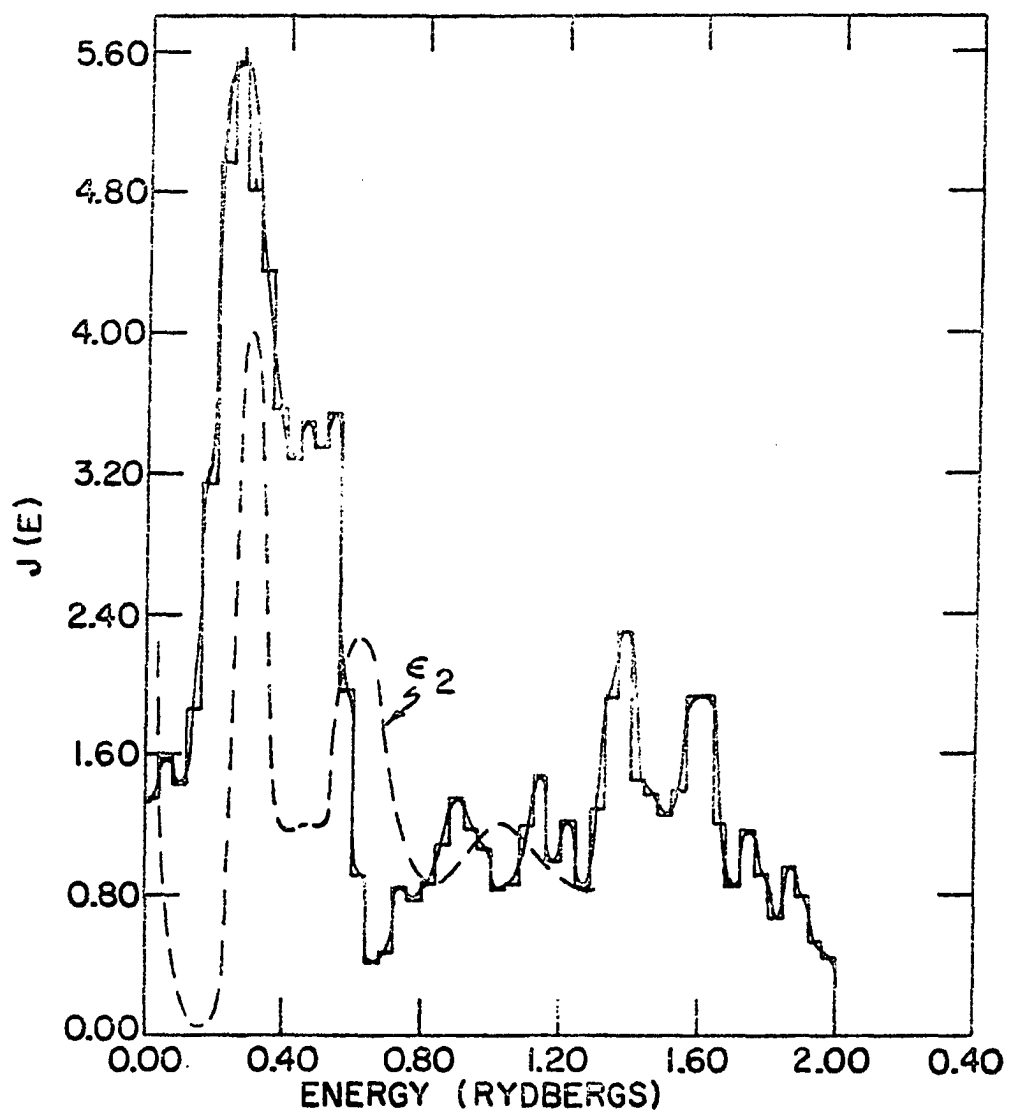
Figure 13. Joint density of states: ReO_3.

of states peak. The low energy maximum begins 3.5 e.v. and extends to 4.2 e.v. where the latter is observed experimentally. Other peaks which are not observed can partially be explained since the probability of intraband transition has been neglected in obtaining the joint density of states. Thus, forbidden transitions indicated by a zero momentum integral are included.

Since a low energy maximum has been detected in our analysis, we conclude that our calculated results have correlated with the observed optical properties of ReO_3.

FERMI SURFACE

Marcus (15) has made a number of de Haas-van Alphen measurements of ReO_3. Mattheiss was the first to give a theoretical description of the Fermi surface. He finds that:

1) The α sheet is centered close to the Γ point. The constancy of the related areas in 100, 110, 111, etc., directions for the measure frequencies, implies that the sheet of the Fermi surface is essentially spherical in shape. The orbit is therefore closed.

2) The β sheet is larger than the α sheet but is also shaped around the Γ point. However, it has a more cubic shape with rounded corners. This orbit is also closed.

3) Finally, the γ sheet consists of tubes which extend out from the Γ point along all x, y, z directions. Besides having an open orbit at the 100, 001, 010 faces, another open orbit moves along the curvature of the tubular structure.

In Figure 14, we give the intersection of the Fermi surface with symmetry points and lines along the 100 and 110 directions for the Mattheiss results and ours. The overall agreement with three sheet-Fermi surface theory is better than expected but two other sheets are found, open as the γ sheet. The spherical sheet about R can be explained by the stabiliz-ation noted in energy bands at R symmetry. Again, no adjust-ments have been made in our calculations to obtain these results.

(a) Mattheiss: ReO_3
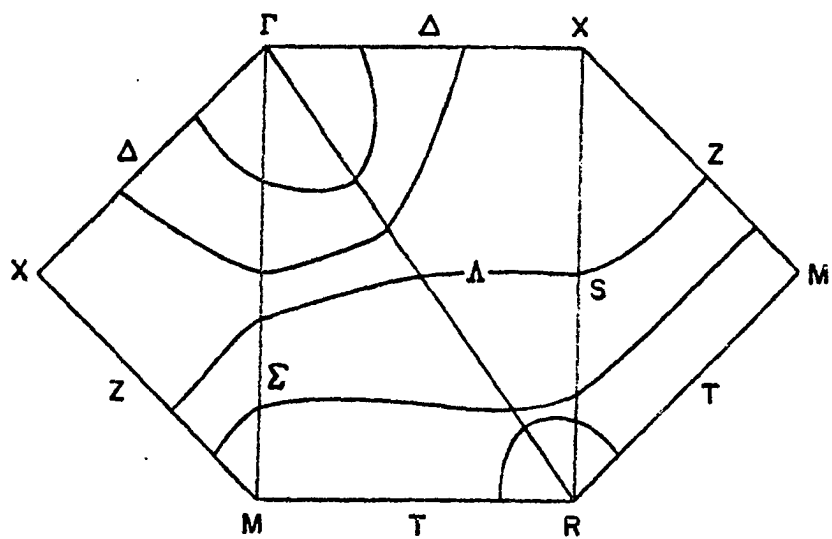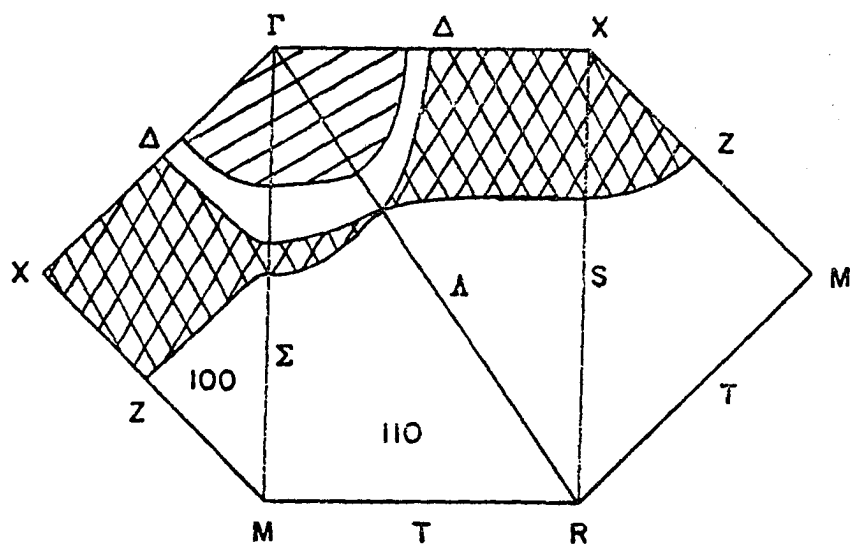
(b) TBA method: ReO_3

Figure 14. Intersection of Fermi surface with planes defined by symmetry points and lines.

SUMMARY

We now give a quantitative, within our TBA limitations, answer to the question "why is rhenium trioxide a conductor?" The $2p\pi$ energies are relatively unchanged from that of the neutral oxygen 2p orbitals because of Madelung effects. But $5d_\pi$ orbitals are stabilized by the Madelung effect of the crystal potential at R and M symmetry to become suitable for bonding with $2p_\pi$ orbitals since $5d_\pi$ -$2p_\pi$ overlap is significant (Table 3). It appears that energy bands which should be considered to have some contribution to the conduction are σ type bands which are immediately above the π band. The metal σ^* or e_g^* orbitals combine with the oxygen $2p_\sigma$ orbitals to form these σ type bands. Thus, even though 2p-2p overlap is small and incapable of promoting conduction of electrons, mixture with $5d_\pi(t_{2g})$ states at M and R symmetry where the minimum occurs in the conduction band allows the non-bonding $2p_\pi$ bands to be the prime cause of conduction in ReO_3.

The small and negative Knight shift of ^{187}Re NMR resonance in ReO_3 measured by Narath and Barham (56) correlates with our calculated absence of tungsten 6s states near the Fermi level.

It is interesting to observe that Mattheiss also has a bonding model of the ReO_3 Fermi surface but with the $5d_\pi$ contribution being the prime source of conduction with small contribution of $2p_\pi$ orbitals. Also, he has an e_g type band

just above this t_{2g} manifold which he attributes to crystal effects of the octahedral electrostatic potential field. The similarity of his model with ours in the existence of an e_g-t_{2g} arrangement suggests that perhaps our TBA method is describing physically the same picture as the APW method. This may explain how our results correlate well with experiment as Mattheiss' results.

We have an e_g* or σ * band where Mattheiss does, but a good portion of the $5d_z^2$-$5d_{x^2-y^2}$ contribution is within the 2s bands which are also σ like. The ability of the TBA method to quantitatively analyze atomic orbital contributions allows us to gain a clearer picture of chemical binding in solids. This is possible because we introduce chemical concepts directly into the TBA model. For instance, we include overlap and electronic interaction terms explicitly instead of using empirical parameters. Then, application of the Mulliken population analysis follows to give a complete picture of chemical binding. We, therefore, not only know what the atomic orbital charge distributions are in the crystal orbitals $\Psi_i(\underline{k},\underline{r})$ for the i th energy band, but have a good idea as to how they got there, e.g. by overlap and Madelung effects.

PART III. TIGHT-BINDING ENERGY BANDS OF
POTASSIUM TANTALATE AND SODIUM TUNGSTEN BRONZE

INTRODUCTION

Cubic strontium titanate, $SrTiO_3$, potassium tantalate, $KTaO_3$, and sodium tungsten bronze, Na_xWO_3 $(0.4 \leq x < 1.0)$ have been the subject of a wide variety of experimental work as is shown in Table 16.

Many workers in the field of perovskite transition metal oxides have attempted to explain the conduction of electrons in the tungsten bronzes, (Table 15).

Table 15. Theoretical models based on various experimental evidence

Name	Atomic orbital constituting lowest conduction band
Sienko (39)	W $5d_{\pi}(t_{2g})$ states
Keller (57)	W 6s states
Mackintosh (58)	Na 3p states
Fuchs (38)	Na states
Goodenough (40)	π bonded O and W 5d (t_{2g}) states

Ours is the first attempt to obtain the tight-binding energy bands of $Na_xWO_3(x=1.0)$. Even though the complete filling of perovskite holes by sodium, $x=1.0$, has not been accomplished at present, this hypothetical substance allows us to study the trend - ReO_3 - $NaWO_3$ - $KTaO_3$ where a metal - non metal transition exists.

Table 16. Summary of experimental data pertinent to energy band structures of transition metal oxides

Experimentalist and method	Observations and conclusions
SrTiO₃	
Gundy(59): absorption measurements	Energy gap is at 3.15 e.v.
Cohen and Blunt(60): reflectivity and electroreflectance in the neighborhood of the fundamental absorption edge	Band gap is observed at 3.4 e.v.
Frederikse et al.(61): magnetoresistance and Shubnikov-de Haas effect	Minima lie along the 100 direction.
Tufte and Stelzer(62): piezo-resistance	Minima lie at the center of the Brillouin zone.
Noland(63): optical transition measurements	Absorption edge is at 3.22 e.v.
DiDomenico and Wemple(64): optical measurements	Band gap is at 3.4 e.v.
Feldman and Horowitz(65): rotary transmission measurements of stress-induced dichroism	A direct transition at zone edge (X) is improbable.
Cardona(66): reflectivity measurements	Absorption peaks observed at: 3.2,4.0,4.86,5.5,6.52,7.4 9.2,9.9,12.5 and 15.3 e.v.
Malitson(67): high precision measurements of the refractive index	The data can be fitted to a Sellmeir relation with the major oscillator at 4.4 e.v.
Baer(68): intraband Faraday rotation	The rotation is negative, monatonically increasing in magnitude as band gap is approached. This implies a p-d fundamental absorption with band gap at 3.4 e.v.

$SrTiO_3$

Table 16(Cont.)

Experimentalist and method	Observations and conclusions
SrTiO$_3$	
Schooley et al.(69): uni-axial stress on the super-conducting critical temp-erature	The presence of supercond-uctivity indicates that the conduction band minima is located off $k=0$ and the effect of the stress indic-ates that the minima is in the 100 direction.
KTaO$_3$	
Frova and Boddy(70): electro-reflectance	Singularities observed in the 100 direction were: 3.57,3.80,4.40,4.88 and 5.5 e.v.
Wemple(71): photoconductivity and reflectance measurements	The photoconductivity peak was observed to be 3.58 e.v. and the absorption band gap to be at 3.50 e.v.
Baer(68): Faraday rotation	The rotation was negative for the same reasons as for SrTiO$_3$ The band gap was estimated to be about 3.80 e.v.
DiDomenico and Wemple(64): absorption measurements	Band gap is 3.9 e.v.
Na$_x$WO$_3$	
Brown and Banks(72):absorp-tion spectra measurements with varying x values	A 4100 Å absorption peak is obtained for a value of x =1.0 by extrapolation of the observed data.

Table 16(Cont.)

Experimentalist and method	Observations and conclusions

Na_xWO_3

Fromhold and Narath(73): nuclear magnetic resonance measurements

Narath and Wallace(74): ibid

Jones et al.(75):ibid

Studies reveal a very small or zero Knight shifts for both the Na and W nuclei. Thus s orbitals of alkali atoms cannot participate to the lowest conduction band but 5d and 6p (but not 6s) orbitals of W may do so.

Greiner et al.(76):magnetic susceptibility measurements

Weak temperature independent paramagnetism is found.

Sienko and Gulick(77): ^{19}F NMR studies of potassium tungsten fluoroxide bronzes

Oxygen was partially substituted by ^{19}F. The Knight shift is less than 0.001%.

Dickens et al.(78): measured reflectance spectra of the $Na_xWO_3, WO_{2.92}, WO_{2.72}, WO_3$

Low energy peak present in the bronzes but not WO_{2+x} (1.39 e.v.). 3.30 e.v. band gap extrapolated from data for x=1.0 .

Vest et al.(51): low temperature specific heat measurements

Obtained electronic specific heat coef. for x=.56 to .86. The extrapolated density of states at x=1 is $2.2X10^{22}$ electron states/e.v.-cc.

Gardner and Danielson(79): measurement of electrical conductivity

The bronzes are conductors from .45 to 1.0 x values. A maximum in conductivity is observed at .75.

Although $SrTiO_3$ tight-binding energy bands have been obtained by Kahn-Leyendecker (41), the related compound $KTaO_3$ has not been studied theoretically. Our theoretical investigation of $KTaO_3$, therefore, provides the first attempt to use TBA energy bands to interpret the optical and insulator properties of $KTaO_3$.

In Table 17 we have $KTaO_3$ and $Na_xWO_3(x=1.0)$ overlap integral values which may be compared with the ReO_3 values in Table 3. Thus, the overlap criterion can be applied to establish a TBA interaction model as was done for ReO_3. For example, if we consider $KTaO_3$, a reasonable TBA interaction vector set is listed in Table 18. Of course, the potassium atom is replaced by sodium if we consider $Na_xWO_3(x=1.0)$.

Attempts to calculate TBA energy bands for $SrTiO_3$ with inclusion of the Ti 4s and 4p orbitals in the Bloch sum basis have failed for the nearest-neighbor model because of the large 4s-4s overlap, about 0.4. The problem exists in the evaluation of the 4s Bloch sum normalization constant in Equation 14. The exponential $\exp(i\underline{k}\cdot\underline{R}_i)$ gives rise to $2\cos(\underline{k}\cdot\underline{R}_i)$ since interactions are in $\pm$ directions. The values of $\underline{k}\cdot\underline{R}_i$ are close to π for $SrTiO_3$, therefore, the cosine is negative. The large value of the 4s-4s overlap integral causes the normalization constant squared to be negative or the impossible situation of an imaginary normalization constant. The failure of the nearest-neighbor model has also been noted by André (80).

Table 17. Overlap integrals in $KTaO_3$ and $Na_xWO_3(x=1.0)$

a	b	Θ_B	ϕ_B	$KTaO_3$ R(a.u.)	S_{AB}	$Na_xWO_3(x=1.0)$ R(a.u.)	S_{AB}
$5d_z^2$	$5d_z^2$	90	0	7.537793	0.012787	7.306311	0.010404
		0	0	7.537793	0.038959	7.306311	0.032668
$5d_{xz}$	$5d_{xz}$	90	0	7.537793	-0.024221	7.306311	-0.018871
		90	90	7.537793	0.004063	7.306311	0.002983
$5d_{x^2-y^2}$	$5d_{x^2-y^2}$	90	0	7.537793	0.030235	7.306311	0.025247
		0	0	7.537793	0.004063	7.306311	0.002983
6s	6s	90	0	7.537793	0.149123	7.306311	0.146516
$6p_z$	$6p_z$	90	0	7.537793	0.073803	7.306311	0.077109
$5d_z^2$	2s	90	0	3.768896	-0.109242	3.653156	-0.105011
		0	0	3.768896	0.218485	3.653156	0.210022
$5d_z^2$	$2p_z$	180	0	3.768896	0.130349	3.653156	0.134755
$5d_{xz}$	$2p_x$	0	0	3.768896	0.095468	3.653156	0.095019
$5d_{x^2-y^2}$	2s	90	0	3.768896	0.189213	3.653156	0.181884
$5d_{x^2-y^2}$	$2p_x$	90	180	3.768896	0.112836	3.653156	0.116701

Table 17(Cont.)

a	b	θ_B	ϕ_B	$KTaO_3$		$Na_xWO_3(x=1.0)$	
				R(a.u.)	S_{AB}	R(a.u.)	S_{AB}
6s	2s	90	0	3.768896	0.260562	3.653156	0.269152
$6p_z$	2s	0	0	3.768896	0.405824	3.653156	0.416765
$6p_z$	$2p_z$	90	0	3.768896	0.102230	3.653156	0.108742
2s	2s	90	45	5.330024	0.004139	5.166342	0.005391
$2p_x$	2s	90	45	5.330024	0.003356	5.166342	0.004384
$2p_z$	$2p_z$	90	45	5.330024	0.000605	5.166342	0.000828
$5d_z^2$	ns[a]	54.7	45	6.527920	0.000000	6.327451	0.000000
$5d_{xz}$	ns	54.7	45	6.527920	0.025464	6.327451	0.036625
$5d_{x^2-y^2}$	ns	54.7	45	6.527920	0.000000	6.327451	0.000000
6s	ns	54.7	45	6.527920	0.355602	6.327451	0.315373
$6p_z$	ns	54.7	45	6.527920	0.170806	6.327451	0.186985
2s	ns	45	90	5.330024	0.163196	5.166342	0.149607

[a]n equals 4 for $KTaO_3$ and 3 for $Na_xWO_3(x=1.0)$.

132

Table 17(Cont.)

a	b	Θ_B	ϕ_B	KTaO$_3$		Na$_x$WO$_3$(x=1.0)	
				R(a.u.)	S$_{AB}$	R(a.u.)	S$_{AB}$
$2p_x$	ns	45	90	5.330024	0.000000	5.166342	0.000000
$2p_z$	ns	45	90	5.330024	0.032728	5.166342	0.041873
$5d_z{}^2$	np_z	54.7	45	6.527920	0.059551	6.327451	0.051505
$5d_{xz}$	np_z	54.7	45	6.527920	-0.002021	6.327451	-0.013406
$5d_{x^2-y^2}$	np_z	54.7	45	6.527920	0.000000	6.327451	0.000000
6s	np_z	54.7	45	6.527920	-0.279541	6.327451	-0.243009
$6p_z$	np_z	54.7	45	6.527920	0.043065	6.327451	0.051631
2s	np_z	45	90	5.330024	-0.191010	5.166342	-0.174044
$2p_x$	np_z	45	90	5.330024	0.000000	5.166342	0.000000
$2p_z$	np_z	45	90	5.330024	-0.013421	5.166342	-0.025070
$5d_z{}^2$	np_x	54.7	45	6.527920	-0.029775	6.327451	-0.025752
$5d_{xz}$	np_x	54.7	45	6.527920	-0.002021	6.327451	-0.013406

133

Table 17(Cont.)

a	b	θ_B	ϕ_B	KTaO₃		Na$_x$WO₃(x=1.0)	
				R(a.u.)	S_{AB}	R(a.u.)	S_{AB}
$5d_{x^2-y^2}$	np_x	54.7	45	6.527920	0.051572	6.327451	0.044604
6s	np_x	54.7	45	6.527920	-0.279541	6.327451	-0.243009
$6p_z$	np_x	54.7	45	6.527920	-0.192713	6.327451	-0.192178
2s	np_x	45	90	5.330024	0.000000	5.166342	0.000000
$2p_x$	np_x	45	90	5.330024	0.046236	5.166342	0.043181
$2p_z$	np_x	45	90	5.330024	0.000000	5.166342	0.000000

Table 18. TBA interaction vector set for KTaO3

Interaction	Vectors in terms of unit cell translation vectors[a]		
	T1	T2	T3
Ta-Ta	1.0	0.0	0.0
	-1.0	0.0	0.0
	0.0	1.0	0.0
	0.0	-1.0	0.0
	0.0	0.0	1.0
	0.0	0.0	-1.0
Ta-O_1	0.5	0.0	0.0
	-0.5	0.0	0.0
Ta-O_2	0.0	0.5	0.0
	0.0	-0.5	0.0
O_1-O_2	-0.5	0.5	0.0
	-0.5	-0.5	0.0
	0.5	0.5	0.0
	0.5	-0.5	0.0
Ta-O_3	0.0	0.0	0.5
	0.0	0.0	-0.5
O_1-O_3	-0.5	0.0	0.5
	-0.5	0.0	-0.5
	0.5	0.0	0.5
	0.5	0.0	-0.5
O_2-O_3	0.0	-0.5	0.5
	0.0	-0.5	-0.5
	0.0	0.5	0.5
	0.0	0.5	-0.5

[a]In terms of components (X, Y, Z), the unit cell translation vectors in Angstrom units are:

$T1$ = (3.980, 0.0, 0.0)
$T2$ = (0.0, 3.980, 0.0)
$T3$ = (0.0, 0.0, 3.980).

Table 18(Cont.)

Interaction	Vectors in terms of unit cell translation vectors		
	T1	T2	T3
Ta-K	0.5	0.5	0.5
	0.5	-0.5	0.5
	-0.5	-0.5	0.5
	-0.5	0.5	0.5
	0.5	0.5	-0.5
	0.5	-0.5	-0.5
	-0.5	-0.5	-0.5
	-0.5	0.5	-0.5
O_1-K	0.0	0.5	0.5
	0.0	0.5	-0.5
	0.0	-0.5	-0.5
	0.0	-0.5	0.5
	0.0	0.5	0.5
	0.0	0.5	-0.5
	0.0	-0.5	-0.5
	0.0	-0.5	0.5
O_2-K	0.5	0.0	0.5
	-0.5	0.0	0.5
	-0.5	0.0	-0.5
	0.5	0.0	-0.5
	0.5	0.0	0.5
	-0.5	0.0	0.5
	-0.5	0.0	-0.5
	0.5	0.0	-0.5
O_3-K	0.5	0.5	0.0
	0.5	-0.5	0.0
	-0.5	-0.5	0.0
	-0.5	0.5	0.0
	0.5	0.5	0.0
	0.5	-0.5	0.0
	-0.5	-0.5	0.0
	-0.5	0.5	0.0

We suggest that the essence of the overlap criterion can best be shown by this evaluation of the Bloch sum normalization constant. If the value of this constant is real, we may conclude that the TBA model is possible. Even though 6s-6s overlap in $KTaO_3$ and $Na_xWO_3(x=1.0)$ is larger than the case of ReO_3 (zero value), the values are small enough to allow the TBA method to be applicable.

The obvious remedy to the $SrTiO_3$ situation is to go further out to next-nearest-neighbors, etc., until the normalization constant converges to a real number.

Since the series ReO_3- $Na_xWO_3(x=1.0)$-$KTaO_3$ is complete in itself in describing metal-non metal transitions in perovskite transition metal oxides, we reserve the $SrTiO_3$ calculation to future work. $KTaO_3$ represents a good model of insulators like $SrTiO_3$.

We will now discuss the input and output aspects of the tight-binding calculations of $KTaO_3$ and $Na_xWO_3(x=1.0)$.

ATOMIC ORBITAL FUNCTIONS, ORBITAL ENERGIES, AND
CRYSTAL POTENTIAL

The radial functions of K,Ta,Na and W atoms are Schmidt orthogonalized linear combinations of STO's (Table 19) obtained using the same method as for ReO_3. The least-squares functions used in the evaluation of overlap and nuclear attraction integrals are listed in Table 20.

The shielding constants listed in Table 4 are used to obtain the Coulomb-exchange integrals needed to calculate the crystal potential (Equation 28). The charge distributions for $KTaO_3$ and Na_xWO_3(x=1.0) are listed in Tables 21 and 22 respectively. The oscillations which exist in the preliminary self-consistency cycles at $\underline{k}$=(0.0,0.0,0.0) can be seen in Figure 15. While the $KTaO_3$ energy bands are converging, the sodium tungsten bronze states are definitely diverging. The latter phenomenon occurred because the 3p states are occupied at the gamma point. As will be seen in the discussion on the Mulliken population analysis of crystal orbitals, the 3p states depopulate as we move from the center of the Brillouin zone. Therefore, the average occupation numbers for 3s and 3p Bloch sums should be close to zero.

Because of the above behavior, the Na_xWO_3(x=1.0) crystal potential cannot reliably be iterated at one point in $\underline{k}$ space. In order to utilize the preliminary iteration as efficiently as

Figure 15. Variation per cycle for energy bands (Rydberg
units) corresponding to atomic orbitals in
$KTaO_3$ and $Na_xWO_3(x=1.0)$ (---- $KTaO_3$ and ____
$NaWO_3$). s and p denote perovskite hole
atomic orbitals (3s and 3p on Na, 4s and
4p on K).

CYCLES
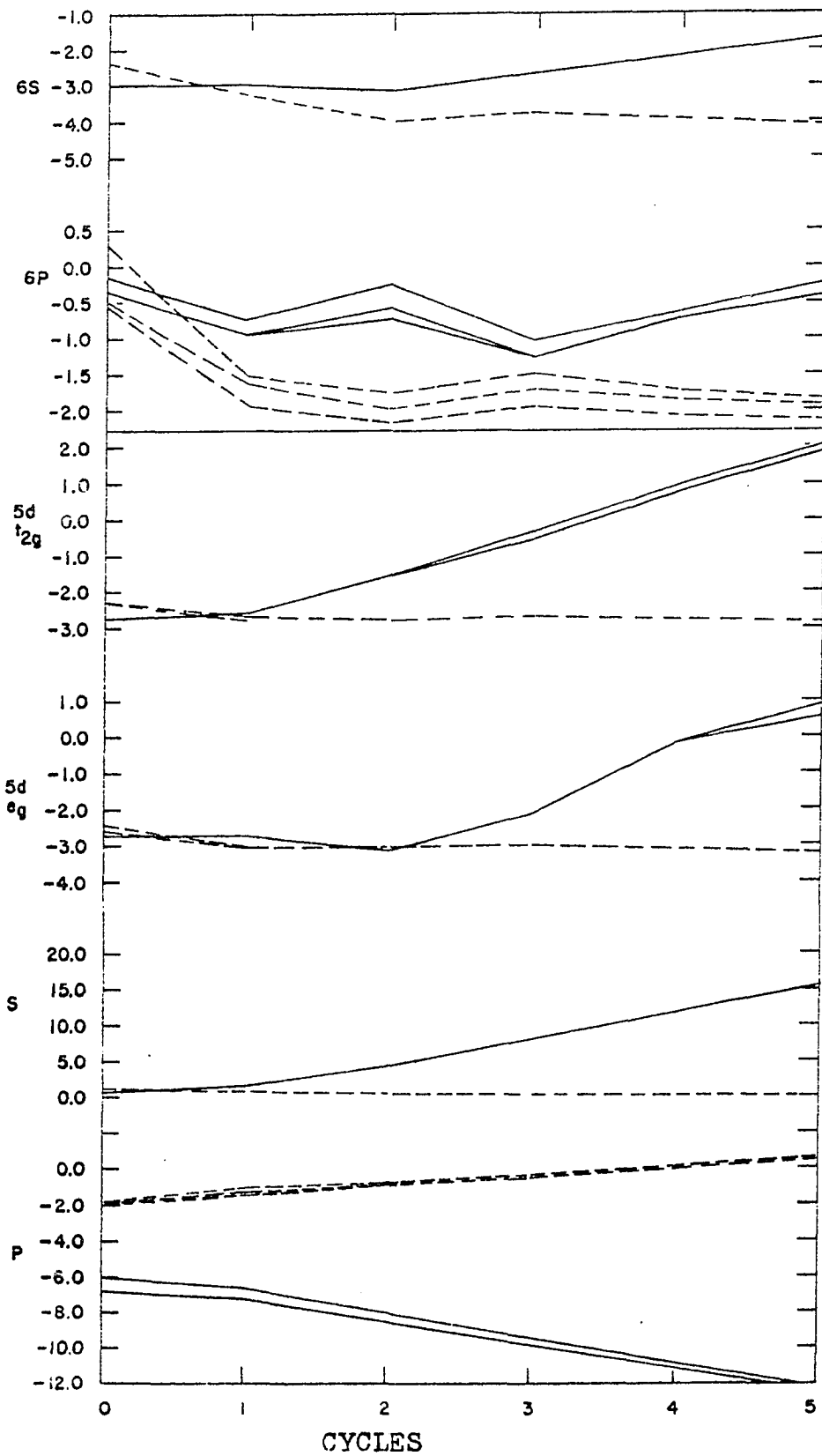
Table 19. Coefficient matrix elements for Schmidt ortho-
gonalized atomic orbital radial function used
in tight-binding calculations of sodium tungsten
bronze and potassium tantalate energy bands

Atomic orbital	$\underline{i}$	$\underline{j}$	T_{ij}	n	ζ
Na 3s	1	1	1.000000	1	10.705400
	1	2	-0.256412	1	10.705400
	2	2	1.032350	2	3.290039
	1	3	0.035387	1	10.705400
	2	3	-0.151461	2	3.290039
	3	3	1.010707	3	0.884802
Na 3p	1	1	1.000000	2	3.641939
	1	2	-0.109832	2	3.641939
	2	2	1.006013	3	0.875209
K 4s	1	1	1.000000	1	18.670288
	1	2	-0.296811	1	18.670288
	2	2	1.043118	2	6.271990
	1	3	0.110129	1	18.670288
	2	3	-0.435717	2	6.271990
	3	3	1.083821	3	2.772440
	1	4	-0.018244	1	18.670288
	2	4	0.072960	2	6.271990
	3	4	-0.199036	3	2.772440
	4	4	1.016745	4	0.920539
K 4p	1	1	1.000000	2	7.580839
	1	2	-0.238385	2	7.580839
	2	2	1.028021	3	2.580910
	1	3	0.045855	2	7.580839
	2	3	-0.211194	3	2.580910
	3	3	1.020888	4	0.910559
Ta 5d	1	1	1.000000	3	19.604000
	1	2	-0.473525	3	19.604000
	2	2	1.106447	4	9.997000
	1	3	0.105200	3	19.604000
	2	3	-0.284400	4	9.997000
	3	3	0.681500	5	4.762000
	3	3	0.577400	5	1.938000
Ta 6s	1	1	1.000000	1	72.584686
	1	2	-0.342833	1	72.584686
	2	2	1.057135	2	26.669189

Table 19(Cont.)

Atomic orbital		$\underline{i}$	$\underline{j}$	T_{ij}	n	ζ
Ta	6s	1	3	0.182006	1	72.584686
		2	3	-0.668358	2	26.669189
		3	3	1.183608	3	14.564799
		1	4	-0.099316	1	72.584686
		2	4	0.382054	2	26.669189
		3	4	-0.877559	3	14.564799
		4	4	1.249496	4	8.609929
		1	5	0.041293	1	72.584686
		2	5	-0.160633	2	26.669189
		3	5	0.389805	3	14.564799
		4	5	-0.689384	4	8.609929
		5	5	1.144889	5	4.597790
		1	6	-0.007583	1	72.584686
		2	6	0.029534	2	26.669189
		3	6	-0.072095	3	14.564799
		4	6	0.130257	4	8.609929
		5	6	-0.240275	5	4.597790
		6	6	1.021850	6	1.857920
Ta	6p	1	1	1.000000	2	34.298294
		1	2	-0.415865	2	34.298294
		2	2	1.083025	3	15.427500
		1	3	0.209432	2	34.298294
		2	3	-0.662656	3	15.427500
		3	3	1.173199	4	8.574400
		1	4	-0.074746	2	34.298294
		2	4	0.244908	3	15.427500
		3	4	-0.518795	4	8.574400
		4	4	1.094313	5	4.251989
		1	5	0.016522	2	34.298294
		2	5	-0.054325	3	15.427500
		3	5	0.117028	4	8.574400
		4	5	-0.273337	5	4.251989
		5	5	1.030778	6	1.837780
W	5d	1	1	1.000000	3	19.929000
		1	2	-0.477561	3	19.929000
		2	2	1.108180	4	10.202000
		1	3	0.113900	3	19.929000
		2	3	-0.307700	4	10.202000
		3	3	0.694000	5	4.982000

Table 19(Cont.)

Atomic orbital		i	j	T_{ij}	n	ζ
W	5d	3	3	0.563100	5	2.068000
W	6s	1	1	1.000000	1	73.588898
		1	2	-0.342941	1	73.588898
		2	2	1.057170	2	27.043488
		1	3	0.182421	1	73.588898
		2	3	-0.669920	2	27.043488
		3	3	1.184391	3	14.786900
		1	4	-0.099891	1	73.588898
		2	4	0.384400	2	27.043488
		3	4	-0.882436	3	14.786900
		4	4	1.251753	4	8.759060
		1	5	0.042293	1	73.588898
		2	5	-0.164625	2	27.043488
		3	5	0.399708	3	14.786900
		4	5	-0.706786	4	8.759060
		5	5	1.151411	5	4.719649
		1	6	-0.007981	1	73.588898
		2	6	0.031108	2	27.043488
		3	6	-0.076006	3	14.786900
		4	6	0.137449	4	8.759060
		5	6	-0.249515	5	4.719649
		6	6	1.023288	6	1.924379
W	6p	1	1	1.000000	2	34.797699
		1	2	-0.416931	2	34.797699
		2	2	1.083435	3	15.672999
		1	3	0.210792	2	34.797699
		2	3	-0.666154	3	15.672999
		3	3	1.174785	4	8.729130
		1	4	-0.077279	2	34.797699
		2	4	0.253140	3	15.672999
		3	4	-0.536281	4	8.729130
		4	4	1.100271	5	4.382429
		1	5	0.017330	2	34.797699
		2	5	-0.056981	3	15.672999
		3	5	0.122881	4	8.729130
		4	5	-0.280071	5	4.382429
		5	5	1.031954	6	1.903520

Table 20.   Least squares functions for Ta, W and K orbitals

Orbital	Least squares function
Ta 5d	0.561897(1.31205) + 0.684028(3.16414) -0.438158(7.63065) + 0.150918(18.4021)
Ta 6s	2.856540(1.41425) - 3.511150(1.99978) +2.434480(2.82772) - 1.997370(3.99845) +1.335460(5.65387) - 0.392740(7.99468)
Ta 6p	1.560500(1.21565) - 1.006810(2.12183) 0.034422(3.70348) + 0.218623(6.46413) -0.093881(11.2826)
W 5d	0.549610(1.40651) + 0.703046(3.32302) -0.476221(7.85101) + 0.166889(18.5489)
W 6s	2.967210(1.47395) - 3.764970(2.07141) +2.701230(2.91104) - 2.228700(4.09102) +1.480270(5.74929) - 0.433006(8.07974)
W 6p	1.576230(1.26262) - 1.027670(2.18974) 0.028008(3.79763) + 0.234639(6.58617) -0.100397(11.4223)
K 4s	1.140140(0.77057) - 0.274258(1.65456) -0.120426(3.55265) + 0.082456(7.62824)
K 4p	1.098740(0.75447) + 0.039917(1.19488) -0.366921(1.89239)

possible, we used the weighted assumed charge distributions after two cycles at $\underline{k}=(0.0,0.0,0.0)$ to obtain input for the final TBA calculation for the 56 $\underline{k}$ vectors. These vectors are determined by the lattice constants of $KTaO_3$ and Na_xWO_3 (x=1.0),which are 3.989 Å (71) and 3.8665 Å (81) respectively, and Table 18.

Table 21. KTaO$_3$ charge distributions

Orbital	Initial charge distribution	Cycle one for 56 k vectors assumed	calculated
5d z 2	0.500000	0.412124	0.404526
5d$_{xz}$	0.300000	0.205142	0.073766
5d$_{yz}$	0.300000	0.206918	0.076799
5d$_{x^2-y^2}$	0.500000	0.394830	0.308389
5d$_{xy}$	0.300000	0.206567	0.072350
6s	0.500000	0.676954	0.547901
6p$_z$	0.033333	0.035517	0.098634
6p$_x$	0.033333	0.038636	0.178331
6p$_y$	0.033333	0.040142	0.385103
2s(1)	1.000000	1.074887	0.830380
2p$_z$(1)	0.666667	0.723710	0.848941
2p$_x$(1)	0.666667	0.760111	0.808833
2p$_y$(1)	0.666667	0.739724	0.790418
2s(2)	1.000000	1.091937	0.732372
2p$_z$(2)	0.666667	0.763929	0.692407
2p$_x$(2)	0.666667	0.771929	0.803928
2p$_y$(2)	0.666667	0.750674	0.751210
2s(3)	1.000000	1.067212	0.759119
2p$_z$(3)	0.666667	0.753050	0.622150
2p$_x$(3)	0.666667	0.727040	0.846893
2p$_y$(3)	0.666667	0.731064	0.794906
4s	0.000000[a]	-0.488564	0.262203
4p$_z$	0.000000	0.021557	0.226848
4p$_x$	0.000000	0.022153	0.117416
4p$_y$	0.000000	0.026123	-0.042396

[a]In order to represent as close as possible to the ReO$_3$ model we chose zero values for potassium orbitals. Even though this choice temporarily violates the charge neutrality of the unit cell, the final iteration over the 56 k vector set corrects for this difference.

Table 22. Na_xWO_3 charge distributions for x=1.0

Orbital	Initial charge distribution	Cycle one for 56 $\underline{k}$ vectors	
		assumed	calculated
$5d_z2$	0.600000	0.540509	0.388784
$5d_{xz}$	0.400000	0.356320	0.082889
$5d_{yz}$	0.400000	0.357455	0.094965
$5d_{x^2-y^2}$	0.600000	0.540394	0.306277
$5d_{xy}$	0.400000	0.357454	0.073552
$6s$	0.500000	0.458284	0.439432
$6p_z$	0.033333	0.025945	0.158390
$6p_x$	0.033333	0.025877	0.142986
$6p_y$	0.033333	0.025530	0.325123
$2s(1)$	1.000000	1.025343	0.832141
$2p_z(1)$	0.666667	0.658260	0.834392
$2p_x(1)$	0.666667	0.692675	0.809648
$2p_y(1)$	0.666667	0.654045	0.551243
$2s(2)$	1.000000	1.025914	0.759421
$2p_z(2)$	0.666667	0.659942	0.884756
$2p_x(2)$	0.666667	0.660065	0.832776
$2p_y(2)$	0.666667	0.692834	0.768167
$2s(3)$	1.000000	1.024786	0.818941
$2p_z(3)$	0.666667	0.692292	0.612055
$2p_x(3)$	0.666667	0.658446	0.831038
$2p_y(3)$	0.666667	0.654157	0.866219
$3s$	0.000000	-0.080707	0.373114
$3p_z$	0.000000	0.096989	0.554747
$3p_x$	0.000000	0.098091	0.052772
$3p_y$	0.000000	0.099100	0.117558

Table 23. $KTaO_3$ and $Na_xWO_3(x=1.0)$ energy parameters[a]

Orbital	Two-electron inter-action energy			One center kinetic energy	Core energy
	$\underline{i}$	$\underline{j}$	$\underline{g}(i,j)$		
Ta 5d	1s	5d	1.413834	9.283373	-93.930159
	2s	5d	1.405152		
	2p	5d	1.408750		
	3s	5d	1.379804		
	3p	5d	1.383094		
	3d	5d	1.392094		
	4s	5d	1.332458		
	4p	5d	1.333250		
	4d	5d	1.347452		
	4f	5d	1.320788		
	5s	5d	1.112624		
	5p	5d	1.073412		
	5d	5d	0.960438		
	6s	5d	0.581030		
	6p	5d	0.573640		
Ta 6s	1s	6s	0.629908	1.370633	-44.801565
	2s	6s	0.626846		
	2p	6s	0.627788		
	3s	6s	0.623608		
	3p	6s	0.624420		
	3d	6s	0.625494		
	4s	6s	0.619166		
	4p	6s	0.619966		
	4d	6s	0.621244		
	4f	6s	0.619850		
	5s	6s	0.606948		
	5p	6s	0.607446		
	5d	6s	0.581030		
	6p	6s	0.444326		
Ta 6p	1s	6p	0.623696	1.412651	-44.134531
	2s	6p	0.621416		
	2p	6p	0.622094		
	3s	6p	0.618870		
	3p	6p	0.619114		
	3d	6p	0.620188		
	4s	6p	0.614456		
	4p	6p	0.614394		
	4d	6p	0.615824		

[a]Rydberg units.

Table 23(Cont.)

Orbital		Two-electron interaction energy			One center kinetic energy	Core energy
		_i_	_j_	g(i,j)		
Ta	6p	4f	6p	0.614470		
		5s	6p	0.601476		
		5p	6p	0.599788		
		5d	6p	0.573640		
		6s	6p	0.444326		
		6p	6p	0.464592		
W	5d	1s	5d	1.505390	10.739013	-100.662215
		2s	5d	1.495006		
		2p	5d	1.499326		
		3s	5d	1.465050		
		3p	5d	1.468974		
		3d	5d	1.479642		
		4s	5d	1.409790		
		4p	5d	1.410822		
		4d	5d	1.427548		
		4f	5d	1.400672		
		5s	5d	1.168008		
		5p	5d	1.126452		
		5d	5d	1.027510		
		6s	5d	0.605248		
		6p	5d	0.597614		
W	6s	1s	6s	0.653252	1.529606	-47.010426
		2s	6s	0.649720		
		2p	6s	0.650798		
		3s	6s	0.646228		
		3p	6s	0.646316		
		3d	6s	0.648222		
		4s	6s	0.641210		
		4p	6s	0.642074		
		4d	6s	0.643516		
		4f	6s	0.642054		
		5s	6s	0.628020		
		5p	6s	0.631162		
		5d	6s	0.605248		
		6s	6s	0.530642		
		6p	6s	0.459920		

Table 23(Cont.)

Orbital	Two-electron inter-action energy			One center kinetic energy	Core energy
	i	j	$g(i,j)$		
W 6p	1s	6p	0.646508	1.552321	-46.311767
	2s	6p	0.644210		
	2p	6p	0.644802		
	3s	6p	0.641214		
	3p	6p	0.641474		
	3d	6p	0.642618		
	4s	6p	0.636332		
	4p	6p	0.636278		
	4d	6p	0.637850		
	4f	6p	0.636292		
	5s	6p	0.622528		
	5p	6p	0.643842		
	5d	6p	0.597460		
	6s	6p	0.459920		
	6p	6p	0.497060		
Na 3s	1s	3s	0.599058	0.485361	-6.210933
	2s	3s	0.579812		
	2p	3s	0.585014		
	3s	3s	0.452126		
	3p	3s	0.375500		
Na 3p	1s	3p	0.589784	0.524253	-5.975097
	2s	3p	0.578078		
	2p	3p	0.579366		
	3s	3p	0.375500		
	3p	3p	0.429974		
K 4s	1s	4s	0.469734	0.457099	-8.549737
	2s	4s	0.463486		
	2p	4s	0.465290		
	3s	4s	0.450782		
	3p	4s	0.452184		
	4s	4s	0.365094		
	4p	4s	0.318634		
K 4p	1s	4p	0.464678	0.491857	-8.347437
	2s	4p	0.460638		
	2p	4p	0.461494		

Table 23(Cont.)

Orbital		Two-electron interaction energy			One center kinetic energy	Core energy
		$\underline{i}$	$\underline{j}$	$g(i,j)$		
K	4p	3s	4p	0.448358		
		3p	4p	0.447218		
		4s	4p	0.318634		
		4p	4p	0.343922		

Atomic orbital parameters used in obtaining tight-binding energy bands are listed in Table 23.

E($\underline{k}$) VS. $\underline{k}$, DENSITY OF STATES, JOINT DENSITY OF STATES AND

RESULTS OF THE MULLIKEN POPULATION ANALYSIS OF $KTaO_3$

The E($\underline{k}$) versus $\underline{k}$ and density of states curves for potassium tantalate are shown in Figure H1 (Appendix H). The energy band values at symmetry points are listed in Table H1. The corresponding results of the Mulliken population analysis are listed in Tables H2-H5 (Appendix H). The Fermi energy is found to be -3.8905 Rydberg units.

The minimum in $KTaO_3$, like ReO_3, conduction band is located at the R symmetry point. This property is evidenced by the rapid drop in valence bands at R accompanied by a minimum in the R_{25}, bands.

The gap between the $2p_{\pi}$ ground state and the t_{2g} type conduction band is 0.3 Ryd. (4.0 e.v.) which is comparable with the observed value of 3.8 e.v. (68). The joint density of states curve shown in Figure 16 with peaks listed in Table 24 gives a peak at 0.3 Ryd. which we identify with this conduction band minimum. Furthermore, most of the peaks compare qualitatively with experimental results (70) as well as resemble the $SrTiO_3$ results (66). The latter agreement suggests a justification for supposing the $KTaO_3$ is a good model for perovskite transition metal oxides which behave as insulators.

The difference between the intermediate e_g states at R_{12} and the top of the valence band is not experimentally available since R_{15},$\rightarrow R_{12}$ transitions are symmetry forbidden as
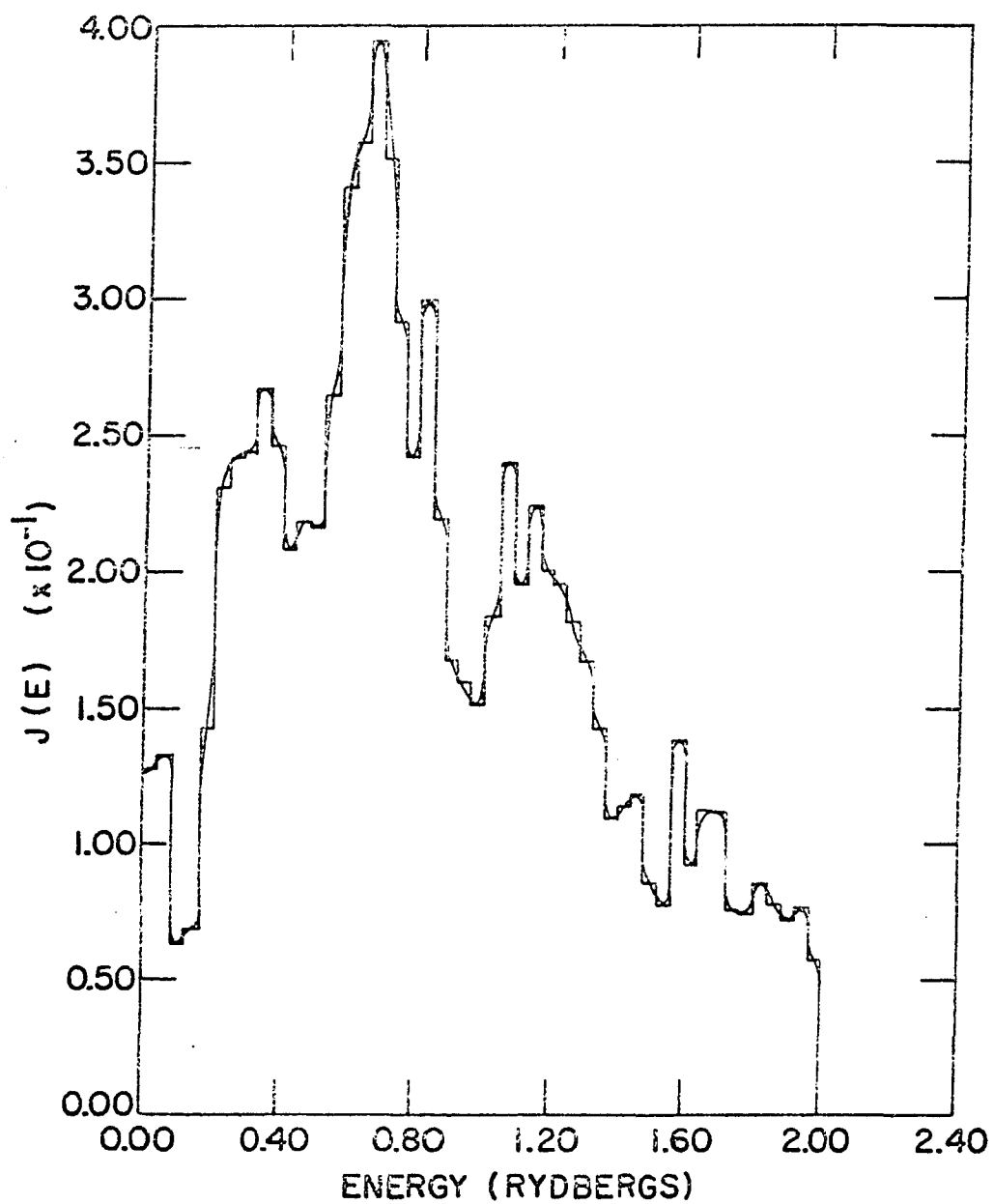
Figure 16. Joint density of states: KTaO₃.

Table 24.   Joint density of states peaks of $KTaO_3$

Rydberg units	Electron-volts	Frova-Boddy results[a]	Cardona results for $SrTiO_3$[a]
0.06	0.816		
0.19	2.58	3.57	3.20
0.28	3.81	3.80	4.00
0.34	4.63	4.40	4.86
0.39	5.31	4.88	5.5
0.46	6.25	5.5	6.52
0.54	7.35		7.40
0.62	8.43		
0.66	8.97		9.20
0.74	10.03		9.9
0.82	11.15		
0.85	11.58		12.5
1.06	14.41		
1.14	15.50		15.3

[a]Results are in electron-volts.

determined by Casella's rules (82). Thus, the 2.58 e.v. peak in the joint density of states (attributed to such a transition) is not obtainable by reflectance spectroscopy.

We now discuss the unusual behavior of 4s and 4p occupation numbers at the symmetry points listed in Tables H2 to H5. The crystal orbitals $\Psi_i(\underline{k},\underline{r})$ are normalized to 1 or $\langle\Psi_i|\Psi_i\rangle = 1$, but large positive and negative n_{i4s} and n_{i4p} values occur. One may argue that the Mulliken population analysis has failed, if we compare the TBA calculation with the usual molecular orbital calculation where negative occupation numbers are forbidden. However, we have a different situation when one applies such a procedure to a crystal. The dependency of

occupation numbers on $\underline{k}$ vectors relaxes the strict require-
ment on positive occupation numbers. However, the average
occupation number over the entire Brillouin zone should be
non-negative since we would then be back to the molecular
situation. The average occupation number may be calculated
to be negative at some stage of iteration of the crystal
potential, but the final number should be positive. For the
most part, our final iteration gives such a result.

The problem of normalization of Bloch sum noted in the
introduction of this part arises in the $KTaO_3$ calculation in
a rather unique way. Because the normalization constant of
6s and 6p Bloch sums at M and R symmetry points is small
(about .1), the TBA method is on the verge of breaking down
for upper states as expected from overlap integrals of 6p-6p
and 6s-6s pairs (Table 17).

The number of electron states/Ryd.-unit cell for $KTaO_3$
is much smaller than the value of 21.1 for ReO_3, in that the
density of states drops abruptly to zero in the band gap
region. Therefore, no estimate of the actual density of
states can practically be made. Within the approximations
used in the TBA method, it is reasonable to assign $KTaO_3$ to
be an insulator as it is thought to be. For the same reason,
no Fermi surface is considered.

E($\underline{k}$) VS. $\underline{k}$, DENSITY OF STATES, JOINT DENSITY OF STATES AND

MULLIKEN POPULATION ANALYSIS OF $Na_xWO_3(x=1.0)$

The E($\underline{k}$) vs. $\underline{k}$ and density of states curves for Na_xWO_3
($x=1.0$) are shown in Figure 11 (Appendix I). The energy band
values at symmetry points are listed in Table 11. The corres-
ponding results of Mulliken population analysis are listed in
Tables 12 to 15 (Appendix I). The Fermi energy is located at
-3.2252 Ryd.

The number of states/Ryd.-unit cell for Na_xWO_3 is found
to be 20.5 or 2.60×10^{22} electron states/e.v.-cm^3 which
corresponds to a value of γ equal to 3.55 millijoules-mole^{-1}
deg^{-2}. The value of 3.0 millijoules-mole^{-1}deg^{-2} from the
extrapolation of experimental (51, 76) values to $x=1.0$ gives
encouraging agreement with our results. Furthermore, it is
interesting that the value of 21.1 for ReO_3 is almost identical
to the 20.5 value for $Na_xWO_3(x=1.0)$.

Let us expand the picture of bands in the Fermi level
region to produce Figure 17 and then use the Mulliken popula-
tion analysis results in Tables 12 to 15 (Appendix I) to
quantitatively determine why Na_xWO_3 should be a conductor at
$x=1.0$.

We no longer have the simple picture postulated for ReO_3
and $KTaO_3$ since most low lying conduction bands cross the
Fermi level nearly perpendicularly. Even the 6s type band
crosses the Fermi level at X symmetry. However, the low lying
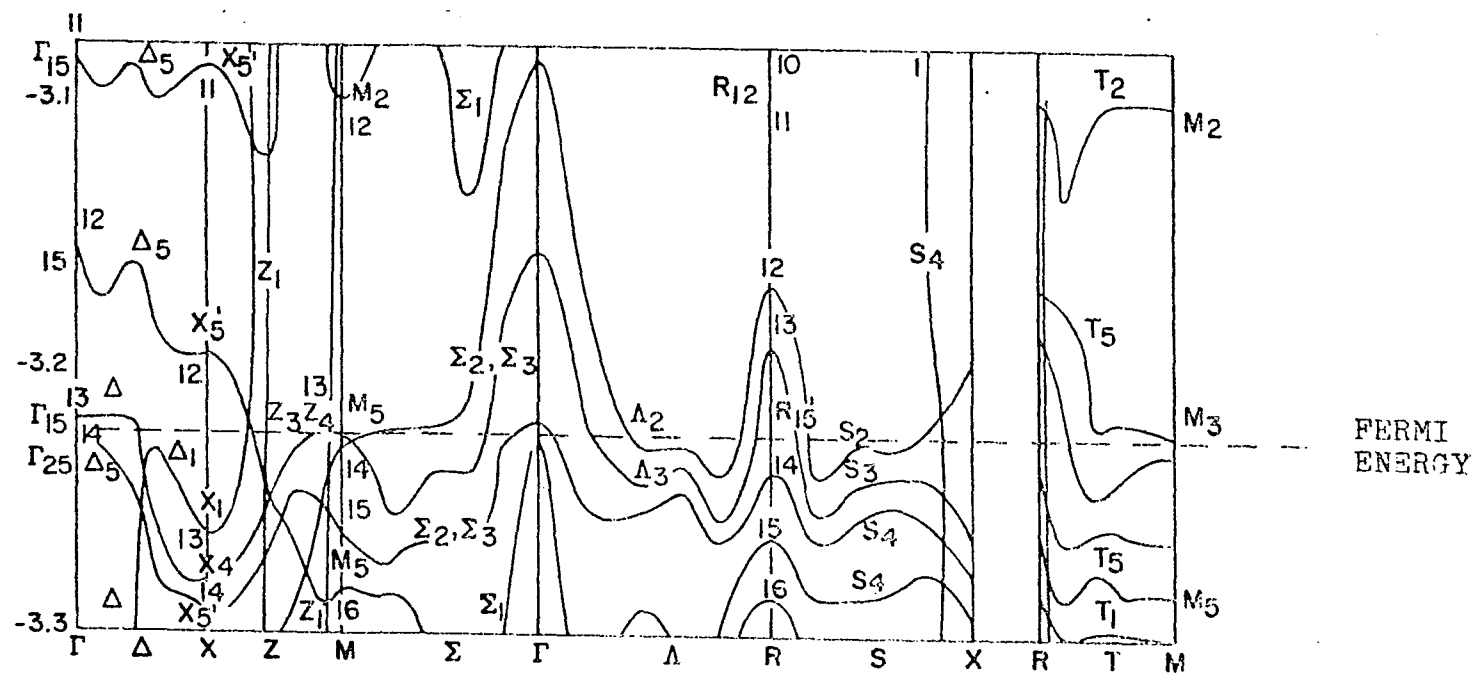
Figure 17. Energy bands of $Na_xWO_3(x=1.0)$ in the region of the Fermi energy (numbers denote i th energy band).

eg type conduction band crosses in many places. We may conclude that conduction is associated primarily with $5d_{eg}$ orbitals.

Projections of the Fermi surface in the 1/48th reduced zone are shown in Figure 18. We predict three Fermi surface sheets which may eventually be correlated with de Haas van Alphen measurements.

The joint density of states is shown in Figure 19 and the corresponding peaks are tabulated (Table 25). Comparison of the low energy peaks with experiment can only be by extrapolation, but agreement with Dicken's results (78) is reasonably close.

Table 25.   Joint density of states peaks for Na_xWO_3
(x=1.0)

Rydberg units	Electron-volts
0.08	1.09
0.18	2.44
0.30	4.08
0.42	5.72
0.54	7.35
0.59	8.03
0.85	11.58
0.98	13.31
1.14	15.51
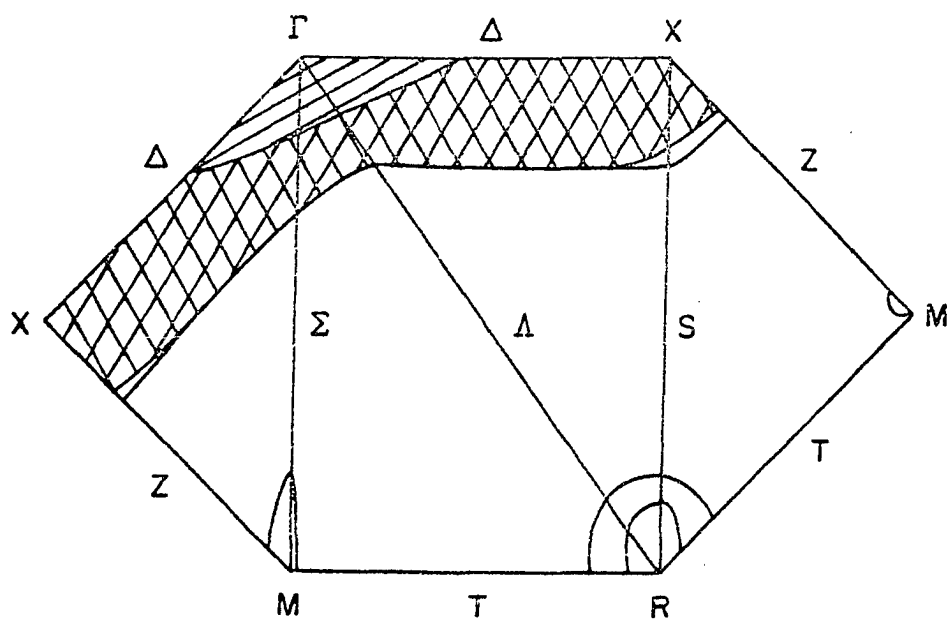
Figure 18.   TBA method: NaWO₃.
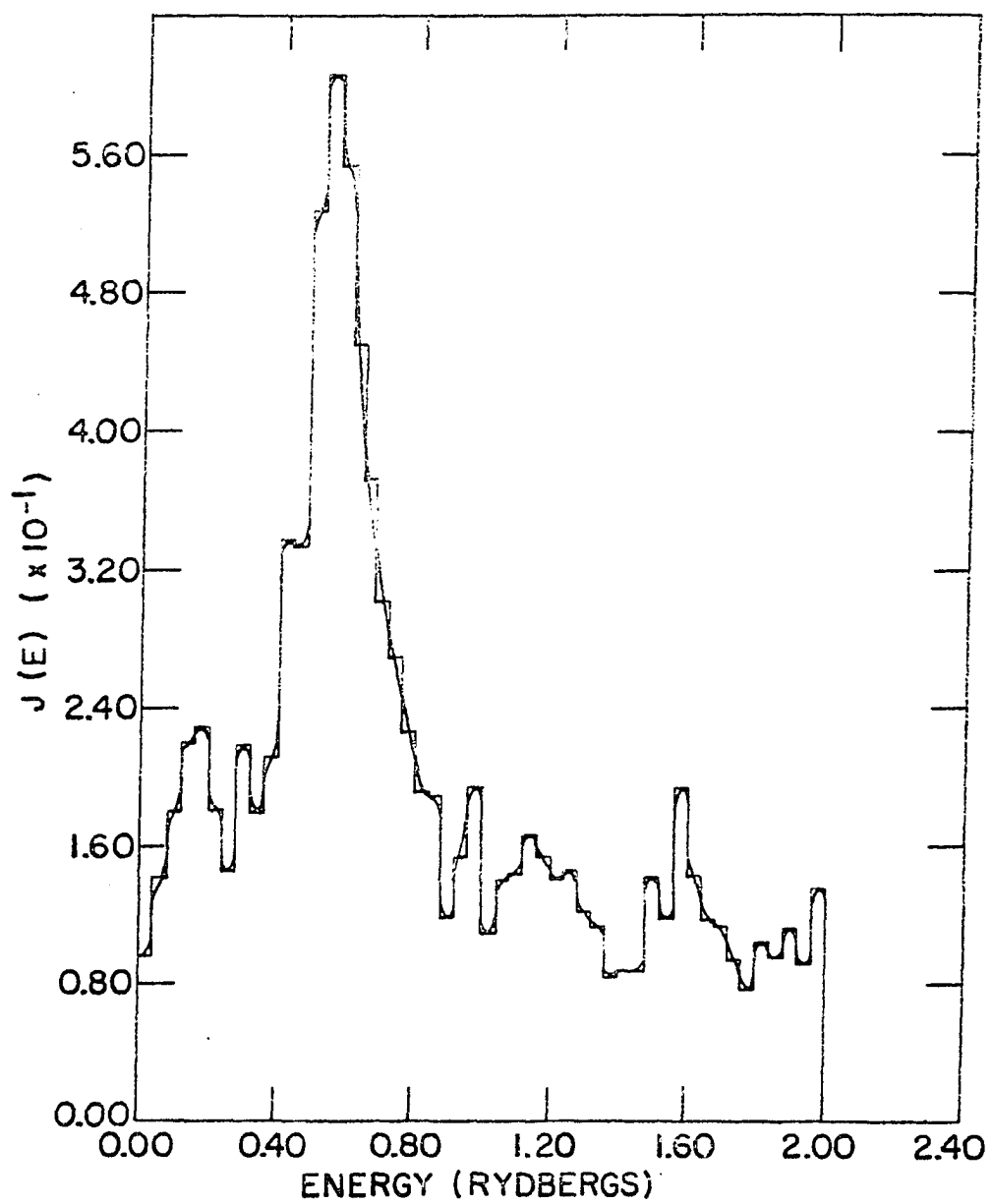
Figure 19. Joint density of states: NaWO$_3$.

PART IV. DISCUSSION

We have utilized the overlap criterion to set up the TBA interaction model for nearest-neighbor atoms. Then we have proceeded in a "semi-rigorous" manner to make theoretically justifiable approximations to make $E(\underline{k})$ vs. $\underline{k}$ calculations practical. The proper choice of good atomic orbital functions and the explicit evaluation of all two-center integrals (overlap, nuclear attraction, Coulomb, and exchange) enables us to quantitatively investigate chemical effects in crystals, eg. Madelung and overlap effects.

The approximation of the crystal potential as a linear combination of atomic potentials is an important part of the LCAO procedure. By using the Mulliken population analysis over all $\underline{k}$ space, we are able to treat this crystal potential in a SCF-MO manner. Thereby, we obtain an internal handle for controlling TBA results instead of the usual a priori semi-empirical procedures. Only bond distances are initially needed.

The role of empirical control on TBA energy bands is purely ad hoc in nature. Instead of parametrizing the crystal potential to make various calculated electronic properties agree with experiment, we proceed to improve the method. For instance, we could seek better convergence in the SCF treatment of charge distributions which occur in the crystal potential. In other words, if we trust the overlap criterion to show when the TBA method is applicable, defic-

iencies in our theoretical results as compared with experiment are thought to reflect the need to increase the rigor of our method. The crux of such a philosophy is some observable trend in preliminary results which reflect qualitative agreement with experimental results.

The series ReO_3, $NaWO_3$, $KTaO_3$ has provided a good model for making further theoretical investigations of perovskite transition metal oxides using the TBA method. The density of states diagrams for these three substances show quantitatively the metal-non metal transition which until present has only been qualitatively understood. In addition, the calculation of the electronic specific heat coefficient and the joint density of states representation of optical spectra provide other avenues between theory and experiment. The results described in this thesis can be said to be better than just qualitatively descriptive of the electronic structure of crystals; perhaps, the LCAO description of crystals gives us a semi-quantitative handle for looking beyond present observable phenomenon to produce some surprising predictions. The consistent agreement of our results with empirical information ,therefore, shows that the molecular picture of crystals can be accurate if we include the effects of translational symmetry.

The SCF procedure will be the subject of further work in this area. More efficient procedures will be sought to obtain convergence of charge distributions. Also the TBA interaction model will be expanded to include more neighboring atoms

in order to handle perovskite oxides which represent borderline cases for application of the TBA method , eg. $SrTiO_3$. With these and other improvements we can ultimately investigate a series of substances which are little understood or may not yet have been synthesized.

BIBLIOGRAPHY

1. Gerstein, B. C., L. D. Thomas and D. M. Silver, J. Chem. Phys. 46, 4288 (1967).

2. Pilar, F. L., "Elementary Quantum Chemistry," McGraw-Hill, Inc., New York (1968).

3. Roothaan, C. C. J., Rev. Mod. Phys. 23, 69 (1951).

4. Ziman, Z. M., "Principles of the Theory of Solids," Cambridge University Press, London (1964).

5. Flodmark, S. F., Internat. Quantum Chem. 1, 147 (1967).

6. Mulliken, R. S., J. Chem. Phys. 23, 1833 (1965).

7. Fenske, R. F. and D. D. Radtke, Inorg. Chem. 7, 479 (1968); _____, K. G. Caulton, D. D. Radtke and C. C. Sweeney, ibid. 5, 960 (1966); _____ and K. G. Caulton, ibid. 7, 1273 (1968).

8. Richardson, J. W. and R. E. Rundle, "A Theoretical Study of the Electronic Structure of Transition-Metal Complexes," ISC-830, Ames Lab (1956).

9. Basch, H. and H. B. Gray, Inorg. Chem. 6, 639 (1967).

10. Mulliken, R. S., J. Chem. Phys. 46, 497,675 (1949).

11. Mattheiss, L. F., Phys. Rev. 181, 987 (1969).

12. Loukes, T. L., "Augmented Plane Wave Method," W.A. Benjamin, Inc., New York (1967).

13. Slater, J. C. and G. F. Koster, Phys. Rev. 94, 1498 (1954).

14. Feinleib, J., W. J. Scouler and A. Feretti, Phys Rev. 165, 765 (1968).

15. Marcus, S. M., Phys. Latters 27A, 584 (1968).

16. Moore, C. E., "Atomic Energy Levels," U.S. National Bureau of Standards Circular 467, U.S. Government Printing Office, Washington, D. C. , (1949 and 1952).

17. Cotton, F. A. and C. B. Harris, Inorg. Chem. **6**, 369,376 (1967).

18. Slater, J. C., "Quantum Theory of Atomic Structure," Vol. I, Mc-Graw Hill, Inc., New York (1960).

19. Cotton, A., Rev. Pure and Applied Chem. **16**, 175 (1966).

20. Pauling, L., J. Chem. Soc. **1948**, 1461 (1948).

21. Condon, E. U. and G. H. Shortley, "THe Theory of Atomic Spectra," Cambridge University Press, New York (1964).

22. Eyring, H., J. Walter and G. E. Kimball, "Quantum Chemistry," John Wiley and Sons, Inc., New York (1944).

23. Mann, J. B., "Atomic Structure Calculations I. and II. I. Hartree-Fock Energy Results and II. Hartree-Fock Wave Functions and Radial Expectation Values; Hydrogen to Lawrencium," LA-3690 and LA-3691, Los Alamos Lab (1967 and 1968).

24. Silver, D. M. and K. Ruedenberg, J. Chem. Phys. **49**, 4306 (1968).

25. Brown, D. A. and N. J. Fitzpatrick, Proc. Cambridge Phil. Soc. **53**, 206 (1967); J. Chem. Soc. **1967**, 316 (1967).

26. Burns, G, J. Chem. Phys. **39**, 1521 (1964).

27. Clementi, E., D. L. Raimondi and W. P. Reinhardt, J. Chem. Phys. **47**, 1300 (1967).

28. Richardson, J. W., R. R. Powell and W. C. Nieuport, J. Chem. Phys. **38**, 796 (1963).

29. Watson, R. T., Solid State and Molecular Theory Group Technical Report No. 12, MIT (1959).

30. Basch, H. and H. B. Gray, Theor. Chim. Acta (Berl.) **4**, 367 (1966).

31. Shavitt, I., "Methods in Computational Physics," Vol. 2, Academic Press, Inc., New York (1963).

32. Gianturco, F. A., J. Chem. Soc. **(A)1969**, 23 (1969).

33. Wolfsberg, M. and L. Helmholz, J. Chem. Phys. $\underline{20}$, 837 (1952).

34. Jørgenson, C. K., Chem. Phys. Letters $\underline{1}$, 11 (1967).

35. Ruedenberg, K., Rev. Mod. Phys. $\underline{34}$, 326 (1962).

36. Ros, P. and G. C. A. Schuit, Theor. Chim. Acta $\underline{4}$, 1 (1966).

37. Sleight, A. W. and J. L. Gillson, Solid State Comm. $\underline{4}$, 1991 (1963).

38. Fuchs, R., J. Chem. Phys. $\underline{42}$, 3781 (1965).

39. Sienko, M. J., Adv. Chem. Ser. No. 39, Am. Chem. Soc., Washington, D. C. (1962).

40. Goodenough, J. B., Bull. Soc. Chim. France $\underline{1965}$, 1200 (1965); _____, J. Appl. Phys. Suppl. $\underline{37}$, $\underline{1415}$ (1966).

41. Kahn, A. H. and A. J. Leyendecker, Phys. Rev. $\underline{135A}$, 1321 (1964).

42. Cardona, M., Phys. Rev. $\underline{140A}$, 651 (1965).

43. Born, M. and T. von Karman, Physik Z. $\underline{13}$, 297 (1912).

44. Born, M. and J. R. Oppenheimer, Ann. Physik $\underline{84}$, 457 (1927).

45. Kaufman, J. J., J. Chem. Phys. $\underline{43}$, s152 (1965).

46. Karian, H. G., "Semi-Rigorous Molecular Orbital Calculation of Transition Metal Complexes," Unpublished M.S. thesis, Chicago, Illinois, De Paul University (1967).

47. Hsia, Y., Can. J. Chem. $\underline{46}$, 2667 (1968).

48. Raffenetti, R., "Even Tempered Orbital Functions," To be published.

49. Cusachs, L. C. and J. H. Corrington, "Atomic Orbitals for Semi-Empirical Molecular Orbital Calculations," To be published.

50. Slater, J. C., "Quantum Theory of Molecules and Solids," Vol. II, McGraw-Hill, Inc., New York (1965).

51. Vest, R. W., M. Griffel and J. F. Smith, J. Chem. Phys. $\underline{28}$, 293 (1958).

52. Sandin, T. R. and P. H. Keeson, Phys. Rev. 177, 1370 (1969).

53. Ferretti, A., D. B. Rogers and J. B. Goodenough, J. Phys. Chem. Solids, 26, 2007 (1965).

54. Cohen, M. H., Phil. Mag. 3, 762 (1958).

55. Brust, D., Phys. Rev. 134, A1337 (1964).

56. Narath, A. and D. C. Barham, Phys. Rev. 176, 479 (1968).

57. Keller, J. M., J. Chem. Phys. 33, 232 (1960).

58. Mackintosh, A. R., J. Chem. Phys. 38, 1991 (1963).

59. Gundy, H. W., Phys. Rev. 113, 795 (1959).

60. Cohen, M. I. and R. F. Blunt, Phys. Rev. 168, 929 (1968).

61. Frederikse, H. P. R., W. R. Hosler and W. R. Thurber, Phys. Rev. 143, 648 (1966); _____, W. R. Hosler, W. R. Thurber, J. Bubiskin and P. G. Siebermann, Phys. Rev. 158, 775 (1967).

62. Tufte, O. N. and E. L. Stelzer, Phys. Rev. 141, 675 (1966).

63. Noland, J. A., Phys. Rev. 94, 724 (1954).

64. DiDomenico, M., Jr. and S. H. Wemple, Phys. Rev. 166, 565 (1968).

65. Feldman, A. and D. Horowitz, Rotary Transmission Measurements, To be published.

66. Cardona, M., Phys. Rev. 140, 651 (1967).

67. Malitson, I., private communication to M. I. Cohen and R. F. Blunt, Phys. Rev. 168, 929 (1968).

68. Baer, W. S., J. Phys. Chem. Solids, 28, 677 (1967).

69. Schooley, J., W. Hosler, M. H. Cohen and C. Koonce, Phys. Rev. 140, 651 (1965).

70. Frova, A. and B. J. Boddy, Phys. Rev. 153, 606 (1967).

71. Wemple, S. H., Phys. Rev. 137, A1575 (1965).

72. Brown, B. W. and E. Banks, J. Amer. Chem. Soc. 76, 963 (1954).

73. Fromhold, A. T. and A. Narath, Phys. Rev. 152, 585 (1966).

74. Narath, A. and D. C. Wallace, Phys. Rev. 127, 724 (1962).

75. Jones, W. H., E. A. Garbaty and R. G. Barnes, J. Chem. Phys. 36, 494 (1962).

76. Greiner, J. D., H. R. Shanks and D. C. Wallace, J. Chem. Phys. 36, 772 (1962).

77. Sienko, M. J. and J. C. Gulick, Abstracts ACS, IN12 (1969).

78. Dickens, P. G., R. M. P. Quilliam and M. S. Whittingham, Mat. Res. Bull. 3, 941 (1968).

79. Gardner, W. and G. C. Danielson, Phys. Rev. 93, 46 (1954).

80. André, J. M., J. Chem. Phys. 50, 1536 (1969).

81. Wechter, M. A., H. R. Shanks and A. F. Voigt, Inorg. Chem. 1, 845 (1968).

82. Casella, R. C., Phys. Rev. 154, 743 (1967).

83. Silver, D. M. and K. Ruedenberg, J. Chem. Phys. 49, 4301 (1968).

84. Edmonds, A. R., "Angular Momentum in Quantum Mechanics," Princeton University Press, New Jersey (1957).

85. Mehler, E. L. and K. Ruedenberg, J. Chem. Phys. 50, 2575 (1969).

86. Lowdin, P., J. Appl. Phys. 33, S251 (1962).

87. Bloch, F., Z. Physik, 52, 555 (1928).

88. Callaway, J., "Energy Band Theory," Academic Press, Inc., New York (1964).

ACKNOWLEDGEMENTS

The author wishes to thank his advisor, Dr. Bernard C. Gerstein, for recognizing the feasibility of the problem and for giving him the opportunity to make the theoretical investigation a reality. Gratitude is expressed to Lowell Thomas for his preliminary work in programing many of the subroutines used in the TBA calculation.

The overlap and nuclear attraction subroutines used are contributed by Dr. David M. Silver. Dr. Silver has written the Coulomb package used in auxiliary programs. The author is very grateful to Dave for taking time out of his busy schedule to aid him in debugging the TBA computer program in early stages of development.

Dr. Klaus Ruedenberg and other people in his group: Dr. Mark Gordon, Dr. Otto Steinborn, Dr. Ernest Mehler and Richard Raffenetti have been very helpful in formulating many aspects of the TBA calculation. The author is appreciative of many useful suggestions made by people in the theoretical physics group: Dr. R. Gupta, Dr. Kenneth Kliewer, Dr. L. Hodges and Dr. Samuel Liu. Of course, the execution of the TBA program would have been impossible without the patience and cooperation of many in the computer services division.

Finally, the author has a special thank you to his wife, Joan, for her patience and encouragement, her typing and keypunching, which has enabled him to complete his thesis.

APPENDICES

Appendix A. Solution of the Secular Determinant

The problem is

$$|\underset{\sim}{H} - E\,\underset{\sim}{S}| = 0 \qquad\qquad (A1)$$

where the Hamiltonian matrix, $\underset{\sim}{H} = \underset{\sim}{b}^{\dagger}\,\mathcal{H}\,\underset{\sim}{b}$ and overlap matrix $\underset{\sim}{S} = \underset{\sim}{b}^{\dagger}\underset{\sim}{b}$ result from the Bloch sum basis set $\underset{\sim}{b} = (b_1, b_2, \ldots b_m)$ where m indicates number of atomic orbitals considered, and the Hamiltonian operator shown in Equation 3. The solution of the secular determinant is carried out in two steps:

1) Orthogonalize the Bloch sums by the Schmidt method to transform $\underset{\sim}{S}$ into an identity matrix.

2) Diagonalize the transformed Hamiltonian matrix to give the eigenvalues and eigenvectors.

The description of the two steps can be lengthy, but a general idea of the procedure is summarized in the following equations:

The transformation is made by an upper triangular matrix $\underset{\sim}{\alpha}$, i.e.,

$$\underset{\sim}{\alpha}^{\dagger}\,|\,\underset{\sim}{H} - E\underset{\sim}{S}\,|\,\underset{\sim}{\alpha} = 0$$

$$= |\underset{\sim}{\alpha}^{\dagger}\,\underset{\sim}{H}\,\underset{\sim}{\alpha} - E\,\underset{\sim}{\alpha}^{\dagger}\,\underset{\sim}{S}\,\underset{\sim}{\alpha}|$$

$$= |\underset{\sim}{\alpha}^{\dagger}\,\underset{\sim}{H}\,\underset{\sim}{\alpha} - E\,\underset{\sim}{I}| = 0 \qquad\qquad (A2)$$

where $\underset{\sim}{I}$ is the identity matrix, i.e., $(\underset{\sim}{I})_{ij} = \delta_{ij}$. The overlap matrix is rewritten as $\underset{\sim}{S} = \underset{\sim}{T}^{\dagger}\,\underset{\sim}{T}$ where $\underset{\sim}{T} = \underset{\sim}{\alpha}^{-1}$. $\underset{\sim}{T}$ is

chosen to be upper triangular, i.e., $T_{ij} = 0$, $i > j$. The elements of this triangular matrix are generally complex functions, thus, $T_{ij} = a_{ij} + ib_{ij}$. It can be shown that

$$T_{ii} = \left[S_{ii} - \sum_{k=1}^{i-1} a_{ki}^2 + b_{ki}^2 \right]^{\frac{1}{2}}$$

and

$$T_{ij} = \frac{S_{ij} - \sum_{k=1}^{i-1} T_{ki}^* T_{kj}}{T_{ii}} \tag{A3}$$

which gives the original matrix elements of $\underset{\sim}{\alpha}$ as:

$$\alpha_{ii} = 1/T_{ii}$$

$$\alpha_{ij} = \frac{-\sum_{k=i}^{j-1} \alpha_{ik} T_{kj}}{T_{jj}} \tag{A4}$$

Therefore, the α_{ij} can be calculated in the following order

$$\alpha_{11}, \; \alpha_{22}, \; \alpha_{12}, \; \ldots, \; \alpha_{1n}, \; \alpha_{33}, \; \alpha_{23}, \ldots \; \alpha_{2n}, \ldots$$

When the eigenvalues and eigenvectors of $\underset{\sim}{H'} = \underset{\sim}{\alpha}^{\dagger} \underset{\sim}{H} \underset{\sim}{\alpha}$ are found, we then have

$$\underset{\sim}{V}^{-1} \; \underset{\sim}{H'} \; \underset{\sim}{V} = \underset{\sim}{E} \quad \text{where} \quad (\underset{\sim}{E})_{ij} = E_i \delta_{ij} \quad \text{and}$$

$\underset{\sim}{V}$ is the eigenvector matrix

or

173

$$\underset{\sim}{V}^\dagger \underset{\sim}{\alpha}^\dagger \underset{\sim}{H} \underset{\sim}{\alpha} \underset{\sim}{V} = \underset{\sim}{E}$$

$$= \underset{\sim}{V}^\dagger \underset{\sim}{\alpha}^\dagger \underset{\sim}{b}^\dagger \underset{\sim}{H} \underset{\sim}{b} \underset{\sim}{\alpha} \underset{\sim}{V} = \underset{\sim}{E}$$

$$= (\underset{\sim}{b} \underset{\sim}{c})^\dagger \underset{\sim}{H}(\underset{\sim}{b} \underset{\sim}{c}) \quad \text{where} \quad \underset{\sim}{c} = \underset{\sim}{\alpha} \underset{\sim}{V}, \text{ or}$$

$$\langle b_i'' | \mathcal{H} | b_j'' \rangle = E_j \delta_{ij}$$

where $b_j'' = \sum_i b_i C_{ij}$. $\hspace{3cm}$ (A5)

Hence, we see that the columns of $\underset{\sim}{C}$ define linear combinations of the Bloch sums which form the function Ψ_i (Equation 1).

The diagonalization procedure follows from the transformation $\underset{\sim}{U}^{-1} \underset{\sim}{H} \underset{\sim}{U} = \underset{\sim}{D}$ where $\underset{\sim}{D}$ is diagonal $D_{12} = D_{21}^* = 0$ for which U is defined as

$$U = \begin{pmatrix} 1_1 & & & & & 0 \\ & \ddots & & & & \\ & & U_{ii} & \cdots & U_{ij} & \\ & & \vdots & 1_1 & \vdots & \\ & & U_{ji} & \cdots & U_{jj} & \\ & & & & & \ddots \\ 0 & & & & & 1_1 \end{pmatrix} \hspace{2cm} (A6)$$

Thus, U is a unit matrix except for the elements U_{ii}, U_{jj}, and U_{ji}. The diagonalization is accomplished by an iteration process which ultimately makes D approximately diagonal. The following sequences are repeated until the values of all of the off-diagonal elements are on the order of 10^{-10} Rydberg

units:

1) Find the largest off-diagonal element of H, H_{ij}

2) Calculate U

3) Make the transformation $U^{-1}H\ U = H'$

The choice of U is basically the same as Jacobi's method for <u>real</u> symmetric matrices, but modifications must be made to account for the complex form of H_{ij}, i.e., $H_{ij} = a + ib$.

If

$$\underset{\sim}{H} = \begin{pmatrix} a & b-ic \\ b+ic & d \end{pmatrix}$$

and

$$\underset{\sim}{U} = \begin{pmatrix} \cos\phi & -\sin\phi\ \exp(-i\theta) \\ \sin\phi\ \exp(i\theta) & \cos\phi \end{pmatrix}$$

then the elements of

$$\underset{\sim}{D} = \underset{\sim}{U}^{-1}\ \underset{\sim}{H}\ \underset{\sim}{U}$$

are

$$D_{11} = a\cos^2\phi + d\sin^2\phi + \left\{ (b-ic)\exp(i\theta) + (b+ic)\exp(-i\theta) \right\} \cdot \sin\phi\cos\phi$$

$$D_{22} = a\sin^2\phi + d\cos^2\phi - \left\{ (b-ic)\exp(i\theta) + (b+ic)\exp(-i\theta) \right\} \cdot \sin\phi\cos\phi$$

$$D_{12} = D_{21}^* = (d-a)\sin\phi\cos\phi\ \exp(-i\theta) + (b-ic)\cos^2\phi - (b+ic)\sin^2\phi\ \exp(-2i\theta) \tag{A7}$$

By setting $D_{12} = 0 = D_{21}^{*}$ and solving for θ and $\emptyset$, we find that D will be diagonal if

$$\tan \theta = \frac{c}{b} = \frac{\sin \theta}{\cos \theta}$$

$$\tan 2\emptyset = \frac{(b^2 + c^2)^{\frac{1}{2}}}{\frac{1}{2}(a-d)} \tag{A8}$$

Using $\sin^2 \theta + \cos^2 \theta = 1$, we obtain

$$\sin \theta = \frac{c}{(b^2+c^2)^{\frac{1}{2}}}$$

$$\cos \theta = \frac{b}{(b^2+c^2)^{\frac{1}{2}}} \tag{A9}$$

By Euler's relation $\exp(i\theta) = \cos \theta + i \sin \theta$, we have

$$\exp(\pm i \theta) = \frac{b \pm ic}{(b^2+c^2)^{\frac{1}{2}}} \quad . \tag{A10}$$

Thus, $\exp(-i\theta)$ is simply

$$\frac{b-ic}{\left[(b+ic)(b-ic)\right]^{\frac{1}{2}}}$$

or $H_{12}/|H_{12}|$.

If we let

$$\lambda = (b^2+c^2)^{\frac{1}{2}}$$

$$\mu = \tfrac{1}{2}(a-d)$$

$$\omega = \text{sign} (\mu) \cdot \frac{\lambda}{(\mu^2 + \lambda^2)^{\frac{1}{2}}}$$

$$\sin \phi = \frac{\omega}{\left[2(1+\sqrt{1-\omega^2}\,)\right]^{\frac{1}{2}}}$$

$$\cos \phi = (1-\sin^2 \phi)^{\frac{1}{2}}$$

then,

$$\underset{\sim}{U} = \begin{pmatrix} \cos \phi & -\sin \phi \, \frac{H_{12}}{|H_{12}|} \\ \sin \phi \, \frac{H_{21}}{|H_{21}|} & \cos \phi \end{pmatrix} \qquad \text{(A11)}$$

and

$$D_{11}= a \cos^2 \phi + d \sin^2 \phi + 2|H_{12}| \sin \phi \cos \phi$$

$$D_{22}= a \sin^2 \phi + d \cos^2 \phi - 2|H_{12}| \sin \phi \cos \phi$$

$$D_{12}=D_{21}^{*}= \left\{(d-a)\sin \phi \cos \phi + |H_{12}| (\cos^2 \phi - \sin^2 \phi)\right\}\frac{H_{12}}{|H_{12}|}$$

$$= 0 \qquad \text{(A12)}$$

Appendix B. Flow Chart for Computer Calculation

The flow chart of our program is outlined below. The matrix elements could have initially been set up in algebraic form. Substitution of overlap and two-center potential integrals (evaluated in elliptical coordinates) and $\underline{k}$ vectors would give the Hamiltonian and overlap matrix elements. The Schmidt orthogonalization of the overlap matrix and diagonalization of the transformed Hamiltonian matrix would then be an easy chore in terms of shorter computer time. However, when we go from cubic to say, hexagonal symmetry, the length of the tables necessary would increase. It is always desirable to make these calculations as automatic as possible via the computer. Our program, therefore, eliminates the need for matrix element tables as well as overlap integral tables, from which are sometimes difficult to interpolate accurate values. In a sense, the TBA program generates all necessary tables within the computer. When the $\underline{k}$ vector is read in, it rapidly makes algebraic substitutions and in about 60 seconds a 25 x 25 matrix problem is solved.

INPUT DATA

1. Unit cell translation vectors
2. Translation vectors in TBA interaction set
3. Overlap, Coulomb-exchange, nuclear attraction integrals calculated by a previous program and stored on tape
4. Indexing parameters
5. Charge distributions
6. Orbital energy parameters

CRYSTAL POTENTIAL

1. Calculate potential matrix elements, $\langle \phi_a | V_b | \phi_a' \rangle$
2. Rotate spherical harmonics and take a proper linear combination of integrals over lattice sites

---

OVERLAP AND $\langle \phi_a | V_a | \phi_b \rangle$ INTEGRALS

Rotate spherical harmonics and take a proper linear combination of integrals after orbital energies are calculated

---

READ **k** VECTORS

CALCULATE MATRIX ELEMENTS BETWEEN BLOCH SUMS

SCHMIDT ORTHOGON-ALIZE BLOCH SUM OVERLAP MATRIX

TRANSFORM HAMILTONIAN MATRIX

DIAGONALIZE H MATRIX TO OBTAIN EIGENVALUES

CALCULATE EIGENVECTORS

DETERMINE THE FERMI ENERGY

MULLIKEN POPULATION ANALYSIS

1. Calculate the occupation numbers of the Bloch sum basis set for each $\underline{k}$ vector

2. By proper weighting of the $\underline{k}$ vector degeneracies in the entire Brillouin zone, obtain the average charge distributions

3. With $\lambda = 8$ and using Equation 29 calculate the assumed charge distribution for the next iteration

GO TO STEP 5 IN INPUT UNTIL SELF CONSISTENCY IS ESTABLISHED

Appendix C. Reduction of Double Sum to Single Sum

Since the sums over $\underline{R}_i$ and $\underline{R}_j$ are over the same vectors, we can write the double sum as N times the single sum, i.e.,

$$\sum_{\underline{R}_i} \sum_{\underline{R}_j} F(\underline{R}_i, \underline{R}_j) = N \sum_{\underline{R}_j} F(\underline{R}_i, \underline{R}_j) \tag{C1}$$

where N is the number of unit cells in the crystal. The proof is as follows:

Because of the periodic boundary conditions

$$F(\underline{R}_i + N_1\underline{t}_1 + N_2\underline{t}_2 + N_3\underline{t}_3) = F(\underline{R}_i) \tag{C2}$$

where $N_1N_2N_3 = N$ and $\underline{t}_1$, $\underline{t}_2$ and $\underline{t}_3$ are the primitive cell translations.

We can also write

$$\underline{R}_i = i_1\underline{t}_1 + i_2\underline{t}_2 + i_3\underline{t}_3 \qquad i_1, i_2, i_3 = \text{integers}$$

$$\underline{R}_j = j_1\underline{t}_1 + j_2\underline{t}_2 + j_3\underline{t}_3 \qquad j_1, j_2, j_3 = \text{integers} \tag{C3}$$

Hence

$$\sum_{\underline{R}_i} \sum_{\underline{R}_j} F(\underline{R}_j - \underline{R}_i) = \sum_{i_1=0}^{N_1-1} \sum_{i_2=0}^{N_2-1} \sum_{i_3=0}^{N_3-1} \sum_{j_1=0}^{N_1-1} \sum_{j_2=0}^{N_2-1} \sum_{j_3=0}^{N_3-1}$$

$$F((j_1-i_1)\underline{t}_1 + (j_2-i_2)\underline{t}_2 + (j_3-i_3)\underline{t}_3) \tag{C4}$$

Let us consider the double sum for integral components along $\underline{t}_1$:

$$\left\{ \sum_{i_1} \sum_{j_1} (j_1 - i_1) \right\}$$

where $(j_1 - i_1) = F((j_1 - i_1)\underline{t}_1)$.

If we expand the sum in the brackets above, we obtain

$$\sum_{i_1} \sum_{j_1} (j_1 - i_1) = \sum_{i_1} (0 - i_1) + (1 - i_1) + (2 - i_1) + \ldots$$

$$+ (N_1 - 1 - i_1)$$

$$= (0-0) + (1-0) + (2-0) + \ldots + (N_1 - 1 - 0)$$
$$+ (0-1) + (1-1) + (2-1) + \ldots + (N_1 - 1 - 1)$$
$$+ \ .$$
$$\vdots$$
$$+ (0 - N_1 + 1) + (1 - N_1 + 1) + \ldots + (N_1 - 1 - N_1 + 1) \qquad (C5)$$

Now if we look at the first two rows above, we see that the terms in each row are identical except for the terms $(N_1 - 1)$ and (-1). However, from the periodic boundary conditions, we know that $F(N_1 \underline{t}_1) = F(\underline{0})$. Therefore, the two terms $(N_1 - 1)$ and (-1) are really identical.

Similar arguments hold for any pair of rows and, hence, all N_1 rows are identical, so we can write

$$\sum_{i_1=0}^{N_1-1} \sum_{j_1=0}^{N_1-1} (j_1-i_1) = N_1 \sum_{j_1} (j_1-i_1)$$

Similarly,

$$\sum_{i_2=0}^{N_1-1} \sum_{j_2=0}^{N_1-1} (j_2-i_2) = N_2 \sum_{j_2} (j_2-i_2)$$

and

$$\sum_{i_3=0}^{N_1-1} \sum_{j_3=0}^{N_1-1} (j_3-i_3) = N_3 \sum_{j_3} (j_3-i_3) \qquad (C6)$$

Therefore, we can write Equation C4

$$\sum_{\underline{R}_i} \sum_{\underline{R}_j} F(\underline{R}_j,\underline{R}_i) = N_1 N_2 N_3 \sum_{j_1} \sum_{j_2} \sum_{j_3}$$

$$F((j_1-i_1)\underline{t}_1 + (j_2-i_2)\underline{t}_2 + (j_3-i_3)\underline{t}_3)$$

$$= N \sum_{\underline{R}_j} F(\underline{R}_j-\underline{R}_i) . \qquad (C7)$$

Since $\underline{R}_j-\underline{R}_i$ is also a crystal translation, we can make the substitution

$$\underline{R}_\ell = \underline{R}_i - \underline{R}_j$$

and then by summing over $\underline{R}_\ell$ instead of $\underline{R}_j$, we merely interchange the order of summation to obtain Equation 48.

Appendix D. Overlap and Related Integrals

The two-center kinetic energy and overlap integrals, are evaluated using a method proposed by Silver and Ruedenberg (63).

This method requires that the coordinate system of the two centers be parallel with their z-axes pointing towards one another. In our calculations, however, the coordinate systems at the two centers are both parallel to that of the crystal as a whole. The problem remains, then, to transform the atomic orbitals at the two centers into coordinate systems of the type necessary for evaluation.

At the center, A, this will be a rotation and at the center B, it will be an inversion of the z'-axes followed by the same rotation as at A. Since the radial part of the atomic orbitals is invariant under such transformations, we need only examine their effect on the spherical harmonics.

The inversion is given simply by

$$Y_{\ell m}(\theta, \phi) = Y_{\ell m}(\pi - \theta', \phi')$$

$$= (-1)^{\ell + m} Y_{\ell m}(\theta', \phi') \tag{D1}$$

with the primes indicating the inverted system.

Since the spherical harmonics forms the bases for the irreducible representations of the three-dimensional rotation group, we can utilize the matrix elements of these representations to accomplish the transformation.

For a complex spherical harmonic on center A

$$Y_{\ell m}(\Theta_A, \phi_A) = \sum_{k=-\ell}^{\ell} D_{km}^{\ell}(\alpha, -\Theta, -\phi)\, Y_{\ell k}(\Theta_A', \phi_A') \tag{D2}$$

where (Θ_A, ϕ_A) and (Θ_A', ϕ_A') are the polar coordinates of the unprimed and primed coordinate systems, respectively, of Figure D1.

α, $-\Theta$ and $-\phi$ are the Euler angles necessary to rotate the $(x'y'z')$ system into coincidence with the (xyz) system. Θ and ϕ are measured from the x' and x axes, respectively, to the z-z' plane. Θ is measured from the z-axis to the z'-axis.

The coefficients are given by

$$D_{km}^{\ell}(\alpha, \beta, \gamma) = \exp(-ik\alpha)\exp(-im\beta)d_{km}^{\ell}(\beta)$$

where

$$d_{km}^{\ell}(\beta) = \sum_t (-1)^t \frac{\left[(\ell+m)!\,(\ell-m)!\,(\ell+k)!\,(\ell-k)!\right]^{\frac{1}{2}}}{(\ell+k-t)!\,(\ell-m-t)!\,(t+m-k)!\,t!}$$

$$(\cos\beta/2)^{2\ell+k-m-2t}(\sin\beta/2)^{2t+m-k} \tag{D3}$$

the index, t, running from max $(0, k-m)$ to min $(\ell-m, \ell+k)$.

If one defines the real spherical harmonics, $\mathcal{Y}_{\ell m}$, as

$$\mathcal{Y}_{\ell m} = N_{(m)}\left\{Y_{\ell -|m|} + I_{(m)}Y_{\ell|m|}\right\} \tag{D4}$$
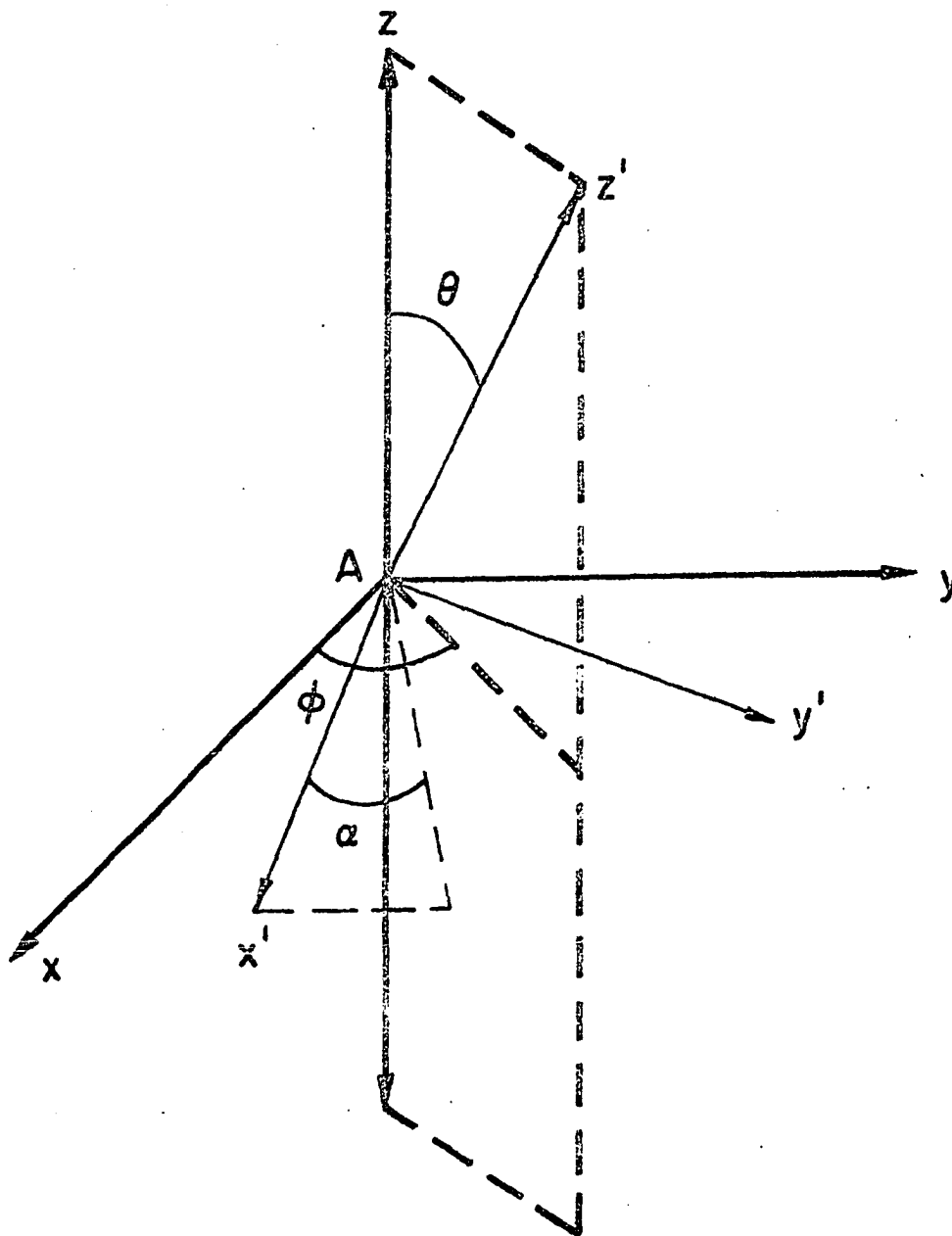
Figure D1. Coordinate systems.

where

$$N_{(m)} = \begin{cases} \sqrt{\tfrac{1}{2}} & m > 0 \\ \tfrac{1}{2} & m = 0 \\ \sqrt{-\tfrac{1}{2}} & m < 0 \end{cases}$$

and

$$I_{(m)} = \begin{cases} (-1)^m & m \geq 0 \\ (-1)^{m+1} & m < 0 \end{cases} \tag{D5}$$

then utilizing Equations D1 and D2 for the necessary transformations, we get as a final expression for the two-centered integrals

$$\langle R_{n\ell}(r_A, \zeta_A) \mathcal{Y}_{\ell m}(\theta_A \phi_A)| F |R_{n'\ell'}(r_B, \zeta_B) \mathcal{Y}_{\ell'm'}(\theta_B, \phi_B)\rangle$$

$$= N^*_{(m)} N_{(m')}(-1)^{\ell'} \Big\{ C(o) \langle R_{n\ell} Y_{\ell o}(\theta_A', \phi_A') | F | R_{n'\ell'} Y_{\ell' o}(\theta_B, \phi_B)\rangle$$

$$+ \sum_{k=1}^{\min(\ell,\ell')} \Big[C(k) + (-1)^{\zeta|m|\,m|+\zeta m'|m'|} C^*(k)\Big] \langle R_{n\ell} Y_{\ell k}(\theta_A'\,\phi_A')$$

$$|F|R_{n'\ell'} Y_{\ell'k}(\theta_B', \phi_B')\rangle \Big\}$$

with

$$C(k) = (-1)^k \Big\{ \exp(i|m|\phi) d^{\ell}_{k-|m|}(-\theta) + I_{(m)} \exp(-i|m|\phi) d^{\ell}_{k|m|}(-\theta) \Big\}$$

$$\cdot \Big\{ \exp(-i|m'|\phi) d^{\ell'}_{k-|m'|}(-\theta) + I_{(m')} \exp(i|m'|\phi) d^{\ell'}_{k|m'|}(-\theta) \Big\} \tag{D6}$$

The dependence on the Euler angle α has dropped out corresponding to the one degree of freedom we have in

choosing the primed coordinate system.

Equation D5 is the overlap integral if F=1 and the potential integral if

$$F = V(\underline{r} - \underline{\rho}_j^{\beta\alpha})$$

If F includes coulomb and exchange operators, it must be transformed in a similar manner.

Appendix E. Potential Integrals

The atomic potential used in the TBA method consists of three operators. These are Coulomb and exchange operators, giving rise to Coulomb and exchange integrals, and a third operator $-2.Z_B/r_B$ for an electron attracted to center B that gives rise to nuclear attraction integrals. The Coulomb and exchange integrals are evaluated by methods programmed for the IBM 360-65 computer (24, 85). The nuclear attraction integrals are of the type

$$\left\langle A_{n\ell m}(\zeta, r_A) \left| \frac{1}{r_B} \right| A_{n'\ell'm'}(\zeta', r_A) \right\rangle$$

where the single-zeta, normalized STO's are

$$A_{n\ell m}(\zeta, r_A) = \frac{(2\zeta)^{n+\frac{1}{2}}}{[(2n)!]^{\frac{1}{2}}} \, r_A^{n-1} \exp(-\zeta, r_A) Y_{\ell m}(\theta, \phi) \qquad (E1)$$

for a function located on atomic center A. The nuclear attraction integrals are evaluated by the use of the expression

$$\left\langle A_{n\ell m}(\zeta, r_A) \left| \frac{1}{r_B} \right| A_{n'\ell'm'}(\zeta', r_A) \right\rangle =$$

$$\delta_{mm'}(-1)^m (2\zeta)^{n+\frac{1}{2}}(2\zeta')^{n'+\frac{1}{2}} \left[(2\ell+1)(2\ell'+1) / (2n)! \cdot (2n')! \right]^{\frac{1}{2}}$$

$$\cdot (R)^{n+n'} \sum_{L=|\ell-\ell'|,2}^{\ell+\ell'} \begin{pmatrix} \ell & \ell' & L \\ 0 & 0 & 0 \end{pmatrix} \begin{pmatrix} \ell & \ell' & L \\ m & -m & 0 \end{pmatrix}$$

$$\cdot \left[E_{n+n'+L}(\rho) + A_{n+n'-L-1}(\rho) \right] . \tag{E2}$$

The summation index L is limited by the constraint that $\ell + \ell' + L = $ even, $\begin{pmatrix} \ell & \ell' & \ell_3 \\ m_1 & m_2 & m_3 \end{pmatrix}$ is the Wigner 3J symbol (84), $R = $ interatomic distance between centers A and B, $\rho = R(\zeta + \zeta')$ and the functions $E_k(\rho)$ and $A_k(\rho)$ are given by (24)

$$E_k(x) = \int_0^1 dt \ t^k \exp(-xt)$$

$$A_k(x) = \int_1^\infty dt \ t^k \exp(-xt) . \tag{E3}$$

These functions are obtained using the recursion relations

$$E_k(x) = \left[k \ E_{k-1}(x) - \exp(-x) \right] / x$$

$$A_k(x) = \left[k \ A_{k-1}(x) + \exp(-x) \right] / x \tag{E4}$$

from the starting functions

$$E_0(x) = \left[1 - \exp(-x) \right] / x$$

$$A_0(x) = \exp(-x)/x . \tag{E5}$$

In order to maintain uniform accuracy, an infinite series is used for computing $E_k(x)$ if the relation,

$$x < (0.072 + 0.012 k_{max}) \ k_{max} \tag{E6}$$

is satisfied:

$$E_k(x) = k! \exp(-x) \sum_{i=0}^{\infty} x^i / (k+i+1)! \tag{E7}$$

The expression given for Equation E2 can be derived by using the LaPlace expansion for r_{Bi}^{-1}, the inverse distance between electron i and nucleus B:

$$r_{Bi}^{-1} = \sum_{L=0}^{\infty} (4\pi/2L+1)^{\frac{1}{2}} \frac{r_<^L}{r_>^{L+1}} Y_{L0}(\Theta_{Ai}, \phi_{Ai}) \tag{E8}$$

where $r_<(r_>)$ is the lesser (greater) of r_{Ai} and R_{AB} and the Y_{LM} are real normalized spherical harmonics. One can then integrate the resulting expression directly and, by interchanging summations, arrive at Equation E2.

The Coulomb and exchange integrals necessary to obtain the crystal potential in Equation ?? are evaluated for single Slater type orbitals (STO's) which are subsequently linearly combined by an auxiliary program. The linear combination is necessary since the atomic orbital functions used in the TBA calculation are multi-STO types (Equation 54).

The STO's used in the computer programs developed by Silver (24) and Mehler (25) for Coulomb and exchange integrals are real spherical harmonics. Since the rotation of spherical harmonics described in Appendix D uses the imaginary spherical harmonics as a basis (only this type is an eigenfunction of the 3-dimensional rotation group), we must be careful in using the integrals. Fortunately, we obtain a

convenient identity which may be demonstrated for the real P_x and P_y functions. By Equation D4, we have after dropping the radial part of P_x and P_y

$$P_x = \frac{Y_1^{-1} - Y_1^{1}}{\sqrt{2}} = \mathcal{Y}_{11}$$

and

$$P_y = \frac{i(Y_1^{-1} + Y_1^{1})}{\sqrt{2}} = \mathcal{Y}_{1\bar{1}}$$

The real normalized spherical harmonics may be linearly combined to give the imaginary normalized spherical harmonics:

$$Y_1^{-1} = \frac{P_x - iP_y}{\sqrt{2}}$$

and

$$Y_1^{1} = \frac{-(P_x + iP_y)}{\sqrt{2}}$$

If we consider the charge distributions $Y_1^{*-1} \cdot Y_1^{-1}$ and $Y_1^{*1} \cdot Y_1^{1}$ for electron one, the corresponding Coulomb integrals of the electrostatic interaction between these distributions and an arbitrary charge distribution $\rho(2)$ for electron two are:

$$\langle Y_1^{-1} \cdot Y_1^{-1} | \rho(2) \rangle = \left\{ \langle P_x P_x | \rho(2) \rangle + \langle P_y P_y | \rho(2) \rangle \right\} / 2$$

$$\langle Y_1^{1} \cdot Y_1^{1} | \rho(2) \rangle = \left\{ \langle P_x P_x | \rho(2) \rangle + \langle P_y P_y | \rho(2) \rangle \right\} / 2$$

Therefore, $\langle Y_1^{-1} \; Y_1^{-1} | \mathcal{P}(2) \rangle = \langle \bar{Y}_1^1 \; \bar{Y}_1^1 | \mathcal{P}(2) \rangle$. Since $\langle P_x P_x | \mathcal{P}(2) \rangle = \langle P_y P_y | \mathcal{P}(2) \rangle$, there exists a one to one correspondence between the imaginary and real spherical harmonics, e.g. $\langle \mathcal{Y}_{11} \mathcal{Y}_{11} | \mathcal{P}(2) \rangle = \langle Y_1^1 \; Y_1^1 | \mathcal{P}(2) \rangle$. The identity allows one to use the numerical values of Coulomb and exchange integrals obtained from real functions to represent the imaginary case.

Some difficulty arose in the evaluation of Coulomb and exchange integrals when $R_{AB}(\zeta_A + \zeta_B) = 360$ where R_{AB} is the internuclear distance expressed in Bohr units and ζ_A and ζ_B are the orbital exponents of STO's located on centers A and B respectively. In auxiliary functions used in the evaluation, $\exp(\pm R_{AB}(\zeta_A + \zeta_B))$ occurs and the computer limit of an exponential is ± 174. Apparently, the present programs are not written to handle this situation. Therefore, we had to apply a reasonable approximation to integrals where this problem arose. The rhenium 5d and 6p functions have large orbital exponents in inner radial region (as have been seen in the discussion on orbital functions) which are neglected in integral evaluations. Therefore, renormalization of these orbitals is necessary since a small part has been cut out. The normalization constant of the 5d is 1.01709 and 6s is 1.004342.

Appendix F. Atomic Orbital Energy Parameters

The one-electron terms which are generally referred to as the core energy, I, is the sum of the kinetic energy and potential energy from the field of the bare nucleus.

The core energy is evaluated from the following integral

$$I = \int_0^\infty P_i \left\{ -\frac{d^2}{dr^2} - \frac{2Z}{r} + \frac{\ell(\ell+1)}{r^2} \right\} P_i \, dv$$

where $P_i(r) = \sum_j c_j R n_j \ell_j(r) r = \sum_j c_j N_j \exp(-\zeta_j r) r^{n_j}$.

Integration gives upon expansion of P_i

$$I = \sum_i \sum_j c_i c_j N_i N_j \left\{ -\frac{\zeta_i^2 (n_i + n_j)!}{(\zeta_i + \zeta_j)^{n_i + n_j + 1}} \right.$$

$$+ \frac{(2.0 n_i \zeta_i - 2Z)(n_i + n_j - 1)!}{(\zeta_i + \zeta_j)^{n_i + n_j}}$$

$$\left. - \frac{(n_j + \ell)(n_i - \ell - 1)(n_i + n_j - 2)!}{(\zeta_i + \zeta_j)^{n_i + n_j - 1}} \right\}$$

The Slater-Condon parameters, F^k and G^k, are calculated via the following integrals:

$$F^k(n_i \ell_i, n_j \ell_j) = \int_0^\infty \frac{2}{r} P_i^2 \, Y_k(n_j \ell_j, n_j \ell_j) dr$$

$$G^k(n_i \ell_i, n_j \ell_j) = \int_0^\infty \frac{2}{r} P_i P_j Y_k(n_i \ell_i, n_j \ell_j) dr$$

where the potential function $Y_k(i,j)$ is

$$Y_k(i,j) = r^{-k} \int_0^r r^k P_i P_j dr + r^{k+1} \int_r^\infty P_i P_j r^{-(k+1)} dr.$$

Brown-Fitzpatrick (25) and Ros-Schuit (36) express the Slater-Condon parameters in terms of Slater type orbitals. The latter formulation has been programed to obtain parameters for the $g(i,j)$ terms in Equation 31.

The derivation of the F^k and G^k expressions are lengthy but straight forward if one utilizes the standard integral

$$\int_a^b x^n \exp(-\mu x) dx = \sum_{i=0}^n \frac{n!}{\mu^{n+1-i}} (-b^i \exp(-\mu b) + a^i \exp(-\mu a)).$$

Appendix G. TBA Results of ReO_3

The i th energy band corresponding to the crystal orbital with function $\Psi_i(\underline{k},\underline{r})$ is numbered along the left column. The eigenvalues of $\Psi_i(\underline{k},\underline{r})$ are listed in Table G1. The % rhenium, O_1, O_2 and O_3 atomic orbital contributions to $\Psi_i(\underline{k},\underline{r})$ are listed in Tables G2, G3, G4 and G5 for $\underline{k} =$ $(0.0,0.0,0.0), (\frac{\pi}{a},0.0,0.0), (\frac{\pi}{a},\frac{\pi}{a},0.0)$ and $(\frac{\pi}{a},\frac{\pi}{a},\frac{\pi}{a})$ respectively. Thus, we have the symmetry points gamma (Γ), X, M and R represented. The subscripts labeling the oxygen atoms O_1, O_2 and O_3 are indicated in parenthesis.

The eigenvalues in Table G1 are listed in Fortran notation where E 0x denotes X 10^x. The energies are in Rydberg units.

The Fermi energy is -1.4828 Rydbergs.

Figure G1. ReO$_3$ energy bands.

TABLE G1   E(K) VS. K: ENERGY BANDS AT THE SYMMETRY POINTS OF THE BRILLOUIN
ZONE OF RHENIUM TRIOXIDE

ENERGY BAND	SYMMETRY POINT GAMMA	X	M	R
1	0.368914E 01	0.441146E 01	0.231985E 03	0.180480E 00
2	0.631159E 00	0.396006E 01	-0.197960E 00	0.175789E 00
3	0.628287E 00	-0.394192E 00	-0.256400E 00	0.123880E 00
4	-0.863311E 00	-0.107109E 01	-0.118808E 01	-0.144122E 01
5	-0.107604E 01	-0.111623E 01	-0.124153E 01	-0.144454E 01
6	-0.108265E 01	-0.120646E 01	-0.124550E 01	-0.146216E 01
7	-0.112029E 01	-0.124299E 01	-0.144844E 01	-0.148081E 01
8	-0.115133E 01	-0.125083E 01	-0.147999E 01	-0.150742E 01
9	-0.115938E 01	-0.148676E 01	-0.149356E 01	-0.151233E 01
10	-0.148002E 01	-0.148984E 01	-0.149545E 01	-0.155368E 01
11	-0.148647E 01	-0.150888E 01	-0.156414E 01	-0.156450E 01
12	-0.148982E 01	-0.162160E 01	-0.166783E 01	-0.165843E 01
13	-0.174371E 01	-0.171831E 01	-0.171873E 01	-0.166219E 01
14	-0.174951E 01	-0.172903E 01	-0.172339E 01	-0.166592E 01
15	-0.175334E 01	-0.175180E 01	-0.184292E 01	-0.202745E 01
16	-0.274463E 01	-0.209894E 01	-0.214084E 01	-0.219596E 01
17	-0.275342E 01	-0.272285E 01	-0.216296E 01	-0.220243E 01
18	-0.328409E 01	-0.305085E 01	-0.292919E 01	-0.240139E 01
19	-0.355427E 01	-0.353293E 01	-0.328207E 01	-0.402056E 01
20	-0.358245E 01	-0.358377E 01	-0.388446E 01	-0.403012E 01
21	-0.360345E 01	-0.422571E 01	-0.433373E 01	-0.446861E 01

197

TABLE G2   MULLIKEN POPULATION ANALYSIS CF CRYSTAL ORBITALS AT
GAMMA SYMMETRY POINT

ENERGY BAND	% RHENIUM ATOMIC ORBITAL CONTRIBUTION								
	$5D\,Z^2$	$5D\,XZ$	$5D\,YZ$	$5D\,X^2-Y^2$	$5D\,XY$	$6S$	$6P\,Z$	$6P\,X$	$6P\,Y$
1	0.0	0.0	0.0	0.0	0.0	25.3	11.8	12.0	11.8
2	2.8	0.1	0.0	0.3	0.1	-0.0	52.2	2.4	32.2
3	0.3	0.0	0.1	2.9	0.0	-0.0	5.8	55.0	25.9
4	0.0	3.4	3.3	0.0	3.5	17.7	10.9	11.2	10.5
5	1.0	15.6	2.5	0.1	40.6	0.0	0.1	0.1	0.2
6	0.0	23.3	33.0	1.0	2.5	0.0	0.0	0.3	0.0
7	0.2	17.1	19.2	0.4	13.0	2.2	3.9	4.9	3.7
8	0.0	0.2	1.5	32.6	0.2	0.1	0.1	1.6	3.0
9	32.8	0.6	0.6	0.0	0.5	0.0	3.5	0.5	0.6
10	0.0	0.0	0.0	0.0	0.0	0.0	0.0	0.3	0.3
11	0.0	0.0	0.0	-0.0	0.0	0.0	0.2	0.7	0.1
12	0.0	0.0	0.0	-0.0	0.0	0.0	0.8	0.0	0.5
13	-0.0	0.1	0.0	0.0	39.5	-0.0	0.0	-0.0	-0.1
14	0.0	39.4	0.1	0.0	0.1	-0.0	-0.1	-0.0	-0.0
15	0.0	0.1	39.6	0.0	0.0	-0.0	-0.0	-0.0	-0.0
16	0.1	0.0	0.0	64.4	0.0	-0.0	-0.0	-0.4	-0.4
17	64.4	0.0	0.0	0.1	0.0	-0.0	-0.6	-0.1	-0.1
18	0.0	0.0	0.0	-0.0	0.0	99.0	0.1	0.1	0.0
19	-1.8	0.0	0.0	-0.0	0.0	-18.0	11.3	0.5	0.4
20	0.1	0.0	0.0	-1.7	0.0	-2.2	0.0	1.2	7.2
21	0.1	0.0	0.0	-0.1	0.0	-24.1	0.2	9.8	3.9

TABLE G2(CCNT.)

ENERGY BAND	% OXYGEN ATOMIC ORBITAL CONTRIBUTICN							
	2S(1)	2P (1) Z	2P (1) X	2P (1) Y	2S(2)	2P (2) Z	2P (2) X	2P (2) Y
1	10.1	0.1	2.8	0.1	10.3	0.1	0.1	2.5
2	0.2	0.6	-0.0	0.4	3.2	C.6	C.0	-C.2
3	5.5	0.0	-0.4	0.2	2.5	0.1	0.6	-0.1
4	-2.7	2.1	13.5	2.0	-2.4	2.0	1.7	11.2
5	0.0	5.2	0.0	13.3	C.0	0.8	13.0	C.4
6	C.0	8.0	C.7	0.9	-0.0	11.3	0.7	C.7
7	-0.6	5.0	6.0	3.7	-C.3	5.6	3.5	1.5
8	-0.9	0.2	27.5	-0.0	-1.3	C.6	0.3	34.1
9	-0.3	-0.0	9.2	0.1	-0.3	-0.0	0.1	9.7
10	0.0	2.7	0.0	46.1	C.0	1.2	45.6	0.0
11	C.0	43.5	C.0	3.3	0.0	3.3	3.3	0.C
12	0.0	4.2	-C.0	C.3	0.C	45.5	0.3	0.0
13	0.0	0.0	0.0	29.8	C.C	0.0	30.6	-C.0
14	C.0	28.6	0.0	0.0	0.0	C.1	0.1	0.0
15	0.0	0.1	0.0	0.0	0.0	29.0	0.0	0.0
16	3.9	-0.0	15.3	-C.0	2.6	0.0	-C.0	14.5
17	1.6	-0.0	3.3	0.0	2.3	-0.0	C.0	4.4
18	-6.8	-C.0	7.0	-0.0	-5.8	-0.0	-0.0	6.6
19	-0.9	-0.1	1.8	-0.0	-1.3	-C.1	0.0	1.5
20	18.0	-C.0	C.5	-0.1	69.4	0.0	-0.0	7.7
21	72.8	-0.0	12.9	-C.0	21.1	-C.0	C.0	5.3

TABLE G2(CONT.)

ENERGY BAND	% OXYGEN ATOMIC ORBITAL CONTRIBUTION			
	2S(3)	2P (3) Z	2P (3) X	2P (3) Y
1	10.6	2.3	0.1	0.1
2	5.0	-0.3	0.0	0.4
3	0.6	-0.0	0.7	0.4
4	-2.4	11.1	1.6	1.6
5	-0.0	1.2	5.1	0.9
6	-0.0	0.1	7.0	10.4
7	-0.2	1.1	4.6	5.5
8	-0.0	0.1	-0.0	0.2
9	-1.6	43.2	0.4	0.5
10	0.0	-0.0	2.6	1.2
11	0.0	0.0	42.1	3.3
12	0.0	0.1	3.9	44.3
13	0.0	0.0	0.1	0.0
14	0.0	-0.0	31.7	0.1
15	0.0	-0.0	0.1	31.2
16	0.0	0.0	-0.0	-0.0
17	2.8	21.9	0.0	0.0
18	-6.4	6.3	-0.0	-0.0
19	94.3	12.4	0.0	0.0
20	-0.3	0.1	0.0	-0.0
21	-2.4	0.5	0.0	-0.0

TABLE G3   MULLIKEN POPULATION ANALYSIS OF CRYSTAL ORBITALS AT X SYMMETRY POINT

ENERGY BAND	% RHENIUM ATOMIC ORBITAL CONTRIBUTION								
	$5D_{Z^2}$	$5D_{XZ}$	$5D_{YZ}$	$5D_{X^2-Y^2}$	$5D_{XY}$	$6S$	$6P_Z$	$6P_X$	$6P_Y$
1	0.1	-0.0	0.1	0.1	-0.0	2.2	47.3	0.0	38.5
2	0.9	-0.0	0.0	0.3	-0.0	0.0	42.0	0.0	50.5
3	1.4	0.1	0.1	4.5	0.1	4.8	0.5	73.7	0.5
4	-0.0	0.0	54.9	1.6	0.0	1.8	0.1	0.6	-0.0
5	23.7	-0.0	1.6	12.6	-0.0	0.3	0.3	0.0	2.1
6	6.9	0.0	5.7	5.5	0.0	11.3	3.9	0.8	2.6
7	-0.0	0.0	0.0	0.0	52.1	0.0	0.0	0.0	0.0
8	0.0	52.6	0.0	0.0	0.0	0.0	0.0	0.1	0.0
9	0.5	0.0	0.0	1.1	0.2	0.4	0.2	0.1	-0.0
10	-0.0	0.0	0.0	0.3	0.0	0.1	-0.2	0.0	-0.0
11	-0.0	0.1	0.0	0.0	0.1	-0.0	1.5	0.0	1.6
12	9.9	0.0	0.6	30.5	0.0	11.8	0.5	0.9	0.4
13	0.1	7.1	0.0	0.3	39.5	-0.0	-0.0	0.7	0.0
14	0.0	39.5	0.0	0.1	7.4	-0.0	0.0	0.1	0.0
15	0.1	0.1	37.0	0.2	0.0	0.0	0.5	-0.0	0.5
16	0.8	0.5	0.0	2.9	0.5	-1.5	0.1	32.4	0.1
17	46.2	0.0	0.0	17.2	0.0	0.2	-0.5	-0.0	-0.7
18	9.1	-0.0	0.0	18.1	-0.0	53.2	-0.6	-1.4	-0.5
19	0.7	0.0	0.0	1.9	-0.0	-16.5	2.4	-0.2	1.9
20	-1.5	0.0	0.0	-1.0	0.0	0.0	1.6	-0.0	2.1
21	1.2	0.0	0.0	3.8	0.0	31.7	0.4	-7.8	0.4

TABLE G3(CONT.)

ENERGY BAND	% OXYGEN ATOMIC ORBITAL CONTRIBUTION							
	2S(1)	2P (1) Z	2P (1) X	2P (1) Y	2S(2)	2P (2) Z	2P (2) X	2P (2) Y
1	0.1	0.2	0.0	0.2	4.5	1.3	0.0	-0.2
2	0.0	0.2	0.0	0.2	2.9	1.2	0.0	-0.9
3	-2.0	0.0	16.2	0.0	0.2	0.1	-0.5	0.2
4	-0.1	0.0	0.1	0.0	0.0	17.3	-0.0	5.4
5	-0.0	0.0	0.0	0.0	-1.6	1.1	-0.0	39.0
6	-0.1	0.4	-0.0	0.4	-0.5	0.4	0.0	19.7
7	-0.0	0.0	0.1	1.1	-0.0	0.0	46.6	0.0
8	-0.0	1.2	0.1	-0.0	-0.0	-0.0	0.0	0.0
9	0.4	16.3	1.7	66.2	0.3	2.4	5.9	0.2
10	0.1	59.7	0.2	7.9	0.0	13.1	0.7	0.0
11	0.0	12.5	0.0	14.2	0.1	33.9	1.5	0.1
12	12.0	2.4	26.6	2.1	0.7	0.0	0.2	0.3
13	0.4	0.8	1.4	5.9	0.1	0.0	36.8	0.1
14	0.1	5.9	0.2	1.3	-0.0	0.0	7.1	-0.0
15	0.1	0.0	0.2	0.0	0.0	29.4	0.0	0.1
16	10.4	0.1	49.9	0.1	0.4	0.0	1.4	0.0
17	0.1	0.0	-0.0	0.0	2.7	-0.0	0.0	17.8
18	10.9	0.0	0.9	0.1	-5.5	-0.0	0.0	9.2
19	1.7	0.1	0.2	0.1	44.3	-0.1	0.0	4.2
20	0.0	0.1	-0.0	0.1	51.8	-0.1	0.0	3.5
21	65.9	0.0	2.3	0.0	-0.5	-0.0	0.1	1.5

TABLE G3(CCNT.)

ENERGY BAND	% OXYGEN ATOMIC ORBITAL CONTRIBUTION			
	2S(3)	2P(3) Z	2P(3) X	2P(3) Y
1	5.2	-0.5	0.0	1.1
2	2.0	-0.8	C.0	1.4
3	0.2	0.1	-0.4	0.1
4	0.3	1.2	-0.0	16.8
5	-0.7	21.5	-0.0	0.0
6	-1.1	43.0	-0.0	1.1
7	-0.0	0.0	0.0	0.0
8	-0.0	0.0	45.9	0.0
9	0.2	0.3	1.4	2.2
10	0.1	0.0	5.3	12.8
11	0.2	0.2	1.3	32.7
12	0.7	0.2	0.2	0.3
13	0.1	0.0	6.6	0.1
14	0.1	0.0	38.1	0.0
15	0.0	0.1	0.1	31.8
16	0.4	0.1	1.4	-0.0
17	2.7	14.2	0.0	-0.0
18	-4.3	10.6	0.0	-0.0
19	55.1	4.5	0.0	-0.1
20	39.6	3.9	0.0	-0.1
21	-0.6	1.4	0.1	-0.0

TABLE G4   MULLIKEN POPULATION ANALYSIS OF CRYSTAL ORBITALS AT
M SYMMETRY POINT

ENERGY BAND	% RHENIUM ATOMIC ORBITAL CONTRIBUTION								
	$5D_{Z^2}$	$5D_{XZ}$	$5D_{YZ}$	$5D_{X^2-Y^2}$	$5D_{XY}$	$6S$	$6P_Z$	$6P_X$	$6P_Y$
1	0.0	-0.0	-0.0	0.0	-0.0	0.0	101.4	0.0	0.0
2	3.6	0.0	0.1	0.1	-0.0	3.9	-0.0	33.3	45.6
3	0.0	0.1	0.0	9.1	-0.0	0.0	-0.0	47.2	33.9
4	33.4	0.0	0.0	0.0	0.0	2.3	0.5	0.2	0.2
5	0.0	54.2	0.0	0.0	0.0	0.0	0.0	0.2	-0.0
6	0.0	0.0	53.7	0.0	0.0	0.0	0.0	0.0	0.2
7	-0.0	0.0	0.0	0.0	32.2	-0.0	0.0	0.1	0.3
8	0.0	-0.1	-0.0	0.2	0.0	0.0	-0.0	0.0	0.0
9	0.3	-0.0	0.1	0.0	0.1	0.0	-0.0	-0.0	0.1
10	0.0	0.1	-0.0	0.1	0.0	0.0	-0.0	0.3	0.4
11	0.0	0.2	0.2	62.1	0.2	0.0	-0.0	-0.0	-0.0
12	-0.0	0.0	0.0	0.1	56.8	-0.1	-0.0	0.0	0.0
13	0.3	35.1	8.9	0.1	0.0	0.2	0.0	0.3	0.0
14	0.0	9.3	36.0	0.8	0.0	0.0	0.0	-0.1	0.1
15	15.0	0.8	0.7	0.0	0.6	22.6	0.1	-0.9	-1.1
16	6.5	0.1	0.2	0.0	0.1	3.4	0.1	14.8	17.8
17	0.1	0.2	0.1	5.8	0.0	0.0	0.0	16.8	14.8
18	42.6	-0.0	-0.0	0.0	0.0	32.4	-1.3	-0.7	-0.7
19	-4.4	0.0	0.0	0.0	0.0	-5.3	-0.7	-0.0	-0.0
20	0.0	0.0	0.0	21.6	0.0	0.0	-0.0	-6.6	-7.1
21	2.7	0.0	0.0	0.0	0.0	40.5	-0.0	-5.1	-4.6

ENERGY BAND   % CXYGEN ATOMIC CREITAL CCNTRIBUTION

ENERGY BAND	2S(1)	2P (1) Z	2P (1) X	2P (1) Y	2S(2)	2P (2) Z	2P (2) X	2P (2) Y
1	0.0	0.0	0.0	0.0	0.0	0.0	0.0	0.0
2	-2.4	-0.0	7.0	1.5	-3.2	-0.0	0.8	9.7
3	-4.2	-0.0	8.8	1.2	-2.8	-0.0	1.3	5.9
4	0.1	0.2	0.5	0.1	0.1	0.2	5.1	0.4
5	-0.0	1.3	0.0	0.0	0.0	0.0	0.0	0.0
6	0.0	0.0	0.0	0.0	-0.0	1.1	0.0	0.0
7	0.0	0.1	0.8	33.2	-0.0	0.0	31.7	1.4
8	0.0	59.3	0.0	1.1	0.0	31.0	0.9	0.0
9	0.0	32.2	0.1	1.0	-0.0	50.2	2.0	0.0
10	0.0	0.0	1.6	44.1	-0.1	4.7	46.7	1.9
11	4.7	0.2	13.6	0.2	4.6	0.2	0.1	13.7
12	-0.0	0.0	2.3	15.1	0.0	0.0	14.0	1.7
13	-0.0	5.4	2.1	0.0	0.1	1.4	0.0	1.5
14	0.1	1.2	-0.0	0.0	0.1	4.9	0.0	0.6
15	4.9	0.1	19.2	1.1	5.4	0.1	0.8	17.6
16	9.1	0.0	14.5	0.7	9.8	0.0	0.7	17.8
17	5.7	0.0	25.8	0.5	4.2	0.0	0.7	24.1
18	4.9	0.0	0.4	0.0	4.7	0.0	0.0	0.5
19	0.4	0.0	-0.0	0.0	0.4	0.0	0.0	-0.0
20	42.1	0.0	2.2	0.1	45.3	0.0	0.0	2.1
21	34.4	0.0	1.2	0.1	31.4	0.0	0.0	1.2

TABLE G4(CONT.)

ENERGY	% OXYGEN ATOMIC ORBITAL CONTRIBUTION			
BAND	2S(3)	2P (3) Z	2P (3) X	2P (3) Y
1	0.1	-1.5	0.0	0.0
2	0.4	0.1	-0.2	-0.2
3	0.0	0.0	-0.3	-0.2
4	-1.2	62.8	0.0	0.0
5	-0.0	0.0	44.1	0.0
6	-0.0	0.0	0.0	44.9
7	0.0	0.0	0.0	0.0
8	0.0	0.0	5.1	2.5
9	0.1	0.1	2.9	4.9
10	0.0	0.0	0.0	0.3
11	0.0	0.0	0.0	0.0
12	0.0	0.0	0.0	0.0
13	0.0	0.1	35.7	8.6
14	0.0	0.0	9.9	36.9
15	2.7	7.6	1.5	1.3
16	2.3	1.3	0.4	0.5
17	0.0	0.0	0.5	0.5
18	-8.6	25.6	0.0	0.0
19	106.2	3.5	0.0	0.0
20	-0.0	0.0	0.1	0.1
21	-2.0	0.3	0.1	0.1

TABLE 65   MULLIKEN POPULATION ANALYSIS OF CRYSTAL ORBITALS AT
R SYMMETRY POINT

ENERGY BAND	% RHENIUM ATOMIC ORBITAL CONTRIBUTION								
	5D Z2 Z	5D XZ	5D YZ	5D X2-Y2	5D XY	6S	6P Z	6P X	6P Y
1	9.0	-0.0	-0.0	0.4	-0.0	0.0	55.6	4.6	22.9
2	0.4	-0.0	-0.0	9.0	-0.0	0.0	3.1	47.5	33.5
3	0.0	-0.0	-0.0	0.0	-0.0	4.1	25.4	33.7	28.2
4	0.0	2.4	1.3	0.0	29.4	-0.0	0.0	0.0	0.1
5	0.0	19.4	10.6	0.1	0.3	-0.0	0.0	0.0	-0.0
6	0.0	12.1	20.9	0.0	4.8	-0.1	0.3	0.1	0.1
7	0.0	0.2	0.0	0.0	0.0	0.0	0.0	0.0	0.0
8	0.1	1.4	2.1	1.2	0.0	0.0	0.0	0.2	0.2
9	0.1	0.4	0.0	0.0	1.4	0.0	0.6	0.0	0.2
10	1.0	0.0	0.0	61.4	0.2	0.0	0.0	0.2	0.1
11	62.0	0.2	0.2	1.0	0.1	0.0	0.2	-0.0	0.0
12	0.4	0.4	0.6	0.1	62.4	-0.1	-0.0	0.0	0.0
13	0.1	57.0	7.3	0.2	0.8	-0.0	0.0	-0.0	-0.0
14	0.3	6.2	56.6	0.0	0.1	-0.1	0.0	-0.0	0.0
15	0.1	0.3	0.3	0.0	0.3	7.5	5.1	7.0	5.7
16	0.1	0.0	0.0	4.3	0.0	-0.0	0.8	18.1	14.8
17	4.1	0.0	0.0	0.1	0.0	0.0	23.0	2.6	8.5
18	0.0	0.0	0.0	0.0	0.0	42.4	2.3	2.6	2.1
19	19.6	0.0	0.0	2.6	0.0	-0.0	-10.7	-0.4	-7.3
20	2.6	0.0	0.0	19.4	0.0	0.0	-1.5	-11.7	-5.2
21	0.0	0.0	0.0	0.0	0.0	45.8	-4.1	-4.4	-4.0

TABLE G5(CONT.)

ENERGY BAND	% OXYGEN ATOMIC ORBITAL CONTRIBUTION							
	2S(1)	2P (1) Z	2P (1) X	2P (1) Y	2S(2)	2P (2) Z	2P (2) X	2P (2) Y
1	-0.6	1.5	0.7	0.6	-2.8	1.5	0.1	3.7
2	-6.0	0.1	7.6	0.9	-4.0	0.1	1.0	5.2
3	-4.6	0.7	5.9	0.8	-3.8	0.7	0.7	5.2
4	0.0	1.2	0.2	28.6	-0.0	0.1	26.5	0.5
5	0.0	31.3	0.1	2.1	0.0	19.6	0.1	-0.0
6	0.0	7.7	0.9	1.9	-0.0	17.0	4.2	1.1
7	-0.0	10.8	0.0	21.5	0.0	11.7	24.1	0.2
8	0.2	11.3	2.2	21.9	0.0	1.6	24.8	1.5
9	0.0	16.3	0.4	2.0	0.0	29.2	0.3	1.6
10	5.4	0.0	15.6	0.1	3.9	0.0	0.0	11.7
11	1.1	0.2	3.1	0.1	2.5	0.2	0.1	6.7
12	0.0	0.0	2.1	16.5	0.0	0.3	15.6	1.1
13	0.0	14.2	1.1	0.5	0.1	1.1	0.1	0.0
14	0.0	2.2	0.7	0.1	0.0	14.4	0.0	2.2
15	-1.4	1.3	24.8	1.3	-1.2	1.3	1.3	22.0
16	5.4	0.0	26.5	0.6	4.4	0.1	0.8	21.1
17	0.9	0.9	3.7	0.4	2.6	0.9	0.1	12.1
18	17.6	0.0	-0.1	0.0	16.2	0.0	0.0	-0.3
19	1.9	0.2	0.1	0.1	35.6	0.2	0.0	2.3
20	57.7	0.0	3.6	0.1	25.6	0.0	0.1	1.4
21	22.5	0.1	0.8	0.1	20.6	0.1	0.0	0.8

TABLE G5(CONT.)

ENERGY BAND	% OXYGEN ATOMIC ORBITAL CONTRIBUTION			
	2S(3)	2P (3) Z	2P (3) X	2P (3) Y
1	-6.5	8.7	0.1	0.5
2	-0.4	0.5	1.0	0.7
3	-3.3	4.9	0.7	0.6
4	-0.0	0.0	4.9	4.8
5	-0.0	0.1	9.8	6.4
6	-0.1	2.2	9.5	17.2
7	0.0	0.0	17.6	13.8
8	0.0	0.1	23.1	8.1
9	-0.1	3.7	14.5	29.4
10	0.1	0.3	0.0	0.0
11	6.0	16.3	0.2	0.1
12	0.1	0.2	0.2	0.0
13	0.0	0.5	14.7	2.3
14	0.0	2.4	1.2	13.0
15	-1.0	22.2	1.4	1.2
16	0.2	1.1	0.9	0.8
17	6.6	32.9	0.1	0.4
18	17.5	-0.3	0.0	0.0
19	52.5	3.0	0.0	0.1
20	7.4	0.4	0.1	0.0
21	20.9	0.9	0.0	0.0

Appendix H.   TBA Results of KTaO$_3$

Using the same notation as in Appendix G, Table H1 contains the eigenvalues of crystal orbital function $\Psi_i(\underline{k},\underline{r})$ for the i th energy band and Tables H2 to H5 are the corresponding % atomic orbital contributions.

The Fermi energy is -3.8905 Rydbergs.
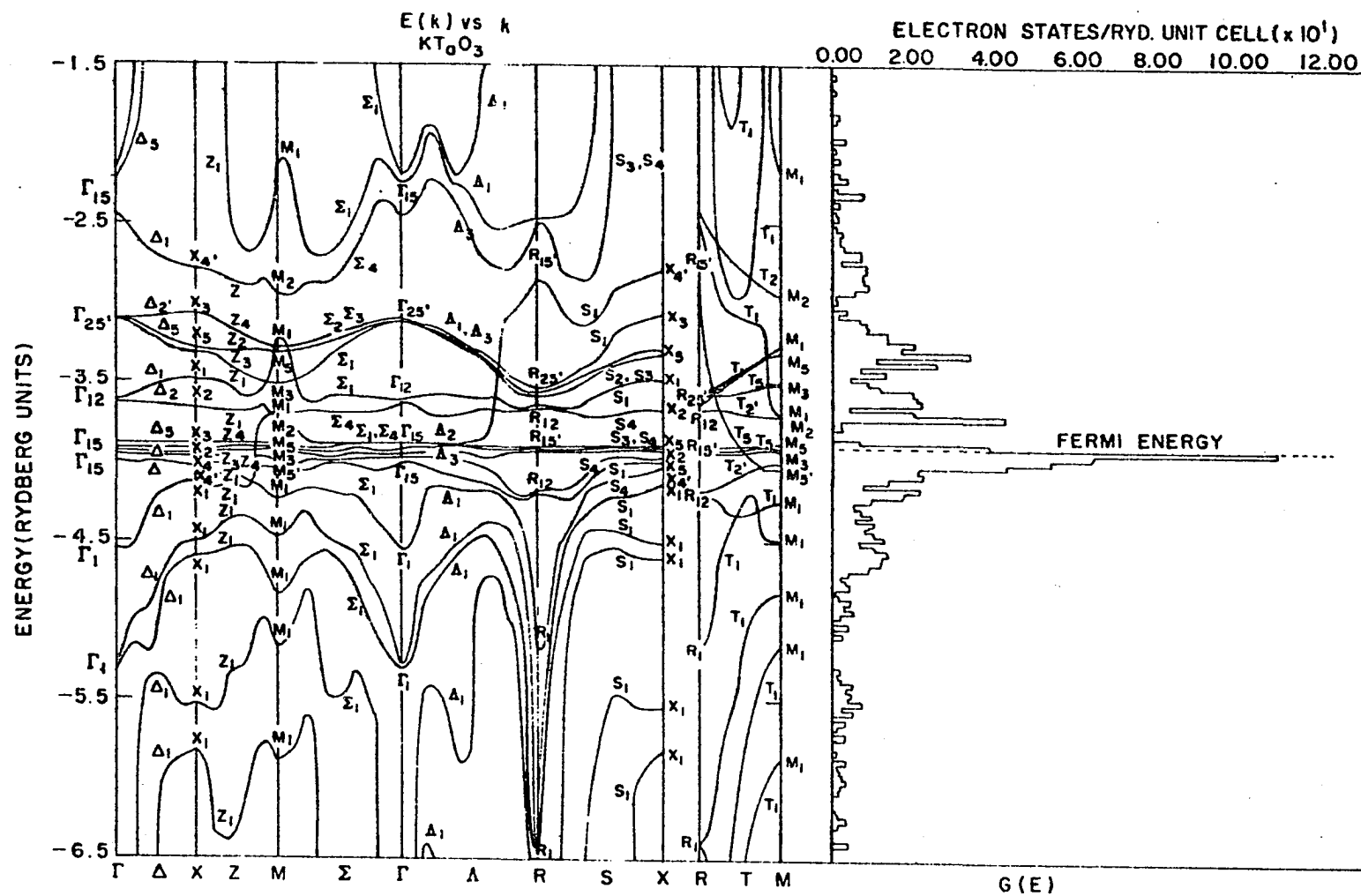
Figure H1. KTaO$_3$ energy bands.

TABLE H1   E(K) VS. K: ENERGY BANDS AT THE SYMMETRY POINTS OF THE BRILLOUIN
ZONE OF POTASSIUM TANTALATE

ENERGY BAND	SYMMETRY POINT GAMMA	X	M	R
1	0.169090E 01	0.701794E 01	0.125720E 04	0.282755E 04
2	0.163503E 01	0.680399E 01	0.237674E 01	0.176071E 01
3	0.156309E 01	0.179607E 01	0.738557E 00	0.160138E 01
4	0.867332E-01	0.162378E 01	0.362849E 00	0.158046E 01
5	-0.218392E 01	0.171296E 00	0.766816E-01	0.938545E 00
6	-0.223361E 01	0.159333E 00	-0.216799E 01	-0.246137E 01
7	-0.243824E 01	-0.279047E 01	-0.293716E 01	-0.250047E 01
8	-0.309717E 01	-0.306559E 01	-0.322630E 01	-0.284783E 01
9	-0.310371E 01	-0.329047E 01	-0.328495E 01	-0.354217E 01
10	-0.312058E 01	-0.332234E 01	-0.332456E 01	-0.355523E 01
11	-0.360746E 01	-0.348923E 01	-0.351424E 01	-0.356930E 01
12	-0.362491E 01	-0.365690E 01	-0.368660E 01	-0.363931E 01
13	-0.388166E 01	-0.389538E 01	-0.372091E 01	-0.366422E 01
14	-0.391499E 01	-0.392919E 01	-0.387496E 01	-0.389963E 01
15	-0.394107E 01	-0.395278E 01	-0.389224E 01	-0.391516E 01
16	-0.395550E 01	-0.395887E 01	-0.391349E 01	-0.392837E 01
17	-0.397562E 01	-0.398559E 01	-0.399299E 01	-0.417548E 01
18	-0.399961E 01	-0.402705E 01	-0.403129E 01	-0.420914E 01
19	-0.455147E 01	-0.412729E 01	-0.424267E 01	-0.516682E 01
20	-0.527699E 01	-0.450757E 01	-0.447299E 01	-0.641118E 01
21	-0.529992E 01	-0.459068E 01	-0.483281E 01	-0.641911E 01
22	-0.685393E 01	-0.552841E 01	-0.515645E 01	-0.668282E 01
23	-0.760151E 01	-0.583213E 01	-0.586593E 01	-0.117929E 02
24	-0.781378E 01	-0.116373E 02	-0.119667E 02	-0.122124E 02
25	-0.991951E 01	-0.140545E 02	-0.129463E 02	-0.244844E 02

TABLE H2 MULLIKEN POPULATION ANALYSIS OF CRYSTAL ORBITALS AT GAMMA SYMMETRY POINT

ENERGY BAND	% TANTALUM ATOMIC ORBITAL CONTRIBUTION								
	$5D\ Z^2$	$5D\ XZ$	$5D\ YZ$	$5D\ X^2-Y^2$	$5D\ XY$	$6S$	$6P\ Z$	$6P\ X$	$6P\ Y$
1	0.1	0.1	0.0	0.1	0.1	0.4	-4.4	-2.2	-0.4
2	0.2	0.0	0.2	0.2	0.1	0.0	-2.0	-4.1	-0.1
3	0.1	0.2	0.0	0.1	0.0	0.5	0.1	0.0	-5.4
4	0.0	-0.0	-0.0	0.0	-0.0	165.1	-6.3	-6.1	-4.8
5	0.9	0.1	0.1	3.0	0.2	0.1	24.7	25.6	48.4
6	3.0	0.0	0.2	1.0	0.3	0.0	51.0	47.2	0.0
7	0.0	0.8	0.8	0.1	0.7	2.0	22.9	25.1	49.4
8	0.0	0.3	8.3	0.0	79.7	0.1	0.8	0.4	0.3
9	0.0	0.1	79.8	0.0	8.6	0.0	-0.0	0.4	0.1
10	0.0	88.2	0.2	0.1	0.2	0.0	0.1	0.1	0.2
11	21.7	0.0	0.6	45.2	0.2	0.0	-0.1	-0.2	-0.1
12	44.1	0.3	0.0	25.6	0.4	0.0	-0.2	-0.0	-0.3
13	0.1	0.0	0.0	0.1	0.0	0.0	0.0	0.0	0.0
14	1.6	0.0	1.1	5.2	1.3	0.2	-0.2	-0.1	-0.4
15	0.3	3.6	1.5	2.1	1.8	6.6	0.0	0.1	-0.1
16	1.9	0.0	3.9	0.7	3.7	0.0	-0.0	-0.0	0.0
17	0.1	5.8	2.0	1.0	1.2	0.0	-0.0	-0.0	-0.2
18	13.8	0.0	0.8	2.6	1.1	0.0	-0.9	-0.7	-0.0
19	-0.0	0.3	0.2	0.2	0.2	85.3	-0.2	-0.3	-0.4
20	1.2	0.0	0.0	5.2	0.0	0.3	-0.2	-0.4	-1.5
21	4.2	0.0	0.0	0.8	0.0	0.0	-1.1	-0.7	0.0
22	0.1	0.2	0.2	0.2	0.2	9.6	1.4	1.6	-0.3
23	1.8	0.1	0.0	4.8	0.0	0.3	1.6	1.4	9.5
24	4.7	0.0	0.0	1.7	0.1	0.0	5.9	5.7	0.0
25	0.1	0.0	0.0	0.0	0.0	27.3	5.2	6.3	6.9

TABLE H2(CONT.)

ENERGY BAND	% OXYGEN ATOMIC ORBITAL CONTRIBUTION							
	2S(1)	2P (1) Z	2P (1) X	2P (1) Y	2S(2)	2P (2) Z	2P (2) X	2P (2) Y
1	-0.0	-0.5	-1.3	0.0	0.1	-0.5	-0.2	-0.3
2	0.1	-0.2	-2.6	0.0	0.0	-0.1	-0.4	-0.0
3	0.0	0.1	-0.0	-0.5	0.0	-0.0	-0.0	-3.4
4	17.1	0.2	0.7	0.2	22.0	0.1	0.1	0.7
5	1.9	-0.3	-0.7	-0.9	5.1	-0.4	-0.4	-1.5
6	4.4	-1.1	-1.1	0.1	-0.0	-1.3	-1.2	-0.0
7	0.3	-0.6	1.0	-1.2	1.4	-0.4	-0.4	1.7
8	0.0	0.0	-0.0	4.3	-0.0	0.6	4.2	0.1
9	0.0	0.0	0.8	0.7	-0.0	3.9	0.3	0.0
10	-0.0	5.0	0.1	-0.0	0.0	0.0	0.0	0.4
11	-2.8	1.8	18.4	2.1	-0.5	0.7	2.6	3.3
12	-0.0	0.3	0.1	0.7	-2.5	2.9	0.2	16.5
13	-0.0	25.9	-0.0	9.5	0.0	14.9	12.7	0.0
14	-0.0	0.1	0.2	6.0	-0.3	35.1	44.8	0.1
15	-0.0	14.2	5.5	22.2	0.1	1.7	1.3	5.7
16	-0.1	4.7	0.0	34.4	0.0	3.1	3.0	0.0
17	-0.0	24.7	0.0	13.4	-0.0	4.8	1.4	-0.0
18	-0.4	17.4	0.2	0.6	-0.0	28.3	25.8	-0.0
19	3.2	2.7	0.9	2.6	0.4	1.0	0.9	0.1
20	15.9	-0.0	5.1	0.6	50.8	0.1	0.1	13.7
21	33.9	0.5	7.7	0.0	0.7	0.7	0.4	0.1
22	0.5	3.6	35.6	2.5	3.7	1.8	2.0	17.5
23	4.9	-0.0	4.8	3.0	12.1	0.3	0.3	46.6
24	9.0	2.2	28.0	0.1	0.0	2.8	2.8	0.1
25	122.2	0.7	5.9	0.9	122.6	0.3	0.5	6.4

TABLE H2(CONT.)

ENERGY BAND	% OXYGEN ATOMIC ORBITAL CONTRIBUTION			
	2S(3)	2P (3) Z	2P (3) X	2P (3) Y
1	0.0	-2.7	-0.2	-0.0
2	0.0	-1.3	-0.4	0.1
3	0.0	0.0	0.2	-0.5
4	16.0	0.7	0.2	0.2
5	1.8	-0.7	-0.3	-0.8
6	4.6	-1.3	-1.0	0.1
7	0.2	1.1	-0.6	-1.2
8	0.0	0.5	-0.0	0.3
9	-0.0	0.3	0.0	4.7
10	-0.0	0.1	5.0	-0.0
11	-0.9	7.3	1.2	0.2
12	-1.8	11.4	0.7	2.5
13	-0.0	-0.0	25.7	11.0
14	-0.0	0.1	0.2	5.4
15	0.2	5.6	11.4	17.0
16	-0.1	-0.0	8.1	36.5
17	-0.0	0.0	29.6	16.4
18	-0.5	0.1	12.1	0.1
19	3.3	1.0	2.6	2.4
20	6.8	2.5	0.0	0.4
21	42.5	10.2	0.3	0.1
22	0.5	33.5	3.9	2.6
23	4.9	6.1	-0.1	3.1
24	9.9	29.1	2.1	0.0
25	119.2	3.6	1.0	1.1

TABLE H2(CCNT.)

ENERGY BAND	% POTASSIUM ATOMIC ORBITAL CONTRIBUTION			
	4S	4P Z	4P X	4P Y
1	-0.1	72.5	34.9	4.2
2	-0.0	37.0	72.6	0.7
3	-0.2	1.0	2.9	104.8
4	-104.9	-0.1	-0.1	-0.9
5	-0.0	-1.5	-1.5	-3.0
6	-0.0	-2.6	-2.4	-0.0
7	-0.7	-0.5	-0.6	-1.2
8	0.0	0.1	0.0	0.0
9	-0.0	0.1	0.2	0.0
10	0.0	0.0	0.0	0.1
11	-0.0	-0.2	-0.5	-0.1
12	-0.0	-0.3	0.0	-0.5
13	-0.0	0.0	0.0	0.0
14	-0.0	-0.1	-0.1	-0.1
15	-0.7	-0.0	-0.0	0.0
16	-0.0	0.1	0.1	-0.0
17	-0.0	-0.0	-0.0	-0.2
18	-0.0	-0.2	-0.1	-0.0
19	-8.9	0.8	0.8	0.9
20	-0.0	-0.1	-0.2	-0.3
21	-0.0	-0.2	-0.1	-0.0
22	-13.0	-3.2	-3.4	-1.4
23	-0.6	-0.6	-0.5	-3.9
24	-0.0	-2.2	-2.1	-0.0
25	-328.9	-0.4	-0.5	-0.4

TABLE H3   MULLIKEN POPULATION ANALYSIS OF CRYSTAL ORBITALS AT
           X SYMMETRY POINT

ENERGY BAND	% TANTALUM ATOMIC ORBITAL CONTRIBUTION								
	5D Z²	5D XZ	5D YZ	5D X²-Y²	5D XY	6S	6P Z	6P X	6P Y
1	0.1	-0.0	0.0	0.0	0.0	0.1	92.9	0.0	0.0
2	0.0	0.0	0.0	0.1	-0.0	0.1	0.0	0.0	90.5
3	0.3	-0.0	0.0	-0.0	0.0	0.5	0.3	0.5	0.0
4	-0.0	0.0	0.0	0.1	0.0	0.3	0.0	0.5	2.9
5	0.0	0.1	0.1	0.0	0.1	1.1	0.0	-2.1	0.0
6	3.0	0.0	0.0	9.9	-0.0	-11.1	0.8	-0.2	1.0
7	1.3	0.4	0.3	3.2	0.4	1.1	0.0	84.9	-0.0
8	0.0	0.0	91.1	0.1	0.0	0.0	0.2	0.1	0.2
9	0.0	5.2	0.0	0.1	87.1	0.0	0.0	0.0	0.0
10	0.1	87.3	0.0	0.3	5.4	0.0	0.0	0.2	-0.0
11	30.9	0.0	0.0	20.5	0.0	0.0	0.7	0.1	1.5
12	16.0	0.3	0.4	26.8	0.3	2.1	1.1	0.9	0.7
13	0.4	0.2	0.0	0.2	1.4	0.2	0.0	-0.0	0.0
14	0.4	1.0	0.1	0.0	0.5	0.0	1.8	0.0	1.2
15	-0.0	0.1	0.0	0.1	3.5	0.2	0.0	-0.0	0.2
16	0.1	2.9	0.0	0.5	-0.2	0.8	0.4	0.0	0.0
17	0.4	0.9	4.6	1.9	0.3	0.7	0.1	0.1	0.3
18	-0.0	1.0	3.3	0.0	0.6	0.1	1.3	0.0	1.7
19	2.6	0.8	0.1	9.2	0.7	1.1	0.4	2.3	0.5
20	-0.1	0.0	0.0	39.4	0.0	-0.2	0.0	8.5	-0.4
21	53.4	-0.0	0.0	-0.2	0.0	0.1	-0.4	2.6	0.1
22	0.4	0.0	0.0	0.2	-0.0	77.7	0.2	2.4	-0.0
23	-5.7	-0.0	0.0	-1.7	-0.0	0.0	0.0	0.2	0.4
24	10.1	-0.0	-0.0	26.7	0.0	-389.3	-3.0	-0.2	-2.5
25	-1.0	-0.0	-0.0	-2.8	-0.0	-1.1	0.0	-5.3	0.0

TABLE H3(CONT.)

ENERGY BAND	% OXYGEN ATOMIC ORBITAL CONTRIBUTION							
	2S(1)	2P (1) Z	2P (1) X	2P (1) Y	2S(2)	2P (2) Z	2P (2) X	2P (2) Y
1	0.0	0.1	0.0	-0.0	0.0	3.1	0.0	0.0
2	-0.0	-0.0	-0.0	0.1	1.7	-0.0	-0.0	1.9
3	0.1	0.1	-0.0	-0.1	-0.1	0.0	0.0	0.0
4	-0.0	-0.1	0.0	0.1	1.4	0.0	-0.0	0.0
5	-28.0	-0.0	-0.0	-0.0	-0.1	0.0	0.5	-0.0
6	0.2	0.0	5.7	0.0	-5.0	0.1	0.0	0.1
7	1.7	0.1	10.5	0.1	0.0	0.0	-0.4	0.0
8	0.1	0.0	0.0	0.0	0.0	4.1	0.0	0.1
9	0.2	-0.0	0.0	-0.7	-0.0	0.0	7.2	0.0
10	0.6	-0.7	0.0	-0.0	0.0	0.0	0.2	0.0
11	0.0	0.3	-0.0	0.2	-2.2	0.6	0.0	29.6
12	0.2	0.0	6.1	0.7	-0.0	1.2	0.3	15.1
13	0.1	22.2	1.5	33.8	0.0	5.2	24.8	0.0
14	0.0	1.2	0.4	0.0	0.0	45.1	5.6	0.3
15	0.5	45.9	1.6	4.1	0.0	0.9	37.9	2.0
16	1.2	6.6	4.6	33.8	0.0	6.4	0.0	2.2
17	1.1	9.8	3.8	12.6	0.4	16.4	3.4	1.2
18	0.8	13.9	0.3	14.5	0.2	16.4	6.7	1.4
19	-0.3	0.0	35.9	0.1	0.5	0.5	11.9	9.4
20	-0.1	0.0	25.7	0.2	-0.3	0.0	0.0	28.3
21	-0.0	0.2	7.6	0.1	0.6	0.1	-0.0	6.4
22	0.1	0.0	1.9	0.2	6.0	0.0	0.1	2.6
23	-0.0	0.4	0.1	0.2	53.0	0.0	-0.0	0.2
24	-1.3	-0.0	-14.7	-0.2	-793.2	0.1	-0.1	0.1
25	-563.6	0.0	0.0	-0.0	-0.1	-0.0	-13.3	-0.0

TABLE H3(CONT.)

ENERGY BAND	% OXYGEN ATOMIC ORBITAL CONTRIBUTION			
	2S(3)	2P (3) Z	2P (3) X	2P (3) Y
1	1.0	1.8	-0.0	0.0
2	0.0	0.0	-0.0	2.9
3	4.4	0.1	0.0	0.0
4	-0.1	0.0	-0.0	0.2
5	-0.1	0.0	0.5	0.0
6	-5.3	0.1	0.0	0.1
7	0.1	0.1	-0.2	-0.0
8	0.0	0.1	0.0	3.9
9	0.0	0.0	0.8	0.0
10	0.0	0.0	6.6	0.0
11	-1.5	18.5	0.0	0.7
12	-0.8	28.0	0.5	0.1
13	0.2	0.0	7.0	2.9
14	0.2	0.3	11.0	31.1
15	0.3	0.6	1.6	0.8
16	0.5	1.2	36.3	2.6
17	0.0	2.5	8.5	31.0
18	0.1	3.3	11.2	23.2
19	0.4	9.4	14.1	0.7
20	0.4	0.0	0.1	0.0
21	-2.7	32.2	0.0	0.0
22	8.6	2.1	0.1	0.0
23	48.6	0.5	-0.0	-0.0
24	-835.0	0.2	-0.1	0.0
25	-0.1	-0.0	-13.6	-0.0

TABLE H3 (CONT.)

ENERGY BAND	% POTASSIUM ATOMIC ORBITAL CONTRIBUTION			
	4S	4P Z	4P X	4P Y
1	-0.0	0.0	0.0	0.8
2	0.0	2.6	-0.0	0.0
3	-0.1	0.4	-0.3	93.8
4	-0.0	94.5	-0.4	0.5
5	127.4	0.0	0.1	0.2
6	0.4	0.7	99.4	0.0
7	-4.5	0.4	0.0	0.4
8	0.0	0.0	-0.0	0.0
9	-0.0	0.0	-0.0	0.0
10	-0.0	0.0	-0.0	0.0
11	-0.0	0.1	0.0	0.1
12	-0.4	0.1	-0.1	0.3
13	-0.0	-0.1	-0.0	-0.1
14	0.0	-0.0	-0.0	0.0
15	-0.0	-0.1	-0.0	-0.0
16	-0.0	0.1	-0.1	-0.1
17	-0.0	-0.0	-0.1	0.1
18	-0.1	0.0	-0.0	0.0
19	-0.0	0.0	-0.3	0.1
20	-1.7	0.0	-0.0	0.1
21	-0.5	0.0	-0.0	0.2
22	-0.9	0.8	-3.5	1.2
23	-0.0	1.2	-0.0	2.2
24	3.1	-8.1	2122.4	-14.5
25	699.9	-0.0	0.9	-0.0

TABLE H4   MULLIKEN POPULATION ANALYSIS OF CRYSTAL ORBITALS AT
            M SYMMETRY POINT

ENERGY BAND	% TANTALUM ATOMIC ORBITAL CONTRIBUTION								
	$5D\ z^2$	$5D\ XZ$	$5D\ YZ$	$5D\ x^2-y^2$	$5D\ XY$	$6S$	$6P\ z$	$6P\ x$	$6P\ y$
1	0.0	0.0	0.0	0.0	-0.0	0.0	97.0	-0.0	-0.0
2	0.6	0.0	0.0	0.0	0.1	3.8	0.0	0.4	1.1
3	0.0	-0.0	0.0	0.0	0.1	2.6	0.0	0.4	1.5
4	-0.0	0.0	0.2	0.0	0.0	0.4	-0.0	0.2	11.7
5	-0.0	0.1	0.0	0.0	0.0	0.6	-0.0	15.5	0.3
6	4.1	0.0	0.0	0.3	0.1	42.1	0.0	6.5	15.7
7	-0.0	0.0	0.1	11.6	0.0	1.0	0.0	44.5	32.3
8	0.4	7.8	28.9	0.6	3.2	7.4	0.0	21.3	10.0
9	0.0	43.5	45.9	1.1	0.4	1.0	0.0	0.8	1.5
10	0.2	44.1	21.2	1.8	3.5	5.7	0.0	13.9	5.2
11	3.4	0.1	0.1	0.3	78.2	0.3	0.0	1.1	0.1
12	60.5	0.1	0.1	7.9	1.2	0.8	0.9	-0.1	0.1
13	6.1	0.0	2.2	66.1	0.0	-0.0	0.1	0.4	2.7
14	0.0	-0.0	-0.8	0.5	0.0	0.0	0.0	0.0	-0.0
15	0.0	-0.8	0.0	0.1	0.1	0.0	-0.0	-0.0	0.0
16	0.0	0.1	0.1	0.1	1.5	0.0	0.0	0.3	0.1
17	0.2	3.8	0.8	-1.2	0.0	0.0	0.0	-0.2	0.1
18	-0.5	0.8	1.2	1.7	0.0	4.6	0.1	-0.0	0.6
19	0.0	1.3	0.0	0.4	0.2	1.1	0.0	15.4	-0.0
20	2.2	0.0	0.3	1.6	4.7	1.2	0.7	-0.0	0.2
21	28.0	0.0	0.2	1.6	1.5	8.2	1.1	-0.0	2.9
22	-0.3	0.0	0.6	5.7	2.9	11.7	0.1	-0.0	19.8
23	-4.8	0.0	0.0	0.0	2.1	8.9	0.0	0.0	0.2
24	6.2	0.5	0.1	37.0	0.5	30.4	-0.0	-53.4	13.6
25	-2.2	-0.0	-0.4	-1.2	0.0	-1.4	-0.0	0.5	-60.2

TABLE H4(CONT.)

ENERGY BAND	% OXYGEN ATOMIC ORBITAL CONTRIBUTION							
	2S(1)	2P (1) Z	2P (1) X	2P (1) Y	2S(2)	2P (2) Z	2P (2) X	2P (2) Y
1	0.0	0.0	0.0	-0.0	0.0	0.0	-0.0	0.0
2	3.1	-0.0	0.2	-0.0	2.1	-0.0	-0.0	0.2
3	-0.0	0.0	0.0	-0.6	-0.8	0.0	-0.5	0.0
4	-0.0	0.0	0.0	0.0	-11.5	-0.0	-0.0	-0.0
5	7.9	-0.0	-0.0	0.0	-0.1	0.0	-0.0	0.0
6	-1.3	0.0	5.9	0.1	-0.6	0.0	1.0	8.6
7	-7.4	-0.0	10.2	0.9	0.3	-0.0	0.8	5.2
8	1.0	-0.1	0.3	1.7	-0.6	-0.2	-0.0	0.1
9	0.2	-0.4	-0.0	0.3	0.1	-0.3	0.0	0.3
10	1.6	-0.4	0.3	1.3	0.1	-0.2	-0.0	0.3
11	0.5	0.0	0.0	15.4	-0.0	0.0	-0.5	-0.0
12	0.7	0.0	0.1	4.1	-0.0	-0.0	0.5	0.9
13	2.2	0.0	-0.5	0.0	1.7	0.5	0.0	1.8
14	0.0	0.7	0.1	0.1	0.0	98.1	0.3	0.7
15	0.0	91.9	0.4	0.5	0.0	0.6	3.6	0.0
16	0.0	4.4	1.1	25.0	0.0	0.6	64.0	0.2
17	0.2	3.1	28.1	0.0	0.5	0.5	0.2	12.5
18	0.3	0.4	6.2	0.7	0.9	0.5	1.0	51.9
19	7.4	0.2	47.6	1.0	0.0	0.0	0.7	-0.0
20	0.1	0.1	0.1	25.6	1.9	-0.0	17.3	3.6
21	-0.0	0.0	0.4	4.6	1.6	-0.0	4.1	7.0
22	0.2	0.0	0.6	14.4	11.4	0.0	4.7	8.4
23	-0.0	0.0	-0.1	0.0	0.1	0.0	3.6	-0.1
24	2573.3	0.0	24.1	0.3	66.6	0.0	0.5	0.2
25	-23.7	-0.0	-0.2	-0.0	-766.0	-0.0	-0.0	0.2

TABLE H4(CONT.)

ENERGY BAND	% OXYGEN ATOMIC ORBITAL CONTRIBUTION			
	2S(3)	2P (3) Z	2P (3) X	2P (3) Y
1	0.0	3.0	0.0	0.0
2	0.5	0.0	-0.1	0.0
3	7.0	0.0	0.0	0.1
4	0.3	0.0	0.1	3.2
5	-0.1	0.0	3.2	0.0
6	9.1	0.2	-0.0	-0.1
7	0.5	0.1	2.8	4.9
8	1.8	0.2	5.4	11.5
9	0.3	0.0	4.8	0.5
10	1.5	0.2	-0.0	0.5
11	0.0	0.5	0.1	0.2
12	-2.8	23.5	0.8	0.5
13	-0.2	2.1	0.1	15.1
14	0.0	0.0	0.1	0.2
15	0.0	0.0	3.7	0.0
16	0.0	0.1	1.2	0.8
17	-0.0	0.4	42.5	9.0
18	0.7	2.9	10.8	15.5
19	0.3	0.6	24.9	0.0
20	6.1	28.5	0.1	7.3
21	-3.8	37.0	0.0	6.1
22	0.1	1.5	0.0	22.0
23	79.3	0.0	0.0	0.0
24	-0.6	0.0	106.2	10.6
25	-0.0	-0.0	-0.2	-62.5

TABLE H4(CONT.)

ENERGY BAND	% POTASSIUM ATOMIC ORBITAL CONTRIBUTION			
	4S	4P Z	4P X	4P Y
1	0.0	0.0	0.0	-0.0
2	0.1	91.4	-0.4	-3.0
3	88.1	0.5	1.4	0.1
4	20.3	0.0	75.1	-0.1
5	4.8	0.0	0.1	67.7
6	3.0	6.8	-0.5	-1.1
7	-0.0	0.0	-1.4	-6.3
8	0.6	0.0	-0.3	-0.9
9	0.1	0.0	-0.3	-0.0
10	0.3	0.1	-0.4	-0.9
11	0.2	0.0	-0.0	-0.0
12	0.2	0.2	0.0	-0.1
13	0.0	0.0	-0.4	-0.1
14	0.0	0.0	-0.0	-0.0
15	-0.0	0.0	0.0	-0.1
16	-0.0	0.0	0.0	-0.0
17	0.0	0.0	-0.0	-0.5
18	-0.0	0.0	-0.0	-0.1
19	0.0	0.0	-0.0	-1.2
20	-1.6	0.2	-0.4	-0.0
21	0.6	0.1	-1.0	0.0
22	0.9	0.3	-4.7	-0.1
23	4.7	0.1	-0.0	-0.0
24	3.4	51.7	-113.4	-2657.7
25	-0.0	-12.7	1007.1	22.9

TABLE H5   MULLIKEN POPULATION ANALYSIS OF CRYSTAL ORBITALS AT
R SYMMETRY POINT

ENERGY BAND	% TANTALUM ATOMIC ORBITAL CONTRIBUTION								
	5D Z^2	5D XZ	5D YZ	5D X^2-Y^2	5D XY	6S	6P Z	6P X	6P Y
1	0.0	-0.0	0.0	0.0	-0.0	93.7	0.0	0.0	0.0
2	0.0	-0.1	-0.1	0.0	-0.2	0.0	1.2	1.4	2.6
3	0.0	-0.1	-0.2	0.0	-0.3	0.0	1.3	0.4	0.0
4	0.0	-1.2	-0.1	0.0	-0.0	0.0	0.6	1.3	0.4
5	0.0	-0.0	-0.0	0.0	-0.0	0.0	0.2	0.2	0.1
6	2.1	0.1	-0.0	6.8	-0.0	-0.0	12.7	12.9	66.7
7	7.3	-0.0	0.8	2.5	0.7	-0.0	46.9	42.5	0.0
8	0.1	0.0	0.8	0.1	0.9	0.2	32.7	39.7	30.6
9	0.0	63.0	2.1	0.0	4.1	0.0	0.1	0.0	0.1
10	0.5	0.7	22.2	0.6	46.6	-0.0	-0.0	0.0	-0.0
11	0.7	4.2	44.1	2.2	17.6	0.0	0.1	0.0	-0.0
12	0.1	0.3	0.4	80.0	0.9	0.0	-0.0	4.0	3.0
13	80.5	0.1	0.4	0.1	0.0	-0.0	6.1	0.4	0.5
14	0.0	0.0	0.2	-0.0	0.2	0.0	0.0	0.0	0.0
15	-0.1	0.0	0.5	0.1	0.6	-0.0	0.2	0.3	0.0
16	0.0	0.1	0.5	0.0	0.4	0.0	1.0	0.8	1.0
17	-0.6	0.1	0.1	-2.0	0.1	-0.0	2.7	2.9	9.2
18	-1.8	0.0	0.0	-0.6	0.1	0.0	9.2	8.2	-0.0
19	0.4	0.0	0.0	0.0	0.0	6.0	1.0	0.9	0.9
20	9.2	0.1	0.1	1.1	0.2	0.0	-7.8	-0.7	-7.8
21	1.2	0.0	0.1	8.8	0.1	0.0	-1.7	-9.3	-5.4
22	0.1	0.2	0.1	0.1	0.1	-0.0	-7.1	-6.4	-3.7
23	0.0	0.4	14.3	0.0	13.9	-0.0	0.0	0.0	1.8
24	0.0	0.0	13.6	0.0	13.9	0.0	0.1	0.2	-0.0
25	0.0	32.1	0.0	0.0	0.0	-0.0	0.4	0.3	0.0

TABLE H5(CONT.)

% OXYGEN ATOMIC ORBITAL CONTRIBUTION

ENERGY BAND	2S(1)	2P (1) Z	2P (1) X	2P (1) Y	2S(2)	2P (2) Z	2P (2) X	2P (2) Y
1	0.0	0.0	2.1	-0.0	0.0	0.0	0.0	2.1
2	0.1	-0.1	-0.0	-1.4	-0.0	-1.4	-1.6	0.0
3	-0.1	-0.2	0.0	-1.4	0.0	-0.5	-0.7	0.0
4	-0.0	-2.6	0.0	-0.1	-0.1	-0.5	-0.1	0.0
5	2.5	0.1	-0.0	0.1	1.6	-0.1	-0.1	0.0
6	-2.2	0.4	2.1	0.9	-11.7	0.2	0.1	7.7
7	-7.3	0.7	5.4	0.3	-0.0	0.1	0.0	0.0
8	-6.1	0.7	1.4	1.4	-4.4	0.3	0.3	0.6
9	-0.0	14.3	0.0	1.2	-0.0	0.0	0.1	0.0
10	0.0	0.1	0.0	18.1	0.0	0.8	1.6	0.0
11	0.0	1.2	0.0	7.5	0.2	1.3	0.5	0.0
12	5.2	0.3	-0.1	0.7	4.9	0.1	0.0	0.1
13	1.4	0.2	0.6	0.1	1.8	0.0	0.0	0.9
14	-0.0	34.4	0.3	4.3	0.0	10.5	11.4	-0.0
15	-0.0	13.1	3.5	11.3	0.0	20.4	23.2	0.0
16	-0.0	0.0	0.0	11.2	-0.0	37.9	34.3	0.1
17	0.4	0.0	15.4	-0.0	1.7	0.0	0.0	55.4
18	1.2	1.3	37.1	0.2	0.0	0.8	0.8	0.0
19	1.2	0.0	29.4	0.0	1.2	0.0	0.0	30.3
20	4.8	-0.0	0.3	0.1	48.2	-0.0	0.4	1.9
21	59.4	0.2	2.0	-0.0	33.0	0.3	-0.0	0.5
22	39.6	0.1	0.3	0.2	22.6	0.5	0.4	0.1
23	0.0	0.2	0.0	22.7	0.8	13.8	13.4	0.0
24	0.0	0.0	-0.0	22.5	0.0	15.4	15.8	0.0
25	0.0	35.6	0.0	0.1	-0.0	0.0	0.0	0.0

ENERGY BAND	% OXYGEN ATOMIC ORBITAL CONTRIBUTION			
	2S(3)	2P (3) Z	2P (3) X	2P (3) Y
1	0.0	2.1	0.0	-0.0
2	0.2	-0.0	-0.1	-1.1
3	-0.1	0.0	0.1	-1.0
4	0.0	0.0	-2.9	-0.8
5	2.7	0.0	0.1	0.1
6	-2.2	2.0	0.4	0.8
7	-8.1	6.8	0.5	0.4
8	-5.1	1.1	0.8	1.3
9	-0.0	0.0	14.1	0.6
10	0.0	0.0	0.2	8.1
11	-0.0	0.1	1.2	18.6
12	0.0	-0.0	0.0	0.0
13	6.9	-1.0	0.3	0.7
14	0.0	0.3	34.5	3.9
15	0.0	3.5	13.2	10.2
16	0.1	0.1	0.0	12.5
17	0.4	14.2	0.0	0.0
18	1.5	40.6	1.3	0.1
19	-0.2	28.7	0.0	0.0
20	49.0	0.7	0.2	0.0
21	10.5	0.2	-0.0	0.1
22	44.3	0.5	0.2	0.1
23	0.0	0.0	0.2	23.2
24	0.0	0.0	0.0	21.9
25	0.0	0.0	35.6	0.2

TABLE H5(CONT.)

ENERGY BAND	% POTASSIUM ATOMIC ORBITAL CONTRIBUTION			
	4S	4P Z	4P X	4P Y
1	0.0	0.0	0.0	0.0
2	6.3	47.9	38.1	8.4
3	0.2	52.1	46.1	4.4
4	1.4	1.3	16.5	86.9
5	81.7	2.6	3.0	5.2
6	0.0	-0.0	-0.0	0.1
7	0.0	0.3	0.3	-0.0
8	2.1	0.2	0.1	-0.0
9	0.0	-0.0	-0.0	0.1
10	0.0	0.1	0.0	0.0
11	0.0	0.1	0.2	0.0
12	0.0	0.0	-0.0	-0.0
13	0.0	0.0	0.0	-0.0
14	0.0	-0.0	-0.0	0.0
15	0.0	0.0	0.0	-0.0
16	0.0	-0.0	-0.0	-0.0
17	0.0	-0.0	-0.0	-0.0
18	0.0	0.0	0.0	-0.0
19	0.0	-0.0	-0.0	-0.0
20	0.0	-0.2	-0.0	-0.1
21	0.0	0.0	-0.1	-0.0
22	8.2	-0.2	-0.1	-0.2
23	0.1	-2.4	-2.4	-0.3
24	0.0	-1.8	-1.7	-0.0
25	0.0	0.1	0.1	-4.0

Appendix I.   TBA Results of $Na_xWO_3(x=1.0)$

Using the same notation as in Appendix G, Table I1 contains the eigenvalues of crystal orbital function $\Psi_i(\underline{k},\underline{r})$ for the i th energy band and Tables I2 to I5 are the corresponding % atomic orbital contributions.

The Fermi energy is -3.2252 Rydbergs.
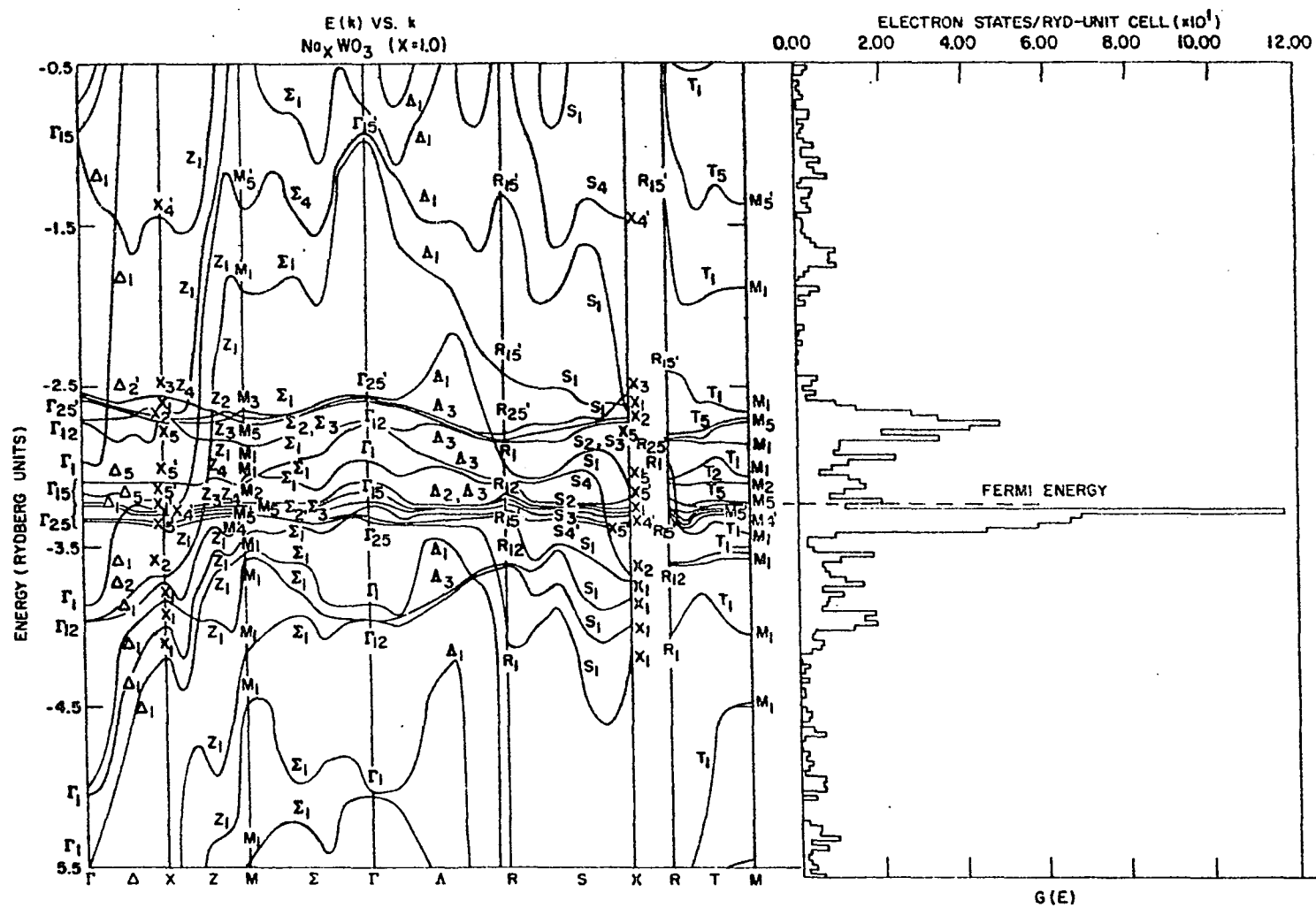
Figure I1. NaWO₃ energy bands.

TABLE I1   E(K) VS. K: ENERGY BANDS AT THE SYMMETRY POINTS OF THE BRILLOUIN
ZONE OF SODIUM TUNGSTEN BRONZE

ENERGY BAND	SYMMETRY POINT GAMMA	X	M	R
1	0.178494E 01	0.497721E 01	0.574128E 03	0.116693E 04
2	-0.738371E 00	0.473387E 01	0.585841E 01	-0.200650E 00
3	-0.925617E 00	0.390161E 01	0.356170E 01	-0.942852E 00
4	-0.954683E 00	0.688576E 00	-0.316201E 00	-0.131859E 01
5	-0.255340E 01	-0.144737E 01	-0.136859E 01	-0.241201E 01
6	-0.255974E 01	-0.255927E 01	-0.189150E 01	-0.278757E 01
7	-0.258314E 01	-0.262527E 01	-0.266169E 01	-0.279475E 01
8	-0.271399E 01	-0.265414E 01	-0.269529E 01	-0.282527E 01
9	-0.271547E 01	-0.269922E 01	-0.271761E 01	-0.301882E 01
10	-0.295949E 01	-0.271037E 01	-0.285791E 01	-0.307885E 01
11	-0.308620E 01	-0.308638E 01	-0.305543E 01	-0.309464E 01
12	-0.315740E 01	-0.319573E 01	-0.309954E 01	-0.316893E 01
13	-0.322106E 01	-0.326368E 01	-0.322471E 01	-0.318935E 01
14	-0.322787E 01	-0.328050E 01	-0.323012E 01	-0.323857E 01
15	-0.332111E 01	-0.329274E 01	-0.326263E 01	-0.326376E 01
16	-0.332646E 01	-0.334659E 01	-0.328530E 01	-0.328558E 01
17	-0.386235E 01	-0.336993E 01	-0.330138E 01	-0.360483E 01
18	-0.396189E 01	-0.367501E 01	-0.341663E 01	-0.360733E 01
19	-0.396253E 01	-0.371564E 01	-0.352958E 01	-0.406588E 01
20	-0.503756E 01	-0.383132E 01	-0.356781E 01	-0.553099E 01
21	-0.505017E 01	-0.400253E 01	-0.404690E 01	-0.555377E 01
22	-0.551776E 01	-0.418687E 01	-0.448079E 01	-0.733287E 01
23	-0.661039E 01	-0.587987E 01	-0.546617E 01	-0.141740E 02
24	-0.719572E 01	-0.770267E 01	-0.625044E 01	-0.165358E 02
25	-0.720820E 01	-0.800292E 01	-0.893844E 01	-0.582785E 02

TABLE 12   MULLIKEN POPULATION ANALYSIS OF CRYSTAL ORBITALS AT
GAMMA SYMMETRY POINT

ENERGY BAND	% TUNGSTEN ATOMIC ORBITAL CONTRIBUTION								
	$5D\ Z^2$	$5D\ XZ$	$5D\ YZ$	$5D\ X^2-Y^2$	$5D\ XY$	$6S$	$6P\ Z$	$6P\ X$	$6P\ Y$
1	-0.0	-0.0	-0.0	-0.0	-0.0	7.5	-0.2	-0.2	-0.2
2	1.0	0.0	0.0	3.4	0.0	0.0	24.3	26.3	33.4
3	3.6	0.0	0.0	1.0	0.0	0.0	42.1	47.1	0.3
4	0.0	0.1	0.2	0.3	0.2	1.6	22.2	14.8	54.2
5	2.2	0.0	38.7	0.6	43.9	0.0	0.0	0.0	0.0
6	0.3	13.6	37.8	1.0	32.2	0.5	0.3	0.3	0.0
7	0.0	73.0	6.3	0.0	6.6	0.3	0.6	0.6	0.1
8	2.2	0.1	2.7	43.1	0.1	0.0	0.1	4.7	3.1
9	43.2	0.1	0.2	2.1	3.0	0.0	4.5	0.2	2.7
10	0.0	0.0	0.5	0.1	0.5	45.9	0.9	0.9	2.5
11	0.4	1.0	0.1	1.3	0.1	1.1	1.3	1.3	1.1
12	0.5	0.0	0.0	0.2	0.0	0.0	0.1	0.1	0.0
13	0.1	10.7	0.5	0.3	0.5	-0.0	0.1	0.1	-0.0
14	0.0	0.0	0.0	0.0	0.0	0.0	0.8	0.8	-0.0
15	0.0	0.0	6.9	0.0	5.7	-0.0	0.2	0.2	0.0
16	0.0	0.8	5.7	0.0	6.8	0.1	0.2	0.3	0.7
17	0.0	0.1	0.0	0.0	0.0	69.0	-0.4	-0.5	-0.8
18	24.7	0.0	0.0	26.6	0.0	-0.0	-0.3	-0.7	-0.1
19	26.7	0.0	0.0	24.8	0.0	0.0	-0.5	-0.1	-0.8
20	-5.7	0.0	0.0	-1.0	0.0	0.0	3.0	2.2	0.1
21	-1.0	0.0	0.0	-5.7	0.0	0.0	0.5	1.3	3.4
22	0.0	0.0	0.0	0.0	0.0	-13.6	1.9	1.9	1.9
23	0.4	0.3	0.1	1.3	0.1	0.6	-0.3	-0.3	-0.2
24	1.3	0.0	0.2	0.4	0.2	0.0	-0.9	-1.2	-0.0
25	0.0	0.2	0.0	0.2	0.0	3.2	-0.5	-0.3	-1.5

232

TABLE I2(CONT.)

ENERGY BAND	% OXYGEN ATOMIC ORBITAL CONTRIBUTION							
	2S(1)	2P (1) Z	2P (1) X	2P (1) Y	2S(2)	2P (2) Z	2P (2) X	2P (2) Y
1	4.7	0.0	0.0	0.0	4.7	-0.0	-0.0	0.0
2	1.7	1.3	0.1	1.4	2.2	1.2	1.3	0.4
3	3.1	0.9	0.1	0.1	0.0	0.3	0.4	-0.0
4	1.0	0.1	-0.1	0.8	3.6	0.6	0.5	-0.2
5	-0.1	0.0	1.2	2.0	0.0	3.5	4.0	0.0
6	0.0	0.6	0.1	1.3	-0.1	4.6	4.0	1.0
7	0.0	5.3	0.0	0.4	0.0	0.5	0.5	-0.0
8	-2.0	0.5	27.8	0.1	-1.1	0.0	-0.0	16.9
9	-0.2	0.3	2.7	1.5	-1.0	-0.0	0.0	14.1
10	-1.9	-0.0	16.3	1.1	-1.6	2.2	1.9	14.3
11	0.0	4.7	1.4	21.8	-0.1	16.7	17.1	4.9
12	-0.0	3.9	0.4	29.3	0.0	14.3	14.2	0.0
13	0.0	32.1	1.6	0.0	-0.0	7.6	7.7	0.1
14	0.0	46.8	0.0	1.9	-0.0	1.4	1.6	0.0
15	-0.0	0.0	0.0	13.0	0.0	31.0	26.9	0.0
16	-0.0	2.8	0.0	24.5	0.0	15.3	19.2	0.0
17	-1.6	0.3	16.0	0.3	-1.3	0.6	0.6	16.0
18	-0.5	0.0	30.4	0.0	-0.1	0.0	0.0	2.8
19	-0.0	0.0	2.0	0.0	-0.5	-0.0	0.0	29.6
20	40.2	-0.0	0.8	0.0	1.0	-0.0	-0.0	-0.0
21	24.1	0.1	0.5	0.0	63.1	0.0	0.0	1.5
22	41.2	-0.0	1.0	0.0	40.8	-0.1	-0.0	0.7
23	0.2	-0.5	-0.6	-0.6	1.3	-0.5	-0.5	0.0
24	1.0	-0.6	-0.6	0.4	0.0	1.2	1.0	-0.0
25	-0.1	1.5	-0.4	0.5	0.2	-0.4	-0.2	-1.4

TABLE I2(CONT.)

ENERGY BAND	% OXYGEN ATOMIC ORBITAL CONTRIBUTION			
	2S(3)	2P (3) Z	2P (3) X	2P (3) Y
1	4.7	0.0	-0.0	-0.0
2	1.6	0.1	1.4	1.5
3	2.7	0.2	0.9	-0.0
4	1.5	-0.2	0.1	0.9
5	-0.1	1.3	0.0	1.8
6	0.0	0.1	0.6	1.5
7	0.0	0.0	5.3	0.4
8	-0.1	1.4	0.4	1.5
9	-2.0	29.3	0.4	0.1
10	-1.8	16.0	-0.0	1.4
11	0.0	1.5	4.7	20.9
12	-0.0	0.5	3.9	29.8
13	0.0	1.5	34.3	0.0
14	0.0	0.1	44.5	1.9
15	0.0	-0.0	0.1	16.3
16	0.0	0.0	2.7	21.1
17	-1.3	14.4	0.3	0.3
18	-0.5	16.1	0.0	0.1
19	-0.5	17.7	0.1	-0.0
20	55.6	1.4	0.0	0.0
21	9.7	0.3	0.1	0.1
22	40.7	0.6	-0.0	0.0
23	0.2	-0.6	-0.5	-0.6
24	0.8	-0.3	-0.4	0.8
25	-0.1	-0.6	1.3	0.1

TABLE I2(CONT.)

ENERGY BAND	% SODIUM ATOMIC ORBITAL CONTRIBUTION			
	3S	3P Z	3P X	3P Y
1	79.0	-0.0	-0.0	-0.0
2	0.0	-0.8	-0.9	-1.1
3	0.0	-1.3	-1.5	-0.0
4	0.3	-0.6	-0.4	-1.5
5	-0.0	0.4	0.4	0.0
6	-0.0	0.1	0.2	0.1
7	-0.0	-0.0	-0.0	-0.0
8	-0.0	-0.0	-0.8	-0.6
9	-0.0	-0.8	-0.0	-0.5
10	-3.1	1.5	1.6	0.8
11	-0.1	-0.5	-0.5	-0.2
12	-0.0	1.5	1.5	0.0
13	-0.0	0.1	0.1	2.7
14	-0.0	0.0	0.0	0.0
15	-0.0	-0.2	-0.2	-0.0
16	-0.0	-0.1	-0.1	-0.0
17	-10.3	-0.4	-0.5	-0.8
18	0.0	0.5	1.0	0.1
19	-0.0	0.5	0.0	0.9
20	0.0	1.4	1.0	0.0
21	-0.0	0.2	0.5	1.4
22	-16.7	-0.1	-0.1	-0.0
23	-0.1	33.8	34.0	32.9
24	-0.0	42.3	53.6	0.7
25	-0.3	22.6	11.2	65.4

TABLE I3   MULLIKEN POPULATION ANALYSIS OF CRYSTAL ORBITALS AT
             X SYMMETRY POINT

ENERGY BAND	% TUNGSTEN ATOMIC ORBITAL CONTRIBUTION								
	5D Z^2	5D XZ	5D YZ	5D X^2-Y^2	5D XY	6S	6P Z	6P X	6P Y
1	0.0	0.0	0.0	0.6	0.0	-0.0	24.3	0.0	88.2
2	0.4	-0.0	0.0	0.1	0.0	0.0	72.2	-0.0	20.3
3	-0.1	-0.0	-0.0	-0.1	-0.0	-1.1	-6.5	-0.0	-18.2
4	-0.3	-0.1	-0.2	-0.6	-0.1	-0.5	-0.0	12.5	-0.4
5	0.0	0.1	0.0	1.2	0.1	1.4	0.0	105.3	0.0
6	1.5	0.6	64.2	3.4	0.1	5.4	0.0	-0.0	-0.0
7	22.5	1.3	20.0	1.2	0.1	12.1	3.5	0.3	0.6
8	20.7	2.5	5.1	24.4	0.6	3.8	0.2	0.5	3.7
9	0.2	22.4	0.1	0.1	67.1	0.2	0.0	0.0	0.0
10	0.1	64.1	0.0	1.6	22.8	0.5	0.0	0.1	0.1
11	5.2	-0.1	0.0	13.8	-0.3	-0.9	-0.1	0.0	-0.0
12	0.5	-0.5	0.1	-0.0	-0.3	0.0	-0.1	0.1	0.0
13	3.0	4.2	0.2	6.8	0.2	6.1	-0.0	0.1	0.2
14	0.1	0.2	0.1	1.5	3.6	0.4	1.1	-0.5	1.0
15	0.3	1.9	0.0	1.6	4.8	1.5	0.6	-0.0	0.3
16	2.0	3.2	2.0	6.1	1.0	4.1	0.8	-0.8	0.0
17	0.8	0.4	8.7	2.0	0.3	2.1	1.5	-0.2	1.8
18	6.7	0.1	0.0	15.9	0.0	0.0	-0.6	3.6	0.1
19	0.2	-0.1	0.1	4.5	0.1	-3.1	-0.7	8.0	0.3
20	4.8	-0.0	0.0	3.8	0.0	6.6	-0.0	0.1	-1.1
21	30.0	0.0	0.0	6.1	0.0	2.1	0.3	0.3	1.0
22	0.0	-0.0	0.0	-0.1	-0.0	53.2	-0.0	1.6	0.9
23	2.5	0.0	0.0	7.3	-0.0	7.6	-0.0	-7.8	-0.0
24	-0.8	-0.0	0.0	-0.6	-0.0	-0.1	0.1	0.4	0.0
25	-0.4	-0.0	0.0	-0.1	-0.0	-2.2	1.0	-0.0	0.0

TABLE I3(CONT.)

ENERGY BAND	% OXYGEN ATOMIC ORBITAL CONTRIBUTION							
	2S(1)	2P (1) Z	2P (1) X	2P (1) Y	2S(2)	2P (2) Z	2P (2) X	2P (2) Y
1	0.0	0.1	0.0	0.0	6.1	1.0	-0.0	0.9
2	-0.0	0.1	-0.0	0.0	0.4	3.1	-0.0	0.2
3	-0.0	0.0	-0.2	-0.1	2.9	-0.3	-0.0	-0.5
4	28.0	-0.0	-0.1	-0.0	0.1	-0.4	1.5	0.0
5	-7.6	0.0	6.1	-0.0	-0.1	0.1	-0.6	0.0
6	-0.1	1.1	0.2	1.2	1.0	4.6	0.0	2.7
7	-0.0	2.9	0.3	3.0	0.7	0.0	0.0	0.3
8	-0.0	0.2	0.0	2.2	0.2	0.9	0.1	26.2
9	-0.0	-0.2	0.0	-0.5	0.0	0.0	7.5	0.1
10	-0.0	-0.6	0.0	0.5	0.0	0.0	2.3	1.5
11	1.8	21.6	2.5	38.0	2.2	0.0	1.1	6.2
12	-0.0	53.2	0.1	30.7	0.9	0.6	2.6	1.1
13	1.8	0.8	25.3	7.5	-0.2	2.1	1.0	1.5
14	0.6	0.2	0.1	0.1	0.7	25.0	29.8	0.6
15	0.7	1.0	2.7	3.9	-0.0	11.9	39.8	0.1
16	0.8	11.2	5.3	0.0	0.0	22.0	13.0	0.8
17	0.2	0.4	5.9	-0.0	0.1	28.1	3.7	2.2
18	6.2	1.8	22.9	-0.0	0.6	0.7	0.1	7.7
19	4.2	5.3	25.6	1.0	0.2	0.1	0.4	1.3
20	0.7	-0.1	1.1	10.1	19.4	0.1	-0.0	39.4
21	-0.0	0.8	0.1	1.1	15.0	0.0	0.0	4.9
22	3.5	0.2	1.3	1.1	21.5	0.0	0.0	2.8
23	123.6	-0.0	1.4	0.0	0.1	0.0	0.7	-0.0
24	0.2	0.3	0.0	0.6	24.8	-0.0	0.0	0.1
25	0.3	-0.0	0.0	-0.4	11.2	-0.0	-0.0	0.1

ENERGY BAND	% OXYGEN ATOMIC ORBITAL CONTRIBUTION			
	2S(3)	2P (3) Z	2P (3) X	2P (3) Y
1	2.5	0.2	-0.0	3.6
2	1.5	0.8	-0.0	0.9
3	1.5	-0.3	0.0	-0.9
4	-0.0	-0.0	1.6	-0.2
5	0.6	0.0	-0.6	0.0
6	1.3	3.3	0.1	7.2
7	3.3	21.6	0.1	0.3
8	-0.2	5.3	0.3	0.3
9	-0.0	0.3	2.6	0.0
10	0.1	0.0	6.9	0.2
11	1.3	5.6	0.3	0.1
12	1.0	1.0	4.7	0.0
13	0.9	0.0	37.6	0.0
14	-0.0	0.0	2.0	32.5
15	-0.1	0.4	13.6	14.8
16	0.6	0.1	28.2	1.0
17	-0.0	0.9	4.5	37.0
18	6.1	25.9	0.2	0.1
19	24.9	17.8	0.1	0.8
20	0.2	0.6	0.1	1.9
21	16.9	13.5	0.0	0.0
22	5.2	3.4	0.0	-0.0
23	-0.1	0.0	0.7	0.1
24	7.4	0.1	0.0	-0.0
25	29.9	0.2	0.0	0.0

TABLE 13(CONT.)

ENERGY BAND	% SODIUM ATOMIC ORBITAL CONTRIBUTION			
	3S	3P Z	3P X	3P Y
1	-0.0	1.4	-29.3	0.3
2	-0.1	0.3	-0.1	0.1
3	0.0	-0.6	125.5	-1.1
4	59.4	-0.0	-0.0	-0.1
5	-7.6	0.3	-0.0	1.2
6	-0.1	1.1	-0.1	1.3
7	-0.3	0.8	-0.2	5.7
8	-0.1	3.1	-0.1	0.2
9	-0.0	0.1	-0.0	0.1
10	-0.7	0.5	-0.0	-0.1
11	-0.0	1.3	0.3	0.2
12	-0.3	2.0	0.0	2.7
13	-0.1	-0.0	0.2	0.7
14	0.6	0.4	0.0	0.1
15	-0.0	0.0	0.1	-0.0
16	-1.8	0.1	0.1	0.1
17	-0.4	0.0	0.2	0.1
18	-2.5	0.1	0.1	4.1
19	-5.0	0.3	1.2	12.4
20	-0.7	12.8	0.2	-0.1
21	-0.0	3.9	-0.0	3.8
22	-3.2	4.8	2.4	1.1
23	-36.6	0.7	-0.4	0.2
24	0.0	49.7	-0.3	18.0
25	-0.0	17.2	-5.0	48.3

239

TABLE 14   MULLIKEN POPULATION ANALYSIS OF CRYSTAL ORBITALS AT M SYMMETRY POINT

ENERGY BAND	% TUNGSTEN ATOMIC ORBITAL CONTRIBUTION								
	$5D\ Z^2$	$5D\ XZ$	$5D\ YZ$	$5D\ X^2-Y^2$	$5D\ XY$	$6S$	$6P\ Z$	$6P\ X$	$6P\ Y$
1	0.0	0.0	0.0	0.0	-0.0	0.0	97.4	-0.0	-0.0
2	-0.4	-0.0	-0.0	-0.6	0.0	-4.4	-0.0	-43.1	0.0
3	-0.0	-0.0	-0.2	-0.1	-0.0	-0.3	-0.0	-0.7	-7.5
4	0.3	0.0	-0.0	0.8	-0.2	38.7	0.1	0.5	16.1
5	3.4	0.0	0.0	1.1	-0.6	3.9	0.1	1.1	57.0
6	0.7	0.1	0.0	2.3	0.1	0.0	0.0	68.0	9.7
7	6.0	32.0	0.6	0.1	23.8	2.8	0.0	7.3	7.5
8	1.2	27.5	52.9	0.0	4.7	0.5	0.0	0.8	1.0
9	0.9	31.0	37.7	0.2	15.0	1.4	-0.0	1.8	1.7
10	37.4	0.6	0.4	0.2	35.9	-0.0	0.5	1.9	1.9
11	9.2	-0.1	-0.1	0.9	11.6	3.6	0.4	1.0	0.6
12	0.4	0.0	0.1	82.2	0.1	-0.0	0.0	0.5	0.6
13	0.0	0.1	-0.1	0.0	-0.0	-0.0	-0.0	0.0	0.0
14	0.0	0.2	-0.3	-0.0	0.0	0.0	0.0	0.1	-0.1
15	0.1	-0.0	-0.0	0.0	0.6	0.2	0.0	0.1	0.0
16	0.1	2.7	5.8	0.0	0.4	0.1	-0.0	-0.1	0.2
17	0.0	5.8	2.6	-0.1	0.1	-0.1	0.0	-0.1	-0.1
18	0.1	0.0	0.0	-0.1	3.8	-2.2	0.5	-0.4	-0.4
19	-0.8	0.6	0.3	-0.0	2.0	0.5	0.0	8.7	2.9
20	-0.1	0.0	0.3	0.4	0.3	0.0	0.0	2.6	9.5
21	45.2	0.0	0.0	0.0	0.4	-1.1	0.9	-0.6	-0.6
22	-2.1	0.0	-0.0	0.1	0.3	59.8	0.1	-1.7	-1.8
23	-0.0	0.0	0.0	12.3	0.0	-0.0	-0.0	-8.7	-7.6
24	-2.1	-0.0	0.0	0.0	1.8	-6.1	-0.0	0.1	0.3
25	0.2	0.0	0.0	0.0	0.2	0.2	-0.0	-5.1	-1.9

TABLE 14(CCNT.)

ENERGY BAND	% OXYGEN ATOMIC ORBITAL CONTRIBUTION							
	2S(1)	2P (1) Z	2P (1) X	2P (1) Y	2S(2)	2P (2) Z	2P (2) X	2P (2) Y
1	0.C	0.0	0.0	-0.0	0.0	0.0	-0.0	0.C
2	11.3	0.0	-1.4	-0.C	-0.9	-0.0	-0.1	-0.0
3	0.4	-0.0	-0.0	-0.0	-3.7	0.0	0.0	-0.2
4	0.6	0.1	0.6	-0.5	5.8	0.1	-0.2	4.2
5	-0.0	0.3	0.0	-0.0	-7.8	0.3	-0.7	1.8
6	-4.6	0.1	6.0	0.1	-1.8	0.0	0.5	0.8
7	3.0	-0.1	0.5	0.3	1.3	0.5	-0.5	0.3
8	0.3	0.1	-0.0	0.0	0.4	0.1	-0.0	-0.0
9	0.8	0.5	-0.1	0.1	-0.4	-0.3	-0.1	0.1
10	2.6	0.2	0.3	1.7	1.3	0.0	0.8	0.2
11	0.2	9.6	0.1	25.2	0.7	9.2	0.8	0.2
12	4.5	0.0	3.0	0.1	3.2	0.1	0.1	3.5
13	-0.0	61.0	0.2	4.1	0.0	10.4	7.5	0.0
14	-0.0	0.8	0.0	10.5	-0.0	59.7	13.6	1.4
15	-0.0	5.8	2.3	18.7	-0.C	2.1	68.8	0.7
16	0.0	1.0	2.2	9.3	0.C	5.7	1.9	1.6
17	0.0	12.2	4.5	0.C	0.1	3.7	0.8	1.0
18	2.7	5.6	8.1	12.8	1.7	5.4	3.9	26.7
19	3.7	2.1	48.5	8.6	1.0	1.8	0.1	7.6
20	0.4	0.2	21.1	3.4	4.2	0.4	1.0	47.8
21	4.C	0.1	1.7	0.1	3.9	0.1	0.1	1.8
22	9.8	0.3	-0.7	2.5	7.9	0.4	0.6	-0.4
23	51.2	0.0	1.5	0.0	53.2	0.0	0.0	1.2
24	0.1	0.3	0.0	2.9	0.0	0.3	1.3	0.0
25	30.7	0.0	0.2	0.1	23.0	0.0	-0.0	0.1

TABLE I4(CONT.)

ENERGY BAND	% OXYGEN ATOMIC ORBITAL CONTRIBUTION			
	2S(3)	2P(3) Z	2P(3) X	2P(3) Y
1	0.0	2.6	0.0	0.0
2	-0.3	-0.0	0.3	-0.1
3	0.0	-0.0	0.1	-1.7
4	15.5	0.7	0.0	-0.1
5	12.3	0.5	-0.0	-0.4
6	0.5	0.0	0.0	0.1
7	0.4	0.2	2.8	0.6
8	0.0	0.1	3.4	6.0
9	-0.0	0.0	3.1	2.1
10	-0.9	14.0	0.0	0.1
11	-0.1	17.0	0.0	-0.0
12	0.0	0.5	0.0	0.1
13	0.0	0.1	14.6	2.0
14	0.0	0.0	2.2	11.3
15	0.2	0.0	0.0	0.5
16	0.3	0.1	22.6	46.6
17	0.0	0.2	44.8	23.7
18	6.3	22.8	0.7	-0.0
19	4.2	0.9	4.4	1.9
20	1.2	0.8	1.3	3.9
21	0.8	37.6	0.0	0.0
22	0.6	1.8	0.1	0.1
23	0.2	0.0	0.2	0.1
24	60.5	0.2	0.0	0.0
25	0.1	0.1	0.1	0.0

TABLE I4(CONT.)

ENERGY BAND	% SODIUM ATOMIC ORBITAL CONTRIBUTION			
	3S	3P Z	3P X	3P Y
1	0.0	0.0	0.0	-0.0
2	-0.0	-6.3	2.6	143.4
3	-0.0	-0.8	113.1	1.6
4	10.9	6.7	0.1	-0.6
5	23.3	2.1	2.0	0.3
6	2.7	0.4	0.8	13.5
7	6.8	2.3	1.4	0.1
8	1.0	0.1	-0.0	0.0
9	2.8	0.4	1.4	0.0
10	-0.6	0.6	0.9	0.0
11	9.8	0.4	0.1	-0.0
12	0.0	0.0	0.8	0.2
13	-0.0	0.0	0.1	0.0
14	0.3	0.0	0.2	-0.0
15	-0.1	0.0	-0.0	-0.0
16	-0.7	0.0	0.1	0.0
17	0.0	0.0	0.4	0.1
18	-1.5	3.1	0.4	0.2
19	0.1	0.8	0.3	-0.1
20	-0.4	0.3	1.3	-0.0
21	0.3	4.7	0.4	0.1
22	7.1	14.6	1.3	-0.5
23	0.1	0.0	-0.7	-3.1
24	39.8	0.6	-0.1	0.0
25	0.4	61.7	-2.9	-7.1

TABLE I5   MULLIKEN POPULATION ANALYSIS OF CRYSTAL ORBITALS AT
R SYMMETRY POINT

ENERGY BAND	% TUNGSTEN ATOMIC ORBITAL CONTRIBUTION								
	5D Z^2	5D XZ	5D YZ	5D X^2-Y^2	5D XY	6S	6P Z	6P X	6P Y
1	0.0	0.0	0.0	0.0	0.0	93.4	0.0	0.0	0.0
2	0.0	-0.2	-0.0	0.0	-0.0	0.2	18.0	17.2	12.8
3	1.2	1.2	0.3	3.3	0.3	-0.0	15.5	12.9	63.9
4	4.5	0.0	0.1	1.7	0.1	-0.0	46.8	50.9	0.0
5	0.0	5.6	3.6	0.0	3.6	0.1	17.5	17.9	19.0
6	0.1	45.9	28.6	0.4	28.4	0.0	0.0	0.0	0.8
7	0.0	0.0	50.7	0.0	51.4	-0.0	0.0	0.0	0.0
8	-0.0	54.6	17.5	0.0	16.9	0.0	0.8	0.8	1.3
9	4.2	-1.0	1.0	24.8	1.1	-0.0	0.7	0.2	-0.0
10	67.6	-0.0	-0.0	13.5	-0.0	-0.0	1.1	0.7	-0.0
11	9.7	-0.0	0.2	43.5	0.2	-0.0	1.2	1.3	3.2
12	0.3	-0.0	-0.2	0.5	-0.2	0.0	0.2	0.2	-0.0
13	0.1	-0.7	0.6	0.1	0.6	0.0	0.2	0.2	0.1
14	-0.1	0.0	0.1	-0.0	0.0	-0.0	0.1	0.1	0.0
15	-0.0	-0.0	0.5	-0.0	0.5	0.0	0.2	0.1	0.0
16	0.0	0.6	0.5	0.0	0.6	0.0	0.9	0.8	1.2
17	-0.1	-0.0	-0.0	0.0	-0.0	0.0	7.4	0.6	11.0
18	-0.0	-0.0	-0.0	-0.1	0.0	0.0	5.6	11.7	1.4
19	0.2	-0.0	-0.0	0.0	-0.0	6.3	1.1	1.6	1.6
20	3.1	-0.0	-0.0	9.1	-0.0	0.0	-3.2	-3.1	-13.2
21	9.2	-0.0	-0.0	3.1	-0.0	0.0	-9.8	-9.9	-0.0
22	0.0	-0.1	-0.1	0.0	-0.1	-0.0	-4.6	-4.6	-4.4
23	0.0	-0.3	-1.8	0.0	-1.8	-0.0	0.0	-0.0	2.1
24	-0.0	-0.0	-1.5	-0.0	-1.6	-0.0	0.3	3.3	-0.0
25	0.0	5.6	0.0	0.0	0.0	0.0	-0.3	-0.3	-0.0

TABLE 15(CCNT.)

ENERGY BAND	% OXYGEN ATOMIC ORBITAL CONTRIBUTION 2S(1)	2P (1) Z	2P (1) X	2P (1) Y	2S(2)	2P (2) Z	2P (2) X	2P (2) Y
1	0.0	0.0	2.2	-0.0	0.0	0.0	0.0	2.2
2	3.4	0.8	0.1	0.2	3.5	-0.0	-0.0	0.0
3	-2.2	3.9	1.3	4.2	-9.9	2.0	1.9	5.3
4	-8.5	0.6	4.9	0.2	-0.0	-0.0	-0.0	0.0
5	3.3	1.2	1.2	0.4	2.8	0.1	0.0	1.1
6	0.1	-0.7	0.0	-0.5	-0.1	2.7	2.8	0.2
7	-0.0	0.0	-0.0	-0.6	0.0	1.2	1.2	-0.0
8	0.8	0.9	0.1	0.0	0.6	1.7	1.8	0.2
9	0.3	11.1	-0.2	13.2	1.8	13.9	14.3	-0.6
10	3.5	0.9	4.4	0.6	0.0	0.0	0.0	0.1
11	1.3	2.3	2.1	4.6	3.4	7.0	7.0	9.7
12	0.0	8.5	0.0	32.0	0.0	12.8	14.3	0.0
13	-0.0	26.0	0.3	3.0	0.0	26.1	24.6	0.2
14	-0.0	37.8	1.3	10.8	0.0	0.1	0.1	0.0
15	-0.0	1.6	1.8	10.2	0.0	36.1	35.0	0.0
16	0.1	14.7	0.0	29.2	0.0	2.5	3.1	1.1
17	0.1	0.5	2.5	0.7	2.7	0.4	-0.0	42.0
18	2.8	0.5	45.5	0.1	0.3	0.7	1.2	5.6
19	0.4	-0.0	29.7	-0.0	0.4	-0.0	-0.0	30.3
20	16.5	-0.1	0.6	0.0	69.0	0.0	-0.0	2.5
21	52.1	0.1	2.1	-0.0	0.0	0.2	0.1	0.0
22	25.9	-0.1	0.0	-0.1	24.7	-0.0	-0.0	0.0
23	0.0	-1.5	0.1	-4.9	0.5	-5.9	-5.9	-0.0
24	0.0	0.1	0.0	-3.6	0.0	-1.5	-1.5	0.0
25	-0.0	9.3	-0.0	-0.3	0.0	0.0	0.0	-0.0

TABLE 15(CONT.)

ENERGY BAND	% OXYGEN ATOMIC ORBITAL CONTRIBUTION			
	2S(3)	2P (3) Z	2P (3) X	2P (3) Y
1	0.0	2.2	C.C	-0.C
2	3.5	0.1	0.7	0.1
3	-2.6	1.5	3.6	3.8
4	-7.8	4.7	0.7	0.2
5	3.2	1.1	1.3	0.5
6	0.0	0.0	-0.7	-0.5
7	-0.0	-0.0	C.C	-C.6
8	C.7	0.1	1.0	0.1
9	-0.1	0.1	13.1	16.7
10	4.7	2.9	0.1	0.1
11	0.9	1.6	1.5	2.5
12	0.0	0.0	9.4	32.0
13	C.0	0.4	25.7	2.2
14	-0.0	1.3	37.3	11.2
15	-0.0	1.8	1.2	10.8
16	C.2	0.0	14.5	27.8
17	1.8	29.8	0.C	C.8
18	1.3	22.2	1.0	0.1
19	-0.1	27.9	-0.C	-0.C
20	16.9	0.5	-0.1	-0.C
21	51.2	1.5	0.1	-0.0
22	26.3	0.1	-C.1	-C.1
23	0.0	0.1	-1.6	-5.1
24	C.0	C.0	C.1	-3.6
25	-0.0	-0.0	9.3	-0.3

TABLE I5(CONT.)

ENERGY BAND	% SODIUM ATOMIC ORBITAL CONTRIBUTION			
	3S	3P Z	3P X	3P Y
1	0.0	0.0	0.0	-0.0
2	40.5	0.1	0.2	-1.0
3	0.2	-2.4	-2.3	-6.9
4	0.0	0.4	0.4	0.0
5	21.3	-0.8	-0.8	-3.1
6	0.1	-2.3	-2.3	-3.1
7	0.0	-1.7	-1.8	-0.0
8	1.9	-0.8	-0.7	-0.4
9	0.1	-4.3	-4.9	-5.6
10	0.0	-0.1	-0.0	-0.0
11	0.0	-1.7	-1.3	-0.7
12	0.0	-5.0	-4.8	-0.0
13	0.0	-0.3	-0.4	-9.1
14	0.0	-0.1	-0.1	-0.0
15	0.0	0.1	0.0	-0.0
16	0.1	0.7	0.7	0.6
17	0.0	-0.1	-0.1	-0.1
18	0.0	0.0	0.0	-0.0
19	0.2	0.2	0.2	0.3
20	0.0	0.5	0.5	0.5
21	0.0	0.0	-0.0	0.0
22	35.8	0.7	0.5	0.3
23	0.1	61.1	62.0	2.8
24	0.0	56.6	56.0	0.0
25	-0.0	-0.4	-0.4	77.9

Appendix J. Translational Symmetry

The TBA approximation depends on a successful amalgamation of a LCAO (linear combination of atomic orbitals) with the translational symmetry possessed by a crystal. Let us discuss the translational symmetry aspect of the problem and show how the LCAO approach enters into the TBA method.

Vectors $R_p = p_1 t_1 + p_2 t_2 + p_3 t_3$ connect equivalent points in ordinary space. The unit cell is defined by the basis vector set t. For an infinite crystal, the components (p_1, p_2, p_3) can assume any integral value. Such vectors R_p are defined as translation vectors.

Let T_1, T_2 and T_3 be translation operators connected with the primitive translations t_1, t_2 and t_3 respectively. Generally T_v (v=1,2 or 3) operates on some function $f(r)$ to give

$$T_v f(r) = f(r + t_v).$$

In terms of a translation vector R_p, a translation operator $T(p)$ is defined as

$$T(p) = T_1^{p_1} T_2^{p_2} T_3^{p_3}$$ where $T_1^{p_1} f(r) = f(r + p_1 t_1)$.

However, if we take a microcrystal, eg. $p_1 = 1000 = p_2 = p_3$, in a bulk solid, we still have the translational symmetry of the particular crystal. That is, the microcrystal is repeated throughout the crystal in a periodic fashion. In general we shall define the microcrystal as containing G unit cells.

By restricting the size of the microcrystal to some finite size, namely G unit cells, we obtain the Born-von-Kármán (43) cyclic boundary condition, i.e.

$$f(\underline{r}+G\underline{t}_v) = f(\underline{r}).$$

In other words, we never pass through the surface of the microcrystal, but instead circle back to the origin. each microcrystal contains G^3 lattice points defined by the inequality $0 \leq p_v \leq G-1$ ($v=1,2,3$). Lowdin(86) calls this inequality the "ground domain (G)". Other equally good ground domains are

$$1 \leq p_v \leq G \text{ and}$$

$$-(G-1)/2 \leq p_v \leq (G-1)/2.$$

The implications of the above boundary conditions are two-fold

1) $T_v^G = 1$.

2) The three translations will now be cyclic operators of order G having eigenvalues $\exp(2\pi i \, \underline{k}_v/G)$ where k_v equals an integer.

The second implication deserves some discussion. The translation operator on a function $f(\underline{r})$ gives us the usual eigenvalue problem where

$$T(p) \, f(\underline{r}) = \lambda_p f(\underline{r}+\underline{R}_p).$$

λ_p is the eigenvalue of translation $\underline{R}_p$. Since $\langle f(\underline{r}) | f(\underline{r}) \rangle$

and $\langle T(p)\ f(r)|T(p)\ f(r)\rangle$ have the same value because of translational symmetry (that is, $f(r)=f(\underline{r}+\underline{R}_p)$), λ_p is a complex number of modulus unity of $\lambda_p=\exp(i\theta_p)$. θ_p is related to the translation vector $\underline{R}_p$ by the expression

$$\theta_p=\underline{k}\cdot\underline{R}_p$$

which is the inner product of $\underline{R}_p$ and the wave vector $\underline{k}$ in reciprocal space. This identification is made via the definition of a wave vector $\underline{k}$

$$\underline{k}=2\pi(K_1\underline{b}_1 + K_2\underline{b}_2 + K_3\underline{b}_3)\ \text{or}$$

$$\underline{k}=k_x\underline{b}_1+k_y\underline{b}_2+k_z\underline{b}_3$$

where the basis set $\underline{b}$ is inversely related to $\underline{t}$. As in recent literature on energy band theory, $\underline{k}$ components are expressed by (k_x, k_y, k_z) which are not integers while K_v $(v=1,2,3)$ are.

The function $f(\underline{r})$ is characterized by a particular vector $\underline{k}$ which appears in the eigenvalue of each translation operator. Thus, $f(\underline{r})$, if a periodic function, gives

$$f(\underline{r}+\underline{R}_p)=\exp(i\underline{k}\cdot\underline{R}_p)f(\underline{r}).$$

This relation is referred to as Bloch's theorem (87).

If a localized function $f(\underline{r})$ is not a function of $\underline{k}$, but is still periodic, we can use Bloch's suggestion (87) to obtain $f(\underline{k},\underline{r})$ by multiplying $f(\underline{r})$ by a phase factor $\exp(i\underline{k}\cdot\underline{R}_p)$ for each translation $\underline{R}_p$. This can be shown for

the q th atomic orbital function $\phi_{q\beta}$ for an electron located at $\underline{r}-\underline{\rho}_\beta$ (see Figure 1) or $\phi_{q\beta}(\underline{r}-\underline{\rho}_\beta)$. For instance, a translation $-\underline{R}_p$ corresponds to the eigenvalue equation

$$T(-p)\phi_{q\beta}(\underline{r}-\underline{\rho}_\beta)=\phi_{q\beta}(\underline{r}-\underline{\rho}_\beta-\underline{R}_p)=\exp(-i\underline{k}\cdot\underline{R}_p)\phi(\underline{r}-\underline{\rho}_\beta).$$

The position vector $\underline{r}-\underline{\rho}_\beta-\underline{R}_p$) is shown in Figure 2. Then $f(\underline{k},\underline{r})=\phi_{q\beta}(\underline{r}-\underline{\rho}_\beta)=\exp(i\underline{k}\cdot\underline{R}_p)\phi_{q\beta}(\underline{r}-\underline{\rho}_\beta-\underline{R}_p)$. In general, we define the sum of $f(\underline{k},\underline{r})$ for all possible translations as the Bloch sum $b_{q\beta}(\underline{k},\underline{r})$ which corresponds to the q th atomic orbital located on atomic site β. That is,

$$b_{q\beta}(\underline{k},\underline{r})=N_{q\beta}^{-\frac{1}{2}}\sum_p \exp(i\underline{k}\cdot\underline{R}_p)\phi_{q\beta}(\underline{r}-\underline{\rho}_\beta-\underline{R}_p).$$

The normalization constant $N_{q\beta}$ of Bloch sum $b_{q\beta}$ is obtained by the evaluation of the self-overlap of un-normalized Bloch sums.

We are now equipt to expand the crystal orbitals $\Psi_m(\underline{k},\underline{r})$ into a linear combination of Bloch sums which for the m th crystal orbital function becomes

$$\Psi_m(\underline{k},\underline{r})=\sum_{q\beta} b_{q\beta}(\underline{k},\underline{r})C_{qm}^\beta(\underline{k}).$$

$C_{qm}^\beta(\underline{k})$ is the corresponding expansion coefficient.

With a knowledge of the linear combination of Bloch sums after one evaluates the coefflients $C_{qm}^\beta(\underline{k})$ for the wave vector coordinates, i.e. (k_x, k_y, k_z), one can classify the energy band symmetry to the proper irreducible repres‑ entations of subgroups of the space group to which the

crystal belongs. Available group theoretical character tables for all of the subgroups of the θ_h space group (88) facilitates this classification for perovskite transition metal oxides which are simple cubic or O_h^1.

Appendix K. Unitary Transformations

Ziman(4) shows how Wannier functions are obtained from
Bloch sums using a unitary transformation. In the tight-
binding limit, atomic orbital functions are obtained in the
same manner:

$$\sum_{\underline{k}} \exp(-i\underline{k}\cdot\underline{R}_\ell) b_{q\alpha}(\underline{k},\underline{r}_\mu) =$$

$$= N^{-\frac{1}{2}} \sum_{q\alpha} \sum_{\underline{k}\,\underline{R}_p} \exp(i\underline{k}\cdot(\underline{R}_p - \underline{R}_\ell)) \phi_{q\alpha}(\underline{r}_\mu - \underline{\rho}_\alpha - \underline{R}_p)$$

$$= \frac{G}{N^{\frac{1}{2}}} \sum_{q\alpha} \sum_{\underline{R}_p} \delta_{\underline{R}_p,\underline{R}_\ell} \phi_{q\alpha}(\underline{r}_\mu - \underline{\rho}_\alpha - \underline{R}_p)$$

$$= \frac{G}{N^{\frac{1}{2}}} \sum_{q\alpha} \phi_{q\alpha}(\underline{r}_\mu - \underline{\rho}_\alpha - \underline{R}_p). \tag{K1}$$

The crux of this unitary transformation is the identity (4)

$$\sum_{\underline{k}} \exp(i\underline{k}\cdot(\underline{R}_p - \underline{R}_\ell)) = G \delta_{\underline{R}_p,\underline{R}_\ell} \tag{K2}$$

where G equals the number of unit cells in the microcrystal.

We will use the unitary transformation to obtain
$\mathcal{F}^{Ave}(\underline{r}_\mu)$ and $n_{q\alpha}$ (note that the position vector $\underline{r}$ is label-
ed to facilitate easier notation).

The Fock operator on electron μ in state $\underline{k}$ is $\mathcal{F}(\underline{k},\underline{r}_\mu)$
defined in Equation 17. $\mathcal{F}(\underline{k},\underline{r}_\mu)$ averaged over $\underline{k}$ space
yields

$$\overset{Ave}{\mathcal{F}}(\underline{r}_\mu) = \frac{1}{G}\sum_{\underline{k}} \exp(i\underline{k}\cdot\underline{R}_\ell)\exp(-i\underline{k}\cdot\underline{R}_\ell)\mathcal{F}(\underline{k},\underline{r}_\mu)$$

$$= -\nabla_\mu^2 - \sum_\gamma 2Z_\gamma/r_{\gamma\mu}$$

$$+ \frac{1}{G}\sum_{\underline{k}}\sum_{q\alpha,t\beta} p_{\underline{k}}(q\alpha,t\beta)\exp(i\underline{k}\cdot\underline{R}_\ell)\exp(-i\underline{k}\cdot\underline{R}_\ell)\cdot$$

$$\cdot \sum_{\underline{R}_\xi}\sum_{\underline{R}_\nu}\exp(-i\underline{k}\cdot\underline{R}_\xi)\exp(i\underline{k}\cdot\underline{R}_\nu)\cdot$$

$$\cdot \frac{1}{N_q^{\frac{1}{2}}N_t^{\frac{1}{2}}}\frac{1}{2}\left\{2\langle\phi_{q\alpha}(\underline{r}_\mu-\underline{\rho}_\alpha-\underline{R}_\xi)\,\phi_{t\beta}(\underline{r}_\mu-\underline{\rho}_\beta-\underline{R}_\nu)|\right.$$
$$\left. -\langle\phi_{q\alpha}(\underline{r}_\mu-\underline{\rho}_\alpha-\underline{R}_\xi)|\phi_{t\beta}(\underline{r}_\mu-\underline{\rho}_\beta-\underline{R}_\nu)\right\} \quad (K3)$$

Bringing the phase factors $\exp(\mp i\underline{k}\cdot\underline{R}_\ell)$ into the double sum over the translation vectors in Equation K3 and using Equation K2 we obtain the transformed expression

$$\overset{Ave}{\mathcal{F}}(\underline{r}_\mu) = -\nabla_\mu^2 - \sum_\gamma 2Z_\gamma/r_{\gamma\mu}$$

$$+ \frac{1}{G}\sum_{q\alpha,t\beta}\sum_{\underline{R}_\xi}\sum_{\underline{R}_\nu}\frac{G^2}{N_q^{\frac{1}{2}}N_t^{\frac{1}{2}}}\delta_{\underline{R}_\xi,\underline{R}_\ell}\delta_{\underline{R}_\nu,\underline{R}_\ell}\left\{\begin{array}{l}Coulomb\\\&exchange\\operators\end{array}\right\}\cdot$$

$$\cdot \sum_{\underline{k}} p_{\underline{k}}(q\alpha,t\beta)$$

and rearrangement after summing over $\underline{R}_\xi$ and $\underline{R}_\nu$ yields

$$\overset{Ave}{\mathcal{F}}(\underline{r}_\mu) = -\nabla_\mu^2 - \sum_\gamma 2Z_\gamma/r_{\gamma\mu} + \sum_{q\alpha,t\beta}\frac{G\cdot G}{N_q^{\frac{1}{2}}N_t^{\frac{1}{2}}}\left\{2\langle\phi_{q\alpha}(\underline{r}-\underline{\rho}_\alpha-\underline{R}_\xi)\phi_{t\beta}(\underline{r}-\underline{\rho}_\beta-\underline{R}_\nu)|\right.$$
$$\left. -\langle\phi_{q\alpha}(\underline{r}-\underline{\rho}_\alpha-\underline{R}_\xi)|\phi_{t\beta}(\underline{r}-\underline{\rho}_\beta-\underline{R}_\nu)\right]$$

$$\cdot \frac{1}{G} \sum_{\underline{k}} p_{\underline{k}}(q\alpha, t\beta) \ . \qquad\qquad (K4)$$

If we let $\underline{r}=\underline{r}'+\underline{R}_v$ and make substitution into Equation K4, we obtain using $\underline{R}_p=\underline{R}_\xi - \underline{R}_v$ (also dropping the prime over the dummy index)

$$\mathcal{F}^{\text{Ave}}(\underline{r}_\mu)= -\nabla_\mu^2 -\sum_\gamma 2Z_\gamma/r_{\delta\mu} + \sum_{q\alpha,t\beta} p^{\text{Ave}}(q\alpha, t\beta) \cdot$$

$$\frac{G \cdot G}{N_q^{\frac{1}{2}} N_t^{\frac{1}{2}}} \left\{ \langle 2\ \phi_{q\alpha}(\underline{r}-\underline{\rho}_\alpha-\underline{R}_p)\ \phi_{t\beta}(\underline{r}-\underline{\rho}_\beta)| \right.$$

$$\left. -\langle\phi_{q\alpha}(\underline{r}-\underline{\rho}_\alpha-\underline{R}_p)|\phi_{t\beta}(\underline{r}-\underline{\rho}_\beta) \right\} \qquad (K5)$$

where $p^{\text{Ave}}(q\alpha, t\beta)$ is the average bond order matrix over $\underline{k}$ space.

In Appendix C, we find basis for making a further simplification of Equation K5 whereby the product of G and the Coulomb and exchange operators for a particular translation $\underline{R}_p$ is essentially a sum over all possible translation vectors where p ranges from 1 to G. Then Equation K5 becomes

$$\mathcal{F}^{\text{Ave}}(\underline{r}) =-\nabla_\mu^2 -\sum_\gamma 2Z_\gamma/r_{\delta\mu} + \sum_{q\alpha,t\beta} p^{\text{Ave}}(q\alpha, t\beta)\frac{G}{N_q^{\frac{1}{2}}N_t^{\frac{1}{2}}}$$

$$\cdot \sum_{p=0}^{G} \left\{ \begin{array}{l} \text{Coulomb and} \\ \text{exhange op-} \\ \text{erators} \end{array} \right\} \qquad (K6)$$

We include p=0 to the sum in Equation K6 in order to establish the convention q = t and $\underline{R}_o=0$.

Let us now proceed to make a similar transformation of the Flodmark population analysis. From Equation 24 we

have an expression for $n_{q\alpha}$ amenable to the unitary transformation. The resulting set of equations for the unitary transformation is

$$n_{q\alpha} = \frac{2}{G} \sum_{\underline{k}} \sum_m^{M_{\underline{k}}} n_{qm}^{\alpha}(\underline{k}) \, \exp(i\underline{k}\cdot\underline{R}_j)\exp(-i\underline{k}\cdot\underline{R}_j)$$

$$= \frac{2}{G} \sum_{\underline{k}} \sum_m^{M_{\underline{k}}} \sum_{t\beta} C_{qm}^{\alpha *}(\underline{k}) \, C_{tm}^{\beta}(\underline{k}) \langle b_{q\alpha}(\underline{k},\underline{r})\exp(-i\underline{k}\cdot\underline{R}_j) | b_{t\beta}(\underline{k},\underline{r})\exp(-i\underline{k}\cdot\underline{R}_j)\rangle$$

$$= \frac{2}{G} \sum_{\underline{k}} \sum_m^{M_{\underline{k}}} \sum_{t\beta} C_{qm}^{\alpha *}(\underline{k}) C_{tm}^{\beta}(\underline{k}) \cdot$$

$$\cdot \exp(i\underline{k}(-\underline{R}_{\xi}+\underline{R}_j))\exp(i\underline{k}\cdot(\underline{R}_v-\underline{R}_j)) \, N_{q\alpha}^{-\frac{1}{2}}N_{t\beta}^{-\frac{1}{2}} \cdot$$

$$\cdot\langle \emptyset_{q\alpha}(\underline{r}-\underline{\beta}_{\alpha}-\underline{R}_{\xi}) | \emptyset_{t\beta}(\underline{r}-\underline{\beta}_{\beta}-\underline{R}_v)\rangle$$

In a manner no different than the unitary transformation of the Fock operator we obtain

$$n_{q\alpha} = \sum_{t\beta} p^{Ave}(q\alpha, t\beta) \frac{G}{N_{q\alpha}^{\frac{1}{2}} N_{t\beta}^{\frac{1}{2}}} \sum_{p=0}^{G} \langle \emptyset_{q\alpha}(\underline{r}-\underline{\beta}-\underline{R}) | \emptyset_t(\underline{r}-\underline{\beta}_{\beta})\rangle \cdot$$

All conventions used previously are utilized for the unitary transformation of the Flodmark population analysis. Thus the quantity $n_{q\alpha}$ can be interpretted in terms of the atomic orbital $q\alpha$ whereby the number of electrons in that orbital on <u>any</u> α site is the average value obtained from the occupation numbers over all $\underline{k}$ space.

Appendix L.   Matrix Elements Between Atomic Orbitals

If $F(\underline{r}_\mu)=1$, we obtain expressions for the overlap matrix elements $\Delta_{q\alpha s\beta}(\underline{k})$. Using Equation 46 we directly obtain Equation 49 for   case $\alpha \neq \beta$ and $q \neq s$. Other cases, i.e. $\alpha=\beta, q\neq s$; $\alpha=\beta, q=s$, need to be specially considered in order to insure that all interactions are included in the sum over interaction vectors. Thus, the convention used to define $\underline{R}_p = \rho_j^{\alpha\alpha} - \rho_1^{\alpha\alpha}$ for $\alpha=\beta$ no longer applies; since one interaction vector, $j=1$, is usually taken as zero. Obviously, $\rho_j^{\alpha\alpha} \neq 0$ ($j=1,...,V$) for general cases. Therefore, we shall use a definition of $\underline{R}_p$ which applies to the special case $\alpha=\beta$;

$$\underline{R}_p = \rho_j^{\alpha\alpha} \quad (j=0,1,2,...V) \quad \text{where}$$

$$\rho_0^{\alpha\alpha} = 0 \text{ for the origin of atom type}$$

located at $\underline{\rho}_\alpha$ in the unit cell.

The latter choice satisfies the "ground domain(G)" discussed in Appendix J.

Using the above convention, we write $\Delta_{q\alpha s\alpha}^{(\kappa)}$ as

$$\Delta_{q\alpha s\beta}(\underline{k}) = GN_{q\alpha}^{-\frac{1}{2}}N_{s\beta}^{-\frac{1}{2}} \sum_{j=0}^{V} \exp(-i\underline{k}\cdot\rho_j^{\alpha\alpha}) \cdot$$

$$\langle \phi_{q\alpha}(\underline{r}_\mu - \rho_j^{\alpha\alpha}) | \phi_{s\beta}(\underline{r}_\mu) \rangle . \tag{L1}$$

Equation L1 can be expressed in a form compatible with economic use of the computer; namely, we shall use Euler's relation to convert the exponential terms in Equation L1 into cosine and sin terms which are more practical to evaluate. Using a parity term derived in Appendix M, we are able to write Equations in the text which apply to the case $\alpha=\beta$ and $q \neq s$.

In the case $\alpha=\beta$ and $q=s$, we obtain the diagonal elements which are obtained from Equation L1 via the Euler relation and are written in terms of cosines

$$\Delta_{q\alpha q\alpha}(\underline{k}) = GN_{q\alpha}^{-1}\langle \phi_{q\alpha}(\underline{r})|\phi_{q\alpha}(\underline{r})\rangle$$
$$+2\sum_{j=1,2}^{V}\cos(\underline{k}\cdot\underline{\ell}_j^{\alpha\alpha})\langle\phi_{q\alpha}(\underline{r}_\mu-\underline{\ell}_j^{\alpha\alpha})|\phi_{q\alpha}(\underline{r}_\mu)\rangle.$$
$$(L2)$$

If the atomic orbital functions are normalized, the overlap term corresponding to the null vector is equal to one.

If the Bloch sums are normalized to unity, i.e. $\Delta_{q\alpha q\alpha}(\underline{k})$ equals one, we need only rearrange Equation L2 to obtain an expression for the normalization constant $N_{q\alpha}$ which is

$$N_{q\alpha}=G\left[1+2\sum_{j=1,2}^{V}\cos(\underline{k}\cdot\underline{\ell}_j^{\alpha\alpha})\langle\phi_{q\alpha}(\underline{r}_\mu-\underline{\ell}_j^{\alpha\alpha})|\phi_{q\alpha}(\underline{r}_\mu)\rangle.\right.$$

Before we move on to a discussion of the Hamiltonian matrix elements, we should comment on the orthogonality of atomic orbital functions.

The diatomic overlap integral $\langle\phi_{q\alpha}(\underline{r}_\mu)|\phi_{s\alpha}(\underline{r}_\mu)\rangle$ which results for the null vector $\underline{\ell}_0^{\alpha\alpha}$ occurs for $\alpha=\beta$ and $q\neq s$.

It is important to stress that this integral is generally non-zero. For instance, if non-orthogonal analytical atomic orbital functions are used , the overlap integral is non-zero when the following conditions on the quantum numbers for orbitals q and s are met:

$$n_q \neq n_s \; ; \; \ell_q = \ell_s \; ; \; m_q = m_s \;.$$

However, if the Schmidt process is applied to the non-orthogonal basis set, the resulting orthogonal functions will automatically give a zero value for the integral for any quantum number set. In any case, the TBA computer program is written to handle either orthogonal or non-orthogonal atomic orbital functions on a given atomic site.

If $F(\underline{r}_\mu)$ equals the TBA Fock operator defined in Equation , off-diagonal $(q \neq s, \alpha \neq \beta)$ matrix elements of $H(\underline{k})$ can be written using Equation 46

$$H(\underline{k})_{q\alpha s\beta} = GN^{-\frac{1}{2}}_{q\alpha}N^{-\frac{1}{2}}_{s\beta} \sum_{j=1}^{V} \exp(-i\underline{k}\cdot(\underline{\rho}_j^{\beta\alpha} - \underline{\rho}_1^{\beta\alpha})) \cdot$$

$$\left\langle \phi_{q\alpha}(\underline{r}_\mu - \underline{\rho}_j^{\beta\alpha}) \Big| \overset{Ave}{\mathcal{F}}(\underline{r}_\mu) \Big| \phi_{s\beta}(\underline{r}_\mu) \right\rangle.$$

If we substitute $\underline{r} = \underline{r}' + \underline{\rho}_\beta$ into Equation ,we obtain the following expression ͻ

$$\overset{Ave}{\mathcal{F}}(\underline{r}_\mu) = -\frac{2}{V} + \sum_p \sum_\gamma V_\gamma(\underline{r}_\mu - \underline{\rho}_p^{\beta\gamma})$$

in terms of interaction vectors $\underline{\rho}_p^{\beta\gamma}$ (dropping the prime due

to the dummy index of integration). Furthermore, the above expression can be rewritten in more useful form

$$\mathcal{H}_{\text{Ave}}(\underline{r}_\mu) = -\nabla_\mu^2 + V_\alpha(\underline{r}_\mu - \underline{\rho}_j^{\beta\alpha}) + \sum_p{}'\sum_\gamma{}' V_\gamma(\underline{r}_\mu - \underline{\rho}_p^{\beta\gamma}).$$

The primes over the summation signs indicate that the interaction vector defined by $p=j$ and $\gamma=\alpha$ is removed from the potential summation. Therefore, Equation L2 becomes

$$H_{q\alpha s\beta}(\underline{k}) = GN_{q\alpha}^{-\frac{1}{2}} N_{s\beta}^{-\frac{1}{2}} \sum_{j=1}^V \exp(-i\underline{k}\cdot(\underline{\rho}_j^{\beta\alpha} - \underline{\rho}_1^{\beta\alpha}))\cdot$$

$$\langle \phi_{q\alpha}(\underline{r}_\mu - \underline{\rho}_j^{\beta\alpha}) | V_\alpha(\underline{r}_\mu - \underline{\rho}_j^{\beta\alpha}) | \phi_{s\beta}(\underline{r}_\mu) \rangle$$

$$+ \sum_p{}'\sum_\gamma{}' \langle \phi_{q\alpha}(\underline{r}_\mu - \underline{\rho}_j^{\beta\alpha}) | V_\gamma(\underline{r}_\mu - \underline{\rho}_p^{\beta\gamma}) | \phi_{s\beta}(\underline{r}) \rangle.$$

$$\text{(L3)}$$

Equation L3 will now be expressed in terms of groups of integrals so that the approximations discussed in context to the TBA method can be applied. That is,

$$H_{q\alpha s\beta}(\underline{k}) = GN_{q\alpha}^{-\frac{1}{2}} N_{s\beta}^{-\frac{1}{2}} \sum_{j=1}^V \exp(-i\underline{k}\cdot(\underline{\rho}_j^{\beta\alpha} - \underline{\rho}_1^{\beta\alpha}))\cdot$$

$$\left[I_0(j) + \sum_p\sum_\gamma I_1(j,p,\gamma) \right]$$

where

$$I_0(j) = \langle \phi_{q\alpha}(\underline{r}_\mu - \underline{\rho}_j^{\beta\alpha}) | V_\alpha(\underline{r}_\mu - \underline{\rho}_j^{\beta\alpha}) | \phi_{s\beta}(\underline{r}_\mu) \rangle$$

and

$$I_1(j,p,) = \langle \phi_{q\alpha}(\underline{r}_\mu - \underline{\rho}_j^{\beta\alpha}) | V_\gamma(\underline{r}_\mu - \underline{\rho}_p^{\beta\gamma}) | \phi_{s\beta}(\underline{r}_\mu) \rangle.$$

We then use Equation 40 to approximate I_0 as

$$I_0(j) = \langle \phi_{q\alpha}(\underline{r}_\mu - \underline{\rho}_j^{\beta\gamma}) | \phi_{s\beta}(\underline{r}_\mu) \rangle \varepsilon_{q\alpha} - \langle \phi_{q\alpha}(\underline{r}_\mu - \underline{\rho}_j^{\beta\alpha}) | -\nabla_\mu^2 \phi_{s\beta}(\underline{r}_\mu) \rangle.$$

In the above, we have operated to the function to the left of the $\mathcal{H}^{eff}_{\alpha}(r_f \; \rho^{\beta\alpha}_j)$ instead of the right. Thus, besides discussions connected with Equation 40, the quantum mechanical implication is that $\mathcal{H}^{eff}_{\alpha}$ is further assumed to be hermitian.

The three-center integrals $I_1(j,p,\gamma)$ are simplified by the Mulliken approximation used in Equation 32. Finally, we can express $H_{q\alpha s\beta}(\underline{k})$ in the form used for computer calculations and shown in Equation 49.

In the case of q=s(or q≠s) and $\alpha = \beta$, we define $H_{q\alpha s\alpha}(\underline{k})$ using the corresponding conventions for overlap matrix elements and using essentially the same approximations as above we are able to write the expression in Equation 49. The only difference with the above is how we express the TBA Fock operator:

$$\mathcal{F}^{Ave}(\underline{r}_\mu) = -\nabla^2_\mu + V_\alpha(\underline{r}_\mu - \underline{\rho}^\alpha_0) + \sum_p \sum_\gamma {}''V_\gamma(\underline{r}_\mu - \underline{\rho}^{\alpha\gamma}_p)$$

where the double primes denote that the null vector is removed from the double sum.

Appendix M. Parity of Overlap Integrals

We want to examine the value of an overlap integral on a translation of coordinate system B (Figure M1) by 2R along the z_2 axis (Figure M2).

Let us investigate the angular part of an overlap type integral between two orbitals having quantum numbers n, ℓ, m and n', ℓ', m' and being separated by the vector $\underline{R} = (R, \Theta, \emptyset)$. That is, we shall use Equation D6 to define

$$\langle \mathcal{Y}_{\ell m}(\Theta_A, \emptyset_A) | 1 | \mathcal{Y}_{\ell m'}(\Theta_B, \emptyset_B) \rangle = \Delta(\underline{R})_{AB}$$

Then,

$$\Delta(\underline{R})_{AB} = N^*(m) N(m') \, (-1)^{\ell'} \sum_k (-1)^k \cdot$$

$$\cdot \left[\exp(-i\gamma_{|m|}) d^\ell_{k\,-|m|}(\beta) + I(m) \exp(i |m|\gamma) \, d^\ell_{k\,|m|}(\beta) \right]$$

$$\cdot \left[\exp(i\gamma_{|m'|}) d^\ell_{k\,-|m|'}(\beta) + I(m') \exp(-i\gamma_{|m'|}) \, d^\ell_{k\,|m|'}(\beta) \right]$$

$$\cdot \langle Y^k_\ell | Y^k_{\ell'} \rangle \tag{M1}$$

where $\gamma = \emptyset$ and $\beta = -\Theta$.

Now if we examine $\Delta(-\underline{R})_{AB}$ we have that

$$-\underline{R} = (R, \pi - \Theta, \pi + \emptyset).$$

Then $\beta' = -(\pi - \Theta) = \Theta - \pi = -(\beta + \pi)$ and $\gamma' = -(\emptyset + \pi) = -\emptyset - \pi = \gamma - \pi$ for Euler angles in the displaced system (Figure M2). Since $\exp(im(\gamma - \pi)) = \exp(im\gamma) \exp(-im\pi) = (-1)^m \exp(im\gamma)$ and

$$d^\ell_{k\,m}(-\beta - \pi) = d^\ell_{k\,m}(\beta + \pi) = (-1)^{\ell + m} \, d^\ell_{-k\,m}(\beta)$$

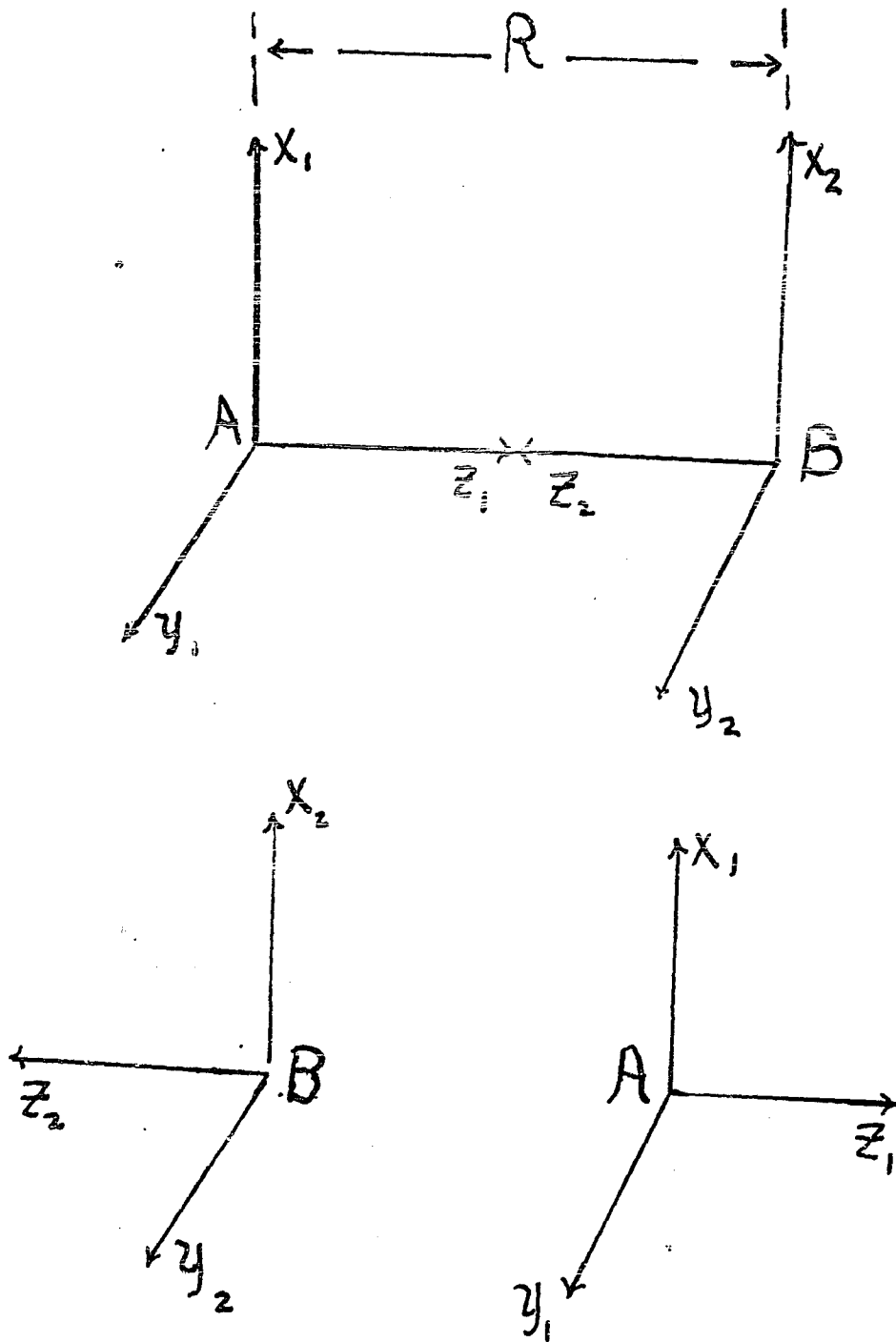Figure M1. The usual overlap coordinate system.

Figure M2. B is translated 2R along the Z_2 axis.

via the symmetry properties of $d^{\ell}_{k\,m}$ as defined by Edmonds (84), we have for the expression in the first bracket in Equation M1

$$\left[\exp(-i|m|(\gamma-\pi)\ d^{\ell}_{k\ -|m|}(-\beta-\pi) + I(m)\ \exp(i|m|(\gamma-\pi))d^{\ell}_{k\ |m|}(-\beta-\pi)\right.=$$

$$= (-1)^{m}\ (-1)^{\ell+m}\left[\exp(-i|m|\gamma)d^{\ell}_{-k\ -|m|}(\beta)\ +I(m)\exp(i|m|\gamma)d^{\ell}_{-k\ |m|}(\beta)\right.\ .$$

The transformation of the quantity in the second brackets in Equation M1 leads to a similiar form with the parity factors appearing out in front (because of orthogonality of ϕ dependent functions m=m' so we are left with a parity factor in and only.

Since $\langle Y^{k}_{\ell}|Y^{k}_{\ell'}\rangle = \langle Y^{-k}_{\ell}|Y^{-k}_{\ell'}\rangle$ (84), substitution of the above form into Equation M1 merely changes the order of summation and we have that

$$\Delta(\underline{R})_{AB} = (-1)^{\ell+\ell'}\Delta(-\underline{R})_{AB}. \qquad (M2)$$

If $F(\underline{r}_{\mu})=V(\underline{r}_{\mu}-\underline{S}^{\beta\alpha}_{j})$, we still would have $(-1)^{\ell+\ell'}$ in front of the negative -$\underline{R}$ integral. Therefore, Equation M2 is a general result to be used in both overlap and Hamiltonián matrix elements.